COLOUR RECONNECTION AND WEAK SHOWERS

Jesper Roy Christiansen

LUNDS
UNIVERSITET

2015

Thesis for the degree of Doctor of Philosophy

Theoretical High Energy Physics
Department of Astronomy and Theoretical Physics
Lund University

Thesis advisor: *Torbjörn Sjöstrand*
Faculty opponent: *Stefan Gieseke*

To be presented, with the permission of the Faculty of Science of Lund University, for public criticism in Lundmarksalen, Sölvegatan 27, on the 13th of November 2015 at 13:00.

Organization	Document name
LUND UNIVERSITY Department of Astronomy and Theoretical Physics Sölvegatan 14A SE–223 62 LUND Sweden	**DOCTORAL DISSERTATION** Date of issue November 2015 Sponsoring organization
Author(s) Jesper Roy Christiansen	
Title and subtitle Colour Reconnection and Weak Showers	

Abstract

This thesis consider the improvement of the simulation tools used to describe high energy particle collisions. These simulation programs are normally referred to as event generators. The emphasis is on two specific parts of the event generation: the introduction of radiation of weak bosons associated with the collision and a new model for colour reconnection.

Each collision contains significant additional radiation of particles, but earlier models have only included QCD and QED radiation. This thesis presents a first attempt at including also the weak radiation. The inclusion of weak emissions allows for a better understanding of already observed data. The weak radiation is also included in the common framework for including multi-jet matrix elements into the description of the radiation.

Colour Reconnection (CR) address the question: between which partons do colour strings form? The new model incorporates three principles, the SU(3) colour rules from QCD, a space-time causality requirement, and a minimization of the potential energy. It also introduces a new type of reconnections producing junction structures. The new model is able to explain the Λ production simultaneously at both LEP and LHC. The effects of CR, both the new model as well as older models, are also considered at potential future e^+e^- colliders. Comparisons between the new model and a string rope model is carried out, which include suggestions for relevant observables.

Key words:
Event generators, hadron collisions, Parton Showers, Weak interactions, Merging, Colour Reconnection, Fragmentation

Classification system and/or index terms (if any):

Supplementary bibliographical information:	Language English
ISSN and key title:	ISBN 978-91-7623-500-3
Recipient's notes	Number of pages 244 / Price
	Security classification

RESUMÉ

Ved CERN (Conseil Européen pour la Recherche Nucléaire) accelererer man protoner og bly-ioner op til næsten lysets hastighed, for derefter at kollidere dem med hinanden. Målet med dette er at forstå, hvordan de mindste ting i universet er bygget op, og hvordan de interagerer. Alle tidligere eksperimentelle data er kombineret til en enkelt teori, kendt som StandardModellen (SM). Håbet er, at de energirige partikelkollisioner vil vise os noget, der ligger udover SM, men før vi kan finde noget nyt, er vi nødt til at være sikre på, at vi forstår SM fuldstændigt.

SM er en yderst elegant teori; den kan dog desværre ikke løses analytisk. For at sammenholde modellen med eksperimentel data er man derfor nødt til at lave nogle approksimationer og antagelser. En af de mest udbredte måder at sammenligne data med teoretiske forudsigelser, er ved hjælp af computersimuleringer, kaldet Monte Carlo simuleringer. Disse programmer simulerer partikelkollisioner ud fra den bedst tilgængelige forståelse af teorien. De kan sammenlignes direkte med de data, der kommer fra rigtige kollisioner, og afvigelser vil være indikationer på fysik udover SM. Denne afhandling omhandler forbedringer af simuleringerne, sådan at vi kan være mere sikre på at potentielle afvigelser virkelig er ny fysik. Det er specielt to områder indenfor simuleringerne, der bliver berørt, den svage partonkaskade og farve omkoblinger.

Når en ladet partikel bliver accelereret udsender den elektromagnetisk stråling i form af fotoner, bremsstrahlung. En kollision mellem to partikler kan ses som en yderst ekstrem acceleration, derfor er store mængder ekstra stråling forventet. Beskrivelsen af denne ekstra stråling kaldes partonkaskaden. Udover at udsende fotoner er det også muligt at udsende gluoner. Disse svarer til fotoner for den stærke kernekraft. Da den stærke kernekraft er mange

gange stærkere end den elektromagnetiske kraft dominerer gluonemissioner totalt billedet. Hidtil har udsendelse af den svage kernekrafts "fotoner" ($W^{\pm}$ og Z) været ignoreret. Dette skyldes, at de er mange gange tungere end protonen. Nu er kollisionsenergien dog blevet så høj, at de bør inkluderes. Inklusion af disse partikler er netop dækket af en svag partonkaskade og er et af hovedemnerne i denne afhandling. Inklusionen af den svage partonkaskade gør det muligt at beskrive produktion af $W^{\pm}$ og Z, som den tidligere partonkaskade ikke kunne forklare.

Den stærke kernekraft er så stærk, at den binder de mest fundamentale partikler (kvarker) sammen til større partikler kaldet hadroner. Et eksempel på en hadron er protonen, som består af to op-kvarker og en ned-kvark. Et af spørgsmålene som en computersimulering må forklare er, hvordan disse kvarker bindes sammen til hadroner. Denne proces kaldes hadronisering. Billedet man forestiller sig er, at der mellem to kvarker er spændt en streng. Denne streng kan så fragmenteres til de forskellige hadroner. Det fungerer fint så længe man bare har to kvarker, da det er oplagt, hvor strengen befinder sig. Men hvis der er mange kvarker, er der også mange forskellige kombinationsmuligheder. Valget mellem disse streng-kombinationer går under navnet farve omkoblinger. I denne afhandling beskrives en nyudviklet model for beskrivelse af dette. Modellen giver en bedre beskrivelse af de forskellige typer af hadroner og deres energier sammenlignet med eksperimentelle data.

Begge tilføjelser er implementeret i det lokalt udviklede Monte Carlo simuleringsprogram, Pythia. Dette er en af de mest udbredte simuleringsprogrammer i verdenen og dermed vil de nye modeller direkte kunne indgå i sammenligningerne mellem teori og data.

PUBLICATIONS

The thesis is based on the following publications:

I Jesper R. Christiansen and Torbjörn Sjöstrand
Weak Gauge Boson Radiation in Parton Showers
JHEP 1404 (2014) 115

II Jesper R. Christiansen and Peter Z. Skands
String Formation Beyond Leading Colour
JHEP 1508 (2015) 003

III Jesper R. Christiansen and Torbjörn Sjöstrand
Colour Reconnection at Future e^+e^- *Colliders*
Eur. Phys. J. C75 (2015) 9, 441

IV Christian Bierlich and Jesper R. Christiansen
Effects of Colour Reconnection on Hadron Flavour Observables
Submitted to Phys. Rev. D

V Jesper R. Christiansen and Stefan Prestel
Merging Weak and QCD showers with Multijet Matrix Elements
LU TP 15-41

Additional publications I have contributed to during my Ph.D. studies but which are not included in the thesis:

VI Torbjörn Sjöstrand et al.
An Introduction to PYTHIA 8.2
Comput. Phys. Commun. 191 (2015) 159-177

VII R. Astalos et al.
Proceedings of the Sixth International Workshop on Multiple Partonic Interactions at the Large Hadron Collider
ariXiv:1506. [hep-ph]

CONTENTS

1 INTRODUCTION

This thesis will be a journey into the wonderful and magnificent world of particle physics. The intellectual journey started already back in ancient Greece with Democritus, who proposed that everything was made out of small indivisible objects, which he named atoms. The main quest of particle physics has ever since been to discover these indivisible, or fundamental, objects and understand their properties. With the ultimate goal of combining all the knowledge into one single theory, "the theory of everything". Most of the major advancements in our understanding of particle physics has been triggered by improvement of technology. What was previously believed to be fundamental, might no longer be fundamental when studied at smaller distances. The most obvious historical example being the atom, which we now know is not fundamental. But a similar situation may very well occur with what we today believe is the set of fundamental particles, when in the future it becomes possible to study these in greater detail. As such the journey of particle physics may be a never ending journey, where it will always be possible to find smaller and more fundamental particles. It might also stop at some point. We simply do not know. The only thing we know for certain is that we have not yet reached the end of the journey.

The modern field of particle physics focuses on the subatomic level. Since these distances are smaller than the wavelength of visible light, it is not possible to study them in an ordinary microscope. Instead huge particle accelerators are used to accelerate the particles to almost the speed of light before colliding them inside enormous detectors. The latest addition to the long history of particle accelerators is the Large Hadron Collider (LHC) with a circumference

of 27 km. It accelerates bunches of respectively protons and leadions before colliding them at an astonishing rate of 40 million times per second. Most of the intriguing physics happens at very short timescales and distances, e.g. the newly discovered Higgs boson has a lifetime of 10^{-22} s. It is therefore not possible to directly observe the fundamental process, instead it has to be inferred from its decay products. To understand how this works, let us imagine wanting to understand what a car is made of, but not being allowed to look inside it. Instead we collide two cars. At low speed the cars will just bounce off each other, and limited new knowledge is gained. When the speed is increased, objects will start to fly out in all directions, and by studying these we may eventually learn what a car is made of. Similarly by studying enough collisions, we hope to be able to understand the fundamental physics behind.

All the knowledge gained through the experiments has been combined into a single theory known as the Standard Model (SM). The SM includes three of the four known forces; the electromagnetic, the weak and the strong nuclear force. So far all attempts to include gravity have been unsuccessful. But on the subatomic level gravity is several orders of magnitude weaker than any of the other forces and can safely be neglected. In fact the agreement between the predictions from the SM and the measured values is extremely good. Best example is the electron magnetic moment, which has both been calculated and measured with a precision of 10^{-12}, and the results agree within the uncertainties [1]. Also at the LHC the SM has been tremendously successful and has been tested at scales spanning more than 10 orders of magnitude with no hints of new physics.

Even with the triumph of the SM at particle accelerators, there are both experimental and theoretical reasons that it can not be the final theory of everything. One of the experimental problems is the existence of dark matter as observed by the rotation of stars in the galactic plane. The stars at the outskirts of galaxies rotate too fast according to the visible matter inside the galaxies. The SM does not contain a suitable particle that can fulfill the role of dark matter, and as such an extension is required. There are a vast number of theories Beyond the Standard Model (BSM) trying to address these problems. They range from simple theories adding a

few extra particles to the more extensive models, which more than double the number of particles. But so far no direct evidence for any of the BSM theories has been observed, even with an extensive search program at the LHC. The newly restarted LHC, with almost twice the energy of the previous run, will hopefully shed some light on what lies in store for us beyond the SM.

The theoretical foundation of the SM is the combination of two of the most far-reaching theories of the 20th century, namely special relativity and quantum mechanics (QM), into what is known as Quantum Field Theory (QFT). In addition the concept of symmetry plays a crucial role, specifically what is known as gauge symmetries. In fact by only specifying the symmetry and the particle content, all possible interactions are given. As such the SM is often written in terms of its symmetries. But even though the SM is mathematically quite elegant, it is extremely difficult to do any calculations within it and approximations have to be used. The most common approximation method is known as perturbation theory. It works well at high energies (e.g. describing the Higgs) but poorly at low energies (e.g. describing the internal structure of the proton). A major part of this thesis focuses on the description of the part of a particle collision not covered by perturbation theory.

1.1 THE PARTICLE ZOO

The search for the most fundamental particles has so far led to a set of particles from which we believe all matter in this Universe is made. The complete set of particles is shown in fig. 1.1. With only this modest set of particles, all data from accelerator experiments over the last 30 years can be described [2]. The set does lack a candidate for dark matter, however, and a potential new fundamental particle may therefore be needed.

The particles are categorized into two groups; matter particles (fermions) and force carriers (gauge bosons and the Higgs). The fermions are further divided into two groups, depending on whether they are affected by the strong force (quarks) or not (leptons). The most well known lepton, and also the earliest discovered fundamental matter particle, is the electron. Together with its neutrino, it makes up the lepton content of the first generation of fermions.

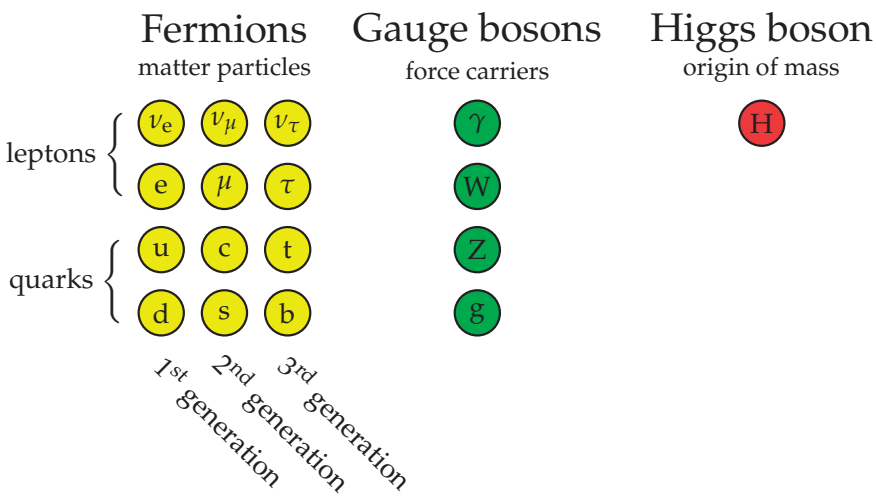

Figure 1.1: The particle zoo of the standard model.

The neutrino is an almost massless and very elusive particle, it can traverse the Earth several times without any interactions. The existence of the neutrino was already proposed in 1930 to explain energy and momentum conservation in radioactive decays, but due to its elusiveness it was not discovered until in 1956. The μ and the τ are heavier copies of the electron and together with their respective neutrinos they form the second and third generations. The properties of the μ and the τ are exactly equal to those of the electron except for their larger masses. However, the additional mass makes them unstable and they are therefore only observed in accelerator experiments or from cosmic rays. Why Nature has chosen to make exactly three generation is one of the big questions of the SM. There are no hindrances for adding an additional generation, but all experimental results indicate exactly three generations.

The quarks are also sorted into generations. The first generation contains the up and down, the second contains the charm and strange, and the third contains the bottom and top. The most familiar of these are the up and down quarks, which form the proton (uud) and the neutron (udd). As such all matter we encounter in our daily life consists only of three different elementary particles, the up and down quarks, and the electron. Similar to the leptons, the higher generations are identical but heavier copies of the first

generation. The top is the heaviest particle of the SM, weighing about 300000 times more than the electron. The strong hierarchy between the different masses is unexplained by the SM, and something that a theory of everything hopefully would address. Another intriguing point about the quarks is that neither of them has been directly detected. Due to the strength of the strong force the quarks are confined into hadrons (e.g. proton, neutron, pion). More information about confinement will come later in the section about the strong force (sec. 1.1.2).

Each force comes with its own set of force carriers. For the electromagnetic (EM) force, it is the well known massless photon. The weak force has three massive force carriers, the $W^{\pm}$ and Z bosons. Due to their relatively high masses they are only produced in high-energy particle collisions and their short lifetime ($\sim 10^{-24}$ s) ensures that they decay long before they even reach the detector. The strong force, also known as quantum chromodynamics, is mediated between "coloured" objects through the emission of gluons. Similar to the photon it is a massless particle, but it is only influential over short distances. This is due to confinement, which ensures that all macroscopic objects are colour neutral. Similar to quarks the gluon can not be directly detected, instead it is inferred from the distribution of hadrons seen at colliders. The final convincing proof (1978-1979) was the discovery of three-jet events[1], where at least one of the jets had to be a gluon jet.

The Higgs boson completes the list of the known elementary particles. It was discovered in 2012 at the LHC, after having evaded discovery for many years at earlier colliders. It was already predicted about 50 years ago, as a mechanism to provide mass to all the SM particles. The simplest introduction of mass breaks gauge invariance, and as such ruins the basic foundation of the theory. The Higgs boson circumvents this problem by using a mechanism known as spontaneous symmetry breaking. It is similar to how a ferromagnetic material randomly selects the direction of the magnetic field when it is cooled, even in an overall symmetric configuration. Since the Higgs has just recently been discovered, detailed measurements of its properties is one of the main goals of the fu-

1 A jet is a collection of (predominantly) hadrons moving almost collinear after the collision.

ture LHC program. The hope is that deviations from the SM predictions will be observed and thereby shed light on potential new BSM physics.

1.1.1 *The weak force*

The weak force is best known for the nuclear β-decays, where for instance a neutron radiates an e^- and a $\overline{\nu}_e$ and transforms into a proton[2] ($n \to pW^{*-} \to pe^-\overline{\nu}_e$). On the more fundamental quark level, what happens is that a d-quark emits a W^{*-} and transforms into a u-quark (see fig. 1.2). The β decays are part of a broader group of interactions known as charged-current interactions, where the interactions are mediated by $W^{\pm}$ bosons. A similar group also exists for the Z-mediated interactions, namely neutral-current interactions.

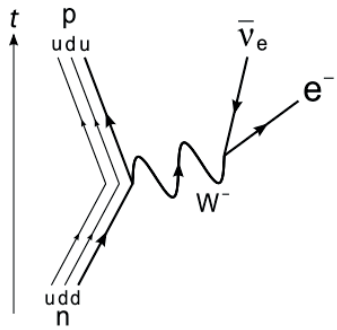

Figure 1.2: Illustration of a β^- decay.

Originally all weak interactions were believed to be point-like, and the first successful description was the Fermi theory. It introduced a four-point interaction with a free parameter, known as the Fermi coupling constant. The Fermi theory successfully described the kinematics of β decays. The modern description of the weak force includes a unification of the weak and the electromagnetic forces into a single force, known as the electroweak force. Therefore the two forces have similar coupling strengths and the only reason the weak force is weaker is due to the mass of its bosons. For collisions with energies well above the masses of the weak bosons, the weak force is just as important as electromagnetism.

2 The $*$ indicates that the mass of the W boson is highly virtual.

1.1.2 *The strong force*

The strong force is also known as Quantum ChromoDynamics (QCD). Due to both the EM force and strong force having a massless force carrier, they share quite a few properties. However, also major differences exist. In this section we will focus on two of the differences.

QCD is a non-Abelian gauge theory and one of the primary consequences of this is that the gluon itself is colour charged. This means that gluons directly interact with other gluons, which is not permitted for photons. Combining this with a coupling constant that is about ten times larger than the EM coupling results in that as soon any coloured object is formed, QCD dominates all other forces by orders of magnitude. At the LHC the incoming objects themselves consist of coloured quarks, which is why it is sometimes referred to as a QCD machine.

One of the most intriguing new phenomena of QCD is confinement: the observation that neither quarks nor gluons can be observed freely, but only inside colour neutral hadrons. To understand how this comes about, imagine moving a quark and an antiquark apart. For ordinary EM (as well as gravity) the force between the particles falls off as $1/r^2$, and therefore only a finite amount of energy is needed to separate them to an infinite distance. For QCD this is not the case, for large distances the strong force becomes constant and the potential therefore rises linearly with the distance. Thus to separate a quark and an antiquark by an infinite distance would require infinite energy. The potential energy stored between the quark and the antiquark is described by a colour string (fig. 1.3). At some point during the separation the energy becomes larger than the energy needed to create a new quark-antiquark pair. And then it becomes energetically favourable to replace the colour string between the quark-antiquark pair with an additional quark-antiquark pair and smaller colour strings (fig. 1.3).

The quarks can be confined into two kinds of hadrons. Either a quark and an antiquark can form a hadron; such hadrons are called mesons. In colour language it is a colour and its anticolour canceling each other. The best known and lightest meson is the pion. The other possible combination is three quarks forming a hadron, which is known as a baryon. The well-known proton and

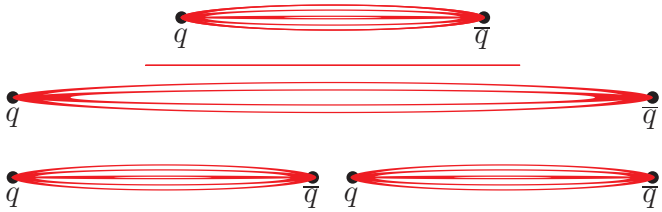

Figure 1.3: Pictorial description of what happens when a quark (q) and antiquark ($\overline{q}$) is separated.

neutron belong to this group. The corresponding colour analogy is three primary colours forming a white colour when added together. Nature is not restricted to only these two groups, in principle it is possible to add and combine them in any way. It is only recently, however, that any hadrons belonging to neither of these two groups have been unambiguously discovered. The discovered exotic quark configuration is the pentaquark (four quarks and one antiquark) by the LHCb collaboration [3].

1.2 MONTE CARLO SIMULATIONS

A pp collision at the LHC is shown in fig. 1.4. The two incoming protons collide and from the collision a huge number of new particles are created, which then move out in all directions. The main goal of particle physics phenomenology is to understand the physics at play in these types of collisions. To answer the question whether such an event is in agreement with SM predictions, and especially whether the number of events is predicted correctly. One of the essential tools in this endeavour is known as event generators. The basic idea is to build a virtual LHC, which simulates pp collisions on ordinary computers. The event generators are built according to our best understanding of the SM. Due to the difficulties with calculations within the SM, parts of the event generation have to rely on approximation and phenomenological models (e.g. string hadronization). The phenomenological models are motivated by the SM whenever possible.

Any QM calculation will only provide a probability for the possible outcomes, and since the SM builds on QM the same holds true

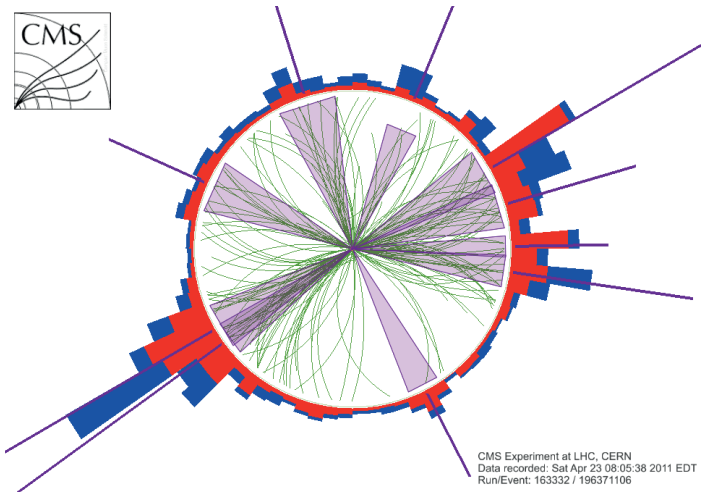

Figure 1.4: An energetic pp collision from the CMS experiment at the LHC. The detector is seen from the end with the collision happening in the center point. Each line represents a charged particle and the blue and red staples indicate energy deposited in the calorimeters.

there. It is first when the actual collision, and thereby measurement happens that Nature will choose one of the possible outcomes [3]. This effect is mimicked in the event generators by using random numbers to decide between the outcomes. The use of random numbers in statistics and integration is referred to as Monte Carlo techniques, hence event generators are sometimes referred to as Monte Carlo simulations.

The history of event generators began more than 35 years ago and has ever since undergone continuous development and refinement leading up to today's modern event generators. Today three major multi-purpose event generators exist: Pythia, Herwig and Sherpa. They all try to encapsulate the description of a full event in a single simulation. In this introduction the description will follow the path chosen by the Pythia program, the other programs share a similar overall structure, but have chosen slightly different paths when limited information from first principles is available. The use of multiple event generators both serves as a validation of the im-

3 In QM this is referred to as wave function collapse [4].

plementations, but also highlights potential constraints of the event generators.

To overcome the large complexity of the collisions, the event generators use a divide-and-conquer approach. The simulation is divided by its different physical mechanisms, which are successively applied to obtain a full event. The ordering of the mechanisms is based on energy, starting with the most energetic mechanism and evolving to softer and softer parts. According to Heisenberg's uncertainty relation this corresponds to begin with the physics happening at the shortest time scales. In this introduction I will divide the simulation into its three main components[4]:

- Hard process: The most energetic part of the event, e.g. the place where for instance Higgs and BSM particles are normally created.
- Parton shower: The simulation of additional radiation associated with the collision.
- Hadronization:The Confinement of the simulated quarks and gluons into the hadrons observed in the experiment.

The next three sections contain a more detailed description of the individual components. For a more detailed description of the physics involved see for example [5] and citations within.

1.2.1 *The hard process*

The probability for a specific process to happen is in particle physics given by its cross section (σ). The calculation of the cross section for pp collisions is factorized into two components (eq. (1.2.1)): the Parton Distribution Functions (PDFs), $f_i(x_1, Q^2)$ and $f_j(x_2, Q^2)$, and the partonic cross section, $\hat{\sigma}^{ij\to X}$.

$$\mathrm{d}\sigma = \int \mathrm{d}x_1 \int \mathrm{d}x_2 \, f_i(x_1, Q^2) \, f_j(x_2, Q^2) \, \mathrm{d}\hat{\sigma}^{ij\to X} \tag{1.2.1}$$

The PDFs can be interpreted as the probability to take out a specific parton, i, with a fixed energy fraction, x, at a specific energy scale,

4 A modern event generator is normally subdivided even further to more than ten different components.

Q^2, from the proton[5]. The PDFs are process independent and can therefore be measured in one process and applied to another. The partonic cross section serves a similar role as the ordinary cross section but on the partonic level. And since the partons are elementary particles, the partonic cross section can be directly calculated through perturbation theory. The fact that it is possible to factorize the cross section is actually quite remarkable. It basically shows that physics at different scales can be treated independently of each other. It is also the foundation of almost all theoretical predictions for the LHC.

At first glance the scale dependence of the PDFs might seem a bit confusing. But it can be understood by interpreting Q^2 as the scale at which the proton is probed. When probing at small Q^2 (corresponding to low resolution) the proton mainly consists of its three valence quarks. However, when the energy is increased the virtual fluctuations start to become visible. A virtual fluctuation is essentially a quark emitting a gluon and reabsorbing it rapidly again. Which in turns leads to gluons becoming more important at higher Q^2. At the LHC the Q^2 is so high that it is sometimes referred to as a gluon collider. Similarly, the virtual fluctuations of gluons should be included (i.e. $g \to q\bar{q} \to g$). The virtual quarks are referred to as sea quarks. Fundamentally it is possible to find all elementary particles inside the proton, but it is normally restricted to the valence quarks, gluons and sea quarks, since the rest provides a negligible contribution.

Mathematically, the evolution of PDFs is governed by coupled differential equations known as the DGLAP (Dokshitzer–Gribov–Lipatov-Altarelli–Parisi) equations (eq. (1.2.2)). The evolution is closely coupled to the probability for an emission to occur (e.g. $g \to gg$, with the probability given by $P_{g \leftarrow g}(z)$, where z is the energy fraction carried away by emitted parton). The gluon evolution contains two contributions: the quark splitting into a gluon and a quark, thereby

5 The interpretation becomes more complicated at higher orders of perturbation theory.

increasing the gluon contribution, and the contribution from the probability that already created gluons remain as gluons.

$$\frac{\mathrm{d}}{\mathrm{d}\log Q} f_g(x,Q) = \frac{\alpha_s(Q^2)}{\pi} \int_x^1 \frac{\mathrm{d}z}{z} \left(P_{g\leftarrow q}(z) \sum_q \left[f_q(\tfrac{x}{z},Q) + f_{\overline{q}}(\tfrac{x}{z},Q) \right] + P_{g\leftarrow g}(z) f_g(\tfrac{x}{z},Q) \right) \tag{1.2.2}$$

The formalism still has an obstacle, namely that the form of the PDFs can not be calculated from first principles. Only the evolution between different scales are known (eq. (1.2.2)). Instead the PDFs have to be determined experimentally. The largest number of constraints on the PDFs comes from Deep Inelastic Scattering (DIS) at ep colliders. DIS is when the electron scatters on one of the quarks inside the proton, thereby directly probing the probability to find a specific quark inside the proton.

The last piece in the cross section calculation is the partonic cross section. This can be calculated from first principles through perturbation theory [6]. Perturbation theory is an expansion in powers of the coupling constant for the field theory. This only works well if the coupling constant is significantly smaller than unity. This is true for the EM coupling constant ($\alpha_{em} \approx 0.0073$) and the QCD coupling at high energies. At low energies the QCD coupling becomes larger than unity, however, and therefore perturbation theory breaks down. This regime is known as non-perturbative QCD.

An excellent way to visualize the power expansion is Feynman diagrams, invented by R. Feynman in 1948. An example of $e^+e^- \to q\overline{q}$ is shown in fig. 1.5. Each vertex corresponds to a fundamental interaction, and thereby contains the coupling constant. The lines corresponds to the propagation of particles from point to point. The Feynman diagrams not only serves as a visualization tool but also as a calculational tool. Each component also has a specific mathematical interpretation, for instance the $e^+e^-\gamma$ vertex always en-

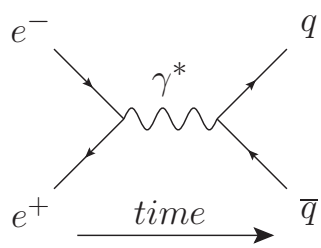

Figure 1.5: The Feynman diagram for $e^+e^- \to \gamma^* \to q\overline{q}$.

ters in the mathematical equation as[6]
$ie\gamma^\nu$. The expression corresponding to the full diagram is known as the Matrix Element (ME). The ME combined with overall energy-momentum conservation, and phase-space integrals makes up the partonic cross section. The partonic cross section for the diagram (fig. 1.5) is given by:

$$\frac{d\hat{\sigma}}{d\Omega} = \frac{\alpha_{em}^2 Q_q^2}{4E_{cm}^2}\left(1+\cos^2\theta\right), \tag{1.2.3}$$

where Q_q is the electrical charge of the quark and $d\Omega = d\varphi\, d\cos\theta$ parameterizes the unit sphere. One of the most intriguing features of the result is the divergence at low energy, which simply means that the probability becomes infinite for infinitely soft scatterings. This divergence is known as an infrared divergence and in the parton shower section it will be described in more details together with collinear divergences. A first interesting consequence of the divergence is that at some point the cross section $gg \to gg$ becomes larger than the measured total pp cross section[7]. At first glance this seems like a contradiction of the theory, since the total pp cross section serves as an upper bound. It is saved, however, by the observation that it is possible to have multiple $gg \to gg$ interactions for each pp collision. And the calculation of the partonic cross section can be used to determine the average number of partonic collisions per pp collision. The inclusion of extra parton interaction is known as Multiple Parton Interactions (MPI) and it contributes to a significant fraction of the particles seen in a typical pp collision.

The diagram drawn in fig. 1.5 only contributes what is known as the Leading Order (LO) ME. The LO diagram is the lowest order, in the power expansion of coupling constants, at which the process is possible. The next term in the power expansion is referred to as Next-to-Leading-Order (NLO). The diagrams for the QCD NLO $e^+e^- \to q\bar{q}$ are shown in fig. 1.6. The complexity grows rapidly with both increasing order as well as increasing number of final state particles. The current state of art is automated calculation of most NLO processes, calculations of a selected set of NNLO pro-

6 γ^ν is a Dirac matrix and e is the electrical charge.
7 A similar divergence also exist for this process.

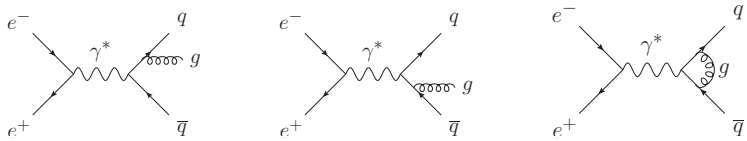

Figure 1.6: The NLO QCD Feynman diagrams for $e^+e^- \to q\overline{q}$.

cesses and a very limited set of N^3LO calculations. The maximal number of outgoing final state partons for LO is about eight, anything beyond that becomes too slow. As can be seen from fig. 1.4, this is not sufficient to describe the full event structure of a pp collision. The most common way to include the extra emissions is known as a parton shower, which is the topic of the next section.

1.2.2 *Parton Shower*

The additional radiation associated with the hard collision can be interpreted in a similar fashion as ordinary bremsstrahlung of a charged particle moving in a magnetic field. The effect is much more extreme, however, which is due to the very rapid acceleration present in the collision as well as the inclusion of QCD, where both the increased coupling constant and the colour-charged gluons enhance the emission rate. A description of this radiation is known as a Parton Shower (PS). The PS iteratively applies the probability for a single parton to split into multiple partons in the collinear limit, e.g. $q \to qg \to qgg \to ...$[8]. These splitting probabilities (also called splitting kernels) are the same as used in the DGLAP equation. As an example of a splitting kernel let us consider the splitting $P_{q\leftarrow q}$. The splitting kernel can be calculated from the $e^+e^- \to q_1\overline{q}_2g_3$ cross section:

$$\frac{d\sigma}{dx_1dx_2}\frac{1}{\sigma_0} = \frac{\alpha_s}{2\pi}\frac{4}{3}\frac{x_1^2+x_2^2}{(1-x_1)(1-x_2)}, \tag{1.2.4}$$

where $x_i = 2E_i/E_{cm}$ and σ_0 is the the cross section for the original $2 \to 2$ process (i.e. the one drawn in fig. 1.5). With the $2 \to 2$ cross section divided out, eq. (1.2.4) corresponds to the probability for both quarks to emit an additional gluon. In the limit where q_1

8 Some PS models use the probability for two partons to split into three instead.

and g_3 are almost collinear, x_2 has to be close to unity ($x_2 \approx 1$) due to momentum conservation. Defining z as the energy fraction the quark keeps ($x_1 = z$)[9] and setting Q^2 equal to the invariant mass of q_1 and the gluon, eq. (1.2.4) can be rewritten as:

$$d\mathcal{P}_{q\to qg} = \frac{\alpha_s}{2\pi}\frac{dQ^2}{Q^2}\frac{4}{3}\frac{1+z^2}{1-z}dz \quad (1.2.5)$$

$$= \frac{\alpha_s}{2\pi}\frac{dQ^2}{Q^2}P_{q\to qg}dz\,, \quad (1.2.6)$$

where $P_{q\to qg} = \frac{4}{3}\frac{1+z^2}{1-z}$ is the same function as in the DGLAP evolution (eq. (1.2.2)). The splitting probability contains two divergences, a soft divergence if z is equal to unity (then $x_3 = 0$ and the gluon has no energy) and a collinear divergence if Q^2 is equal to zero ($x_2 = 1$). The high probability for collinear emissions leads to the jet structures seen in the event display (fig. 1.4).

The definition of the evolution variable, Q^2, is not unique, with some common choices being the transverse momentum or the angle of the emission. Both of these choices are preferred over virtuality, since they better conserve the coherence of QCD. Coherence here refers to a destructive interference of emission amplitudes that leads to a reduction of the total emission rate.

Since the PS allows for an unlimited number of emissions it is essentially an all-order calculation, however, the calculation for each order is an approximation. This can be compared to the hard ME calculation, where each order is exact, but the overall calculation has to be cut off at a certain point.

Another advantage of the PS is that it naturally includes resummation. To understand the need for resummation it is easiest to consider an analogy for radioactive decays. The probability for a single atom to decay, after a specific amount of time, is not only given by the differential probability, but must also include the probability that it has not already decayed. Similar for emissions the probability to have an emission at low scale ($\approx$ late time) must include the probability that no emissions at higher scales ($\approx$ earlier

9 Different definition of z in this section compared to the DGLAP evolution.

times) occurred. This leads to that the probability to have exactly one emission, at a scale Q, is given by

$$d\mathcal{P}_{q\to qg} = \Delta(Q^2_{max}, Q^2)\,\frac{dQ^2}{Q^2}\frac{\alpha_s}{2\pi}P_{q\to qg}(z)dz\,\Delta(Q^2,\mu_f^2)\,, \quad (1.2.7)$$

where Q_{max} is the starting scale, μ_f is a low energy cut-off scale and $\Delta(Q_1^2, Q_2^2)$ is the no emission probability (also called Sudakov form factors) given by

$$\Delta(Q_1^2, Q_2^2) = \exp\left(-\sum_{a,b,c}\int_{Q_2^2}^{Q_1^2}\frac{dQ'^2}{Q'^2}\int\frac{\alpha_s}{2\pi}P_{a\to bc}(z')dz'\right) \quad (1.2.8)$$

The collinear approximation works well in describing the structure of partons inside the jets, but it does not incorporate the interference needed to describe separated high-energy jets. This is the region of phase space where hard ME calculation works well, since in general only a few of these are present per event. The obvious question is then if we can combine the best of two worlds, and use ME calculation where they are available and rely on the PS to take care of the rest. One of the biggest problems with a naive addition is the possibility for double-counting. The same three-jet event can either come directly as a hard ME or come as a $2 \to 2$ hard ME with a PS emission, and of course including both leads to a double-counting. The way this is avoided is by separating the phase-space into regions that are covered either by the hard ME or by the PS. This whole procedure is known as merging and together with matching (the combination of NLO calculations with the PS) are the largest improvement to the event generators during the last ten years.

All the above discussion about PS focused exclusively on the emission of gluons. It is also possible to include emissions of photons, which follow exactly the same recipe except for being suppressed by an order of magnitude compared to the gluon emissions ($\alpha_s/\alpha_{em} \sim 10$). This has already been studied in great detail, especially at lepton colliders, where the leptons will emit photons but no gluons. Another possibility is the emission of $W^\pm$ and Z bosons, which, in addition to the coupling constant suppression, also has a mass suppression. For low energy collisions the production of $W^\pm$ and Z bosons only needs to be included in the hard ME, since it will

predominantly be the hardest part of the collision. If the energy is increased sufficiently above the $W^{\pm}$ and Z masses, e.g. the 13 TeV LHC or even more at a potential 100 TeV pp collider, the production of weak bosons is no longer guaranteed to be the hardest part of the collision and as such need to be included in the PS. The implementation and consequences of a weak shower constitutes a major part of this thesis. The introduction will restrict itself to one aspect of it, namely the fact that the weak bosons are massive.

The introduction of mass for the emitted particle naturally changes the splitting kernels. The easiest way to study this is to calculate the $q\bar{q} \to q\bar{q}Z$ ME, while only allowing radiation from the final state particles (similar to eq. (1.2.4)):

$$\frac{1}{\sigma_0}\frac{d\sigma}{dx_1\,dx_2} = \frac{\alpha_{weak}}{2\pi}\left(\frac{x_1^2+x_2^2+2r_3(x_1+x_2)+2r_3^2}{(1-x_1)(1-x_2)} - \frac{r_3}{(1-x_1)^2} - \frac{r_3}{(1-x_2)^2}\right), \tag{1.2.9}$$

where $r_3 = m_W^2/E_{cm}^2$ and α_{weak} is the corresponding weak coupling constant for either the Z or the $W^{\pm}$ bosons. In the massless limit ($r_3 \to 0$) it is easy to see that the same kinematical expression as earlier is obtained. The expression also seems to have the same divergences at $x_1 = 1$ and $x_2 = 1$, however, these are no longer part of the available phase-space. Part of the energy has to go into the $W^{\pm}$ mass, and as such it is not possible to conserve momentum if one quark is assigned half the energy. With the divergences gone it is possible to do an integration over the full phase-space which will have the following structure:

$$\sigma^{gg\to u\bar{u}Z}\frac{1}{\sigma_0} = \frac{\alpha_{weak}}{2\pi}\left[C_1\log^2\left(\frac{E_{cm}^2}{M_W^2}\right) + C_2\log\left(\frac{E_{cm}^2}{M_W^2}\right) + C_3\right], \tag{1.2.10}$$

where C_1, C_2 and C_3 are numerical constants[10]. The first term has the highest power of the logarithm thus being the most important, and therefore is normally referred to as Leading Logarithm

10 A similar integration can also be done for the gluon splittings with the introduction of a lower cut-off.

(LL). The second term is referred to as the Next-to-LL (NLL). The collinear approximation only formally captures the LL component of the result, however, it normally does better than what naively would be expected from a LL approximation. The LL approximation also provides a very simple tool to probe the expected size of the weak effects at a given center-of-mass energy. Simply inserting the jet energy in $(\alpha_{\text{weak}}/(2\pi))\log^2(E^2_{\text{jet}}/M^2_W)$ for respectively 200 GeV, 1 TeV and 5 TeV gives $\sim$ 0.06, 0.4 and 1. This clearly highlight why it has earlier been a good approximation to neglect weak correction, but that this will no longer be true when the energy is pushed well beyond the $W^{\pm}$ mass.

1.2.3 *Hadronization*

The last big piece in the simulation chain is hadronization: the transformation from the quarks and gluons used in the hard process and the PS to the actual observed hadrons in the experiments. The hadronization phase is one of the least understood parts of the simulation chain since it belongs to the non-perturbative regime of QCD. This has led to several phenomenological models being developed with emphasis on different aspects of QCD. One of the most successful models is the Lund string fragmentation model, which will be the focus of this introduction. The model explains the hadronization by spanning colour strings between the partons and later fragment these into the observed hadrons.

Before entering the underlying fragmentation formalism, let us consider an essential question, both to this thesis and to the string fragmentation, namely, between which partons do strings form? As an example consider the case of two quarks (q_1 and q_2) and two antiquarks ($\overline{q}_1$ and $\overline{q}_2$). These can either connect as $q_1 - \overline{q}_1$ and $q_2 - \overline{q}_2$ (fig. 1.7a), $q_1 - \overline{q}_2$ and $q_2 - \overline{q}_1$ (fig. 1.7b), or potentially even more complicated colour structures. The decision on which colour configuration to choose is known as Colour Reconnection (CR)[11]. The name originates from the first studies of CR at LEP more than twenty years ago, where it was considered in $e^+e^- \to W^+W^- \to q\overline{q}q\overline{q}$. The quark and the antiquark from the same $W^{\pm}$ decay has

11 Or slightly more precise, it is called CR whenever alternatives to the leading-colour topologies are considered.

to be colour connected just when the decay happens. But it might be possible for both the pairs to share the same colour, since QCD only contains a limited number of colours. When the quark and antiquark start to move apart it may become favourable to reconnect the colours and choose to form the string between the quark from one $W^{\pm}$ decay and the antiquark from the other $W^{\pm}$ decay, hence the name colour reconnection.

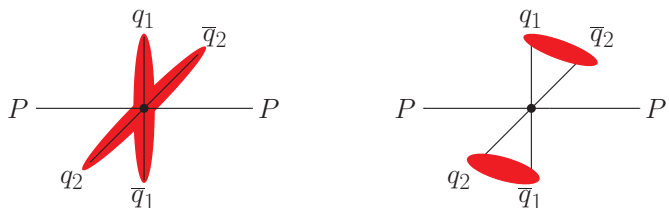

Figure 1.7: Example of two different string configuration for two quarks (q_1 and q_2) and two antiquarks ($\overline{q}_1$ and $\overline{q}_2$). The quarks and antiquarks are imagined to originate from a single pp collision.

Since not much is known from first principles, there is a significant freedom in designing a CR model. There is one principle, however, which is a common trend between all CR models, namely the minimization of potential energy. Since the evolution of the event generators is not carried out in ordinary space, but rather in $p_{\perp}$, no trivial definition of the potential energy is available. Two different measures are predominantly used, either the invariant mass of the string, m_{string}, or the logarithm of the invariant mass, $\log m_{\text{string}}$. The first represents the total energy available in the string while the later expresses the available potential energy. The later measure is normally referred to as the λ measure. In addition to the different definitions of the potential energy, the models also differ in which partons are allowed to reconnect.

At e^+e^- colliders CR effects are expected to be limited, but they become exceedingly more relevant and complicated at pp colliders. With the increased number of final state coloured particles and the ordering from the PS being spoiled between different MPIs, the effects of CR are much more apparent. Experimentally, the need for CR can be seen when considering the average transverse momentum as a function of multiplicity. Without CR this distribution is

expected to be constant, since additional MPIs do not increase the average transverse momentum. Since CR lowers the total multiplicity, thereby requiring additional activity from MPIs, and since it tends to form boosted strings by reconnecting collinear partons, the average transverse momentum increases with increased CR. With the strong correlation between the amount of CR and final state activity, the CR predicts a rise of average transverse momentum with multiplicity, in agreement with observations.

CR plays a significant role in this thesis with the development of a new CR model to explain discrepancies observed at the LHC (Paper II) and further phenomenological studies at both LHC (paper IV) and a potential future e^+e^- collider (paper III). The main features of the model is the inclusion of more complicated reconnections (known as junctions) and determination of allowed reconnections based on the colour rules from QCD.

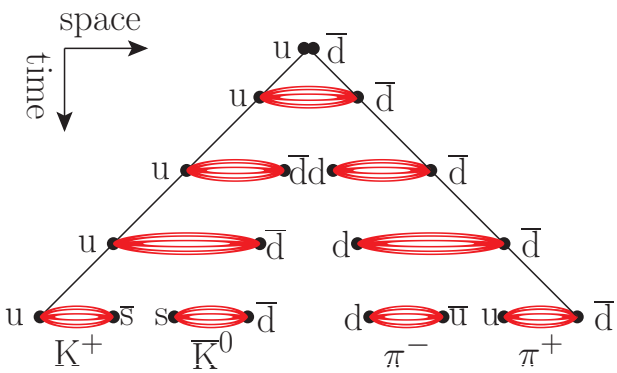

Figure 1.8: Illustration of a string fragmenting into several hadrons.

The fragmentation of a string into hadrons is depicted in fig. 1.8. The large string is divided by successive quark-antiquark pair formation until each string corresponds to exactly one hadron. There are two major considerations at each fragmentation step: how is the energy distributed between the two new strings and what is the flavour and spin of the newly formed quark-antiquark pair.

The energy sharing is determined by the Lund symmetric fragmentation function:

$$f(z) \propto \frac{(1-z)^a \exp\left(\frac{-bm_\perp^2}{z}\right)}{z}, \tag{1.2.11}$$

where z is the energy fraction taken by hadron formed, $m_\perp^2 = p_\perp^2 + m^2$, and a and b are two free parameters of the model. The string is fragmentated by starting from the two end points and recursively fragment off hadrons according to eq. (1.2.11) until no more energy is left in the string. The derivation of the function relies on the symmetric structure of the problem, i.e. the probability for a specific fragmentation to happen should not depend on whether we start from the right or the left end.

The flavour choice is decided by considering the whole fragmentation as a QM tunneling process, where larger masses are exponentially suppressed:

$$\mathcal{P} \propto \exp\left(-\frac{\pi m_{\perp q}^2}{\kappa}\right), \tag{1.2.12}$$

where κ is the string tension. The consequence is that $s\bar{s}$ are suppressed by 70 % compared to the $u\bar{u}$ and $d\bar{d}$ pairs and all other quarks can safely be neglected in the fragmentation process[12]. It is still possible to form hadrons with charm and bottom quarks, but the quarks have to have been produced in either the hard process or the PS. The transverse momentum is included in a similar way for all hadrons. This leads to all hadrons sharing a similar $p_\perp$ spectrum with large $p_\perp$ being heavily suppressed[13].

In the fragmentation depicted by fig. 1.8 only mesons are produced. To include the production of baryons, diquarks are introduced. A diquark is the combination of two quarks (or two antiquarks to form an antidiquark) into an effective (semibound) state. The colour rules from QCD allows the interpretation of two colours as a single anticolour. Thereby it is possible to simply insert an antidiquark-diquark pair in the above formalism. The antidiquark-diquark pair always has to be inserted together in order not to violate the baryon number conservation of QCD. The diquark mass is larger than that of a single quark, which in turn leads to a suppression of baryon production.

The diquark formalism is not the only baryon production mechanism. Another example is the junction mechanism. A junction is

12 The exact value of the parameter is tuned to experimental data

13 Later decays of the hadrons alter the $p_\perp$ spectra.

a point where three string pieces meet (fig. 1.9). The junction string topology can be seen as a similar extension to a baryon as the string is to a meson. The junction naturally carries a baryon number, thus at least one baryon has to be formed when it is hadronized. In the diquark production mechanism a diquark and an antidiquark are produced simultaneously, so there is a large correlation between the ensuing baryon and antibaryon. This is not necessarily true for junctions, since a junction and an antijunction can be separated by several (and potentially hard) gluons. Junctions have predominantly been used in the description of beam baryons (e.g. the proton in pp collision). The new CR model introduce a new use for the junction structures, by introducing them as possible colour configurations (see fig. 1.10). This naturally leads to an enhancement of the baryon production, which is one of the key prediction of the new CR model.

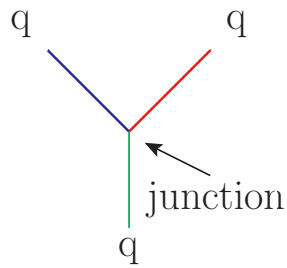

Figure 1.9: Example of a junction connected to three quarks. Each line here is intended as a simplified representation of a more extended string, as drawn e.g. in fig. 1.8.

One of the key concepts of the fragmentation is its universality. Basically, no matter how a string is formed it should hadronize according to the same rules. This has led to the fragmentation parameters being determined in the clean environment of the $e^+e^- \to q\bar{q}$

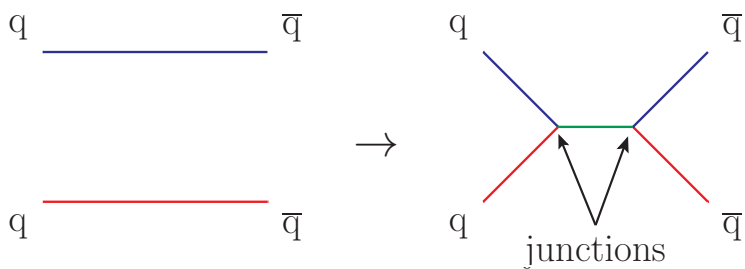

Figure 1.10: Two ordinary strings reconnecting two form a junction and an antijunction.

collisions and then applied directly to pp collisions. If any discrepancy is then observed at pp colliders it will have to be due to new physics present in pp collisions, which is not present (or at least negligible) at e^+e^- colliders. One such example is CR, which only plays a small role at e^+e^- colliders, compared to the more important role at hadron colliders. Another example could be that overlapping strings should be hadronized differently from non-overlapping ones, and such overlaps occur much more frequently at hadron colliders. One of the key aspects for most models trying to explain observed discrepancies is the larger final state activity in pp collisions.

The last piece of the whole simulation chain is the decay of unstable hadrons. A large fraction of the hadrons produced in the fragmentation will decay almost immediately, and certainly before they reach any detector equipment. The decays are carried out according to their experimentally measured lifetime and branching fractions.

1.3 SUMMARY

The world of fundamental particle physics is a both beautiful and elegant world. From a few fundamental principles the behaviour of all matter can be deduced, in principle. In reality, the world becomes slightly more messy and complex when confronted with our limitation in calculation techniques. In order to provide a sufficient description of high-energy collisions several physic concepts happening at potentially different scales need to be included. The most common framework for handling this challenge is event generators. They divide the complex collision into smaller manageable pieces and solve them separately, at least to some approximation. The overall goal is to create a virtual particle collider built on the knowledge of the theory and capable of describing real experiments. A typical pp collision as seen from the point of view of such a simulation is shown in fig. 1.11. The two protons collide to form a bunch of outgoing hadrons, all described by the physics cocktail included in the event generators.

Event generators have had tremendous success at describing the measured data at both hadron and lepton colliders. But with the

huge complexity of the model, there will always be regions of the model with room for improvement. The rest of this thesis will focus on exactly such areas, specifically, a new colour reconnection model and the introduction of a weak parton shower.

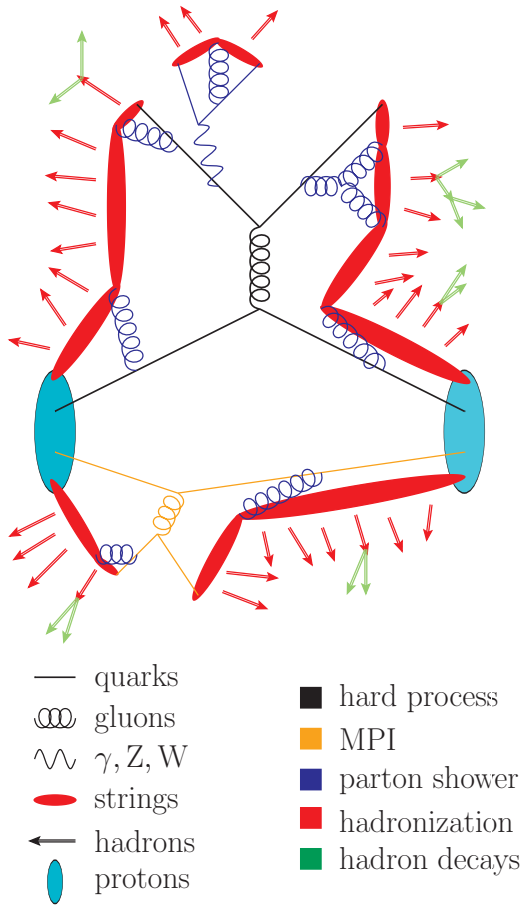

Figure 1.11: An example of how a pp collision is seen from a event generator's perspective. The hard process is a dijet event with a radiated weak boson and an additional MPI. The two protons are artificially separated in the drawing in order to see what happens.

BIBLIOGRAPHY

[1] D. Hanneke, S. Fogwell, and G. Gabrielse, "New Measurement of the Electron Magnetic Moment and the Fine Structure Constant," *Phys. Rev. Lett.* **100** (2008) 120801, arXiv:0801.1134 [physics.atom-ph].

[2] M. Thomson, *Modern Particle Physics*. Cambridge University Press, 2013.

[3] **LHCb** Collaboration, R. Aaij *et al.*, "Observation of $J/\psi p$ Resonances Consistent with Pentaquark States in $\Lambda_b^0 \to J/\psi K^- p$ Decays," *Phys. Rev. Lett.* **115** (2015) 072001, arXiv:1507.03414 [hep-ex].

[4] J. J. Sakurai and J. Napolitano, *Modern Quantum Mechanics*. Addison-Wesley, 2011.

[5] A. Buckley *et al.*, "General-purpose event generators for LHC physics," *Phys. Rept.* **504** (2011) 145–233, arXiv:1101.2599 [hep-ph].

[6] M. E. Peskin and D. V. Schroeder, *An introduction to quantum field theory*. Westview Press, 1995.

2

OVERVIEW OF THE PAPERS

This section contains a brief summary of the papers that constitute this thesis. The articles can be separated into two groups. Papers I and V explain the implementation of a weak shower and how to use it for merging in PYTHIA. Paper II, III and IV concerns the development, implementation and phenomenological consequences of a new colour reconnection model. Below follows a more detailed resume as well as a section on my contributions to each individual article.

2.1 WEAK GAUGE BOSON RADIATION IN PARTON SHOWERS

The PS formalism had previously only been implemented to include QED and QCD emissions. This article presents a first inclusion of weak gauge boson emissions in the PS. The main motivations were to firstly understand why the PS has a difficult time describing W(Z) + jets observables. Secondly, the incorporation of the weak PS means that the weak Sudakov resummation will enter on equal footing with the QCD one. Especially it ensures that the competition between the different types of emissions is treated correctly.

There are two obvious technical new effects in the implementation of the weak PS: the mass of the weak gauge bosons and the flavour change of the W emission. The flavour change is handled according to the CKM matrix, and additional care has only to be taken for the evaluation of PDFs. The emission of massive particles were already considered in a hidden-valley framework [1], which turns out be directly applicable to the weak PS. Due to the massive bosons the collinear approximation does not provide acceptable re-

sults. This is circumvented by introducing an extensive use of ME correction for all weak emissions. The ME corrections also need to be separated depending on the type of $2 \to 2$ process.

The new PS is compared to data recorded from the ATLAS experiment and, with the inclusion of a k-factor, the new PS describes the inclusive W(Z) + jet production well. The individual $p_\perp$ distributions for jets are also well described, however, the new PS fails to describe the φ angle between the two leading jets. Additional studies focused on the production of hadronically-decaying weak bosons inside jets are also performed. Due to the profuse ordinary QCD emissions a broad spectrum of "background" jet masses is generated, making the weak bosons challenging to find, but not impossible. Lastly the effect of the weak Sudakov is considered at both 14 TeV and 100 TeV pp colliders. The effects are seen to be about $\sim 12\%$ at 14 TeV and increasing to $\sim 25\%$ at 100 TeV for the maximal considered jet energies.

2.1.1 *My contributions*

The original idea for the paper was conceived by Torbjörn Sjöstrand. The final framework constitute a combined effort of both Torbjörn and me, with the largest contributions from Torbjörn. The code implementation in Pythia was done exclusively by me, and I also carried out all the phenomenological analyses. I wrote a first draft for section 3-5, but they were then edited by Torbjörn.

2.2 String formation beyond leading colour

This paper describes the implementation of a new handling of colours for both colour reconnection and beam remnants in Pythia. The theoretical motivation for the work was to incorporate the SU(3) colour rules from QCD into the model. The new model also includes junction structures, which can be used to explain the enhancement of the Λ production observed at LHC.

The new colour treatment in the beam remnant model combines colours from scattered partons in the MPIs to lower the total number of strings connected to the beam. The probability to form the different colour configurations are based on the QCD colour rules,

with an additional suppression of high colour states due to saturation. The new model differs from the old model for particle production at high rapidities. At the measured rapidities it is difficult to tell whether the new model describes the data better, however.

The new CR model is built on three main principles: the SU(3) colour rules, a space-time causality requirement, and the minimization of the λ measure. Each string is assigned a colour and only colour-compatible and causally connected strings are allowed to reconnect. All reconnections that lower the total λ measure are carried out until a local minimum is reached.

The advantages of the new model is that it can simultaneously describe the Λ production at both LEP and LHC, which no earlier PYTHIA tune had been able to. It still has problems describing the identified particle's $p_\perp$ spectra individually, and also the $\langle p_\perp \rangle$ vs. mass. The effect on the top mass measurement is also considered, which shows an uncertainty of about 0.14 ± 0.11 GeV, which is of similar magnitude as earlier observations [2].

2.2.1 *My contributions*

The original idea for the model was conceived by Peter Skands. During the development of the final model, we both contributed with ideas for improvements. The code implementation and the phenomenological studies were carried out exclusively by me. I wrote the first draft for section 2.3.1, 3 and 4.

2.3 COLOUR RECONNECTION AT FUTURE e^+e^- COLLIDERS

This paper studies the phenomenological effects of CR at e^+e^- colliders. In addition to the CR model introduced in paper II, two older CR models, which were reimplemented [3] in PYTHIA 8 and another CR model, introduced in connection with the top mass measurement at LHC [2], are also considered.

The first study uses the fully hadronic W-mass measurement as a probe to test CR instead. With the expected statistical uncertainty it is shown that a new collider will be able to constrain the CR models severely. Especially if the measurement is repeated at higher center-of-mass energies, where the effect is significantly larger.

The new CR models are also compared to dedicated CR studies at LEP. Only a single of the new CR models is ruled out with more than three sigma. A measurement of the total multiplicity in respectively semi-leptonic and fully hadronic WW events is suggested as an observable sensitive to CR.

Finally the uncertainty introduced in hadronic measurement at e^+e^- colliders due to CR are highlighted through the study of a Higgs parity measurement. It is argued that CR needs to be included for measurements aiming at a precision below 5 %.

2.3.1 *My contribution*

The model comparisons were suggested by Torbjörn Sjöstrand, but afterward were carried out by me with limited guidance from Torbjörn. The reimplementation of the old models and all the phenomenological studies were carried out by me. I wrote the first draft for the paper except parts of the introduction and the old model descriptions. The paper was later edited by Torbjörn, but to a significant lesser extent than paper I.

2.4 Effects of colour reconnection on hadron flavour observables

This paper presents a comparison of two models, the CR model from paper II and a string rope model [4] for hadronic flavour observables at LHC.

The models are compared to data for fully inclusive identified particle ratios at a center-of-mass energy of both 200 GeV and 7 TeV. Both models are capable of describing the Λ/K_s ratio, but fail to describe the p/π ratio.

The main point of the article is to suggest a measurement of particle ratios as a function of the total multiplicity. Earlier models predict no dependency on the multiplicity, whereas both new models predict an increase of the baryon fraction with multiplicity. This would therefore serve as an excellent probe to test the new models.

A connection between collective flow and CR has been suggested [5]. To test this for the new models, a prediction for Λ/K_s as a function of the $p_\perp$ was considered, separated into different multiplicity re-

gions. The new CR model shows similar trends as observed in heavy-ion collisions, as opposed to the string rope model where no effect is observed.

2.4.1 *My contribution*

The idea for the paper was fully conceived by Christian Bierlich (another Ph. D. student at Lund university) and me. He contributed with the string rope model and I contributed with the new CR model. We both contributed to the common phenomenological studies. I wrote the parts related to the new CR model and we both contributed equally to the common sections.

2.5 MERGING WEAK AND QCD SHOWERS WITH MULTIJET MATRIX ELEMENTS

This paper presents an inclusion of the weak parton shower into the merging framework of PYTHIA 8. The new merging scheme allows for reclusterings of $W^{\pm}$ emissions in the same manner as ordinary QCD emissions. The choice between the different paths is determined by their respective PS probabilities and the insistence on a $p_{\perp}$-ordering of the emissions. As an obvious consequence $W^{\pm}+$ jets no longer has to recluster to a Drell-Yan process, but can also originate through a QCD dijet process with a radiated $W^{\pm}$. Earlier the $W^{\pm}+$ jets configurations could lead to unordered histories, where the scale setting and Sudakov treatment could not be unambiguous determined. The new merging solve these problems.

The new merging scheme is compared to data from ATLAS and CMS and shows a significant improvement over the previous method. Especially in the high $S_{\perp}$ region, where the better scale setting and handling of Sudakov form factors lead to a lower prediction, which is in better agreement with data.

Another advantage of including the weak shower is the natural handling of weak resummation. The effects are studied at a potential future 100 TeV proton collider, which shows effect of about 30 % at jet $p_{\perp}$ scale of 20 TeV.

2.5.1 *My contribution*

The paper was a combined effort from Stefan Prestel and me. Stefan is an expert on matching and merging, and I have the knowledge on the implementation of the weak parton shower. We both contributed to the development, implementation and phenomenological studies of the new merging scheme. I wrote the first draft for sections 2, 5 and 6.

BIBLIOGRAPHY

[1] L. Carloni, J. Rathsman, and T. Sjöstrand, "Discerning Secluded Sector gauge structures," *JHEP* **04** (2011) 091, arXiv:1102.3795 [hep-ph].

[2] S. Argyropoulos and T. Sjöstrand, "Effects of color reconnection on $t\bar{t}$ final states at the LHC," *JHEP* **1411** (2014) 043, arXiv:1407.6653 [hep-ph].

[3] T. Sjöstrand and V. A. Khoze, "On Color rearrangement in hadronic W+ W- events," *Z.Phys.* **C62** (1994) 281–310, arXiv:hep-ph/9310242 [hep-ph].

[4] C. Bierlich, G. Gustafson, L. Lönnblad, and A. Tarasov, "Effects of Overlapping Strings in pp Collisions," *JHEP* **1503** (2015) 148, arXiv:1412.6259 [hep-ph].

[5] A. Ortiz Velasquez, P. Christiansen, E. Cuautle Flores, I. Maldonado Cervantes, and G. Paic, "Color Reconnection and Flowlike Patterns in *pp* Collisions," *Phys.Rev.Lett.* **111** no. 4, (2013) 042001, arXiv:1303.6326 [hep-ph].

ACKNOWLEDGEMENTS

It has been both a pleasure and a privilege to do my Ph.D studies at the theoretical high energy physics group at Lund. I hoped to work on the line between theoretical and experimental particle physics and this was exactly the opportunity I was given.

First of all I would like to thank Torbjörn Sjöstrand. No matter what question I came along with you always took the time to thoroughly answer it. You have also shown me the value of thinking things through before starting to implement them, even though I sometimes still fail to follow.

I would also like to thank Peter Skands for being my supervisor on the project I did while I was at CERN (and a slight bit there after). It was always a pleasure to discuss the more perplexing and obscure colour configuration allowed within QCD, even though I at times just seemed to get more and more confused. At the same time I would also like to thank the whole CERN theory department for the warm welcome, and especially the other Ph.D. students for making the stay that much more enjoyable.

Christian Bierlich and Stefan Prestel, the two collaborators during my Ph.D. studies, deserve my gratitude. Christian was not only a great collaborator but also a great sparring partner for any potential crazy ideas regarding CR and strings. Stefan showed me that with dedication and hard work, it is possible to get a lot done in a short amount of time.

This thesis would not have been the same without the proof reading and suggestions from Christian Bierlich, Leif Lönnblad, Johan Relefors and Torbjörn Sjöstrand.

Furthermore I would like to thank the whole theory division in Lund for their warm and open welcome. Without you this thesis would have not been the same and the time spent here not as en-

tertaining. Notably, I would like to thank my fellow Ph.D. students for all the fun during the day-to-day time and the occasional Danish "fika".

I

WEAK GAUGE BOSON RADIATION
IN PARTON SHOWERS

LU TP 14-02
MCnet-14-01
January 2014

Weak Gauge Boson Radiation in Parton Showers

Jesper R. Christiansen and Torbjörn Sjöstrand

Department of Astronomy and Theoretical Physics,
Lund University, Sölvegatan 14A,
SE-223 62 Lund, Sweden

JHEP 1404 (2014) 115

Abstract

The emission of W and Z gauge boson is included in a traditional QCD + QED shower. The unitarity of the shower algorithm links the real radiation of the weak gauge bosons to the negative weak virtual corrections. The shower evolution process leads to a competition between QCD, QED and weak radiation, and allows for W and Z boson production inside jets. Various effects on LHC physics are studied, both at low and high transverse momenta, and effects at higher-energy hadron colliders are outlined.

I.1 INTRODUCTION

The appearance of high-quality LHC data has been matched by high-quality theoretical cross section calculations. One example is $W/Z + n$ jets, where NLO cross sections are available for up to $W + 5$ jets [1]. In most of these studies the emphasis is on QCD issues, specifically all real and virtual corrections to the Born-level W/Z production graph are of a QCD nature. Separately there has been a range of studies concentrating on weak corrections to processes at lepton and hadron colliders, see [2–18] for a representative but not exhaustive selection. In this article we will concentrate on jet production at the LHC and other future hadron colliders from this latter weak point of view, i.e. study weak real and virtual corrections to QCD processes, as a complement to the QCD path. Such weak corrections grows like $\alpha_W \ln^2(E^2/m^2_{W/Z})$, where E is the energy scale of the hard process, and thus become non-negligible at high energies.

The possibility of large weak virtual corrections was highlighted by one set of calculations [9, 10], which gave a jet rate reduced by by up to 30% at around the LHC kinematical limit. This study included both $\mathcal{O}(\alpha_W)$ virtual corrections to $\mathcal{O}(\alpha_s^2)$ processes and $\mathcal{O}(\alpha_s)$ ones to $\mathcal{O}(\alpha_W\alpha_s)$ ones, however. Here we are only interested in the former, which appears to be significantly less [12], but still not negligible.

Cancellation between real and virtual corrections is familiar from QCD and QED. The appearance of soft and collinear singularities for the emission of a gluon or photon are compensated by infinitely negative virtual corrections, with only finite $\mathcal{O}(\alpha)$ terms remaining after the cancellation of infinities ($\alpha = \alpha_s$ or α_{em}, respectively). In some calculations a fictitious photon mass is used to regularize these divergences, rather then the more familiar dimensional regularization scheme, but such a mass has to be sent to zero at the end of the calculation. For weak calculations the finite physical W/Z mass guarantees finite real and virtual corrections throughout. That is, the negative $\mathcal{O}(\alpha_W \ln^2(E^2/m^2_{W/Z}))$ corrections to the two-jet rate induced by virtual W/Z loops should be compensated by the class of two-jet events with an additional real W/Z in the final state. A complication, relative to QCD and QED, is that the flavour change

of $W^{\pm}$ leads to Bloch-Nordsieck violations [5], where the real and virtual effects do not fully cancel.

The finite mass also means that classes of events with or without a W/Z are completely separated. This is not only an advantage. Consider, for instance, how the character of a high-energy quark jet is changed by the possibility of W/Z emissions in addition to the conventional g/γ ones. Recall that high-$p_\perp$ jets at the LHC easily can acquire masses around or above the W/Z mass already by g radiation. A W/Z produced inside a jet and decaying hadronically may then be rather difficult to distinguish from QCD emissions. It is therefore natural to consider strong, electromagnetic and weak emissions in one common framework when confronting data.

Traditionally there exists two possible approaches to describe multiple emissions: matrix elements (ME) and parton showers (PS). Formally ME is the correct way to go, but that presupposes that it is possible to calculate both real and virtual corrections to high orders. If not, the ME approach breaks down in the divergent soft and collinear limits. Here the PS approach is more sensible, since it includes Sudakov form factors to restore unitarity. In recent years a main activity has been to combine the ME and PS approaches to achieve the best overall precision [19].

Up until now, showers have only included QCD and QED emissions, and W/Z production has been viewed solely as a task for the ME part of the overall description. In this article we extend the showering machinery to contain also the emission of the W and Z gauge bosons, on equal footing with QCD and QED emissions. This has some advantages for high-$p_\perp$ jets, precisely where W/Z decay products may be hidden in the core, among other quarks and gluons. The shower formalism directly couples the real emissions to the virtual corrections, by Sudakov factors. It thereby becomes straightforward to study residual non-cancellation of real and virtual corrections as a function of jet selection criteria. Another advantage is that multiple emission of W/Z bosons is a natural part of the formalism, even if this only becomes important at very high jet energies. In the other extreme, the shower mechanism may also be relevant for the production of W/Z plus multijets at lower $p_\perp$ scales, both as a test of the shower approach as such and as a building block for merging/matching approaches.

The development of a weak shower formalism faces several challenges. One such is the W/Z masses, that induce both kinematical and dynamical complications. These will mainly be overcome by matching to several relevant ME expressions, thereby guaranteeing improved precision relative to a PS-only based description.

The new showers are implemented as parts of the Pythia 8 event generator [20, 21]. Thereby they can be combined with the existing QCD and QED shower implementations, and with all other aspects of the complete structure of hadron-collider events. This allows us to study the consequences at LHC for W/Z production in general, and for the structure of high-$p_\perp$ jets in particular.

In Section 2 we develop the shower formalism needed for W and Z bosons, including several new aspects. This formalism is validated in Section 3. In Section 4 it is then applied to study consequences for jets and W/Z production at the LHC. A brief outlook towards results for even higher-energy colliders is found in Section 5. Finally Section 6 provides a summary and outlook.

I.2 The Weak Shower

In this section we describe how the production of $\mathrm{W/Z} + n$ jets is handled. To be more precise, the bulk of the study will be concerned with $n \geq 2$, i.e. from where production of W/Z inside a jet becomes possible. The $n = 0, 1$ processes do not have a direct overlap with QCD jets, and an existing shower formalism is appropriate to handle them, as will be described further below.

In principle, the introduction of W/Z emission in showers would only involve the introduction of two new splitting kernels. In practice, the large W/Z masses lead to large corrections, both in the kinematics handling and in the splitting behaviour. In order to provide a reasonably accurate description, within the limits of the shower approach, several matrix elements are used as templates to provide a correct dependence on the W/Z masses.

Also other problems will appear, that are new relative to the already existing QCD/QED formalism, notably that the weak force has spin-dependent couplings and that the emission of a W boson changes the flavour of the radiating quark. Further, a complete description would need to include full γ^*/Z^0 interference, but in the

following these interference terms will be neglected. That is, for low virtualities a pure γ^* is assumed, and for higher virtualities a pure Z^0. This should be a good first approximation, since the bulk of the shower activity should be in the two peak regions.

I.2.1 *The basic shower formalism*

The starting point for shower evolution is the DGLAP evolution equation, which can be written as

$$\mathrm{d}\mathcal{P}_{a\to bc} = \frac{\alpha}{2\pi}\,\frac{\mathrm{d}Q^2}{Q^2}\,P_{a\to bc}(z)\;, \tag{I.2.1}$$

with $\alpha = \alpha_\mathrm{s}$ or α_em, Q^2 some evolution variable expressing the hardness of the $a \to bc$ branching and z the energy-momentum sharing between the daughters b and c. Some further azimuthal φ dependence may or may not be included. The branchings can be of the character $\mathrm{q} \to \mathrm{qg}$, $\mathrm{g} \to \mathrm{gg}$, $\mathrm{g} \to \mathrm{q\bar{q}}$, $\mathrm{f} \to \mathrm{f}\gamma$ ($\mathrm{f} = \mathrm{q}$ or ℓ), and $\gamma \to \mathrm{f\bar{f}}$. To this list we now want to add $\mathrm{q} \to \mathrm{q'W}$ and $\mathrm{q} \to \mathrm{qZ^0}$, including subsequent decays $\mathrm{W} \to \mathrm{f\bar{f}'}$ and $\mathrm{Z} \to \mathrm{f\bar{f}}$. The W/Z production mechanism is directly comparable with that of g/γ, whereas the decays happen with unit probability and therefore are slightly separated in character from the corresponding $\mathrm{g} \to \mathrm{q\bar{q}}$ and $\gamma \to \mathrm{f\bar{f}}$ ones. The difference obviously is related to the W/Z being massive and the g/γ ones massless.

To set the coupling notation, consider the case that the W/Z masses are set to zero. Then the evolution equations for a quark can be written in a common form

$$\begin{aligned}
\mathrm{d}\mathcal{P}_{\mathrm{q}\to\mathrm{q}X} &= \frac{\alpha_{\mathrm{eff}}}{2\pi}\frac{\mathrm{d}Q^2}{Q^2}\frac{1+z^2}{1-z}\,, && \text{(I.2.2)}\\
\alpha_{\mathrm{eff}} &= \alpha_{\mathrm{s}}\frac{4}{3} \;\text{ for }\; \mathrm{q}\to\mathrm{qg}\,, && \text{(I.2.3)}\\
&= \alpha_{\mathrm{em}}\, e_{\mathrm{q}}^2 \;\text{ for }\; \mathrm{q}\to\mathrm{q}\gamma\,, && \text{(I.2.4)}\\
&= \frac{\alpha_{\mathrm{em}}}{\sin^2\theta_W\cos^2\theta_W}\,(T_{\mathrm{q}}^3 - e_{\mathrm{q}}\sin^2\theta_W)^2 \;\text{ for }\; \mathrm{q}_L\to\mathrm{q}_L\mathrm{Z}\,, && \text{(I.2.5)}\\
&= \frac{\alpha_{\mathrm{em}}}{\sin^2\theta_W\cos^2\theta_W}\,(e_{\mathrm{q}}\sin^2\theta_W)^2 \;\text{ for }\; \mathrm{q}_R\to\mathrm{q}_R\mathrm{Z}\,, && \text{(I.2.6)}\\
&= \frac{\alpha_{\mathrm{em}}}{2\sin^2\theta_W}\,|V_{\mathrm{qq}'}^{\mathrm{CKM}}|^2 \;\text{ for }\; \mathrm{q}_L\to\mathrm{q}'_L\mathrm{W}\,, && \text{(I.2.7)}\\
&= 0 \;\text{ for }\; \mathrm{q}_R\to\mathrm{q}'_R\mathrm{W}\,. && \text{(I.2.8)}
\end{aligned}$$

Here L/R denotes left-/right-handed quarks, $T_{\mathrm{q}}^3 = \pm 1/2$ for up/down-type quarks, and V^{CKM} is the CKM quark mixing matrix.

It will be assumed that the incoming beams are unpolarized, i.e. that incoming fermions equally often are left- as righthanded. Since QCD interactions are spin-independent, a left- or righthanded helicity is picked at random for each separate fermion line at the hard interaction. (Usually this association is unique, but in cases like uu $\to$ uu a choice is made that favours a small scattering angle, using $1/\hat{t}^2$ and $1/\hat{u}^2$ as relative weights.) Since the gauge-boson emissions preserve helicity (for massless fermions), the choice at the hard process is propagated through the full shower evolution. The emission rate for a single W/Z boson is not affected by this helicity conservation, relative to what spin-averaged splitting kernels would have given, but the rate of several W/Z bosons is increased. This is most easily realized for the W case, where a first emission fixes the fermion line to be lefthanded, and a second W therefore can be emitted twice as often as with a spin-averaged branching kernel.

The formalism for FSR and ISR, for the case of massless gauge bosons, is outlined in [22]. A brief summary is as follows, for the case that on-shell masses can be neglected.

For FSR the evolution variable for branchings $a \to bc$ is $\mathrm{p}^2_{\perp\mathrm{evol}} = z(1-z)Q^2$ where Q^2 is the off-shell (timelike) virtuality of parton a. The evolution equation becomes

$$\mathrm{d}\mathcal{P}_a = \frac{\alpha(\mathrm{p}^2_{\perp\mathrm{evol}})}{2\pi}\,\frac{\mathrm{d}\mathrm{p}^2_{\perp\mathrm{evol}}}{\mathrm{p}^2_{\perp\mathrm{evol}}}\,P_{a\to bc}(z)\,\Delta_a(p^2_{\perp\mathrm{max}},\mathrm{p}^2_{\perp\mathrm{evol}})\,, \qquad \text{(I.2.9)}$$

where Δ_a is the Sudakov form factor, i.e. the no-emission probability from the initial maximal scale $p^2_{\perp\mathrm{max}}$ down to the current $\mathrm{p}^2_{\perp\mathrm{evol}}$ one [19]. It is obtained from an exponentiation of the real-emission probability in such a way that unitarity is restored: the total probability for parton a to branch, or to reach a lower cutoff scale $p^2_{\perp\mathrm{min}}$ without branching, adds to unity. A dipole shower [23] approach is used to set the kinematics of a branching. That is, for a QCD shower, colour is traced in the $N_C \to \infty$ limit, and thus the radiating parton a can be associated with a "recoiler" r that carries the opposite colour. A gluon is split into two possible contributions by its colour and anticolour, both as a radiator and as a recoiler. The $a + r$ system preserves its four-momentum in a branching and, if viewed in its rest frame, the a and r three-momenta are scaled down without a change in direction to give a the mass Q. In this frame z $(1-z)$ is the fraction of the modified a energy that b (c) takes.

For ISR it is most convenient to use backwards evolution [24], i.e. to start at the hard interaction and then proceed towards earlier branchings at lower evolution scales. That is, the $a \to bc$ branching process is now interpreted as parton b becoming "unbranched" into a. Parton b has a spacelike virtuality with absolute value Q^2, and the evolution variable is $\mathrm{p}^2_{\perp\mathrm{evol}} = (1-z)Q^2$. The evolution equation now depends on PDF ratios

$$\mathrm{d}\mathcal{P}_b = \frac{\alpha(\mathrm{p}^2_{\perp\mathrm{evol}})}{2\pi}\,\frac{\mathrm{d}\mathrm{p}^2_{\perp\mathrm{evol}}}{\mathrm{p}^2_{\perp\mathrm{evol}}}\,\frac{x_a f_a(x_a,\mathrm{p}^2_{\perp\mathrm{evol}})}{x_b f_b(x_b,\mathrm{p}^2_{\perp\mathrm{evol}})}\,P_{a\to bc}(z)\,\Delta_b(p^2_{\perp\mathrm{max}},\mathrm{p}^2_{\perp\mathrm{evol}};x_b)\,, \qquad \text{(I.2.10)}$$

where again the Sudakov form factor is obtained by an exponentiation of the real-emission expression, to preserve unitarity. The parton coming in from the other side of the event defines a recoiler r, such that $z = x_b/x_a = (p_b + p_r)^2/(p_a + p_r)^2$. With b originally

moving parallel with the incoming beam particle with a fraction x_b of the beam momentum, the branching requires a redefinition of kinematics such that afterwards parton a is parallel with the beam and carries a fraction x_a. Accordingly, all the outgoing partons produced by the $b + r$ collision are boosted and rotated to a new frame.

Both ISR and FSR are evolved downwards in $p^2_{\perp\mathrm{evol}}$, starting from a $p^2_{\perp\mathrm{max}}$ scale typically set by the hard interaction at the core of the event. A branching at a given scale sets the maximum for the continued evolution. At each step all the partons that potentially could branch must be included in the sum of possibilities. There are always two incoming partons that can radiate, while the number of outgoing ones increases as the evolution proceeds.

A third component of perturbative parton production is multiparton interactions (MPI). These can also conveniently be arranged in a falling $p_\perp$ sequence, and by unitarity acquires a "Sudakov" factor in close analogy with that in showers [25]. Therefore both ISR, FSR and MPI can be combined in one common sequence of falling $p_\perp$ scales [26]:

$$\begin{aligned}\frac{\mathrm{d}\mathcal{P}}{\mathrm{d}p_\perp} &= \left(\frac{\mathrm{d}\mathcal{P}_{\mathrm{MPI}}}{\mathrm{d}p_\perp} + \sum \frac{\mathrm{d}\mathcal{P}_{\mathrm{ISR}}}{\mathrm{d}p_\perp} + \sum \frac{\mathrm{d}\mathcal{P}_{\mathrm{FSR}}}{\mathrm{d}p_\perp}\right) \\ &\times \exp\left(-\int_{p_\perp}^{p_{\perp\mathrm{max}}} \left(\frac{\mathrm{d}\mathcal{P}_{\mathrm{MPI}}}{\mathrm{d}p'_\perp} + \sum \frac{\mathrm{d}\mathcal{P}_{\mathrm{ISR}}}{\mathrm{d}p'_\perp} + \sum \frac{\mathrm{d}\mathcal{P}_{\mathrm{FSR}}}{\mathrm{d}p'_\perp}\right) \mathrm{d}p'_\perp\right) ,\end{aligned} \tag{I.2.11}$$

with a combined Sudakov factor. Each MPI gives further incoming and outgoing partons that can radiate, so the ISR and FSR sums now both run over an increasing number of potentially radiating partons. The decreasing $p_\perp$ scale can be viewed as an evolution towards increasing resolving power; given that the event has a particular structure when activity above some $p_\perp$ scale is resolved, how might that picture change when the resolution cutoff is reduced by some infinitesimal $\mathrm{d}p_\perp$? That is, let the "harder" features of the event set the pattern to which "softer" features have to adapt. Specifically, energy–momentum conservation effects can be handled in a reasonably consistent manner, where the hardest steps almost follow the standard rules, whereas soft activity is reduced by the competition for energy, mainly between ISR and MPI.

For massless particles only kinematics variables such as $p_\perp$ can set the scale. For weak showers the W/Z mass introduces an alternative scale, and this opens up for ambiguities. Consider if a combination such as $p^2_{\perp\text{evol}} + km^2_{W/Z}$, with k as a free parameter, is used as ordering variable for W/Z emission (but otherwise not affecting kinematics). Then an increased k will shift W/Z emissions to occur earlier in the combined evolution, which gives them a competitive advantage relative to QCD/QED emissions. We will later study the impact of such possible choices.

A key feature for the efficient generator implementation is that the real and virtual corrections exactly balance, i.e. that eq. (I.2.11) contains exactly the same $d\mathcal{P}$ expressions in the prefactor and in the Sudakov factor. This holds for QCD and QED emissions to leading-log accuracy, and also for Z^0 ones, but not for $W^\pm$ emissions, due to the above-mentioned Bloch-Nordsieck violations. It comes about by a combination of two facts. Firstly, a real emission of a $W^\pm$ in the initial state changes the flavour of the hard process, while a $W^\pm$ loop does not. Secondly, the incoming state is not isospin invariant, i.e. the proton is not symmetric between u and d quarks, nor between other isospin doublets. Together this leads to a mismatch between real and virtual Sudakov logarithms, that is not reproduced in our implementation. In that sense our results on the reduced rate of events without a W emission are not trustworthy. But only the $qq' \to qq'$ processes with both quarks lefthanded are affected, not ones where either quark is righthanded, nor $qg \to qg$ processes [6]. Also, real and virtual corrections cancel for final-state emissions, so only initial-state ones contribute. The total error we make on this count therefore is small, in particular compared with true NLO corrections beyond our accuracy.

I.2.2 *Merging generics*

One of the key techniques that will be used in the following is matrix-element merging [27–29]. It can be viewed as a precursor to PowHeg [30, 31].

In a nutshell the philosophy is the following. Assume a Born cross section σ_B, usually differential in a number of kinematical variables that we do not enumerate here. The real NLO correction to

this is $\mathrm{d}\sigma_R$, differential in three further kinematical variables, with ratio $\mathrm{d}K_{ME} = \mathrm{d}\sigma_R/\sigma_B$. The parton-shower approximation also starts from σ_B and multiplies this with $\mathrm{d}K_{PS}$, which represents the shower branching kernel, cf. eq. (I.2.1), summed over all possible shower branchings from the Born state, differential in Q^2, z and φ. At this stage the Sudakov form factor has not yet been introduced. Now ensure that $\mathrm{d}K_{PS} \geq \mathrm{d}K_{ME}$ over all of phase space, which may be automatic or require some adjustment, e.g. by a multiplicative factor. Then begin the evolution of the shower from a starting scale Q^2_{max} downwards, with a first (= "hardest") branching at a Q^2 distributed according to

$$\mathrm{d}K_{PS}(Q^2, z, \varphi) \exp\left(- \int_{Q^2}^{Q^2_{max}} \mathrm{d}Q^2 \int \mathrm{d}z \int \frac{\mathrm{d}\varphi}{2\pi} \mathrm{d}K_{PS}(Q^2, z, \varphi) \right) . \tag{I.2.12}$$

Since $\mathrm{d}K_{PS}$ is an overestimate, accept a branching with a probability $\mathrm{d}K_{ME}/\mathrm{d}K_{PS}$. This replaces the $\mathrm{d}K_{PS}$ prefactor in eq. (I.2.12) by $\mathrm{d}K_{ME}$, but leaves the Sudakov unchanged. Now use the veto algorithm trick: when a Q^2 scale is not accepted, set $Q^2_{max} = Q^2$ and continue the evolution down from this new maximal scale. This gives a distribution

$$\mathrm{d}K_{ME}(Q^2, z, \varphi) \exp\left(- \int_{Q^2}^{Q^2_{max}} \mathrm{d}Q^2 \int \mathrm{d}z \int \frac{\mathrm{d}\varphi}{2\pi} \mathrm{d}K_{ME}(Q^2, z, \varphi) \right) \tag{I.2.13}$$

(for proof see e.g. [21]). Here the dependence on the original $\mathrm{d}K_{PS}$ is gone, except that the shower Q^2 definition is used to set the order in which the phase space is sampled. The soft and collinear divergences leads to eqs. (I.2.12) and (I.2.13) being normalized exactly to unity; a first emission is always found. In practice a lower cutoff Q^2_{min} is always introduced; if the evolution falls below this scale then an event of the Born character is assumed. This preserves unitarity.

This completes the description of ME merging. In PowHeg the hardness scale is not based on any specific shower, but fills a similar function. More importantly, to achieve full NLO accuracy,

PowHeg normalizes the differential cross section in eq. (I.2.13) to $\sigma_B + \sigma_V + \int d\sigma_R$, where σ_V are the virtual corrections, including PDF counterterms. We will not here aim for a corresponding NLO accuracy, but keep open the possibility to multiply by an overall "K factor", which catches the bulk of the NLO effects.

A simple application of ME merging is $W/Z + 1$ jet, starting from the Born W/Z production process [29]. The $q\bar{q} \to Zg$ (or $q\bar{q}' \to Wg$) final state can be reached by two shower emission histories, which match the t- and u-channel Feynman graphs of the matrix elements. It is found that $1/2 < dK_{ME}/dK_{PS} \leq 1$, so that Monte Carlo rejection is straightforward. (The original result was found for an evolution in virtuality rather than in $p_\perp^2$, but both give the same result since $dQ^2/Q^2 = dp_\perp^2/p_\perp^2$ and z is the same.) The $qg \to Zq$ (or $qg \to Wq'$) process has one shower history, with a $g \to q\bar{q}$ branching, that corresponds to the u-channel Feynman diagram, while the s-channel quark exchange diagram has no shower correspondence. In this case $1 \leq dK_{ME}/dK_{PS} \leq (\sqrt{5}-1)/(2(\sqrt{5}-2)) < 3$, which requires the shower emission rate to be artificially enhanced for Monte Carlo rejection to work. For both processes agreement is found in the $p_\perp \to 0$ limit, as it should, with increasing discrepancies at larger $p_\perp$, but still only by a modest factor right up to the kinematical limit.

It is plausible that the (uncorrected) PS underestimate of the $qg \to Zq$ emission rate at least partly is related to it missing one Feynman graph. If so, the shower description of $W/Z+ \geq 2$ partons can be expected to do even worse, since it misses out on further diagrams. This is the behaviour observed in data [32–34]. By starting up from QCD $2 \to 2$ processes as well, but avoiding doublecounting, it is the hope to bring up this rate.

Given that the ME merging approach has been used to select the hardest emission, a normal shower can be attached for subsequent emissions from this scale downwards. Normally these emissions would be based on the shower algorithm pure and simple. In some cases it may be convenient to use the merging approach also for subsequent emissions, notably for massive particles in the final state, where the suppression of collinear radiation may not be fully described by the shower [28, 35]. Although the ME is not the correct one for consecutive emissions, it still encodes the suppression

from mass terms to a reasonable approximation, at least as well as a shower could. The one modification is to apply it to changed kinematical conditions, e.g. to a gradually decreasing dipole mass for FSR. We will come back to this point.

I.2.3 *Pure final-state emissions*

As a starting point for FSR we consider the simplest possible case, when a Z or W is radiated in the final state of an *s*-channel process such as $q_0\overline{q}_0 \to g^*(0) \to q\overline{q} \to q(1)\,\overline{q}(2)\,Z^0(3)$ (or $q_0\overline{q}_0 \to g^*(0) \to q(1)\,\overline{q}'(2)\,W(3)$). Using CalcHEP [36] for these and subsequent ME calculations, the matrix element can be written as

$$\frac{1}{\sigma_0}\frac{d\sigma}{dx_1\,dx_2} = \frac{\alpha_{\text{eff}}}{2\pi}\left(\frac{x_1^2+x_2^2+2r_3(x_1+x_2)+2r_3^2}{(1-x_1)(1-x_2)} - \frac{r_3}{(1-x_1)^2} - \frac{r_3}{(1-x_2)^2}\right) . \tag{I.2.14}$$

Here $x_i = 2p_0p_i/p_0^2 = 2E_i/E_{\text{cm}}$, with the latter expression valid in the rest frame of the process, and $r_i = m_i^2/E_{\text{cm}}^2$, here with the quarks assumed massless. In order to arrive at the above result, the ME was integrated over three angular variables. Setting $r_3 = 0$ the kinematics dependence reverts to the familiar one for three-jet events in e^+e^- annihilation, as it should. The α_{eff} values are provided in eqs. (I.2.5)–(I.2.8).

Owing to the W/Z mass, the phase space for a weak emission is considerably different from that of a QCD one. Notably the soft and collinear divergences lie outside the physical region. Within the accessed region we would like to use the matrix-element merging approach to achieve as accurate a description as possible. As a first step, an overestimate is obtained by

$$\frac{1}{\sigma_0}\frac{d\sigma}{dx_1\,dx_2} \le \frac{\alpha_{\text{eff}}}{2\pi}\frac{N}{(1-x_1)(1-x_2)} , \tag{I.2.15}$$

with $N = 8$. This translates into an overestimate

$$d\mathcal{P}^{\text{over}}_{q\to qZ} = \frac{\alpha_{\text{eff}}}{2\pi}\frac{dp^2_{\perp\text{evol}}}{p^2_{\perp\text{evol}}}\frac{N}{1-z} , \tag{I.2.16}$$

which later is to be corrected.

The emission of heavy bosons in final state radiation has already been considered in the context of massive Hidden-Valley photons [35], and therefore only a short review is provided here. Consider the process $p_0 \to p_{13} + p_2 \to p_1 + p_2 + p_3$, where all particles are allowed to be massive. While the matrix elements are described by x_1 and x_2 (after a suitable integration over angles), the parton shower is described in terms of

$$\mathrm{p}^2_{\perp\mathrm{evol}} = z(1-z)(m_{13}^2 - m_1^2) \tag{I.2.17}$$

and z, which in the massless limit equals $x_1/(x_1+x_3)$. For a massive case it is convenient to start out from two massless four-vectors $p_1^{(0)}, p_3^{(0)}$ and then create the massive ones as linear combinations

$$\begin{aligned} p_1 &= (1-k_1)p_1^{(0)} + k_3 p_3^{(0)} \,, & \text{(I.2.18)}\\ p_3 &= (1-k_3)p_3^{(0)} + k_1 p_1^{(0)} \,, & \text{(I.2.19)}\\ k_{1,3} &= \frac{m_{13}^2 - \lambda_{13} \pm (m_3^3 - m_1^2)}{2m_{13}^2} \,, & \text{(I.2.20)}\\ \lambda_{13} &= \sqrt{(m_{13}^2 - m_1^2 - m_3^2)^2 - 4m_1^2 m_3^2} \,. & \text{(I.2.21)} \end{aligned}$$

This new energy sharing corresponds to a rescaled

$$z = \frac{1}{1-k_1-k_3}\left(\frac{x_1}{2-x_2} - k_3\right) \,. \tag{I.2.22}$$

The $\mathrm{p}^2_{\perp\mathrm{evol}}$ and z expressions, can be combined to give the Jacobian

$$\frac{\mathrm{d}\mathrm{p}^2_{\perp\mathrm{evol}}}{\mathrm{p}^2_{\perp\mathrm{evol}}}\,\frac{\mathrm{d}z}{1-z} = \frac{\mathrm{d}x_2}{1-x_2+r_2-r_1}\,\frac{\mathrm{d}x_1}{x_3 - k_1(x_1+x_3)} \,. \tag{I.2.23}$$

Note that the shower expressions so far only referred to emissions from the $\mathrm{q}(1)$, whereas the matrix elements also include emissions from the $\overline{\mathrm{q}}(2)$ and interferences. For a ME/PS comparison it is therefore necessary either to sum the two PS possibilities or split

the ME expression. We choose the latter, with a split in proportion to the propagators, which gives a probability for the $q(1)$

$$P_1 = \frac{(m_{13}^2 - m_1^2)^{-1}}{(m_{13}^2 - m_1^2)^{-1} + (m_{23}^2 - m_2^2)^{-1}} = \frac{1 - x_1 + r_1 - r_2}{x_3} \,. \quad \text{(I.2.24)}$$

Thus we arrive at the ME/PS correction factor

$$\begin{aligned} W_1 = \frac{W_{ME,1}}{W_{PS,1}} &= \frac{(1 - x_1 + r_1 - r_2)(1 - x_2 + r_2 - r_1)}{N} \\ &\times \frac{x_3 - k_1(x_1 + x_3)}{x_3} \frac{1}{\sigma_0} \frac{\mathrm{d}\sigma}{\mathrm{d}x_1 \, \mathrm{d}x_2} \,. \end{aligned} \quad \text{(I.2.25)}$$

All the explicit dependence on m_3 is located in k_1 in the last factor, but obviously implicitly the whole kinematics setup is affected by the value of m_3.

The emission of W bosons introduces flavour changes in the shower, and thus also the need for implementing the full CKM-matrix in the emissions, eq. (I.2.7). The change of flavour to top is excluded due to the high mass of the top quark, which significantly reduces W emission off b quarks. All quarks are considered massless in the ME weights, but proper masses are included in the kinematics calculations, as demonstrated above.

The ME merging technique, viewed as a correction to the LO expression, is properly valid only for the first branching. The arguments for including a sensible behaviour in the soft and collinear regions remain, however. Therefore eq. (I.2.25) can be applied at all steps of the shower evolution. That is, starting from an original $q\overline{q}$ dipole, the downwards evolution in $p_{\perp\mathrm{evol}}^2$ gradually reduces the dipole mass by the $g/\gamma/W/Z$ emissions. When a W/Z is emitted, the ME correction is based on the current dipole mass and the emission kinematics. This is particularly relevant since it may be quite common with one or a few QCD emissions before a W/Z is emitted.

In non-Abelian theories the radiated gauge bosons themselves carry charge and can themselves radiate. For QCD emissions this is well approximated by the dipole picture, where each emission of a further gluon leads to the creation of a new dipole. Similarly the emission of a W/Z leads to more weak charges, with the possibility

of non-Abelian branchings $W^{\pm} \to W^{\pm}Z^0$ and $Z^0 \to W^+W^-$. So far we have not included these further branchings, and therefore preserve the original $q\bar{q}$ weak-dipole when a W/Z is emitted. This will imply some underestimation of multiple-W/Z production rate.

New $q\bar{q}$ pairs can be created within the shower evolution, e.g. by gluon branchings $g \to q\bar{q}$. These are considered as new weak dipoles, and can thus enhance the rate of W/Z emissions.

I.2.4 *Pure initial-state emissions*

As a starting point for ISR we here instead consider a process such as $q(1)\,\bar{q}(2) \to Z(3)\,g^*(4)$ (or $q(1)\,\bar{q}'(2) \to W(3)\,g^*(4)$), where the subsequent $g^* \to q_0\bar{q}_0$ (or $g^* \to gg$) decay has been integrated out. This matrix element can then be written as

$$W_{\mathrm{ME}} = \frac{\hat{s}}{\hat{\sigma}_0}\frac{\mathrm{d}\hat{\sigma}}{\mathrm{d}\hat{t}} = \frac{\alpha_{\mathrm{eff}}}{2\pi}\left(\frac{\hat{t}^2+\hat{u}^2+2\hat{s}(m_3^2+m_4^2)}{\hat{t}\hat{u}} - \frac{m_3^2 m_4^2}{\hat{t}^2} - \frac{m_3^2 m_4^2}{\hat{u}^2}\right). \tag{I.2.26}$$

The ISR kinematics is already set up to handle the emission of a massive particle, e.g. in $b \to gb$, with a b quark in the final state. The ME correction machinery [29] has only been set up for the emission of a massless particle, however, so some slight changes are necessary. For the case that the W/Z is emitted by the incoming parton 1 the Mandelstam variables become

$$\hat{s} = (p_1+p_2)^2 = \frac{m_4^2}{z}\,, \tag{I.2.27}$$

$$\hat{t} = (p_1-p_3)^2 = -Q^2 = -\frac{p_{\perp\mathrm{evol}}^2}{1-z}\,, \tag{I.2.28}$$

$$\hat{u} = m_3^2+m_4^2-\hat{s}-\hat{t} = m_3^2+m_4^2-\frac{m_4^2}{z}+\frac{p_{\perp\mathrm{evol}}^2}{1-z}\,. \tag{I.2.29}$$

It turns out that the massless DGLAP-kernel eq. (I.2.2) is not an overestimate for the ME eq. (I.2.26). Instead the following slightly modified splitting kernel is used

$$\mathrm{d}\mathcal{P}_{q\to qX} = \frac{\alpha_{\mathrm{eff}}}{2\pi}\frac{\mathrm{d}Q^2}{Q^2}\frac{1+z^2(1+r^2)^2}{1-z(1+r^2)} \tag{I.2.30}$$

where $r = m_3/m_{\text{dipole}} = m_3/m_4$. The standard DGLAP kernel is recovered in the massless limit. Using the Jacobian $\mathrm{d}\hat{t}/\hat{t} = \mathrm{d}p^2_{\perp\text{evol}}/p^2_{\perp\text{evol}}$, the shower emission rate translates to

$$W_{\text{PS1}} = \frac{\hat{s}}{\hat{\sigma}_0}\frac{\mathrm{d}\hat{\sigma}}{\mathrm{d}\hat{t}} = \frac{\alpha_{\text{eff}}}{2\pi}\frac{\hat{s}^2 + (m_3^2 + m_4^2)^2}{\hat{t}(\hat{t} + \hat{u})} \,. \tag{I.2.31}$$

Adding the emission from parton 2, easily obtained by $\hat{t} \leftrightarrow \hat{u}$, gives

$$W_{\text{PS}} = W_{\text{PS1}} + W_{\text{PS2}} = \frac{\alpha_{\text{eff}}}{2\pi}\frac{\hat{s}^2 + (m_3^2 + m_4^2)^2}{\hat{t}\hat{u}} \,. \tag{I.2.32}$$

In this case it is convenient to use $W = W_{\text{ME}}/W_{\text{PS}}$ as ME correction factor. That is, the full ME is compared with the sum of the two PS possibilities, unlike the FSR case, where the ME is more easily split into two parts each compared with a single shower history.

It can most easily be seen that the modified DGLAP kernel is an upper estimate by taking the ratio of the PS weight with the ME one,

$$W = \frac{W_{\text{ME}}}{W_{\text{PS}}} \leq \frac{\hat{t}^2 + \hat{u}^2 + 2\hat{s}(m_3^2 + m_4^2)}{\hat{s}^2 + (m_3^2 + m_4^2)^2} \tag{I.2.33}$$

$$= \frac{\hat{t}^2 + \hat{u}^2 + 2\hat{s}^2 + 2\hat{s}\hat{t} + 2\hat{s}\hat{u}}{\hat{t}^2 + \hat{u}^2 + 2\hat{s}^2 + 2\hat{s}\hat{t} + 2\hat{s}\hat{u} + 2\hat{t}\hat{u}} \leq 1 \tag{I.2.34}$$

A new upper estimate for the range of allowed z values is needed, since the standard one enters unphysical regions of the modified DGLAP kernel, turning the PS weight negative. This is not a surprise, since the standard upper estimate does not include massive emissions. The upper estimate chosen is

$$z \leq \frac{1}{1 + r^2 + \frac{p^2_{\perp\text{evol}}}{m^2_{\text{dipole}}}} \tag{I.2.35}$$

This limit should ensure that the emitted particle will always have enough energy to become massive and have the chosen $p^2_{\perp\text{evol}}$. It is not formally proven to be an upper limit, but works for all studied cases.

The handling of CKM weights for W emission becomes slightly more complicated in ISR than in FSR, owing to the presence of PDFs in the evolution. The PDF ratio in eq. (I.2.10) is generalized to an upper estimate

$$R^{\mathrm{PDF}}_{\mathrm{max}} = \frac{\sum_a |V^{\mathrm{CKM}}_{ab}|^2 \, x_b f_a(x_b, p^2_{\perp \mathrm{max}})}{x_b f_b(x_b, p^2_{\perp \mathrm{max}})} \tag{I.2.36}$$

used in the downwards evolution with the veto algorithm. For a trial emission the relevant part of the acceptance weight then becomes

$$\frac{1}{R^{\mathrm{PDF}}_{\mathrm{max}}} \frac{\sum_a |V^{\mathrm{CKM}}_{ab}|^2 \, x_a f_a(x_a, \mathrm{p}^2_{\perp \mathrm{evol}})}{x_b f_b(x_b, \mathrm{p}^2_{\perp \mathrm{evol}})} \, . \tag{I.2.37}$$

Once a branching has been accepted, the new mother flavour a is selected in proportion to the terms in the numerator sum.

Like for final-state radiation, the ME merging weight will be used not only for a W/Z emission in direct association with the hard process, but for all branchings in the backwards evolution. All final-state particles are then lumped into one single effective particle, like the g^* above.

I.2.5 *Mixed initial–final-state emissions*

In addition to the pure-final or pure-initial topologies, the two other relevant possibilities are with one or two quark lines flowing through the hard $2 \to 2$ topologies, i.e. $\mathrm{qg} \to \mathrm{qg}$ and $\mathrm{qq}' \to \mathrm{qq}'$.

It would have been tempting to use the ME correction factors as above for FSR and ISR. Unfortunately this does not give a particularly good agreement with the $\mathrm{qg} \to \mathrm{qgZ}^0$ matrix element. Specifically, whereas s-channel processes tend to populate the available phase space with only a $\mathrm{d}p^2_\perp / p^2_\perp$ fall-off, the coherence between ISR and FSR in t-channel processes leads to a destructive interference that reduces emissions at large angles [37]. Thus emission rates depend on the $\hat{t}$ of the core $2 \to 2$ process, not only on its $\hat{s}$. Therefore we have chosen to base the ME corrections on the full $2 \to 3$ kinematics.

The general strategy will be to use that the three-body phase space can be split into two two-body ones, with an intermediate state i, e.g.

$$\mathrm{d}\Phi_3(1+2+3) = \mathrm{d}\Phi_2(1+i)\,\frac{\mathrm{d}m_i^2}{2\pi}\,\mathrm{d}\Phi_2(i\to 2+3)\,. \qquad \text{(I.2.38)}$$

One of the $\mathrm{d}\Phi_2$ factors will be associated with the QCD hard $2\to 2$ process, whereas the rest comes from the shower branching. This way it is possible to compare the $2\to 3$ ME with the $2\to 2$ ME + shower in the same phase space point, with proper Jacobians.

To begin with, consider the simpler first process, $\mathrm{qg}\to\mathrm{qg}$, with an additional Z^0 emission, labeled as $\mathrm{q}(a)\,\mathrm{g}(b)\to\mathrm{q}(1)\,\mathrm{g}(2)\,\mathrm{Z}^0(3)$. We will first outline the procedures for FSR and ISR separately, and then explain how to combine the two, and how to modify for $\mathrm{W}^\pm$ emission.

For FSR the intermediate state is the virtual quark that emits the Z^0, $\mathrm{q}(a)\,\mathrm{g}(b)\to\mathrm{q}^*(i)\,\mathrm{g}(2)\to\mathrm{q}(1)\,\mathrm{g}(2)\,\mathrm{Z}^0(3)$, which gives the phase space separation

$$\mathrm{d}\Phi_3(a+b\to 1+2+3) = \mathrm{d}\Phi_2(a+b\to i+2)\,\frac{\mathrm{d}m_i^2}{2\pi}\,\mathrm{d}\Phi_2(i\to 1+3)\,. \qquad \text{(I.2.39)}$$

Rewriting the second $\mathrm{d}\Phi_2$ in terms of angles in the i rest frame, the $2\to 3$ ME can be expressed as

$$\mathrm{d}\sigma_{\mathrm{ME}} = \frac{|M_{2\to 3}|^2}{2\hat{s}}\,\mathrm{d}\Phi_3 = \frac{|M_{2\to 3}|^2}{2\hat{s}}\,\mathrm{d}\Phi_2(i+2)\,\frac{\mathrm{d}m_i^2}{2\pi}\,\frac{\beta_{13}}{4}\,\mathrm{d}(\cos\theta^*)\,\frac{\mathrm{d}\varphi^*}{2\pi}\,, \qquad \text{(I.2.40)}$$

with

$$\beta_{jk} = \sqrt{\left(1-\frac{m_j^2}{m_{jk}^2}-\frac{m_k^2}{m_{jk}^2}\right)^2 - 4\frac{m_j^2}{m_{jk}^2}\frac{m_k^2}{m_{jk}^2}}\,,\quad m_{jk}^2 = (p_j+p_k)^2\,, \qquad \text{(I.2.41)}$$

which simplifies to $\beta_{13} = 1 - m_3^2/m_i^2$ if $m_1 = 0$.

The $2 \to 2$ ME combined with the shower instead gives an answer

$$\mathrm{d}\sigma_{\mathrm{PS}} = \frac{|M_{2\to2}|^2}{2\hat{s}}\,\mathrm{d}\Phi_2'(i+2)\,\frac{\alpha_{\mathrm{eff}}}{2\pi}\,\frac{\mathrm{d}p_{\perp\mathrm{evol}}^2}{p_{\perp\mathrm{evol}}^2}\,\frac{N\,\mathrm{d}z}{1-z}\,\frac{\mathrm{d}\varphi^*}{2\pi}\,. \tag{I.2.42}$$

Here $\mathrm{d}\Phi_2'(i+2)$ represents the outgoing i before it acquires a mass by the $q^* \to qZ^0$ branching, as assumed for the initial $2 \to 2$ QCD process. The correct phase space, used in the ME expression, is scaled down by a factor $\beta_{i2} = 1 - m_i^2/\hat{s}$. To compare the two rates, it is necessary to convert between the standard two-body phase-space variables and the shower ones. The relationship $p_{\perp\mathrm{evol}}^2 = z(1-z)m_i^2$ gives $\mathrm{d}p_{\perp\mathrm{evol}}^2/p_{\perp\mathrm{evol}}^2 = \mathrm{d}m_i^2/m_i^2$. For z it is convenient to define kinematics in the i rest frame, $p_i^* = m_i(1;0,0,0)$, with 2 along the $-z$ axis. Then, with $m_1 = 0$,

$$p_1^* = \frac{m_i^2 - m_3^2}{2m_i}\,(1;\sin\theta^*,0,\cos\theta^*)\,, \tag{I.2.43}$$

$$p_0^* = p_1^* + p_2^* + p_3^* = \left(\frac{\hat{s}+m_i^2}{2m_i};0,0,-\frac{\hat{s}-m_i^2}{2m_i}\right)\,. \tag{I.2.44}$$

Now insert into eq. (I.2.22), with $k_1 = m_3^2/m_i^2$ and $k_3 = 0$,

$$z = \frac{1}{1-m_3^2/m_i^2}\,\frac{x_1}{x_i} = \frac{m_i^2}{m_i^2-m_3^2}\,\frac{p_0^*p_1^*}{p_0^*p_i^*} = \frac{1}{2}\left(1+\frac{\hat{s}-m_i^2}{\hat{s}+m_i^2}\,\cos\theta^*\right)\,, \tag{I.2.45}$$

from which $\mathrm{d}(\cos\theta^*)/\mathrm{d}z$ can be read off. This gives a ME correction weight to the shower

$$\begin{aligned} W_{\mathrm{FSR}} &= \frac{\mathrm{d}\sigma_{\mathrm{ME}}}{\mathrm{d}\sigma_{\mathrm{PS}}} = \frac{|M_{2\to3}|^2\,\mathrm{d}\Phi_2(i+2)}{|M_{2\to2}|^2\,\mathrm{d}\Phi_2'(i+2)}\,\frac{\beta_{13}}{4\,\alpha_{\mathrm{eff}}\,N}\,\frac{p_{\perp\mathrm{evol}}^2\,\mathrm{d}m_i^2}{\mathrm{d}p_{\perp\mathrm{evol}}^2} \\ &\qquad \times (1-z)\,\frac{\mathrm{d}(\cos\theta^*)}{\mathrm{d}z} \\ &= \frac{|M_{2\to3}|^2}{|M_{2\to2}|^2}\,\beta_{i2}\frac{\beta_{13}}{2\,\alpha_{\mathrm{eff}}\,N}\,m_i^2\,(1-z)\,\frac{\hat{s}+m_i^2}{\hat{s}-m_i^2} \\ &= \frac{|M_{2\to3}|^2}{|M_{2\to2}|^2}\,\frac{1}{2\,\alpha_{\mathrm{eff}}\,N}\,\frac{p_{\perp\mathrm{evol}}^2}{z}\,\frac{\hat{s}}{\hat{s}-m_i^2}\,\frac{m_i^2-m_3^2}{m_i^2}\,. \end{aligned} \tag{I.2.46}$$

For ISR the intermediate state instead is the $2 \to 2$ QCD process $\mathrm{q}(a)\,\mathrm{g}(b) \to (\mathrm{q}^*\mathrm{g})(i)\,\mathrm{Z}^0(3) \to \mathrm{q}(1)\,\mathrm{g}(2)\,\mathrm{Z}^0(3)$, where the q^* is the spacelike quark after having emitted the Z^0. Thus the phase space separation here is

$$\mathrm{d}\Phi_3(a+b \to 1+2+3) = \mathrm{d}\Phi_2(a+b \to i+3)\,\frac{\mathrm{d}m_i^2}{2\pi}\,\mathrm{d}\Phi_2(i \to 1+2)\,. \tag{I.2.47}$$

The first $\mathrm{d}\Phi_2$ is rewritten in terms of angles in the $a+b$ rest frame, giving

$$\mathrm{d}\sigma_{\mathrm{ME}} = \frac{|M_{2\to3}|^2}{2\hat{s}}\,\mathrm{d}\Phi_3 = \frac{|M_{2\to3}|^2}{2\hat{s}}\,\frac{\beta_{i3}}{4}\,\mathrm{d}(\cos\theta)\,\frac{\mathrm{d}\varphi}{2\pi}\,\frac{\mathrm{d}m_i^2}{2\pi}\,\mathrm{d}\Phi_2(1+2)\,, \tag{I.2.48}$$

while the shower gives

$$\mathrm{d}\sigma_{\mathrm{PS}} = \frac{\alpha_{\mathrm{eff}}}{2\pi}\,\frac{\mathrm{d}\mathrm{p}^2_{\perp\mathrm{evol}}}{\mathrm{p}^2_{\perp\mathrm{evol}}}\,\frac{(1+z^2(1+r^2)^2)\,\mathrm{d}z}{1-z(1+r^2)}\,\frac{\mathrm{d}\varphi}{2\pi}\,\frac{|M_{2\to2}|^2}{2m_i^2}\,\mathrm{d}\Phi_2(1+2)\,. \tag{I.2.49}$$

The relation $m_i^2 = z\hat{s}$ gives $\mathrm{d}m_i^2/\mathrm{d}z = \hat{s}$. To relate $\cos\theta$ and $\mathrm{p}^2_{\perp\mathrm{evol}}$ it is convenient to go via the spacelike virtuality Q^2 of the q^* propagator, which by definition is related as $\mathrm{p}^2_{\perp\mathrm{evol}} = (1-z)Q^2$. In the rest frame, $p_{a,b} = (\sqrt{\hat{s}}/2)\,(1;0,0,\pm1)$, p_3 can be written as

$$p_3 = \frac{\sqrt{\hat{s}}}{2}\,\left(\frac{\hat{s}+m_3^2-m_i^2}{\hat{s}};-\beta_{i3}\sin\theta,0,-\beta_{i3}\cos\theta\right)\,, \tag{I.2.50}$$

and thus

$$Q^2 = -(p_a-p_3)^2 = \frac{1}{2}\left(\hat{s}-m_3^2-m_i^2+\hat{s}\beta_{i3}\cos\theta\right)\,, \tag{I.2.51}$$

i.e. $\hat{s}\beta_{3i}\mathrm{d}(\cos\theta)/\mathrm{dp}^2_{\perp\mathrm{evol}} = 2/(1-z)$. Put together, this gives

$$\begin{aligned} W_{\mathrm{ISR}} &= \frac{\mathrm{d}\sigma_{\mathrm{ME}}}{\mathrm{d}\sigma_{\mathrm{PS}}} = \frac{\frac{|M_{2\to3}|^2}{2\hat{s}}\,\frac{\beta_{i3}}{4}\,\mathrm{d}(\cos\theta)\,\frac{\mathrm{d}m_i^2}{2\pi}}{\frac{|M_{2\to2}|^2}{2m_i^2}\,\frac{\alpha_{\mathrm{eff}}}{2\pi}\,\frac{\mathrm{dp}^2_{\perp\mathrm{evol}}}{\mathrm{p}^2_{\perp\mathrm{evol}}}\,\frac{(1+z^2(1+r^2)^2)\,\mathrm{d}z}{1-z(1+r^2)}} \\ &= \frac{|M_{2\to3}|^2}{|M_{2\to2}|^2}\,\frac{\hat{s}\beta_{i3}\mathrm{d}(\cos\theta)}{\mathrm{dp}^2_{\perp\mathrm{evol}}}\,\frac{z\mathrm{p}^2_{\perp\mathrm{evol}}}{4\alpha_{\mathrm{eff}}}\,\frac{1-z(1+r^2)}{1+z^2(1+r^2)^2} \\ &= \frac{|M_{2\to3}|^2}{|M_{2\to2}|^2}\,\frac{1}{2\alpha_{\mathrm{eff}}}\,\frac{z\mathrm{p}^2_{\perp\mathrm{evol}}(1-z(1+r^2))}{(1-z)(1+z^2(1+r^2)^2)}\,. \end{aligned} \tag{I.2.52}$$

Two further aspects need to be considered. Firstly, the $2 \to 3$ ME expression should be compared with the sum of the FSR and ISR contributions. This could become tedious, so here a simpler route is to split the ME into two parts, one that is used for the FSR reweighting, and another for the ISR one. The relative fractions are chosen by the respective propagator, which gives an additional factor

$$\begin{aligned} W_{\mathrm{split,FSR}} &= \frac{m^{-2}_{i(\mathrm{FSR})}}{m^{-2}_{i(\mathrm{FSR})} + Q^{-2}_{(\mathrm{ISR})}} = \frac{|(p_a - p_3)^2|}{|(p_a - p_3)^2| + (p_1 + p_3)^2} \\ &= 1 - W_{\mathrm{split,ISR}}\,. \end{aligned} \tag{I.2.53}$$

Secondly, there are some differences for W emission. As in the *s*-channel case, the ISR has to include CKM-weighted PDFs and choices of incoming flavour. The flavours in the hard process are also different for ISR and FSR: a process like $\mathrm{ug} \to \mathrm{dgW}^+$ has a QCD subprocess $\mathrm{dg} \to \mathrm{dg}$ for ISR and $\mathrm{ug} \to \mathrm{ug}$ for FSR. Since QCD is flavour-blind, and the MEs are for massless quarks, this is only a matter of bookkeeping.

The matrix elements for processes like $\mathrm{qq}' \to \mathrm{qq}'\mathrm{Z}^0$ and $\mathrm{q\bar{q}}' \to \mathrm{q\bar{q}}'\mathrm{Z}^0$, $\mathrm{q}' \neq \mathrm{q}$, are pure *t*-channel. They therefore have a somewhat different structure from the $\mathrm{qg} \to \mathrm{qgZ}^0$ ones. The general pattern from four radiating partons can be quite complex, so for the purpose of a correction to the parton shower we have chosen to neglect the cross-terms between emission from the q and q′ flavour lines. That is, the $2 \to 3$ ME used for correcting emissions off the q flavour line is obtained by letting couplings to the q′ line vanish. As we will show later on, this is a reasonable approximation. From

there on, the procedure is as for $qg \to qgZ^0$. That is, the remaining ME is split into one part associated with FSR and another with ISR. For each of them a correction from PS to ME is done using either W_{FSR} or W_{ISR}.

For $qq \to qqZ^0$ it is not possible to separate by couplings. Instead the fermion lines are picked probabilistically with equal probability for each combination. Thereafter each line is considered as in the $qq' \to qq'Z^0$ case.

Finally, a $q\overline{q} \to q\overline{q}$ process is handled as pure s-channel, just like a $q\overline{q} \to q'\overline{q}'$ process.

The description so far has been formulated in terms of corrections to a W/Z emission as the first branching attached to a $2 \to 2$ QCD process, i.e. what the matrix elements have been calculated for. But for it to be useful, the corrections must be applicable for emissions at any stage of the shower, i.e. following a number of earlier QCD, QED and weak emissions. To do that, the whole system is converted to a pseudo $2 \to 2$ process, for which the ME correction procedure can be applied as above. In particular, this should guarantee a proper account of W/Z mass effects.

For FSR, a recoiler is always chosen in the final state. For a process like $qq' \to qq'$ the initial q' flavour is considered as recoiler to q, however many branchings have occurred. For $qg \to qg$, in a consecutive branching $g \to g_1g_2$ the new recoiler is chosen to be the one of g_1 and g_2 that forms the largest invariant mass together with q. The kinematics of the branching process is first boosted longitudinally to the rest frame of the two incoming partons of the original $2 \to 2$ process, and thereafter boosted to the rest frame of the radiator + recoiler. The momenta of the two incoming partons, still along the beam axis, are rescaled (down) to the same invariant mass as the outgoing state. Thus a consistent $2 \to 2 \to 3$ kinematics is arrived at, and ME corrections can applied to this sequence as before.

For ISR there is always a unique recoiler, given by the opposite incoming parton. In this case a core $2 \to 2$ process is constructed in its rest frame, with incoming partons that need not agree with the original ones, while the original outgoing partons are scaled (up) to the same invariant mass. Thus the scattering angle is preserved,

in some sense. The relevant Z emission is then added on to this kinematics, and the ME correction weight can be found.

1.2.6 *Doublecounting with weak Born processes*

Throughout the description, doublecounting issues have appeared. The $2 \to 3$ ME has been split into two parts, one used for the FSR ME corrections, and the other for the corresponding ISR ones. Within either of ISR or FSR, the possibility of radiation from two incoming or two outgoing partons is also taken into account. There remains one significant source of doublecounting, however, namely the production of a W/Z as a Born process, followed by further QCD emissions. That is, starting from $q\bar{q} \to Z^0$, first-order topologies $q\bar{q} \to gZ^0$ and $qg \to qZ^0$ will be generated, and from those $q\bar{q} \to ggZ^0$, $q\bar{q} \to q'\bar{q}'Z^0$, $qg \to qgZ^0$ and $gg \to q\bar{q}Z^0$. It is therefore possible to arrive at the same set of $2 \to 3$ processes either from a weak or a QCD base process, which opens up for another type of doublecounting.

The two production paths, here denoted "weak" or "QCD" by the base process, are expected preferentially to populate different phase space regions. To begin with, consider only ISR emission, and recall that branchings are ordered in $p_{\perp\mathrm{evol}}$, which approximately translates into ordering in ordinary $p_\perp$. In the weak path, the Z^0 and its recoiling parton therefore are produced at a larger $p_\perp$ scale than the further parton produced by the next PS branching. By contrast, in the QCD path the Z^0 will be added at the lower $p_\perp$. Similarly, FSR in the weak path allows one parton to split into two preferentially nearby partons, which thereby both tend to be opposite to the Z^0, while FSR in the weak path would preferentially place the Z^0 close to either outgoing parton.

What complicates the picture above is the use of ME corrections for the QCD path, which are there to include W/Z mass effects and ISR/FSR interference, but as a consequence also weights up the singular regions associated with the weak path. This makes the doublecounting issue more severe than if either path only had non-singular tails stretching into the singular region of the other path. As a technical side effect, the Monte Carlo efficiency of the QCD path elsewhere can become low, since the upper limit for the

ME/PS ratio, needed to set the trial sampling rate, becomes larger the closer to the "unexpected" singularities the QCD path is allowed to come. By contrast, the PYTHIA description of W/Z production only performs ME corrections for the first emission, as already discussed, so the weak path is not corrected by any $2 \to 3$ MEs.

The solution we have adopted to this issue is to separate the full $2 \to 3$ phase space into two non-overlapping regions, in the spirit of the $k_\perp$ clustering algorithm [38, 39]. That is, for a $2 \to 3$ phase-space point define distances

$$d_{iB} = p_{\perp i}^2 \,, \tag{I.2.54}$$

$$d_{ij} = \min\left(p_{\perp i}^2, p_{\perp j}^2\right) \frac{1}{R^2} \left((y_i - y_j)^2 + (\varphi_i - \varphi_j)^2\right) \,, \tag{I.2.55}$$

that represent the relative closeness to the ISR and FSR singularities, respectively, with R providing the relative normalization of the two. Then find the smallest of these distances, disregarding d_{ij} combinations that are not associated with ME singularities, such as Z^0g or qq. Associate the phase-space point with the weak path if a parton is closest to the beam or two partons closest to each other, and with the QCD path if the Z^0 is closest to the beam or to a quark.

Starting from weak production, this means that a check is made after the shower has emitted two partons, and if the phase-space point lies in the QCD-path region the event is rejected. Events with at most one branching thus are not affected, and emissions subsequent to the first two are not checked any further. Starting from a QCD event, the emission of a Z^0 is vetoed if it falls in the weak-path region. Not much should be made of the asymmetric treatment, in one case the veto of the whole event and in the other only of the branching: were it not for the ME correction on the QCD path then neither path would populate the "wrong" region to any appreciable extent. The weak-path choice is motivated by starting out from a $q\bar{q} \to Z^0$ cross section that is inclusive, so that the addition of the QCD path should be viewed as swapping in a better description of a region that already is covered. A corresponding argument for the QCD-path evolution is less obvious, and it is simpler to operate as if Z^0 emissions into the wrong region do not form a part of the shower evolution.

1.2.7 *Other shower aspects*

In the description so far the choice of W/Z mass has not been mentioned. The practical implementation is such that a new W/Z mass is chosen each time a trial W/Z emission is to be defined, according to a relativistic Breit-Wigner with running width. This allows the W/Z mass distribution to be reweighted by the mass dependence of matrix elements and of phase space.

In addition, by default there is a lower cutoff at 10 GeV for the W/Z mass. This is intended to avoid doublecounting between the PS description of γ^* production below this scale and the ME description of γ^*/Z^0 production above it. For the purposes of this study the contribution below 10 GeV is negligible. More relevant is the absence of the γ^* contribution above 10 GeV, and the γ^*/Z^0 interference contribution everywhere. This could become a further extension some day, but would involve relatively minor corrections to the overall picture, which is dominated by the W/Z peak regions.

The emitted weak bosons are decayed after the evolution of the full parton shower, into the possible decay channels according to their partial widths. In order to achieve a better description of the decay angles, a ME correction is applied. For FSR this is corrected to the ME of a four-body final state, e.g. $g^* \to u\bar{u} \to u\bar{u}Z \to u\bar{u}e^+e^-$. The ME is based on the helicity previously chosen for the radiating fermion line. Since the weak boson is already produced, all overall factors that do not depend on the decay angles are irrelevant, including the W/Z propagators. An upper estimate of the ME expression is obtained by taking four times the maximum obtained for six different decay directions ($\pm\hat{x}, \pm\hat{y}, \pm\hat{z}$ in the W/Z rest frame); empirically this always works. Then standard hit-and-miss Monte Carlo is used to pick the decay direction. For ISR the same method is applied, the only difference is the change of ME to the $u\bar{u} \to g^*Z \to g^*e^+e^-$. In the case of the mixed-initial-final state, the same two MEs are applied and the choice between them is made depending on where in the shower algorithm the emission is produced.

After the decay of the weak boson, a new parton shower is started, with the two decay products defining the first dipole.

The implementation of the weak shower only works for $2 \to 2$ or $2 \to 1$ hard processes. The reason behind this is that the mixed initial and final state ME correction relies on a $2 \to 2$ hard process. And if the starting point would be a $2 \to 3$ process, it is not always possible to identify a unique $2 \to 2$ process.

I.3 VALIDATION

In this section we collect some checks on the functioning of the weak-shower implementation. This provides insight into the approximations made and their limitations. Needless to say, many further checks have been made.

I.3.1 *Control that parton showers offer overestimates*

As the implementation relies heavily on correcting the shower behaviour by a ME/PS ratio, it is relevant to study the correction procedures. Specifically, the uncorrected PS should everywhere have a higher differential rate than the corresponding ME-corrected one has.

Results for the s-channel process, as a function of the evolution variable, can be seen in Fig. I.1. The FSR results are obtained with $N = 8$ in eq. (I.2.16), and so the rather crude overestimate of the ME expression is not unexpected. The ISR uses an overestimate specifically designed for the weak shower eq. (I.2.30), which does a better job at imitating the behaviour of the ME. The difference between the two curves is largest for small $p_{\perp\text{evol}}$, whereas for larger momenta the agreement improves. This is expected since the mass of the weak bosons is more important in the low-$p_{\perp\text{evol}}$ region. The reason that the PS without any correction does not diverge for $p_{\perp\text{evol}} \to 0$ is the purely kinematic restriction from the emission of a heavy boson. Around the PS peak the ratio between the uncorrected and the corrected number of events goes above 100. The generation of weak emissions therefore is rather inefficient, leaving room for improvements. But it should be remembered that the QCD shower part produces more trial emissions than the weak shower one does, and that therefore the overall simulation time should not be significantly affected by the weak shower. Similar results but as a function

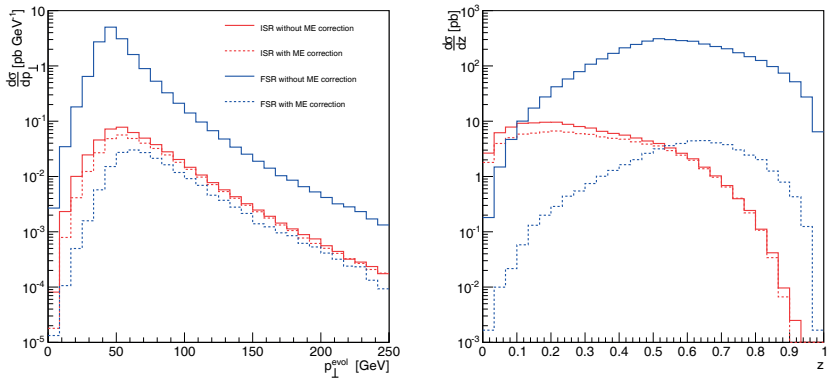

(a) (b)

Figure I.1: The differential cross section as a function of (a) $p_{\perp evol}$ and (b) z for weak boson emission in s-channel processes. The differential cross sections are shown both with and without including the ME corrections and are separated into ISR and FSR. The center of mass energy was 7 TeV and the minimum $p_{\perp hard}$ was set to 50 GeV.

of the energy-sharing variable, z, can also be seen in Fig. I.1. The FSR overestimate has the same structure as the ME and only an overall factor differs between the two. The ISR overestimate gets slightly worse for high and low values of z.

For the t-channel processes the PS is not guaranteed to be an overestimate of the ME. Indeed, for all the processes there are emissions with weights above unity, and significantly so. This indicates a divergence in the ME that is not covered in the PS. It turns out that the problematic type of events contain a low-$p_\perp$ parton in the final state, quark or gluon, or two almost collinear partons. This can be seen in Fig. I.2 for the ug $\to$ ugZ process, where the weight becomes high as the quark becomes collinear with the gluon. These types of events were discussed in the double-counting section: in a PS approach they should be produced by a Drell–Yan weak boson production followed by QCD emissions, and not by emission of weak bosons within the PS. Once the doublecounting cuts are introduced, Fig. I.2, the weights are much better behaved than before. The hard cutoff at $\Delta R = 2\pi/3$ is due to momentum conservation in the three-particle final state. Some very few phase-space points remain with

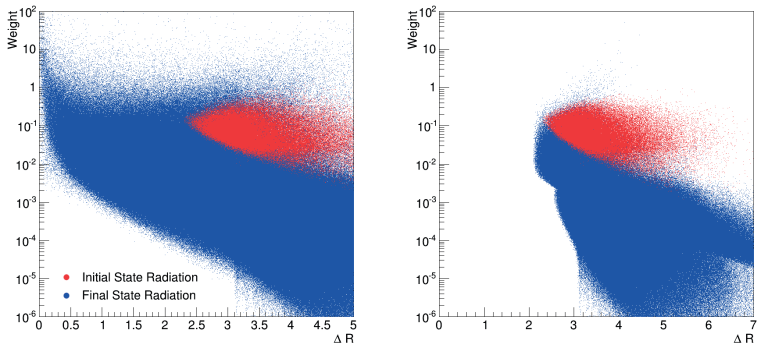

Figure I.2: Scatter plots showing the weight distributions as a function of ΔR between the final state quark and the final state gluon for the process ug $\to$ ugZ. In (a) all trial emissions are included, whereas the no-double-counting cuts have been imposed in (b). The ISR points masks part of the FSR ones. The starting minimum $p_\perp$ of the hard process was set to 50 GeV and only the weak shower was enabled. $R = 0.6$ was used in the clustering step for (b).

weights above unity. Events in such points are always accepted, but only with the standard unit weight, so the PS produces too few events in these regions. Given the tiny fraction involved, this effect should be small in most phenomenological studies. Similar to what was seen for the s-channel overestimate, the ISR overestimates behave nicely. Almost all the ISR weights stay within a band between 0.01 and 1. In addition to the aforementioned problem with weights above unity, the FSR has a large bulk of trial emissions with very low weights, making the generation inefficient.

1.3.2 *Transverse momentum distribution of the weak boson*

It is possible to validate the implementation of the PS by comparing it to ME calculations for $2 \to 3$ processes, and to this end we have used CalcHEP to generate events according to various MEs. Strictly speaking this only ensures that the first emission is correct and does not reveal anything about how the PS describes later emissions.

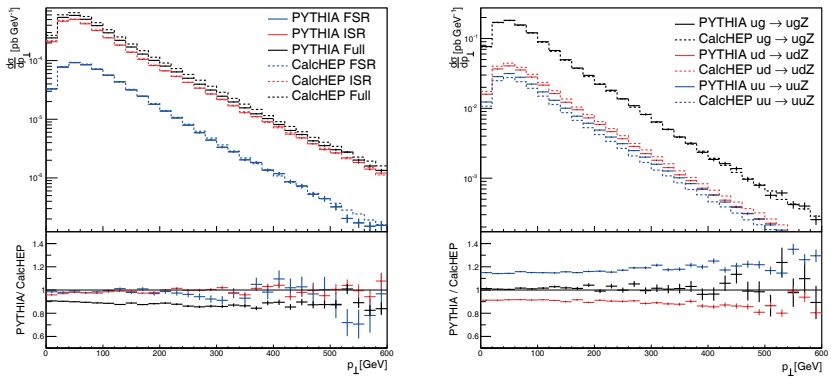

(a) (b)

Figure I.3: Comparison between CalcHEP and PYTHIA 8 results for representative (a) s-channel $d\bar{d} \to u\bar{u}Z$ and (b) t-channel processes. The center of mass energy was 8 TeV and the following phase-space cuts were applied to avoid divergent regions: $p_{\perp u} > 100$ GeV, $p_{\perp g} > 100$ GeV, and $M_{ug} > 150$ GeV.

In order for the comparison to be meaningful, the Sudakov factors have to be removed from the PS. This can be achieved by a veto on each emission after statistics on it has been collected. The evolution thus continues downwards from the vetoed scale as if there had been no branching, which cancels the Sudakov. To match the choices made for the ME calculations, the factorization and renormalization scales are held fixed at the Z^0 mass throughout the shower evolution. In addition the starting scale for the emissions was set to $\sqrt{s}$ in order to fill up the full phase space.

For comparisons in pure s-channel processes, an ISR and an FSR part can be read off from the full ME, using the coupling structure. It is therefore possible to compare these parts individually with their respective PS type. Since the PS is already corrected to these MEs, a perfect match is expected and also observed, see Fig. I.3. For the combined case, this is no longer true, since the PS does not include the interference effects present in the full ME answer. This difference amounts to the order of 10% in the chosen phase-space region, with similar numbers in several other phase-space regions that have been tested. The PS is only expected to be an

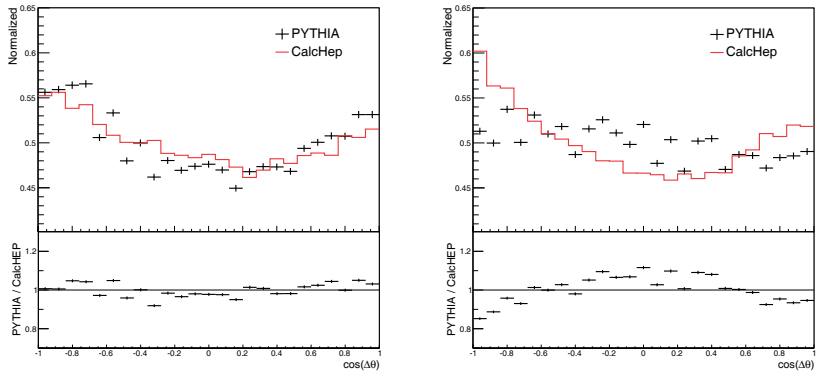

(a) (b)

Figure I.4: Angular distributions in the $2 \to 4$ process $ug \to uge^+e^-$ between (a) the u quark and the electron and (b) the gluon and the electron, defined in the W rest frame. To avoid divergent phase-space regions the same cuts are applied as in Fig. I.3.

approximation to the full MEs, and therefore the discrepancy just shows with which accuracy the PS works.

Since the *t*-channel processes do not admit a natural split between ISR and FSR, only the combined results are relevant. The $ug \to ugZ$, $ud \to udZ$ and $uu \to uuZ$ comparisons are shown in Fig. I.3. For the quark-gluon hard process a perfect match is expected and observed, since the full ME correction is used. It also shows that, at least in this part of phase space, the small problem with weights above unity is negligible (not a surprise given the cuts chosen). The $ud \to udZ$ and $uu \to uuZ$ cases both have a discrepancy between the MEs and the PS. In both cases this comes from the PS ignoring interference between emissions of weak bosons from different fermion lines. For the latter case there is a further problem, namely that the applied ME correction is that of $ud \to udZ$ and not $uu \to uuZ$.

I.3.3 *Angular distributions of the weak boson decay products*

The angles between the decay products of the weak boson and the other partons in a $2 \to 4$ process (e.g. $q\bar{q} \to q\bar{q}Z^0 \to q\bar{q}e^-e^+$)

are by construction matched to the angles calculated from the correct MEs for s-channel processes, separately for ISR and FSR. The same s-channel-derived corrections are used also for t-channel processes. To check the validity of this approach, the angular distributions between the partons and the leptons have been studied for the $ug \to uge^+e^-$ case, see Fig. I.4. The angle is defined in the rest frame of the decaying weak boson. Since only the shape is relevant, all the curves are normalized to unit area. The angle between the quark and the electron is well described by this ME correction, whereas the same can not be said for the angle between the electron and the gluon: the PS prediction is almost flat, while the ME has peaks around the collinear and anti-collinear regions. Note the suppressed zero on the y axis of the figure, however, such that both distributions stay within $\pm 20\%$ of being flat.

The discrepancy could influence relevant observables, one obvious candidate being the isolation of leptons: if the the gluon and the electron are less likely to be collinear, there is a higher probability for the electron to be isolated. It should be noted that these calculations are in the rest frame of the decaying weak boson, and that the decay products of a boosted Z^0 will tend to be collimated with each other and with the emitting parton, away from the g direction.

I.3.4 W *emission in QED hard processes*

So far all the validation tests shown have been for the emission of Z^0 bosons. For QCD hard processes and the emission of a single weak boson these results translate directly to the $W^\pm$ cases. This does not apply for a hard QED process, e.g. $q\bar{q} \to \gamma^* \to e^+e^-$. Here the emission of a Z^0 can be split into ISR and FSR parts, as before, whereas a $W^\pm$ additionally can couple to the γ^*. Then an attempted split into ISR and FSR becomes gauge dependent, and can individually become negative for certain regions of phase space.

To study this phenomenon, consider the simplest possible s-channel FSR case, $\gamma^* \to u\bar{d}W^-$, and compare it with the three related $\gamma^* \to u\bar{u}Z^0$, $g^* \to u\bar{d}W^-$ and $g^* \to u\bar{u}Z^0$ ones. In each case two possible Feynman diagrams for the emission of a W off a

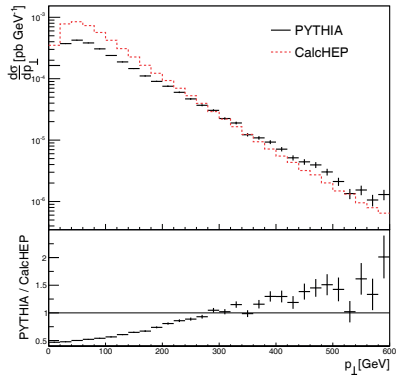

Figure I.5: Comparison between the $2 \to 3$ ME calculation and the prediction from the PS for the $u\bar{u} \to u\bar{d}W^-$ process, including only electroweak diagrams. Similar cuts as in Fig. I.3 were applied.

quark are included and, in Feynman gauge, the squared MEs take the common form

$$|M|^2 = c\left(\alpha_1 A(x_1, x_2) + \alpha_2 A(x_2, x_1) + 2\beta B(x_1, x_2)\right) \quad \text{(I.3.1)}$$

$$A(x_i, x_j) = \frac{(1-x_1)(1-x_2) - r^2}{(1-x_i)^2}\,, \quad \text{(I.3.2)}$$

$$B(x_1, x_2) = \frac{x_1 + x_2 - 1 + r^2(x_1 + x_2) + r^4}{(1-x_1)(1-x_2)}\,, \quad \text{(I.3.3)}$$

with the same definitions as before for x_1, x_2 and r. The c, α_1, α_2 and β are coefficients that depend on the specific process. For the three reference processes the coefficients are $\alpha_1 = \alpha_2 = \beta = 1$, suitably normalized, cf. eq. (I.2.14).

For the $\gamma^* \to u\bar{d}W^-$ process, however, the coefficients become $\alpha_1 = e_u^2 = 4/9$, $\alpha_2 = e_d^2 = 1/9$ and $\beta = e_u e_d = -2/9$. This gives a cross section that is negative over a large fraction of the phase space. The reason obviously is that we have neglected a third diagram specific to this case, involving the triple-gauge-boson vertex $\gamma^* \to W^+W^-$, which restores positivity.

The introduction of a complete electroweak gauge boson shower is beyond the scope of this study. For now we therefore handle cases like this using the same shower couplings and ME corrections as for the cases with a gluon propagator. To estimate the effect

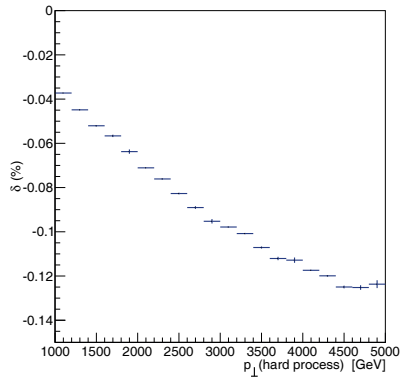

Figure I.6: Weak corrections to di-jet production. δ is calculated by removing all events with a weak boson emission, $\delta = -\sigma(2 \to 3)/\sigma(2 \to 2)$.

of this approximation, the $2 \to 3$ ME for $u\bar{u} \to u\bar{d}W^-$ with all electroweak diagrams included, but not QCD ones, was compared to the prediction from the PS, see Fig. I.5. This includes s- and t-channel exchange of $W^{\pm}$, Z and γ, and is dominated by the t-channel contributions for the studied regions of phase space. The comparison looks reasonable for large $p_\perp$ values, but for small values the ME rate is about twice as large as the PS one. Such a qualitative agreement should be good enough, given the dominance of QCD processes at the LHC.

I.4 STUDIES OF JET PHENOMENA AT LHC ENERGIES

We now turn to studies of how the introduction of a weak shower changes different observables at the LHC. Three representative examples have been chosen. Firstly, weak corrections to the exclusive di-jet production, and some other generic rate measures. Secondly, how likely it is to find a W/Z decaying hadronically inside a high-$p_\perp$ QCD jet. Thirdly, whether it is possible to describe the inclusive W/Z + jets cross sections that the ordinary PS fails to describe. PYTHIA version 8.181 was used for all the phenomenological studies. The choice of PDF was CTEQ6L [40], with a NLO running α_s.

1.4.1 *Exclusive di-jet studies*

The calculation of Moretti, Nolten and Ross (MNR) [9, 10] showed large negative $\mathcal{O}(\alpha_s^2\alpha_w)$ corrections to jet production at hadron colliders, in the range 10–30% for jets with $p_\perp > 1$ TeV. To put these numbers in perspective, we simulate $2 \to 2$ QCD hard processes with only the weak shower turned on. The weak correction is then defined by the rate at which at least one W/Z boson is produced, Fig. I.6. That rate increases for larger $p_\perp$ of the hard process, partly by the PDF change from gluon-dominated to quark-dominated hard processes, partly by the intrinsic logarithmic increase of the emission rate. In our calculations the corrections are only in the range 4–14%, i.e. less than half of the corresponding MNR numbers. The comparison is not fair, however, since we only study $\mathcal{O}(\alpha_w)$ corrections to $\mathcal{O}(\alpha_s^2)$ hard processes, whereas MNR additionally includes $\mathcal{O}(\alpha_s)$ corrections to $\mathcal{O}(\alpha_s\alpha_w)$ hard processes.

There is another difference between MNR and our PS, in that MNR includes Bloch-Nordsieck violation effects, whereas the PS approach is based on exact balance between real and virtual corrections to the di-jet production. But, as mentioned earlier, the BN violations are expected to be small at the LHC, and therefore the comparison should still be sensible.

1.4.2 *Resummation and competition between the QCD shower and the weak shower*

With the availability of a weak shower it is possible to study the effect of multiple weak boson emissions. This probability is largest for high-$p_\perp$ jets, but even for $2 \to 2$ QCD processes with $p_\perp > 1$ TeV the probability for more than a single weak boson emission is found to be about one per mille at LHC energies, Fig. I.7. For most (if not all) analyses the experimental uncertainty will be significantly above this probability, and it is therefore a good approximation to neglect the effects coming from other than the first W/Z boson. As already mentioned the possibility of pure electroweak shower evolution, like $\gamma^*/Z^0 \to W^+W^-$, is not included here.

In a PS it is possible to tell when the weak emission occurs in the ordered shower evolution, as opposed to a ME calculation. It

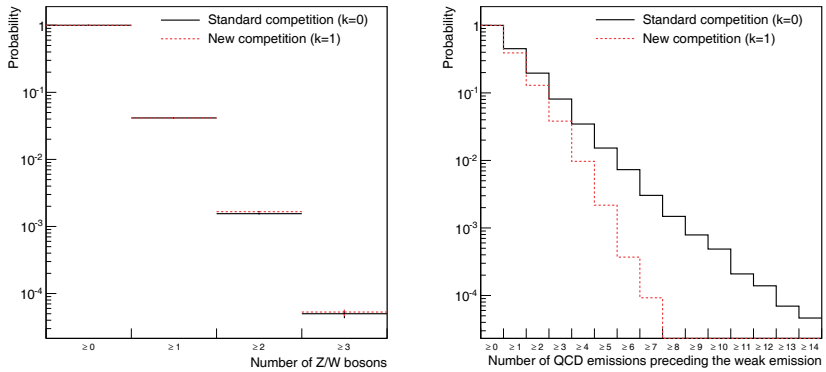

(a) (b)

Figure I.7: Probability (a) for multiple emissions of weak bosons and (b) for the number of QCD emission preceding the weak emission. The center-of-mass energy was set to 14 TeV and the hard process $p_\perp$ was above 1 TeV.

is therefore of interest to study the competition between QCD and weak emission. The non-negligible W/Z mass could make for ambiguities, which we explore by comparing the normal $p_{\perp evol}$ ordering with an alternative $p^2_{\perp evol} + km^2_{W/Z}$ one for weak branchings, with $k = 1$ taken as the extreme alternative. In Fig. I.7 we show how many QCD branchings occur before the weak one, where a long tail is significantly reduced by the larger weak scale choice. The probability of having at least one preceding QCD emission is of order 40% in both extremes, however, underlining that large jets masses are common in the QCD evolution. Furthermore, the total number of weak bosons only varies by about 2% between the two choices of evolution scale. The chances of constraining k from data thus are limited. One possibility is to study the energy distributions inside a jet, but the problem here is the low experimental rate (to be discussed later). Another possibility is weak boson production in association with jets, where especially the events with a high jet multiplicity could be influenced by the choice of k, a topic that will be studied later in this section.

In fixed-order perturbation theory there is no concept of an ordered evolution, and thus not of how many QCD emissions precede the weak one. The shower results here could be an indication

of how high orders that need to be used, in matching and merging schemes, so as to describe multijet production in association with a W/Z. Assuming a ME-to-PS matching at the W/Z emission scale, say, Fig. I.7 suggests that at most 1% of the W/Z have more than five QCD emissions at a higher scale than the W/Z itself for a $p_\perp > 1$ TeV jet. Thus, taking into account the two original jets, it would be necessary to include up to W/Z + 7 jets so as not to miss relevant multijet topologies down to the 1% level. This is entirely feasible with current technology. Thus the W/Z emission in showers does not address otherwise unapproachable topologies, but it is likely to address some issues considerably faster. And jet numbers will rise dramatically for matching scales below the W/Z one, making showers unavoidable in that region.

I.4.3 *Substructure of a jet with weak bosons inside the jet*

If a W/Z is radiated from a high-$p_\perp$ jet, it is probable that the W/Z will be boosted along the jet direction, and that the W/Z decay products will fall within a reasonably-sized jet cone. For leptonic decays it should still be possible to separate the decay products from the other components of the jet, but for hadronic decays the distinction will be more difficult. One possibility is to study the jet substructure and jet-jet invariant masses for signs of bumps at the W and Z masses.

One key challenge is the low W/Z emission rate, around 4% for $p_\perp > 1$ TeV events in total, and not all of that inside jets. Another is that the QCD evolution itself produces a rich substructure, with a high rate in the W/Z mass region. Thus the signal of W/Z production inside jets would be small bumps sitting on top of a large but smooth QCD background.

Before searching for W/Zs inside jets, let us take a step back and consider some of the more basic properties of W/Zs produced inside jets, Fig. I.8. It is expected that the $p_\perp$ distribution for the weak bosons will be significantly harder than for those produced in Drell-Yan. The Drell-Yan production peaks at a few GeV, whereas the emissions peak at the mass of the weak bosons, mainly by simple phase-space effects in the PS.

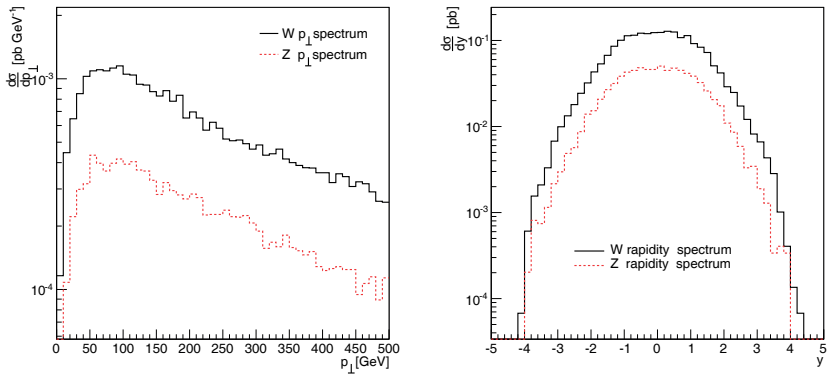

(a) (b)

Figure I.8: The (a) $p_\perp$ and (b) rapidity distributions for W/Z emissions, for $2 \to 2$ QCD processes with a transverse momentum above 1 TeV.

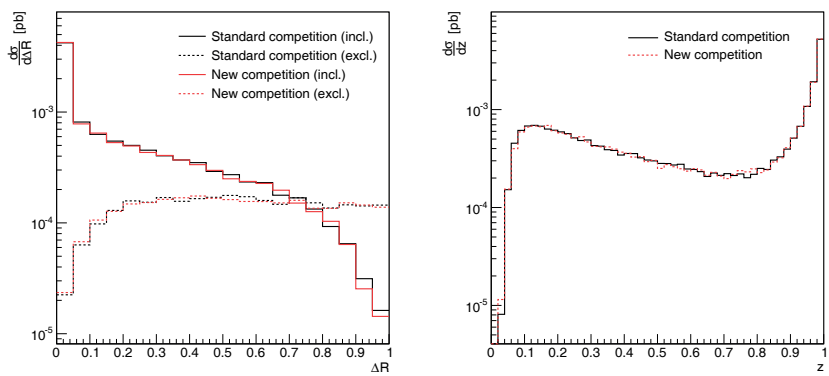

(a) (b)

Figure I.9: The (a) ΔR and (b) energy sharing distributions for radiated W/Zs. The anti-$k_\perp$ jet algorithm has been used with $R = 1$ and minimum transverse momentum of 100 GeV. The hard process was $2 \to 2$ QCD processes with transverse momentum above 1 TeV. The ΔR distributions were calculated both with (inclusive) and without (exclusive) including the weak boson in the jet clustering algorithm.

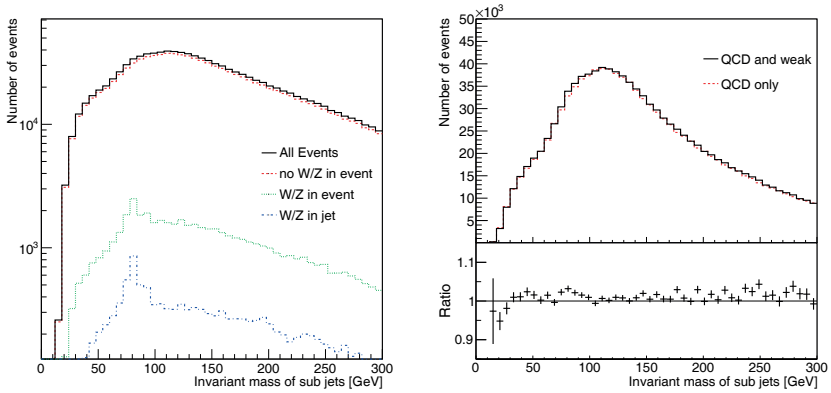

(a) (b)

Figure I.10: The invariant mass of all subjet configurations found by applying trimming method to a fat jet. In (a) the distribution for several different event selections. In (b) a comparison between simulations with or without the weak shower included.

The location of the weak boson within the jet is different from that of the normal QCD emission. This can be most easily realized by considering the ΔR and energy sharing distributions, Fig. I.9. The energy sharing distribution for QCD has a peak around zero due to the soft divergence. Weak emissions do not have soft divergencies, but instead have a hard cut-off due to the mass. The peaks observed at respectively $\Delta R = 0$ and $z = 1$ are due to isolated weak bosons produced from either ISR or large-angle FSR emissions. This is in agreement with the $\Delta R = 0$ peak disappearing when the weak boson is excluded in the jet clustering.

The above distributions are shown for two different competition schemes, the standard $p_{\perp evol}$ ordered and the new $p^2_{\perp evol} + M^2_{W/Z}$ ordered. The two schemes give essentially the same results for all the distributions and thus none of the observables provide any separation power between the schemes.

Returning to the hadronically decaying W/Z inside jets, a simple phenomenological study has been carried out to determine whether is possible to locate these. First all jets with $p_\perp > 1$ TeV are found according to the anti-$k_\perp$ algorithm with $R = 1$, using FastJet [41]. Afterwards these jets are split into subjets by the trimming algorithm, with parameters $Z = 0.05$ and $r_{tr} = 0.2$. The invariant mass

of all subjet pairs is shown in Fig. I.10. Unfortunately no peak is visible to the naked eye, due to the large background. As a check, if only those events are singled out that contains a W/Z the signal stands out, and even more so for those jets that contain a W/Z.

As a further step, mass spectra are compared with or without weak radiation in the shower, Fig. I.10, together with the ratio. It is possible to see a difference between the two runs, but note that only statistical uncertainties have been included (1 000 000 events, corresponding to about 77 fb^{-1}), and not any detector smearing effects.

I.4.4 *Weak boson production in association with jets*

Inclusive weak boson production in association with jets for a long time has been known to be poorly described by the PYTHIA shower approach alone. The PS can describe the emission of the first jet to a decent level of agreement with data, but for additional jets the shower predictions fall below the observed data, increasingly so for more jets. The use of ME corrections for the first emission is not the reason it works out there: as we have already discussed, the uncorrected PS overestimates the $q\bar{q} \to Zg$ process and underestimates the $qg \to Zq$ one, but by small amounts over most of phase space, and in such a way that the sum of the two comes out approximately right. Rather we would like to attribute the problem to the absence of weak emissions in showers, and are now in a position to check this hypothesis.

The new shower framework has been compared with the W + jets and Z + jets data from the ATLAS experiment [34, 42] using the Rivet framework [43]. The PYTHIA results are obtained as the sum of two components, one "weak (production) path" where the starting topology for shower evolution is a W/Z, and the other a "QCD (production) path" where the starting topology is a $2 \to 2$ QCD process. The former, being leading order, is well known to miss out on an overall K factor, which we address by normalizing this component to the inclusive W rate. For the Z production this rate is not quoted, so we instead normalize to $Z + 1$ jet. Empirically there does not seem to be a corresponding need for a large K factor in QCD $2 \to 2$, in the context of tunes where α_s is among the

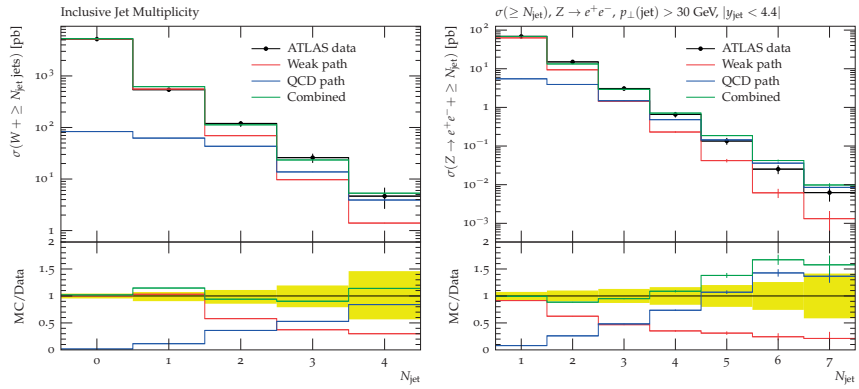

(a) (b)

Figure I.11: The inclusive jet multiplicity rates for (a) W + jets and (b) Z + jets.

free parameters, and so none has been used here. Doublecounting between the two paths is avoided as already discussed.

The inclusive W/Z cross sections as a function of the number of associated jets are shown in Fig. I.11. The weak production starts to fall off at higher jet multiplicities, as foretold, where the QCD path becomes the dominant production channel. It is clear that the addition of the QCD path, absent in previous comparisons between data and Pythia, plays a key role in achieving a much improved agreement with data. The agreement for the first four jets is very good both for W and Z, the only slight problem being the $W + 1$ jet bin. For higher jet multiplicities the PS start to overestimate the production. The discrepancy might very well be within tuneable parameters, for instance a small change in α_s will have a large influence at high jet multiplicities. And given all the approximations made, the overall agreement might be better than one had initially expected.

Next we turn to more exclusive quantities, beginning with the jet $p_\perp$ spectra. These are known to fall off too rapidly for the weak path alone, Fig. I.12. But here again the QCD path provides a slower drop that nicely takes over with increasing $p_\perp$, giving a good overall agreement. This is not really surprising, given that the likelihood of emitting a W/Z increases with increasing $p_\perp$ of the QCD process.

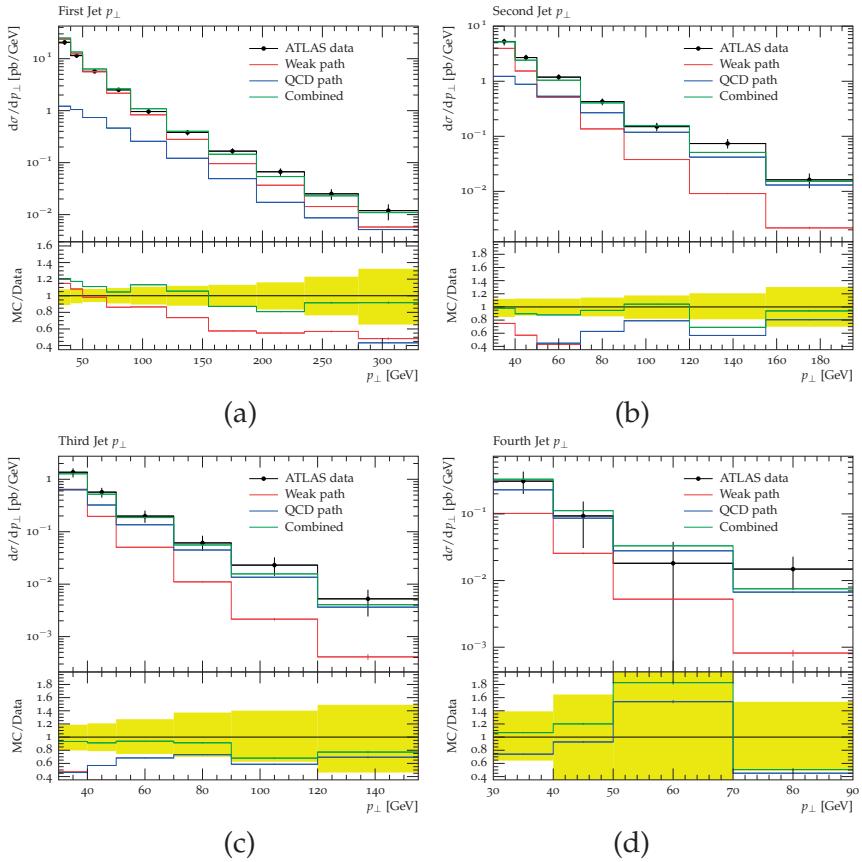

Figure I.12: The $p_\perp$ distributions for the four hardest jets in W + jet production.

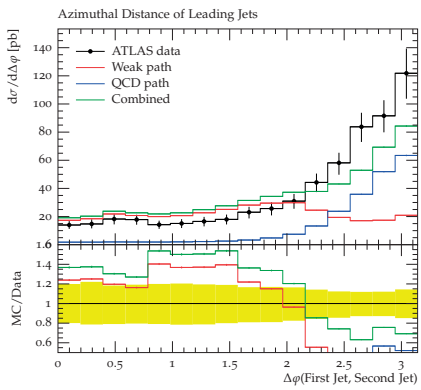

Figure I.13: The $\Delta\varphi$ distributions for between the leading and sub-leading jets in W + jet production.

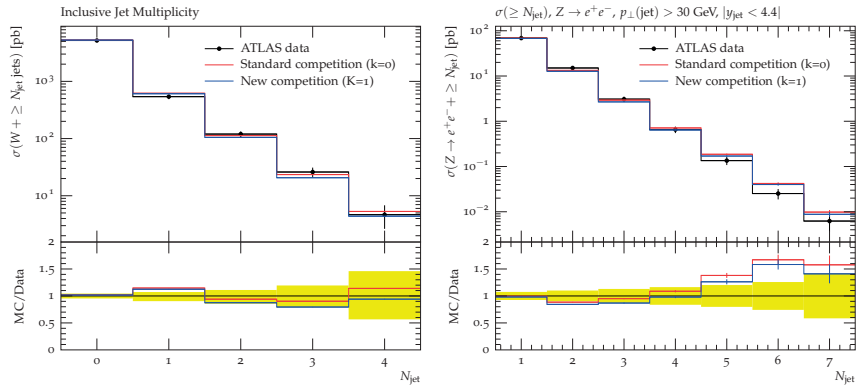

(a) (b)

Figure I.14: The inclusive jet multiplicities for two different competitions, (a) for W + jets and (b) for Z + jets.

A further check is provided by the φ angle between the two leading jets. The QCD path starts out from two back-to-back jets, and part of that behaviour could be expected to survive the emission of a weak boson. For the weak path the jets come from ISR, and are therefore not expected to be particularly anticorrelated in φ. This is also what is observed in Fig. I.13: the weak path is almost flat in $\Delta\varphi$, whereas the QCD path gives a clear peak around $\Delta\varphi = \pi$. Combining the two production channels does not give overwhelming agreement between data and the event generator, however, with data having a stronger peak structure.

As mentioned previously, the implementation introduces a new parameter, k, that changes the competition between the weak shower and the QCD shower. To test whether any of the weak boson plus jets observables are sensitive to the choice of k, two different simulations have been carried out. The first simulation uses the standard $p_{\perp evol}$ competition with $k = 0$ and the second uses $k = 1$, thus the weak bosons are produced earlier in the shower. Fig. I.14 shows the inclusive jet multiplicities for the two different competitions. It may be counterintuitive that the new competition produces a lower number of weak bosons. The explanation is that the QCD emissions can open new paths that allows weak emissions. Consider for instance a $gg \to gg$ process at a hard scale of 75 GeV. This process can not radiate any weak bosons with the new com-

petition, due to it requiring the weak emissions to happen prior to any QCD emissions (since 75 GeV is below the W mass). In the standard competition it is possible to have a QCD emission prior to the weak emission, thus enabling for instance a gluon splitting into two quarks followed by the emission of a weak boson. This was also verified, by considering only those events that had a hard scale significantly above the Z mass. And for these, the two curves were equal within statistical uncertainties. The difference between the two competitions is not very large, however, and given the experimental uncertainty these observables do not provide any significant discrimination power. More differential distributions were also tested, but none allowed a better distinction between the competitions. Thus so far it has not been possible to find observables that can actually tell the two competitions apart.

I.5 PROSPECTS FOR FUTURE COLLIDERS

The emission rate of weak bosons is expected to scale as $\alpha_w \ln^2(\hat{s}/M^2_{Z/W})$, and thus the effect of a weak PS is higher for colliders with a higher center-of-mass energy. One of the suggestions for a possible next step beyond the LHC is a new 100 TeV pp collider. In this section we will redo some of the phenomenological studies presented in the last section, but now with the center-of-mass energy cranked up accordingly.

The weak virtual corrections to the di-jet exclusive cross section at 100 TeV are shown in Fig. I.15. As before this equals the probability to emit at least one weak boson, up to a minus sign. For the di-jet with a $p_\perp$ around 30 TeV the corrections reach about 30%, a significant increase compared to the maximal 14% for LHC energies. Clearly one will need to consider weak corrections for all processes that can have jets at large $p_\perp$.

Since the emission rate for a single weak boson is enhanced significantly, also the rate of multiple weak emissions goes up, Fig. I.16. This is of special interest since currently the matching and merging schemes only describe a single emission of a weak boson. The probability for radiating at least 2 weak bosons stays within a few percent for inclusive di-jet production. The effects may be larger for more exclusive observables. For instance, if you consider the pro-

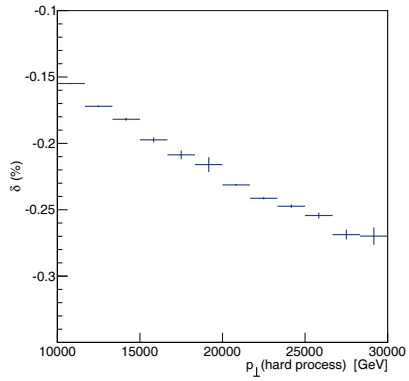

Figure I.15: Weak virtual correction to di-jet production at a 100 TeV pp collider, cf. Fig. I.6.

duction of a weak boson in association with jets, you would have an additional weak boson in ∼10 % of the events (under the conditions of Fig. I.16).

It is also interesting to note that the larger available phase space means that more QCD emissions can precede that of a weak boson, Fig. I.16. To again obtain a one percent accuracy the simulations now need to include up to 11 QCD emissions before the weak one, which is beyond current ME capability. A matching to a shower that can cover at least the softer W/Z emissions, relative to the large scales of the hard process, there offers obvious advantages.

I.6 SUMMARY AND OUTLOOK

In this article we have described an implementation of weak gauge boson emission as an integrated part of a standard parton-shower machinery, outlined its consequences and compared it with some relevant data. This is a first, to the best of our knowledge.

The challenges of obtaining a realistic description have been larger than might have been foreseen. For instance, the matching to first-order matrix elements for W/Z emission is a natural way to obtain a realistic description of corrections induced by the gauge boson masses, an issue not encountered for QCD and QED showers. A first step thus is to consider W/Z emission off s-channel $2 \to 2$ QCD

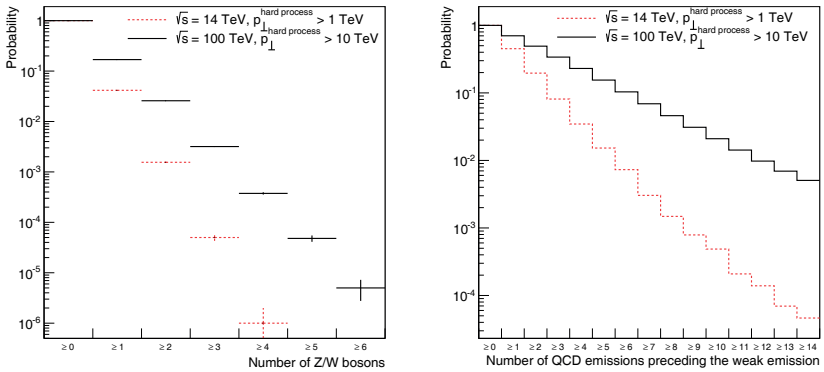

(a) (b)

Figure I.16: Probability (a) for multiple emissions of weak bosons and (b) for the number of QCD emissions preceding the weak emission. The center of mass energy was set to 100 TeV and the hard process $p_\perp$ was above 10 TeV. The standard competition was used.

processes, where initial- and final-state radiation can be cleanly separated (by dropping interference effects), and use these matrix elements to correct the shower behaviour also for other processes. But such a factorized description then performs rather poorly for t-channel-dominated QCD processes, necessitating a more complex matrix-element-correction machinery. The main drawback is that, in a shower language, there now arises doublecounting issues between what should be classified as QCD emission off a weak process and weak emission off a QCD process, and this has to be resolved. At the end of the day the weak-emission machinery therefore becomes more cumbersome than intended.

Possibly the most satisfying outcome of this study is the so much improved description of $W/Z + n$ jet data. A widespread misconception is that showers are bound to *under*estimate emission rates, in spite of several studies to the contrary [27–29]. The poor performance of PYTHIA for $W/Z + n$ jets, with a clear trend to the worse for increasing n, has fed this myth. Now we see that the discrepancies essentially disappear once the possibility of weak showers is introduced, at least within experimental errors and reasonable model variations, e.g. of α_s. This is not to say that everything is

perfect; as always the shower does better for azimuthally-averaged quantities than in more differential distributions.

Apart from this insight, has the outcome been worth the effort? Not surprisingly we have shown that, even at the highest LHC scales, W/Z emissions usually occur early in the shower evolution, such that the dominant $W/Z + n$ jet topologies can be generated perfectly well by standard matrix elements technology. So from that point of view the answer would be no.

However, in step with the computational advances has come the realization that "raw" order-by-order matrix elements are not enough. Essentially all matching/merging techniques for combining the different fixed-n-jet results adopt a parton-shower perspective to overcome doublecounting issues. Notably a fictitious shower history is used to define the Sudakov form factors that are needed to turn inclusive matrix elements into exclusive ones [44]. In the CKKW-L approach [45] these Sudakovs are derived from a shower algorithm, meaning that the overall reliability of the matching/merging procedure is dependent on the quality of this algorithm. Here the lack of W/Z emission as a possibility can force the adoption of less natural shower histories [46]. The new machinery thus opens the road to a better combined description, even in cases when no real W/Z emissions are taken from the shower itself. Further, the shower histories are used to reweight the fixed α_s couplings of the ME calculations to ones running as a function of the relevant branching scales, so also here improvements are possible.

So what lies in the future?

Firstly, we hope that the extended shower will prove useful in its own right. In particular it offers a convenient tool for studying how the structure of jets is affected by real and virtual weak-emission corrections, interleaved into the standard QCD (+ QED) framework. Thus it is easy to get a first understanding of where effects could be significant, and the general order of such effects, both for jets and for the event as a whole. The low computer-time cost means that weak showers could be included routinely in event generation of any process, as a reminder/warning of complications that may occur, both from readily visible lepton pairs, from missing neutrino momenta and from the stealth mode of hadronically decaying weak bosons.

Input from higher-order matrix elements will still be needed for precision studies. But, secondly, we have already stressed the improvements of matching/merging strategies that are made possible by including W/Z emission as part of the shower evolution, so an obvious step is to actually upgrade the existing matching/merging strategies available with Pythia [46–48].

Thirdly, there are some issues that have not been addressed. One is that we have not included the full γ^*/Z^0 interference structure; currently the QED machinery includes pure γ^* effects up to some mass scale, while the pure Z^0 kicks in above this scale. Furthermore not all electroweak branchings are included as part of the shower, such as $W^\pm \to W^\pm\gamma$, $Z^0 \to W^+W^-$ or $W^\pm \to W^\pm Z^0$. One could even imagine to include the Higgs in the game. However, this is on a slope of rapidly falling shower-language relevance, so it is not clear whether the investment in time would be worth it.

acknowledgements

Work supported in part by the Swedish Research Council, contract number 621-2010-3326, and in part by the MCnetITN FP7 Marie Curie Initial Training Network, contract PITN-GA-2012-315877.

bibliography

[1] Z. Bern, L. J. Dixon, F. Febres Cordero, S. Hoeche, H. Ita, D. A. Kosower, D. Maitre and K. J. Ozeren, Phys. Rev. D **88** (2013) 014025 [arXiv:1304.1253 [hep-ph]].

[2] M. Kuroda, G. Moultaka and D. Schildknecht, Nucl. Phys. B **350** (1991) 25.

[3] G. Degrassi and A. Sirlin, Phys. Rev. D **46** (1992) 3104.

[4] M. Beccaria, G. Montagna, F. Piccinini, F. M. Renard and C. Verzegnassi, Phys. Rev. D **58** (1998) 093014 [hep-ph/9805250].

[5] M. Ciafaloni, P. Ciafaloni and D. Comelli, Phys. Rev. Lett. **84** (2000) 4810 [hep-ph/0001142].

[6] M. Ciafaloni, P. Ciafaloni and D. Comelli, Nucl. Phys. B **589** (2000) 359 [hep-ph/0004071].

[7] A. Denner, PoS HEP **2001** (2001) 129 [hep-ph/0110155].

[8] M. Melles, Phys. Rept. **375** (2003) 219 [hep-ph/0104232].

[9] S. Moretti, M. R. Nolten and D. A. Ross, Phys. Rev. D **74** (2006) 097301 [hep-ph/0503152].

[10] S. Moretti, M. R. Nolten and D. A. Ross, Nucl. Phys. B **759** (2006) 50 [hep-ph/0606201].

[11] P. Ciafaloni and D. Comelli, JHEP **0609** (2006) 055 [hep-ph/0604070].

[12] U. Baur, Phys. Rev. D **75** (2007) 013005 [hep-ph/0611241].

[13] A. Banfi, G. P. Salam and G. Zanderighi, JHEP **0707** (2007) 026 [arXiv:0704.2999 [hep-ph]].

[14] J. H. Kuhn, A. Scharf and P. Uwer, Phys. Rev. D **82** (2010) 013007 [arXiv:0909.0059 [hep-ph]].

[15] G. Bell, J. H. Kuhn and J. Rittinger, Eur. Phys. J. C **70** (2010) 659 [arXiv:1004.4117 [hep-ph]].

[16] S. Dittmaier, A. Huss and C. Speckner, JHEP **1211** (2012) 095 [arXiv:1210.0438 [hep-ph]].

[17] W. J. Stirling and E. Vryonidou, JHEP **1304** (2013) 155 [arXiv:1212.6537 [hep-ph]].

[18] J. M. Campbell, K. Hatakeyama, J. Huston and F. Petriello *et al.*, arXiv:1310.5189 [hep-ph].

[19] A. Buckley *et al.*, arXiv:1101.2599 [hep-ph].

[20] T. Sjöstrand, S. Mrenna and P. Z. Skands, Comput. Phys. Commun. **178**, 852 (2008) [arXiv:0710.3820 [hep-ph]].

[21] T. Sjöstrand, S. Mrenna and P. Z. Skands, JHEP **0605** (2006) 026 [hep-ph/0603175].

[22] T. Sjöstrand and P. Z. Skands, Eur. Phys. J. C **39** (2005) 129 [arXiv:hep-ph/0408302].

[23] G. Gustafson and U. Pettersson, Nucl. Phys. B **306** (1988) 746.

[24] T. Sjöstrand, Phys. Lett. B **157** (1985) 321.

[25] T. Sjöstrand and M. van Zijl, Phys. Rev. D **36** (1987) 2019.

[26] R. Corke and T. Sjöstrand, arXiv:1011.1759 [hep-ph].

[27] M. Bengtsson and T. Sjöstrand, Phys. Lett. B **185** (1987) 435.

[28] E. Norrbin and T. Sjöstrand, Nucl. Phys. B **603** (2001) 297 [hep-ph/0010012].

[29] G. Miu and T. Sjöstrand, Phys. Lett. B **449** (1999) 313 [hep-ph/9812455].

[30] P. Nason, JHEP **0411** (2004) 040 [hep-ph/0409146].

[31] S. Frixione, P. Nason and C. Oleari, JHEP **0711** (2007) 070 [arXiv:0709.2092 [hep-ph]].

[32] V. M. Abazov *et al.* [Do Collaboration], Phys. Lett. B **658** (2008) 112 [hep-ex/0608052].

[33] S. Chatrchyan *et al.* [CMS Collaboration], JHEP **1201** (2012) 010 [arXiv:1110.3226 [hep-ex]].

[34] G. Aad *et al.* [ATLAS Collaboration], JHEP **1307** (2013) 032 [arXiv:1304.7098 [hep-ex]].

[35] L. Carloni, J. Rathsman and T. Sjöstrand, JHEP **1104** (2011) 091 [arXiv:1102.3795 [hep-ph]].

[36] A. Belyaev, N. D. Christensen and A. Pukhov, Comput. Phys. Commun. **184** (2013) 1729 [arXiv:1207.6082 [hep-ph]].

[37] R. K. Ellis, G. Marchesini and B. R. Webber, Nucl. Phys. B **286** (1987) 643 [Erratum-ibid. B **294** (1987) 1180].

[38] S. Catani, Y. L. Dokshitzer, M. H. Seymour and B. R. Webber, Nucl. Phys. B **406** (1993) 187.

[39] G. P. Salam, Eur. Phys. J. C **67** (2010) 637 [arXiv:0906.1833 [hep-ph]].

[40] J. Pumplin, D. R. Stump, J. Huston, H. L. Lai, P. M. Nadolsky and W. K. Tung, JHEP **0207** (2002) 012 [hep-ph/0201195].

[41] M. Cacciari, G. P. Salam and G. Soyez, Eur. Phys. J. C **72** (2012) 1896 [arXiv:1111.6097 [hep-ph]].

[42] G. Aad *et al.* [ATLAS Collaboration], Phys. Rev. D **85** (2012) 092002 [arXiv:1201.1276 [hep-ex]].

[43] A. Buckley, J. Butterworth, L. Lönnblad, H. Hoeth, J. Monk, H. Schulz, J. E. von Seggern and F. Siegert *et al.*, arXiv:1003.0694 [hep-ph].

[44] S. Catani, F. Krauss, R. Kuhn and B. R. Webber, JHEP **0111** (2001) 063 [hep-ph/0109231].

[45] L. Lönnblad, JHEP **0205**, 046 (2002) [hep-ph/0112284].

[46] L. Lönnblad and S. Prestel, JHEP **1203** (2012) 019 [arXiv:1109.4829 [hep-ph]].

[47] L. Lönnblad and S. Prestel, JHEP **1302** (2013) 094 [arXiv:1211.4827 [hep-ph]].

[48] L. Lönnblad and S. Prestel, JHEP **1303** (2013) 166 [arXiv:1211.7278 [hep-ph]].

II

STRING FORMATION BEYOND
LEADING COLOUR

COEPP-MN-15-1
LU-TP-15-16
MCNET-15-09

String Formation Beyond Leading Colour

Jesper R. Christiansen[1,2], Peter Z. Skands[2,3]

[1]: Department of Astronomy and Theoretical Physics, Lund University, Sölvegatan 14, Lund, Sweden

[2]: Theoretical Physics, CERN, CH-1211, Geneva 23, Switzerland

[3]: School of Physics and Astronomy, Monash University, VIC-3800, Australia

JHEP 1508 (2015) 003

Abstract

We present a new model for the hadronisation of multi-parton systems, in which colour correlations beyond leading N_C are allowed to influence the formation of confining potentials (strings). The multiplet structure of $SU(3)$ is combined with a minimisation of the string potential energy, to decide between which partons strings should form, allowing also for "baryonic" configurations (e.g., two colours can combine coherently to form an anticolour). In e^+e^-collisions, modifications to the leading-colour picture are small, suppressed by both colour and kinematics factors. But in pp collisions, multi-parton interactions increase the number of possible subleading connections, counteracting their naive $1/N_C^2$ suppression. Moreover, those that reduce the overall string lengths are kinematically favoured. The model, which we have implemented in the PYTHIA 8 generator, is capable of reaching agreement not only with the important $\langle p_\perp \rangle \, (n_{\text{charged}})$ distribution but also with measured rates (and ratios) of kaons and hyperons, in both ee and pp collisions. Nonetheless, the shape of their $p_\perp$ spectra remains challenging to explain.

II.1 INTRODUCTION

The description of hadronic final states at high-energy colliders involves a complicated cocktail of physics effects, dominated by QCD [1–3]. For the calculation of *inclusive* hard-scattering cross sections, factorisation allows most of the complicated long-distance physics to be represented in the form of universal parton distribution functions (PDFs) [4], while the short-distance parts can be calculated perturbatively. Perturbative aspects, such as hard-process matrix elements, parton showers, and decay (chains) of short-lived resonances, are generally coming under increasingly good control, due to a combination of advances: better amplitude calculations (including better automation and better interfaces [5–12]), better parton-shower algorithms (e.g. ones based on QCD dipoles [13–19]), and better techniques for how to combine them (matching and merging, see [3, 12, 20–22] and references therein). These successes build on an extensive prior experience with perturbative approximations to QCD at both fixed and infinite order, and the tractable nature of the perturbative expansions themselves.

To describe the full (*exclusive*) event structure, however, several additional soft-physics effects must be accounted for, such as hadronisation, multiple parton interactions (MPI), Bose-Einstein correlation effects, and beam remnants. These are connected with the rich structure of QCD beyond perturbation theory and are vital, each in their own way, to the understanding of issues such as underlying-event/pileup effects on isolation and accurate jet calibrations, and the interpretation of identified-particle rates and spectra.

For these aspects, explicit calculations can only be performed in the context of simplified phenomenological models, constructed so as to capture the essential features of full (nonperturbative) QCD. An example relevant to this paper is the Lund string model of hadronisation [23, 24], whose cornerstone is the observation that the static QCD potential between a quark and an antiquark in an overall colour-singlet state grows linearly with the distance between them, for distances larger than about 0.5 fm [25]. This is interpreted as a consequence of the gluon field between the charges forming a high-tension "string" (with tension $\kappa \sim 1\,\mathrm{GeV/fm}$), which subsequently fragments into hadrons.

While the details of the string-breaking process may be complicated (the Lund model invokes quantum tunnelling to describe this aspect [23]), the first question that any hadronisation model needs to address is therefore simply: *between which partons do confining potentials arise?* In string-based models, this is equivalent to answering the question between which partons string pieces should be formed. Traditionally, Monte Carlo event generators make use of the leading-colour (LC) approximation to trace the colour flow on an event-by-event basis (see [3, 26]), leading to partonic final states in which each quark is colour-connected to a single (unique) other parton in the event (equivalent to a leading-colour QCD dipole [27]). Gluons are represented as carrying both a colour and an anticolour charge, and are hence each connected to two other partons. At the level of strings, this is interpreted as gluons forming transverse "kinks" on strings whose endpoints are quarks and antiquarks [23]. Studies at *ee* colliders show this to be a quite reasonable approximation in that environment, and the traditional Lund string model, implemented in PYTHIA [28–30], is capable of delivering a good description of the vast majority of *ee* collider data (for recent studies, see, e.g., [31–34]).

The question of *colour reconnections* (CR) — broadly, whether other string topologies than the LC one could lead to non-negligible corrections with respect to the LC picture — was studied at LEP [35–42], chiefly in the context of CR uncertainties on W mass determinations in $ee \to WW$ [43], with conclusion that excluded the very aggressive models and disfavoured the no CR scenario at 2.8 standard deviation [44]. The uncertainty on the W mass from this source ended up at $\Delta m_W \sim 35\,\text{MeV}$, corresponding to about 0.05%.

There are strong physical reasons to think that CR effects *should* be highly suppressed at LEP, however. Firstly, there is a "trivial" parametric suppression of beyond-LC effects of order $1/N_C^2 \sim 10\%$. Secondly, the two W decay systems are separate colour-singlet systems, with a space-time separation of order of the inverse W width, $\Gamma_W \sim 2\,\text{GeV}$. This separation implies that interference effects between the two systems should be highly suppressed for wavelengths shorter than $1/\Gamma_W$, i.e., there can be essentially no perturbative cross-talk between them. This line of argument motivated the phrasing of CR models that operate only at the non-perturbative

level as the most physically reasonable [43], an observation that we shall also adhere to in the present work. Thirdly, the QCD coherence of perturbative parton cascades implies that, inside each W (or Z) decay system, angles of successive QCD emissions tend to be ordered from large to small [45], so that there is very little space-time overlap between the QCD dipoles inside each system. This means that, even if one were to allow to set up confining potentials between non-LC-connected partons, these would tend to correspond to *larger* opening angles and therefore they would have a higher total potential energy (longer strings) than the equivalent LC ones. The LC topology should therefore also be *dynamically* favoured over any possible non-LC ones. All these factors contribute to an expectation of quite small effects, at least in the context of e^+e^- collisions.

Moving to pp collisions (and using pp as a shorthand to for any generic hadron-hadron collision, including in particular also $p\bar{p}$ ones), the situation changes dramatically. Trivially, one must now include coloured initial-state partons, with associated coloured beam remnants. But more importantly, the modern understanding of the underlying event (UE) and of soft-inclusive (minimum-bias/pileup) physics in general, especially at high particle multiplicities, is that they are dominated by contributions from multiple parton interactions (MPI) [46]. In a pp event that contains several MPI systems, there is a non-negligible possibility of phase-space overlaps between final states from different MPI systems. Moreover, since the MPI scattering centres must all reside within the proton radius, which is of the same order as the transverse size of QCD strings, the initial-state (beam) jets will all "sit" right on top of each other, a situation which should affect the fragmentation especially at high rapidities. Finally, unlike the case for angular-ordered partons inside a jet, there is no perturbative principle that predisposes colour-connected partons from different MPI or beam-remnant systems to have small opening angles; indeed a recent study [47] found that such "inter-MPI/remnant" invariant masses (denoted i-type and n-type in [47]) tend to be among the largest in the events, corresponding to a high potential energy in a string context, and hence with the most to gain from potential reconnections. For these reasons, we expect qualitatively larger effects in pp collisions.

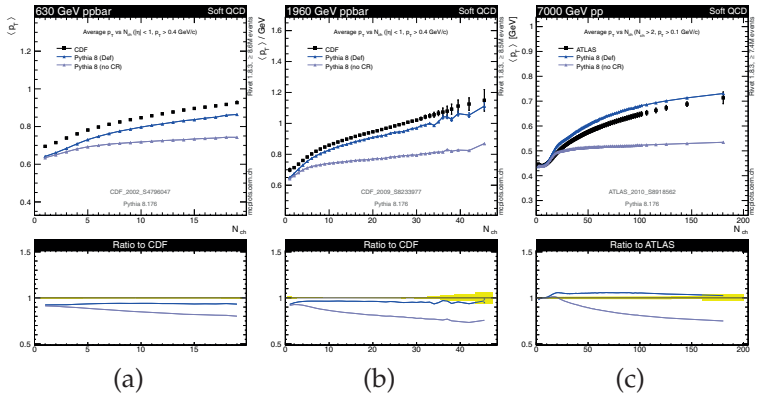

Figure II.1: Measurements of $\langle p_\perp \rangle (n_{Ch})$ in minimum-bias events at 630 GeV [50] (a), 1960 GeV [51] (b), and 7000 GeV [53] (c), compared to PYTHIA 8.175 [29] (tune 4C [56]), with and without colour reconnections switched on. (Plots from mcplots.cern.ch [55].)

There are also tantalising hints from hadron-collider data that nontrivial physics effects are present at the hadronisation stage in pp collisions. The most important such clue is furnished by the dependence of the average (charged) particle $p_\perp$ on the particle multiplicity, $\langle p_\perp \rangle (n_{\mathrm{ch}})$. Measurements of this quantity in minimum-bias events, first made at the ISR [48] and since by UA1 [49], CDF [50, 51] and the LHC experiments [52–54], reveal that $\langle p_\perp \rangle$ grows with n_{ch}, as can be seen in the plots in fig. II.1 (from mcplots.cern.ch [55]). This cannot be accounted for by independently hadronising MPI systems, for which the expectation would be that $\langle p_\perp \rangle (n_{\mathrm{ch}})$ should be almost flat, as is also illustrated by the "no CR" curves in fig. II.1. (If each MPI hadronises independently, then per-particle quantities such as $\langle p_\perp \rangle$ should be independent of the number of MPI, which is correlated with n_{Ch} [46].) The observation that $\langle p_\perp \rangle$ increases with n_{Ch} therefore strongly suggests that some form of collective hadronisation phenomenon is at play, correlating partons from different MPI systems.

Given these arguments, and the realisation [57] that precision kinematic extractions of the top quark mass at hadron colliders (see e.g., [58–64] for experimental methods and [65] for a recent phenomenology review) can be significantly affected by colour re-

connections[1], several toy models have appeared [47, 57, 68–71], relying mainly on potential-energy minimisation arguments to reconfigure the partonic colour connections for hadronisation. Although these models have had some success in describing the $\langle p_\perp \rangle (n_{\mathrm{Ch}})$ distribution (as e.g., in fig. II.1), the lack of rigorous underpinnings have implied that large uncertainties remain, which still contribute about a 500 MeV uncertainty on the hadronic top mass extraction [62, 65, 71]. In this paper, we take a first step towards creating a more realistic model, combining the earlier string-length minimisation arguments with selection rules based on the colour algebra of $SU(3)$. Our treatment amounts to taking the LC connections produced by the shower as a starting point, complemented by an $SU(3)$-weighted randomization over the set of possible subleading topologies that would have been present in a full-colour treatment. The missing colour information should thereby be restored, at least in a statistical sense.

An alternative line of argument, pursued in particular in the EPOS model [72], invokes the notion of hydrodynamic collective flow to explain the $\langle p_\perp \rangle (n_{\mathrm{Ch}})$ distribution (as well as the so-called CMS "ridge effect" [73, 74] and a host of other pp observables [72]). Certainly, the presence of hydro effects in pp is a hypothesis that, if confirmed, would have far-reaching consequences, and it will be an important task for future experimental and phenomenological studies to find ways of disentangling CR effects from hydro ones. In this context, our paper should therefore also be viewed as an attempt to see how far one can get *without* postulating genuine (pressure-driven) collective-flow effects in pp. Within this context, it is important to note that CR can mimic flow effects to some extent, via the creation of boosted strings [75]. Alternatively, it is possible that the effective string tension could be rising, as in the idea of colour ropes [76], with recent work along these lines reported on by the Lund group [77]. Finally, we note that non-hydro rescattering has also been proposed [78] as a potential mechanism contributing to the rise of $\langle p_\perp \rangle (n_{\mathrm{Ch}})$, though the explicit model of parton-parton rescattering effects presented in [78] found only very small effects. The possibility of Boltzmann-like elastic (or even inelastic) final-

1 For completeness we note that, similarly to above, much smaller effects are expected in e^+e^- environments [66, 67].

state hadron-hadron rescattering is still open. As usual, nature's solution is likely to involve an interplay of effects at different levels. Nevertheless, before exploring further effects at the hadron level, we believe it makes good sense to first examine the hadronisation process itself, which is the topic of this work.

Finally, we note that colour flows beyond LC have also been invoked in the context of J/ψ formation [79–82], and as a potential mechanism to generate diffractive topologies in ep and pp collisions [83, 84].

In section II.2, we briefly recapitulate the treatment of colour space for the existing MPI models in PYTHIA, and present the new model that we have developed, combining the minimisation of the string potential with the multiplet structure of QCD. In section II.3, we constrain the resulting free model parameters on a selection of both ee and pp data, discussing the physics consequences of the new colour-space treatment as we go along. In section II.4, we consider implications for precision extractions of the top quark mass at hadron colliders. Finally, in section II.5, we summarise and give an outlook.

II.2 THE MODEL

In this section, we present the colour-space model that we have developed, which allows strings to form not only between LC-connected partons, but also between specific non-LC-connected ones, following combination rules that approximate the multiplet structure of full-colour QCD. We begin with a brief summary of the current modelling, in section II.2.1. We then turn to a general discussion of coherence effects beyond leading N_C in section II.2.2. Finally, in section II.2.3, we present the detailed implementation of the new model.

We emphasise that there is a conceptual difference between colour-space *ambiguities*, such as those explored in this work, and physical colour *reconnections*. The subleading-colour effects we discuss here arise naturally in "full-colour" $SU(3)$ and do not involve any physical exchange of colour or momentum (although explicit algorithms may of course still employ an iterative-reconnection scheme to find the potential-energy minimum). Strictly speaking,

the term colour *reconnections* should be reserved to describe effects related to *dynamical* reconfigurations of the colour/string space that involve explicit exchange of colours and momentum, via perturbative gluon exchanges or non-perturbative string interactions. Effects of this type are not explored directly in this work, instead we refer the interested reader to the SK string-interaction models presented in [43, 66, 67]. Somewhat sloppily, we follow the entrenched convention in the field and use the acronym "CR" for effects of either kind here.

II.2.1 *Existing MPI Models and Colour Space*

In a naive LC picture, each MPI scattering system is viewed as separate and distinct from all other systems in colour space. The very simplest colour-space options in the old PYTHIA 6 MPI model [46] and the first HERWIG (and HERWIG++) MPI models [85, 86] go a step further, representing each MPI final state as two quarks (or gluons), colour-connected directly to each other, i.e., treating each MPI system as a separate hadronising colour-singlet system. However, this ignores that the incoming partons are coloured, and hence that the total colour charge of each MPI scattering system is in general non-zero. These particular models therefore violate colour conservation and are unphysical.

To be LC-correct one must take into account that each MPI-initiator parton should cause one or two strings to be stretched to its remnant (one for quarks, two for gluons). This conserves colour, but still has the implication that no strings would be stretched *between* different MPI systems. This situation is illustrated in fig. II.2a. Physically, this can lead to arbitrarily many strings being stretched across the central rapidity region, one or two for each MPI (corresponding to adding their total colour chargers together as scalar quantities, rather than as $SU(3)$ vectors).

However, already in the context of earlier works [46, 87], it was noted that even this picture cannot be quite physically correct. Since all the MPI initiators on each side are extracted from one and the same (colour-singlet) beam particle, and since they are extracted at a rather low scale of order the perturbative evolution cutoff $p_{\perp 0} \sim$ one to a few GeV, there is presumably some over-

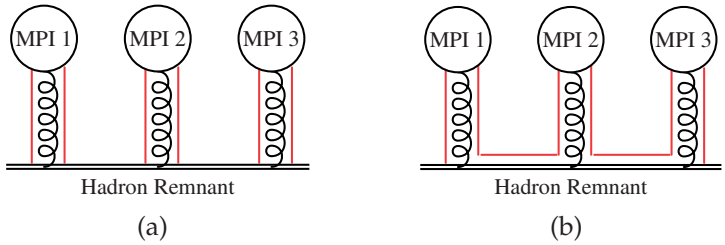

Figure II.2: (a): in a strict LC picture, each MPI initiator gluon increases the "colour charge" of the beam remnant by two units. (b): allowing different MPI initiators to be connected in a colour chain reduces the total colour charge of the remnants. Here for example, no strings will be stretched directly between the shown remnant and the final states of MPI 2. (Note that the colour assignments shown are for illustration only, and would be represented by Les Houches Colour Tags [5, 6] in a real event generator.)

lap and accompanying saturation effects, implying that they are not completely independent. Not knowing the exact form of the correlations, a pragmatic solution is to minimise the total colour charge of the remnant (and hence the number of strings stretched to it), by allowing the different MPI systems to be colour-connected to each other along a "chain" in colour space, as illustrated in fig. II.2b. Variations of this are used in the current forms of both the PYTHIA [46, 87] and HERWIG++ [47] MPI models, reducing the number of strings/clusters especially in the remnant-fragmentation region at high rapidities. It is, however, still fundamentally ambiguous exactly which systems to connect and how. In the example of fig. II.2, it is arbitrary that it happens to be the colour of MPI 1 and the anticolour of MPI 3 which end up connected to the remnant. For a more detailed discussion of this aspect, see e.g. [87]. An interesting physics point is that, in this picture, the particle production at very forward rapidities is controlled essentially by how large one allows the colour charge of the remnant to become, which in turn depends on the number of MPI and their mutual colour correlations. This could presumably be revealed by studies correlating the particle production in the central region (sensitive to the number of MPI) with that in the forward region (sensitive to the total charge of the remnant).

In the absence of any further CR effects, the relationship between the number of MPI and the average particle multiplicity at central rapidities is still approximately linear. Consequently, the per-particle spectra in high-multiplicity events (with many MPI) are similar to those in (non-diffractive) low-multiplicity events (with few MPI)[2]. This is what leads to the simple expectation of the flat $\langle p_\perp \rangle (n_{\mathrm{Ch}})$ spectrum exhibited by the "no CR" curves that were shown in fig. II.1 in the previous section. However, as was also remarked on there, the experimental data convincingly rule out such a constant behaviour. This observation is the main reason additional non-trivial final-state CR effects have been included in both HERWIG++ and PYTHIA.

In the original (non-interleaved) MPI model in PYTHIA 6 [28, 46], the parameters `PARP(85)` and `PARP(86)` allowed to force a fraction of the MPI final states to be two gluons colour-connected to their nearest neighbours in momentum space. The physical picture was that the hardest interaction built up a "skeleton" of string pieces, onto which a fraction of the gluons from MPI were grafted (by brute force) in the places where they caused the least amount of change of string length. This effectively minimised the increase in string length from those gluons. An important factor contributing to the revival of the question of CR in hadron collisions was the tuning studies of this model, carried out by Rick Field on underlying-event and minimum-bias data from the CDF experiment at the Tevatron [50, 88, 89]. His resulting "Tune A" and related tunes [90, 91] were the first to give good fits to the available data at the time, but the surprising conclusion was that in order to do so this "colour-space grafting" had to be done nearly all the time.

An alternative set of CR models, which relied on physical analogies with overlapping strings in superconductors, were developed only in the context of e^+e^- collisions [43, 66, 67], chiefly with the aim of studying potential CR uncertainties on the W mass, see [92] and references therein. As far as we are aware, this class of mod-

2 For very low multiplicities, well-understood bias effects cause the average particle $p_\perp$ to increase (if the event is required to contain only one particle, then that particle must be carrying all the scattered energy), while for high multiplicities, the contribution from hard-jet fragmentation also generates slightly harder spectra.

els has not yet been applied in the context of the more complex environment of hadron-hadron collisions.

In the new (interleaved) MPI model in PYTHIA 6 [14, 28], showers and MPI were carried out in parallel, with physical colour flows. This was too complicated to handle with the old CR model. A new "colour annealing" CR scenario was developed [57, 69, 93] which, after the shower evolution had finished, allowed for a fraction of partons to "forget" their LC colour connections, with new ones determined based on the string area law (shorter strings are preferred), following a simplified annealing-like algorithm, in a similar spirit to an earlier model by Rathsman, called the "Generalized Area-Law" (GAL) model [68]. The fraction of partons that forgot their LC colour connections was assumed to grow with the number of MPI, with a per-MPI probability given by the parameter `PARP(78)`. A further parameter, `PARP(77)`, allowed to suppress the reconnection probability for fast-moving partons. Although still intended as a toy model, the new colour-annealing models obtained good agreement with the Tevatron minimum-bias and underlying-event data, e.g. in the form of the Perugia family of tunes [94, 95]. The most recent incarnations, the Perugia 2011 and 2012 tunes, also included LHC data and were among the main reference tunes used during Run 1 of the LHC [95]. However, a study comparing independent MPI+CR tunings at different collider energies revealed different preferred CR parameter values at different CM energies [96], implying that the modelling of this aspect, or at least its energy dependence, was still inadequate.

In PYTHIA 8, the default MPI colour-space treatment is similar to that of the original PYTHIA 6 model, although starting out from a more detailed modelling of the colour flow in each MPI. With a certain probability, controlled by the parameter `ColourReconnection:range`, all the gluons of each lower-$p_\perp$ interaction can be inserted onto the colour-flow dipoles of a higher-$p_\perp$ one, in such a way as to minimise the total string length [71]. The effects of this model was already illustrated in fig. II.1. A set of alternative CR scenarios was also presented in [71], but were still mostly intended as toy models in the context of estimating uncertainties on the top-quark mass.

Finally, in the most recent developments of the HERWIG++ MPI model, an explicit scenario for colour reconnections has likewise been introduced [47], based on a simulated-annealing algorithm that minimises (sums of) cluster masses. In the context of the cluster hadronisation model [97], the minimisation of cluster masses fulfils a similar function as the minimisation of string lengths above. The two minimisations differ in that the string length measure is closely related to the product of the invariant masses rather than the sum used in the cluster model. The main model parameter is the probability to accept a favourable reconnection, p_{reco}. The study in [47] emphasised in particular that the largest pre-reconnection cluster masses are spanned between hard partons and the remnants (denoted *n*-type clusters), with inter-MPI ones (spanned directly between partons from different MPI systems and denoted *i*-type) having the second-largest masses. The former again indicates that there is a non-trivial interplay with the non-perturbative hadronisation of the beam remnant, while the latter reflects the lack of a priori knowledge about the colour correlations *between* different MPI systems. Similarly to the qualitative conclusions made with the PYTHIA CR models, the HERWIG++ study found that quite large values of $p_{\text{reco}} \sim 0.5$ were required to describe hadron-collider data.

II.2.2 *Beyond Leading Colour*

To illustrate the colour-space ambiguity between different MPI systems, and between them and the beam remnant, let us take the simple case of double-parton scattering (DPS), with all the initiator partons being gluons. What happens in colour space when we extract *two* gluons from a proton? Even if we imagine that the two gluons are completely uncorrelated, QCD gives several possibilities for their superpositions:

$$\mathbf{8} \otimes \mathbf{8} = \mathbf{27} \oplus \mathbf{10} \oplus \overline{\mathbf{10}} \oplus \mathbf{8} \oplus \mathbf{8} \oplus \mathbf{1} \,. \tag{II.2.1}$$

The highest-charge multiplet, here the **27** (a "viginti-septet"), effectively corresponds to the LC configuration: symmetric addition of the two gluons, each carrying two units of (LC) colour charge (one colour and one anticolour), for a total of 4 string pieces required to

be attached to the remnant[3]. However, note that the probability for this to occur is

$$P_{\mathrm{LC}} = \frac{27}{64} < 50\% \,, \tag{II.2.2}$$

hence the naive expectation that subleading topologies should be suppressed by $1/N_C^2$ is badly broken already in this very simple case[4]. The decuplets (octets) correspond to coherent-superposition topologies with a lower total colour charge and consequently only three (two) string pieces attached to the remnant. The singlet represents the special case in which the two MPI-initiator gluons have identical and opposite colours, with total colour charge 0 (generating a diffractive-looking topology from the point of view of the remnant). In QCD, for two random (uncorrelated) gluons, there is a $1/64$ probability for this to happen purely by chance.

The other possible two-parton combinations are:

$$\mathbf{3} \otimes \mathbf{8} = \mathbf{15} \oplus \overline{\mathbf{6}} \oplus \mathbf{3} \,, \tag{II.2.3}$$

$$\mathbf{3} \otimes \overline{\mathbf{3}} = \mathbf{8} \oplus \mathbf{1} \,, \tag{II.2.4}$$

$$\mathbf{3} \otimes \mathbf{3} = \mathbf{6} \oplus \overline{\mathbf{3}} \,, \tag{II.2.5}$$

where strict LC would correspond to populating only the **15** (quindecuplet), **8** (octet), and **6** (sextet), respectively. The relative weights (probabilities) for each multiplet in each of these combinations are illustrated in fig. II.3, along with diagrams exemplifying corresponding colour flows (with thick lines indicating partons, thin ones colour-flow lines). For each multiplet, three vertical bars indicate the probability associated with that multiplet in strict Leading Colour (LC), in our model (defined below), and in $SU(3)$ (QCD), respectively. The filled circles represent the *ratio* between our model and QCD, so for those *unity* indicates perfect agreement. Note that, since the subleading multiplets are absent in LC, only two non-zero bars appear for them. Below, we shall also consider the probability

3 Assuming each string can only carry one unit of flux, or equivalently a 4-unit "colour rope", see [77].

4 In general, the highest-charge multiplet in the combination of k gluons represents a fraction $(k+1)^3/8^k$ of the possibilities.

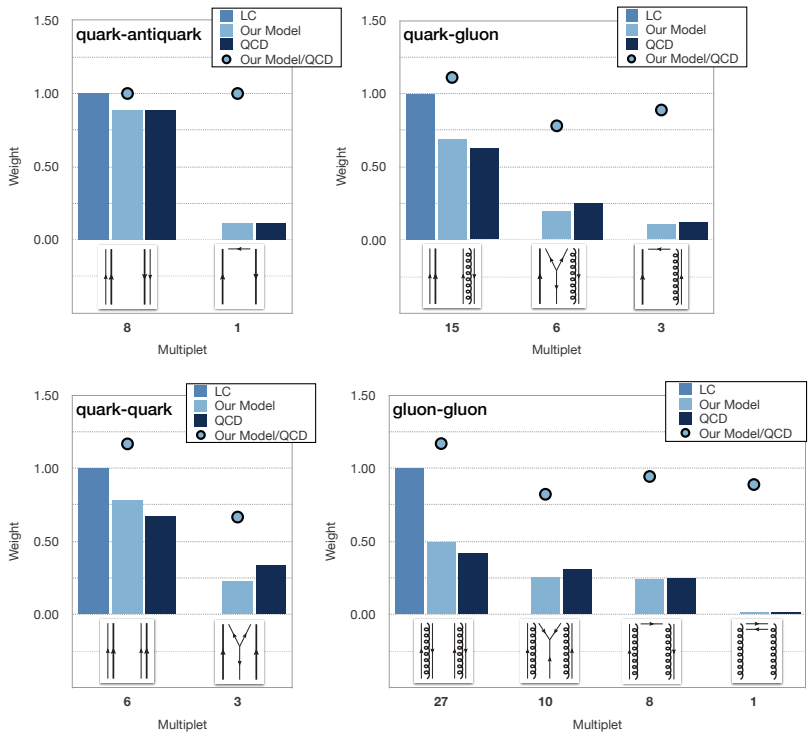

Figure II.3: Illustration of the possible colour states of two random (uncorrelated) partons. In strict LC, only the completely incoherent superposition is populated. Our model (described below) gives a systematically better approximation. Filled circles show the ratio between our model and full $SU(3)$. The diagrams below the histograms attempt to illustrate corresponding colour-flow configurations, with thick and thin lines denoting partons and colour-flow lines, respectively.

for three uncorrelated triplets to form an overall singlet, which is $1/27$ in QCD:

$$\mathbf{3} \otimes \mathbf{3} \otimes \mathbf{3} \quad = \quad \mathbf{10} \oplus \mathbf{8} \oplus \mathbf{8} \oplus \mathbf{1} \ , \tag{II.2.6}$$

while in our simplified model it will come out to be $2/81 = (1 - \frac{1}{3})/27$.

We emphasise that we only use these composition rules for colour-unconnected partons, which in the context of our model we approximate as being totally uncorrelated. LC-connected partons are always in a singlet with respect to each other, and colour neigh-

bours (e.g., the two colour lines of a gluon or those of a $q\bar{q}$ pair produced by a $g \to q\bar{q}$ splitting) are never in a singlet with respect to each other.

The approximation of colour-unconnected partons being totally uncorrelated, combined with a set of specific colour-space parton-parton composition rules, such as those of $SU(3)$ or the simplified ones defined below, allow us to build up an approximate picture of the possible colour-space correlations that a complicated parton system can have, including randomised coherence effects beyond Leading Colour. Due to the subleading correlations, there are many possible string topologies that could represent such a parton system, including but not limited to the LC one. The selection principle that determines how the system collapses into a specific string configuration will be furnished by the minimisation of the string potential, as we shall return to below.

Our model thus consists of two stages. First, we generate an approximate picture of the possible colour states of a parton system. Then, we select a specific realisation of that state in terms of explicit string connections. This is done at the time when the system is prepared for hadronisation, i.e., after parton showering but before string fragmentation.

By maintaining the structure of the (LC) showers unchanged, we neglect any possibility of reconnections occurring already at the perturbative level. Though perturbative gluon exchanges and/or full-colour shower effects might mediate such effects in nature, we expect their consequences to be suppressed relative to the non-perturbative ones considered here. This is partly due to the coherence and collinear-enhancement properties already acting to minimise the mass of LC dipoles inside each perturbative cascade, and partly due to the space-time separation between different systems (be they different MPI systems, which are typically separated by transverse distances of order $1/\Lambda_{\mathrm{QCD}}$ inside the proton, or different resonance-decay systems separated by $1/\Gamma_{\mathrm{res}}$). Thus, at high $Q \gg \Lambda_{\mathrm{QCD}}$ or $Q \gg \Gamma_{\mathrm{res}}$ we don't expect any cross-talk between different MPI or different resonance systems, respectively. The case can be made that perturbative reconnection effects could still be active at longer wavelengths, but we expect that such semi-soft

effects can presumably be absorbed in the non-perturbative modelling without huge mistakes.

II.2.3 *The New Model*

Our simplified colour-space model is defined as follows. Rather than attempting to capture the full correlations (which we have emphasised are not a priori known anyway and would require a cumbersome matrix-based formalism), we note that the main subleading parton-parton combination possibilities of real QCD can be encoded in a single "colour index", running from 1 to 9 (with corresponding indices for anti-colours).

Quarks are assigned a single such colour index, antiquarks a single anticolour index, and gluons have one of each, with the restriction that their colour and anticolour indices cannot be the same. Thus, formally our model has 9 different quark colour states and 72 kinds of gluon states. We emphasise that these indices should not be confused with the ordinary 3-dimensional $SU(3)$ quark colour indices (red, green, and blue); rather, our index labels the possible colour states of two-parton (and in some cases three-parton) *combinations*. Thus, for example, a quark and an antiquark are in an overall colour-singlet state if the colour index of the former equals the anticolour index of the latter, otherwise they are in an octet state, cf. eq. (II.2.4). We note that a similar index was used already in the models of "dipole swing" presented in [98, 99], though here we generalise to parton combinations involving colour-epsilon structures as well, cf. fig. II.3.

Confining potentials will be allowed to form between any two partons that have matching colour and anticolour indices. Since LC-connected partons are forced to have matching colour and anticolour indices, the "original" (LC) string topology always remains possible, but now further possibilities also exist involving partons that *accidentally* have matching indices, illustrated in fig. II.4.

Furthermore, two *colour* indices are allowed to sum coherently to a single *anticolour* index within three separate closed index groups: [1,4,7], [2,5,8], and [3,6,9]. E.g., two quarks carrying indices 2 and 5 respectively, are allowed to appear to the rest of the event as carrying a single combined anti-8 index. These index combinations

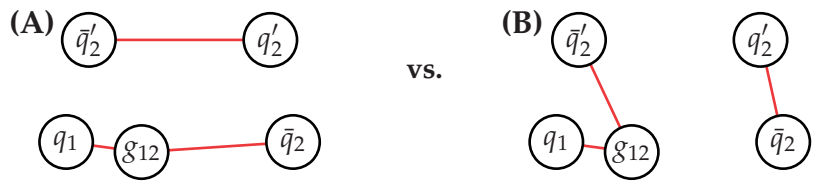

Figure II.4: Illustration of a multi-parton state with a rather simple colour-space ambiguity. Subscripts indicate colour-space indices. *(A):* the "original" (LC) string topology. *(B):* an alternative string topology, allowed by the accidentally matching "2" indices.

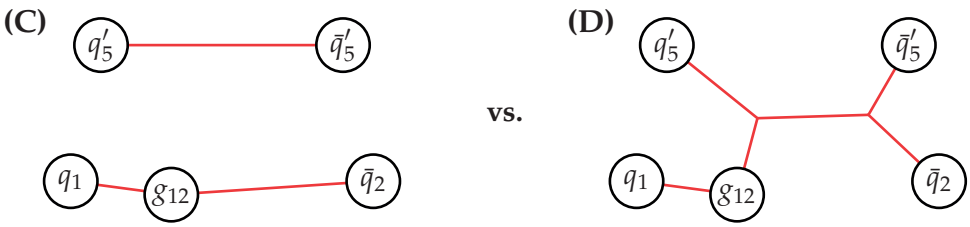

Figure II.5: Illustration of a similar multi-parton state as in fig. II.4, but now with index assignments resulting in a junction-type colour-space ambiguity. The orientation of the top $q'_5 - \bar{q}'_5$ dipole has also been reversed relative to fig. II.4. *(C):* the original (LC) string topology. *(D):* an alternative string topology with a junction and an antijunction, allowed by the cyclically matching "2" and "5" indices.

represent the antisymmetric ε_{ijk} colour combinations that were pictorially represented as Y-shaped "colour junctions" in fig. II.3. A junction can therefore be interpreted as the string extension of a baryon with the baryon number (ε_{ijk}) located in the centre of the Y-shape [100]. An explicit example of a parton system whose colour state includes such a possibility is shown in fig. II.5. A model for string hadronisation of such topologies was developed in [100] and has subsequently also been applied to the modelling of baryon beam remnants [87]. We reuse it here for hadronisation of junction-type colour-index combinations.

The new model can be divided into two main parts: a new treatment of the colour flow in the beam remnant and a new CR scheme.

The two models are independent and can therefore in principle be combined both with each other as well as with other models. (Note, however, that the old PYTHIA 8 CR scheme is inextricably linked with the colour treatment of the beam remnant and therefore only works together with the old beam-remnant model.) Both of the models occasionally result in complicated multi-junction configurations that the existing PYTHIA hadronisation cannot handle. Rather than attempting to address these somewhat pathological topologies in detail, this problem is circumvented by a clean-up method that simplifies the structure of the resulting systems to a level that PYTHIA can handle.

The next two sections describe respectively the details of the new beam-remnant model and the new CR scheme, including technical aspects and the algorithmic implementation. Afterwards the junction clean-up method is described.

Colour Flow in the Beam Remnant

It being an inherently non-perturbative object, we do not expect to be able to use perturbative QCD to understand the structure of the beam remnant. Instead, we rely on conservation laws; the partons making up the beam remnant must, together with those that have been kicked out by MPI, sum up to the total energy and momentum of the beam particle, be in an overall colour-singlet state, with unit baryon number (for a proton beam), carrying the appropriate total valence content for each quark flavour, with equal numbers of sea quarks and antiquarks. The machinery used to conserve all these quantities should be consistent with whatever knowledge of QCD we possess, such as the standard single-parton-inclusive PDFs to which our framework reduces in the case of single-parton scattering.

In this work the focus is on the formation of colour-singlet states, including the use of $SU(3)$ epsilon tensors. This naturally leads to a modification of the treatment of baryon number conservation, due to the close link between baryons and the epsilon tensors in $SU(3)$. The modelling of energy/momentum and flavour conservation is not touched relative to the existing modelling of those aspects, and thus only a small review is presented here (for more details see [87]).

The overall algorithm can be structured as follows:

1. Determine the colour structure of the already scattered partons.
2. Add the minimum amount of partons needed for flavour conservation.
3. Add the minimum amount of gluons required to obtain a colour-singlet state.
4. Connect all colours.
5. With all the partons determined find their energy fractions.

The conservation of baryon number is not listed as a separate point, but naturally follows from the formation of junctions. Let us now consider each of these points individually starting from the top.

To calculate the colour structure of the beam remnant, let us return to the DPS example of earlier. With a probability of $27/64$, the two gluons form a completely incoherent state, leaving four colour charges to be compensated for in the beam remnant (two colours and two anticolours). However the three valence quarks alone are insufficient to build up a **27** (eq. (II.2.6)), and therefore a minimum of one additional gluon is needed. Then two of the quarks can combine to form a $\bar{\mathbf{3}}$, which can form an **8** with the remaining valence quark, which then can enter in a **27** with the added gluon. Conversely, if the two gluons had been in an octet state instead, the additional gluon would not have been needed. Thus, in order to determine the minimal number of gluons needed in the beam remnant, we need to know the overall colour representation of all the MPI initiators combined.

While it could be possible to choose this representation purely statistically, based on the (simplified or full) $SU(3)$ weights, we note two reasons that a lower total beam-remnant charge is likely to be preferred in nature. Firstly, to determine the most preferred configuration the string length needs to be considered. Since the beam remnants reside in the very forward regime, strings spanned between the remnant and the scattered gluons tend to be long, and as such a good approximation is to minimise the number of strings spanned to the beam. This corresponds to preferring a low-charge

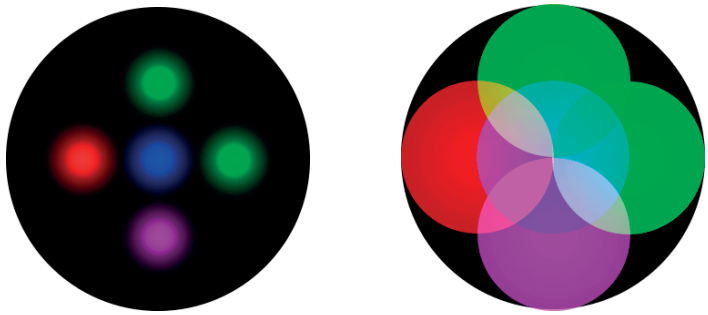

(a) $Q^2 \gg \Lambda^2_{\mathrm{QCD}}$ (b) $Q^2 \sim \Lambda^2_{\mathrm{QCD}}$

Figure II.6: A proton (black) with five distinct colour sources (e.g., four MPI-initiator partons plus one representing the beam remnant), chosen so that they add to a singlet (with magenta = antigreen). Shown are two different resolution scales representative of (a) the perturbative stage, during which the MPI systems are considered as being uncorrelated in colour space, and (b) the nonperturbative stage, at which the beam remnant is considered and we assign higher weights to states with lower total QCD charge in order to mimic saturation effects.

colour-multiplet state for the remnant, and as a consequence also minimises the number of additional gluons required. Secondly, a purely stochastic selection corresponds to the assumption that the scattered partons are uncorrelated in colour space. For hard MPIs (at $Q \gg \Lambda_{\mathrm{QCD}}$), this is presumably a good approximation, since the typical space-time separation of the collisions are such that two independent interactions do not have time to communicate. This is illustrated by fig. II.6a. However, after the initial-state radiation is added, the lower evolution scale implies larger spatial wavefunctions, allowing for interference between different interactions, illustrated by fig. II.6b. An additional argument is that at a low evolution scale the number of partons is low, thus to combine to an overall singlet the correlation between the few individual partons needs to be large. To provide a complete description of this cross-talk, multi-parton densities for arbitrarily many partons would be needed, ideally including colour correlations and saturation effects. Although correlations in double-parton densities has been the topic of several recent developments [101–109], the field is still not at a stage at which it would be straightforward

to combine explicit double-parton distributions with the standard single-parton-inclusive ones (which a code like PYTHIA must be compatible with), nor to generalise them to arbitrarily many partons. The only formalism we are aware of that addresses all of these issues (in particular flavour and momentum correlations for arbitrarily many partons) while reducing to the single-parton ones for the hardest interaction remains the one developed in the context of the current PYTHIA beam-remnant model [87]. In this study, we supplement the momentum- and flavour-correlation model of [87] with a simple model of colour-space saturation effects appropriate to the $SU(3)$-multiplet language used in this work. Noting that saturation should lead to a suppression of higher-multiplet states, we use a simple ansatz of exponential suppression with multiplet size, M:

$$p(M) = \exp\left(-M/k_{\text{saturation}}\right) \tag{II.2.7}$$

where p is the probability to accept a multiplet of size M and $k_{\text{saturation}}$ is a free parameter that controls the amount of suppression.

Everything stated above for the two-gluon case can be generalised to include quarks and an arbitrary number of MPI. The calculation just extends to slightly more complicated expressions:

$$\mathbf{8} \otimes \mathbf{3} \otimes \bar{\mathbf{3}} \otimes \mathbf{8} \otimes \ldots \;=\; \ldots \tag{II.2.8}$$

where quarks enter as triplets, antiquarks as antitriplets and gluons as octets. The statistical probability to choose any specific multiplet can be calculated in a similar fashion, either in full or simplified QCD. There is however still an ambiguity in how the colours are connected. For instance consider two quarks and one antiquark forming an overall triplet state. The colour calculation will not tell us which of the quarks are in a singlet with the antiquark. In the case of ambiguities, the implementation is to choose randomly. The CR algorithm applied later may anyhow change the initial colour topology, lessening the effect of the above choice.

At the level of the technical implementation, the choice of colour state for the scattered partons is transferred to the final state particles of the event using the LC structure of the MPI and PS. For

example, if the two gluons are in the octet state, one of the LHE colour tags (see [5, 6]) is changed accordingly, and is propagated through to the colour of the final state particles.

As a special case the overall colour structure of the beam remnant is not allowed to be a singlet. This is to avoid double-counting between diffractive and non-diffractive events. In the DPS example, if the gluons form a colour singlet, they essentially make up (part of) a pomeron, and thus should fall under the single-diffractive description. It would be interesting to look into the interplay between MPI and diffraction in more detail using the colour-multiplet language developed here, but this would require its own dedicated study, beyond the scope of this work.

The conservation of flavour is relative straightforward and follows [87]. The principle used is to add the minimum needed flavour. For example if only an s quark is scattered from a proton, the remnant will consist of an $\bar{s}$ plus the three valence quarks.

With the flavour structure and colour multiplet of the beam remnant known, it is now possible to calculate explicitly how many gluons need to be added to obtain a colour-singlet state. Again the idea is to add the minimum number of gluons to the beam remnant. Colour-junction structures, which we have argued can arise naturally in the colour structure of the scattered partons, complicate this calculation slightly. To achieve an overall colour-singlet state the number of junctions minus the number of antijunctions has to match that of the beam particle. Taking this into account the minimal number of gluons is given by

$$N_{\text{gluons}} = \max\left(0, \frac{(N_{\text{colour}} - N_{\text{quarks}} + \|N_{\text{junctions}} - N_{\text{antijunctions}} - b\|)}{2}\right); \tag{II.2.9}$$

where b is the beam baryon number (1 if the beam is a baryon, 0 if the beam is a meson, and -1 if the is an antibaryon). The division by two is due to the gluons carrying two colour lines. Without junctions, the number of gluons is simply the number of colour lines to the remnant minus the number of available quarks to connect those colour lines to. It is easiest to understand how junctions change this, by noting that the creation of a junction basically takes two colour

charges and turn into one anticolour. Thus the number of required connections goes down by one for each additional junction needed.

After the gluons are added, all the colour connections and junction structures are assigned randomly between the remaining colours, with one exception: if the beam particle is a baryon and a junction needs to be constructed (similarly for an antibaryon and an antijunction), two of the valence quarks will be used to form the junction structure (possibly embedded in a diquark), if they have not already been scattered in the MPIs.

With finally the full parton structure known, including both flavours and explicit colours, the last step of the construction of the beam remnant is the assignment of energy fractions (x values) to each remnant parton, according to modified PDFs. To obtain overall energy-momentum conservation, the individual partons are scaled by an overall factor. The scaling becomes slightly more complicated by the introduction of primordial $k_\perp$. Details on the modified PDF versions and the scaling can be found in [87].

Colour Flow in the Whole Event

As discussed above, the CR model is applied after the parton-shower evolution has finished (and after inclusion of the beam-remnant partons as described in the preceding subsection), just before the hadronisation. The model builds on two main principles: a simplified $SU(3)$ structure of QCD, based on indices from 1 to 9, to tell which configurations are possible; and the potential energy of the resulting string systems, as measured by the so-called λ measure [23], to choose between the allowed configurations.

The starting point for the model is the LC configuration emerging from the showers + beam remnants. Thus between each LC-connected pair of partons a tentative dipole is constructed. This configuration is then changed by allowing two (or three) dipoles to reconnect, and this procedure is iterated until no more reconnections occur. In each step of the algorithm, four different types of reconnections can occur, illustrated in fig. II.7:

1. simple dipole-type reconnections involving two dipoles that exchange endpoints (fig. II.7a);

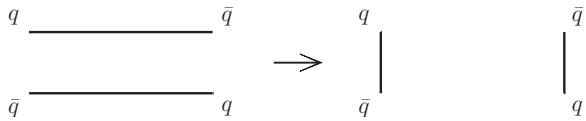

(a) Type I: ordinary dipole-style reconnection

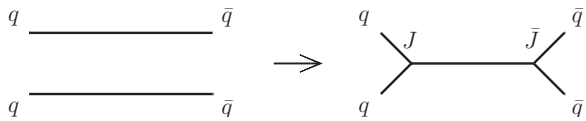

(b) Type II: junction-style reconnection

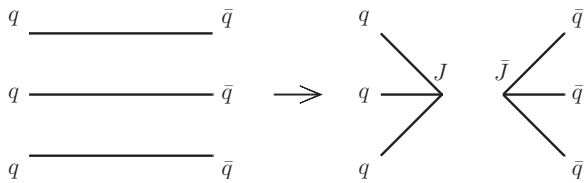

(c) Type III: baryon-style junction reconnection

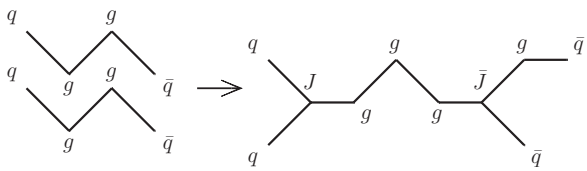

(d) Type IV: zipper-style junction reconnection

Figure II.7: The four different allowed reconnection types. Type I (a) is the ordinary string reconnection. Type II (b) is the formation of a connected junction antijunction pair. Type III (c) is the formation of junction and antijunction, which are not directly connected. Type IV (d) is similar to type II except that it allows for gluons to be added between the two junctions.

2. two dipoles can form a junction-antijunction structure (fig. II.7b);

3. three dipoles can form a junction-antijunction structure (fig. II.7c);

4. two multi-parton string systems can form a junction and an antijunction at different points along the string and connect them via their gluons (fig. II.7d).

Note that, although mainly dipoles between quarks are shown in the illustrations, all dipoles (q-$\bar{q}$, q-g, g-$\bar{q}$ and g-g) are treated in the same manner in the implementation. Within an LC dipole, the quark and antiquark are assumed to be completely colour coherent, so that the probabilities for two dipoles to be in a colour-coherent state can be found by the standard $SU(3)$ products. In full QCD, the probabilities for type I (dipole) and II (junction) reconnections for q-$\bar{q}$ dipoles are given by eq. (II.2.4) and (II.2.5) as $P_{\mathrm{I}}^{q\bar{q}} = 1/9$ and $P_{\mathrm{II}}^{qq} = 1/3$, respectively. For gg dipoles, the calculation is complicated slightly by the fact that eq. (II.2.1) takes into account both the colour and anticolour charges of both of the gluons. With a probability of $P_{\mathrm{I}}^{gg} = 8/64 = 1/8$ each, either "side" (colour or anticolour) of the gluons are allowed to reconnect (for a $1/64$ probability that CR is allowed on both sides). And with a total probability of $P_{\mathrm{II}}^{gg} = 20/64 = 5/16$ either one *or* the other side is allowed a junction-type reconnection (both sides would be equivalent to a dipole-style reconnection already counted above). For simplicity, the index rules described in the beginning of this section have been defined to treat $q\bar{q}$, qg, and gg dipoles all on an equal footing. The result is a compromise of $P_{\mathrm{I}} = 1/9$ for all dipole-type reconnections and $P_{\mathrm{II}} = 2/9$ for all junction-type reconnections. Differences between $q\bar{q}$ and gg combinations still arise due to gluons being prevented from having the same colour and anticolour indices, and since the combination of two type-II reconnections is equivalent to a type-I reconnection. A comparison between the weights resulting from our simplified treatment and the multiplet weights in full QCD for the simple case of two-parton combinations was illustrated in fig. II.3. Note also that the probability for a type-III reconnection among three uncorrelated $q\bar{q}$ dipoles (essentially creating a baryon from three uncorrelated quarks) is $P_{\mathrm{III}}^{qqq} = 1/27$ in full QCD (among

the 27 different ways to combine 3 quarks, only one is a singlet) while it is only 2/3 as large in our model; $P_{\mathrm{III}} = 2/9 \times 1/9 = 2/81$. Although our model should be a significant step in the right direction, we therefore still expect a tendency to underestimate baryon production. When tuning the model below, we shall see that we are able to compensate for this by letting junction-type reconnections appear somewhat more energetically favourable compared with dipole-type reconnections.

To recapitulate the model implementation, each dipole is assigned a random index value between 1 and 9. Two dipoles are allowed to do a type-I reconnection if the two numbers are equal, providing the 1/9 probability. Type-II reconnections are allowed if the two numbers modulo three are equal and the indices are different (e.g. 1-4 and 1-7), thereby providing the 2/9 probability. Three dipoles are allowed to do the type-III reconnection if they all have the same index modulo three and are all different (1-4-7). The type-IV reconnection follows the same principles: a dipole needs to have the same index, and a junction needs to have different-but-equal-under-modulo-three index. The exact probability for type-IV reconnections depend on the number of gluons in the string.

The number of allowed colour indices can in principle be changed (the 9 above), e.g. to vary the strength of CR. However, the type-II, -III, and -IV reconnections rely on the use of modulo, thus care should be taken if junction formation is allowed. A different method to control the strength of the CR will be discussed below.

The above colour considerations only tell which new colour configurations are *allowed* and not whether they are *preferable*. To determine this, we invoke a minimisation of the λ string-length measure. The λ measure can be interpreted as the potential energy of a string, more detailed it is the area spanned by the string prior to hadronisation. It is closely connected to the total rapidity span of the string, and thereby also its total particle production. The minimisation is carried out by only allowing reconnections that lower the λ measure, which ensures that a local minimum is reached.

A further complication is that, while the λ-measure for a quark-antiquark system with any number of gluon kinks in between is neatly defined by an iterative procedure [23], the measure defined there did not include junction structures. The first extension to

handle these were achieved by starting from the simple measure between a quark antiquark dipole [100]:

$$\lambda^{q\bar{q}} \;=\; \ln\left(1+\frac{s_{q\bar{q}}}{2m_0^2}\right) \tag{II.2.10}$$

where $s_{q\bar{q}}$ is the dipole mass squared and m_0 is a constant with dimensions of energy, of order Λ_{QCD}. For high dipole masses, the "1" in eq. (II.2.10) can be neglected, splitting the λ-measure neatly into two parts: one from the quark and one from the antiquark end (in the dipole rest frame):

$$\lambda^{q\bar{q}} \overset{s\gg m_0^2}{\to} \ln\left(\frac{s}{2m_0^2}\right) \;=\; \ln\frac{\sqrt{2}E_q}{m_0}+\ln\frac{\sqrt{2}E_{\bar{q}}}{m_0}\,. \tag{II.2.11}$$

The extension to handle a junction system used the same method, going to the junction rest-frame and adding up the "λ-measures" from all the three (anti-)quark ends. The end result became

$$\lambda^{q_1q_2q_3} = \ln\frac{\sqrt{2}E_1}{m_0}+\ln\frac{\sqrt{2}E_2}{m_0}+\ln\frac{\sqrt{2}E_3}{m_0} \tag{II.2.12}$$

where the energies are calculated in the junction rest frame[5]. This procedure worked well in the scenarios considered in that study, since all the dipoles had a relative large mass. However, in the context of our CR model, we will often be considering dipoles that have quite small masses. In that case, continuing to ignore the "1" in eq. (II.2.10) can lead to arbitrarily large negative λ measures. Among other things, such a behaviour could allow soft particles with vanishing string lengths to have a disproportionately large impact on dipoles with a large invariant mass. Generalising this behaviour to soft junction structures results in similar effects, namely that soft particles can have a disproportionately large effect.

5 Note: we use a slightly different definition of m_0 here compared to the original paper [100]

An alternative measure is here proposed to remove the problem with negative string lengths,

$$\lambda' = \ln\left(1 + \frac{\sqrt{2}E_1}{m_0}\right) + \ln\left(1 + \frac{\sqrt{2}E_2}{m_0}\right) \tag{II.2.13}$$

where the energies are calculated in the rest-frame of the dipoles. This measure is always positive definite. In the case of massless particles the λ'-measure can be rewritten to

$$\lambda' = \ln\left(1 + \frac{s}{2m_0^2} + \frac{\sqrt{2s}}{m_0}\right) \tag{II.2.14}$$

where again s is the invariant mass squared of the dipole and m_0 is a constant. The two measures agree in the limit of large invariant masses ($s \gg m_0$). The implementation includes a few alternative measures as options, but the above is chosen as the default measure and therefore also the one that the parameters are tuned for.

A final complication regarding the λ measure is that the form above cannot be used to describe the distance between two directly connected junctions. Instead the same measure as described in [100] is also used in this study ($\lambda = \beta_1\beta_2 + \sqrt{(\beta_1\beta_2)^2 - 1}$, where β_1 and β_2 are the 4-velocities of the two junction systems).

Since the λ-measure for junctions introduces additional approximations, a tuneable parameter is added to control the junction production. Several options for this parameter are possible and we settled on a $m_{0\mathrm{j}} \neq m_0$ in the λ-measure for junctions. A higher $m_{0\mathrm{j}}$ means a lower λ measure, resulting in an enhancement of the junction production. We cast the free parameter as the ratio,

$$\texttt{junctionCorrection} \;:\; C_j = m_{0\mathrm{j}}/m_0\,, \tag{II.2.15}$$

thus a value C_j above unity indicates an enhancement in junction production, and vice versa. The possibility of a junction enhancement can be seen as providing a crude mechanism to compensate for the intrinsic suppression of junction topologies in the colour-space model. Indeed, in the section on tuning below we find that values above unity are preferred in order to fit the observed amounts of baryon production.

(a) Ordinary pseudoparticle (b) Junction pseudoparticle

Figure II.8: The figure shows how two gluons are turned into a pseudoparticle depending on whether they are connected via an ordinary string (a) or a junction (b). The (gg) represents the formed pseudoparticle.

In the context of CR, it is generally the dipoles with the largest invariant masses which are the most interesting; they are the ones for which reconnections can produce the largest reductions of the λ measure. However, as evident from the above discussion, dipoles with *small* invariant masses can actually be the most technically problematic to deal with. It was therefore decided to remove dipoles with an invariant mass below m_0 from the colour reconnection. Technically this is achieved by combining the small-mass pair into a new pseudo-particle. For an ordinary dipole this is a trivial task (fig. II.8a), but if the dipole is connected to a junction the technical aspects becomes more complicated (fig. II.8b). The easiest way to think of this is as an ordinary diquark, but in addition to these we can have digluons, which will have three ordinary (anti-)colour tags. Note that we do not intend these to represent any sort of weakly bound state; we merely use them to represent a low-invariant-mass collection of partons whose internal structure we consider uninteresting for the purpose of CR. The pseudo-particles are formed after the LC dipoles are formed, and also after any colour reconnections if the new dipoles have a mass below m_0. Increasing m_0 will therefore lower the amount of CR. Only small effects occur for variations around the Λ_{QCD} scale, however increasing m_0 beyond 1 GeV introduces a significant reduction of CR.

The complete algorithm for the colour reconnection can be summarised as below.

1. Form dipoles from the LC configuration.
2. Make pseudoparticles of all dipoles with mass below m_0.
3. Minimise λ-measure by normal string reconnections.

4. Minimise λ-measure by junction reconnections.

5. If any junction reconnections happened return to point 3.

The choice to first do the normal string reconnections before trying to form any junctions is due to the algorithm not allowing to remove any junction pairs.

Since each reconnection is required to result in a lower λ-measure than the previous one, the minimisation procedure is only expected to reach a local minimum. A possible extension to reach the global minimum would be to use simulated annealing [110]. This is, e.g., the approach adopted in the HERWIG++ CR model [47]. However this would also require the implementation of inverse reconnections (i.e. a junction and an antijunction collapsing to form strings, and the unfolding of pseudo-particles.). Secondly the computational time needed to find the global minimum would slow down the event generation speed very significantly. For purposes of this implementation, we therefore restrict ourselves to a local deterministic minimisation here, noting that an algorithm capable of reproducing the full expected area-law exponential would be a desirable future refinement.

Hadronisation of Multi-Junction Systems

The existing junction hadronisation model [87] was developed mainly for the case of string systems containing a single junction (in the context of baryon-number violating SUSY decays like $\tilde{\chi}^0 \to qqq$). For such systems, the strategy of is to take the two legs with lowest energy in the junction rest-frame and hadronise them from their respective quark ends inwards towards the junction, until a (low) energy threshold is reached, at which point the two endpoints are combined into a diquark (which contains the junction inside). This diquark then becomes the new endpoint of the last string piece, which can then be fragmented as usual.

The case of a junction-antijunction system was also addressed in [87] (arising e.g., in the case of $e^+e^- \to \tilde{t}\,\tilde{t}^* \to \bar{q}\bar{q}\,qq$), but the new treatment of the beam remnants presented here, as well as the new CR model, can produce configurations with any number of colour-connected junctions and antijunctions. This goes beyond what the existing model can handle.

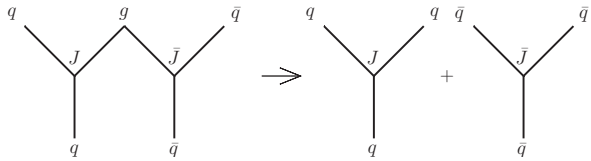

(a) Single gluon split

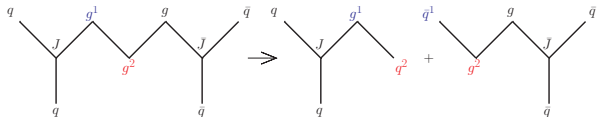

(b) Multi gluon split

Figure II.9: The figure shows how connected junctions are separated if they are connected by respectively a single gluon (a) or multiple gluons (b). The indices indicate where the split happens and which particles each gluon splits into.

The systems of equations describing such arbitrarily complicated string topologies are likely to be quite involved, with associated risks of instabilities and pathological cases. Rather than attempting to address these issues in full gory detail, we here adopt a simple "divide-and-conquer" strategy, slicing the full system into individual pieces that contain only one junction each, via the following 3 steps:

- If a junction and an antijunction are connected with a single gluon between them, that gluon is forced to split into two light quarks (u,d and s) that each equally share the 4-momentum of the gluon (corresponding to $z = \frac{1}{2}$). Since the gluon is massless, the two quarks will have to be parallel (fig. II.9a).

- If a junction and an antijunction are connected with at least 2 gluons in between, the gluon pair with the highest invariant mass is found, and is split according to the string-fragmentation function. The highest invariant mass is chosen due to it having the largest phase space and being the most likely to have a string breakup occur. The split is done in such a way that the two gluons are preserved but each of them give up part of their 4-momentum to the new quark pair. The new quark that is colour-connected to one of the gluons will be par-

allel to the other gluon (fig. II.9b, where the indices indicate who is parallel with whom.).

- After the two rules above have been applied, only directly-connected junction-antijunctions are left. If all three legs of both junctions are connected to each other, the system contains no partons and can be thrown away. If two of the legs are directly connected, the junction-antijunction system is equivalent to a single string piece and is replaced by such, see fig. II.10a. Finally, the case of a single direct junction-antijunction connection is dealt with differently, depending on whether the system contains further junction-antijunction connections or not. In the former case, illustrated in fig. II.10b, the maximum number of junctions are formed from the partons directly connected to the junction system. The remaining particles are formed into normal strings. In the example of fig. II.10b, three quarks are first removed to form a junction system; the remaining q and $\bar{q}$ then have no option but to form a normal string. The current method randomly selects which outgoing particles to connect with junctions. One extension would be to use the string measure to decide who combines with whom. (However the effect of this might be smaller than expected, since the majority of the multi-junction configuration comes from the beam remnant treatment, which later undergoes CR.)

  For cases with a single direct junction-antijunction string piece and no further junctions in the system, illustrated in fig. II.10c, the λ-measure is used to determine whether the two junctions should annihilate or be kept [87] (essentially by determining whether the strings pulling on the two junctions cause them to move towards each other, towards annihilation, or away from each other). If the junctions survive, a new $q\bar{q}$ pair is formed by taking momentum from the other legs of the junction. Otherwise the junction topology is replaced by two ordinary strings. An option to always keep the junctions also exists.

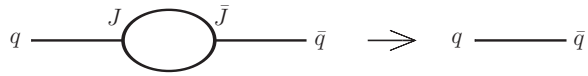

(a) Doubly-connected $J\bar{J}$ system

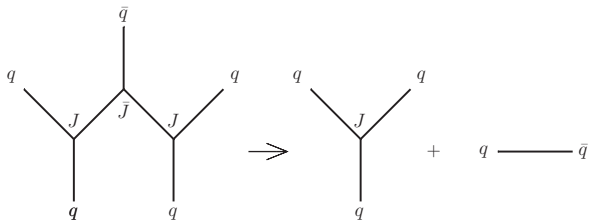

(b) Multiple $J\bar{J}J\cdots$ Connections

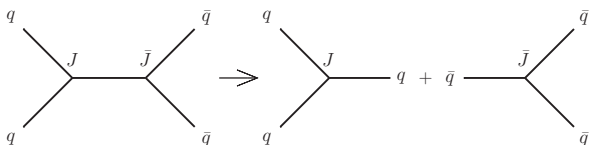

(c) A single $J\bar{J}$ Connection

Figure II.10: The figure shows how directly connected junctions are separated. Fig. a shows the replacement of a doubly-connected junction-antijunction system by an ordinary string piece. Fig. b shows the method used to reduce systems with more than two interconnected junctions. Fig. c shows the split-up of a system containing exactly one junction-antijunction connection, into two separate junction systems.

Space-Time Structure

By default, we do not account for any space-time separation between different MPI systems. This is motivated by the observation that, physically, the individual MPI vertices can at most be separated by transverse distances of order the proton radius, which by definition is small compared with the length of any string long enough to fragment into multiple particles.

We do note, however, that in order for reconnections to occur between two string pieces, they should be in *causal contact*; if either string has already hadronised before the other forms, there is no space-time region in which reconnections between them could physically occur. In the rest frame of a hadronising string piece, we take

the formation time of the corresponding QCD dipole to be given roughly by the inverse of its invariant mass, $\tau_{\text{form}} \sim 1/m_{\text{string}}$. Alternative measures (e.g., the $k_\perp$ evolution variable of the PS) could also have been used, and to allow at least a range of variations of the exact definition, a free parameter is introduced. The time at which the string piece begins to hadronise is related to the inverse of Λ_{QCD}, $\tau_{\text{had}} \sim 1/\Lambda_{\text{QCD}}$. In order for reconnections to be possible between two string pieces, we require that they must be able to resolve each other during the time between formation and hadronisation, taking time-dilation effects caused by relative boosts into account. There are several ways in which this requirement can be formulated at the technical level, and accordingly we have implemented a few different options in the code. In principle, the two strings can be defined to be in causal contact if the relative boost parameter fulfils:

$$\gamma\,\tau_{\text{form}} < C_{\text{time}}\,\tau_{\text{had}} \Rightarrow \frac{\gamma\,c}{m_{\text{string}} r_{\text{had}}} < C_{\text{time}} \tag{II.2.16}$$

where C_{time} is a tuneable parameter and $r_{\text{had}} (= \tau_{\text{had}}\,c \equiv 1$ fm) is a fixed constant given by the typical hadronisation scale. There are however two major problems with this definition: first it is not Lorentz invariant; the two dipoles will not always agree on whether they are in causal contact or not. This can be circumvented, by either requiring both to be able to resolve each other (strict) or just either of them to be able to resolve the other (loose). Secondly, the emission of a soft gluon from an otherwise high-mass string changes m_{string} significantly for each of the produced string pieces, which gives an undesirable infrared sensitivity to this measure, reminiscent of the problems associated with defining the λ string-length measure itself. One way to avoid this problem is to consider the *first* formation time of each colour line, i.e. the dipole mass at the time the corresponding colour line was first created in the shower, which we have implemented as an alternative option. No matter the exact definition of formation time and hadronisation time, all models agree that reconnection between boosted strings should be suppressed. A final extremely simple way to capture this in a Lorentz-invariant way is to apply a cut-off directly on the

boost factor γ, which thus provides a simple alternative to the other models.

These different methods have all been implemented and are available in PYTHIA, via the mode `ColourReconnection:timeDilationMode`. The C_{time} parameter introduced above is specified by `ColourReconnection:timeDilationPar` and controls the size of the allowed relative boost factor for reconnections to occur. As such it can be used to tune the amount of CR. Its optimal value will vary depending on the method used, but after the methods are tuned they produce similar results (see section II.3 for details).

A final aspect related to space-time structure that deserves special mention is resonance decays. By default, these are treated separately from the rest of the event. Physically, this is well motivated for longer-lived particles (e.g., Higgs bosons), which are expected to decay and hadronise separately. For shorter-lived resonances the separation of the MPI systems and resonance decays is physically not so well motivated. E.g., most Z/W bosons and top quarks will decay before hadronisation takes place, $\Gamma \gg \Lambda_{\text{QCD}}$, and as such should be allowed to interact with the particles from the MPI systems, ideally with a slightly suppressed probability due to the decay time.

Currently, only two extreme cases are implemented, corresponding to letting CR occur *before* or *after* (all) resonance decays. The corresponding flag in PYTHIA is called `PartonLevel:earlyResDec`. When switched on, CR is performed *after* all resonance decays have occurred, and all final-state partons therefore participate fully in the CR. Since no suppression with resonance lifetime is applied, this gauges the largest possible impact on resonance decays from CR. When switched off, CR is performed *before* resonance decays, hence involving only the beam remnant and MPI systems. It is equivalent to assuming an infinite lifetime for the resonances, and hence estimates the smallest possible impact on resonance decays from CR. An optional additional CR can be performed between the decay products of the resonance decays, with the physics motivation being $H \to WW \to q\bar{q}q\bar{q}$ studies.

To summarise, we acknowledge that the treatment of space-time separation effects and causality is still rather primitive in this model.

The derivation of a more detailed formalism for these aspects would therefore be a welcome and interesting future development.

II.3 CONSTRAINTS AND TUNING

The tuning scheme follows the same procedure as for the Monash 2013 tune [34]. However at a more limited scope, since only CR parameters, and ones strongly correlated with them, are tuned. As a natural consequence of this, the Monash tune was chosen as the baseline. As discussed in section II.2.3, several options are available for the choice of CR time-dilation method, which naturally results in slightly different preferred parameter sets. Here, we consider the following three modes:

- Mode 0: no time-dilation constraints. m_0 controls the amount of CR (mode 0);
- Mode 2: time dilation using the boost factor obtained from the final-state mass of the dipoles, requiring all dipoles involved in a reconnection to be causally connected (strict);
- Mode 3: time dilation as in Mode 2, but requiring only a single connection to be causally connected (loose).

This allows to investigate the consequences of some of the ambiguities in the implementation of the model. For the purpose of later studies that may want to focus on a single model, we suggest to use mode 2 as the "standard" one for the new CR. The parameters described in this section will therefore correspond to that particular model, with parameters for the others given in appendix A. Note that this section only contains the main physical parameters; for a complete list we again refer to appendix A.

II.3.1 *Lepton Colliders*

We begin with e^+e^- collisions. Only small effects are expected in this environment, due to the $p_\perp$-ordering of the shower and the absence of MPIs. Only CR and string-fragmentation variables were studied, since the shower was left untouched. The fragmentation

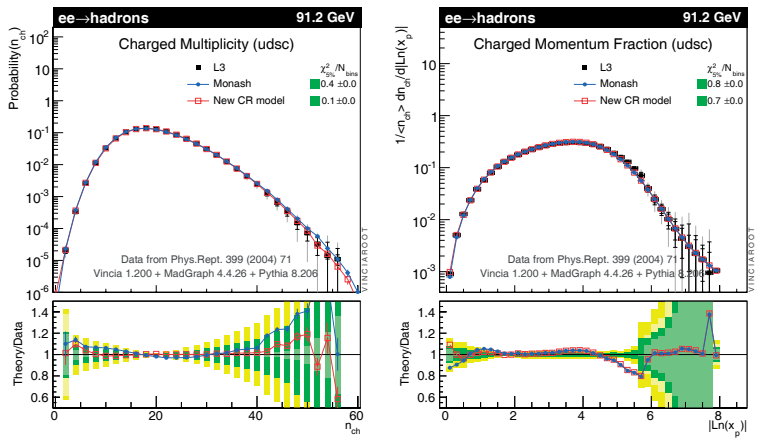

(a) (b)

Figure II.11: Charged-particle multiplicity (a) and momentum fraction (b) spectra, in light-flavour tagged data from the L3 collaboration [111]. (Plots made with VINCIAROOT [112]. The ratio panes follow the now-standard "Brazilian" colour conventions, with outer (yellow) bands corresponding to 2σ deviations and inner (green) bands corresponding to 1σ deviations.)

model contains three main parameters governing the kinematics of the produced hadrons: the non-perturbative $p_\perp$ produced in string breaks, controlled by the $\sigma_\perp$ parameter (`StringPT:sigma`), and the two parameters, a and b, which control the shape of the longitudinal (z) fragmentation function. For pedagogical descriptions, see e.g. [2, 23, 30, 34]. Since the effects are expected to be small, we made the choice of keeping $\sigma_\perp = 0.335$ GeV unchanged, adjusting only the longitudinal (a and b) parameters. Changing the minimal number of parameters also helps to disentangle the effects of CR from the retuning. As a verification, a tune with a smaller $\sigma_\perp$ (0.305 GeV) was considered, however after retuning a and b the two tunes described the LEP data with a similar fidelity. (The choice of testing a lower $\sigma_\perp$ was made since the CR model tends connect more collinear partons leading to shorter strings, but a harder $p_\perp$ spectrum of the produced hadrons [75].)

The determination of the two parameters of the Lund fragmentation function, a and b, is complicated slightly by the fact that they are highly correlated; choosing both of them to be quite small often produces equally good descriptions of fragmentation spectra as choosing both of them large, corresponding to a relatively elongated and correlated χ^2 "valley". By simultaneously considering both variables and comparing them to both multiplicity and momentum spectra, cf. fig. II.11 (with the *"New CR model"* curve showing our new model, and *"Monash"* the baseline Monash 2013 tune), we here settled on a low-valued pair, as compared with the default Monash values:

```
StringZ:aLund = 0.38 # was 0.68
StringZ:bLund = 0.64 # was 0.98
```

The new CR also alters the ratio between the identified-particle yields, especially so for baryon production due to the introduction of additional junctions. Thus the flavour-selection parameters of the string model also need to be retuned, by comparing with the total identified-particle yields, see e.g. [34]. As expected the effects are minimal in e^+e^- collisions, and only small changes are required. The modifications were therefore done with a view to providing a better description also for pp colliders, but staying within the uncertainties allowed by the LEP data. This resulted in an adjustment of the parameters for the diquark over quark fragmentation probability and the strangeness suppression:

```
StringFlav:probQQtoQ = 0.078 # was 0.081
StringFlav:probStoUD = 0.2 # was 0.217
```

As expected the diquark over quark probability is reduced due to the introduction of junctions. More surprisingly is the increased suppression of strange quarks, since the model a priori should not influence flavour selection. The technical implementation of the junction hadronisation does, however, introduce a slight enhancement of the strangeness production, due to an even probability for a gluon to split into an u, d or s quarks when separating junction

systems. This is not visible at LEP, but at pp colliders the slightly lower strangeness fragmentation is favoured.

The final set of fragmentation parameters we define is more technical. For junction systems and beam remnants, a separate set of parameters controls the choice of total spin when two, already produced, quarks are combined into a diquark. Unlike diquarks produced by ordinary string breaks (whose spin is controlled by the parameter `StringFlav:probQQ1toQQ0`), which can only contain the light quark flavours (u, d, s), and for which the significant mass splittings between the light-flavour spin-3/2 and spin-1/2 baryon multiplets necessitates a rather strong suppression of spin-1 diquark production (relative to the naive factor 3 enhancement from spin counting), junction systems in particular can allow the formation of baryons involving heavy flavours, which have smaller mass splittings and which therefore might require less suppression of spin-1 diquarks. We note also that diquarks produced in string breakups are produced within the linear confinement of the string, whereas junction diquarks come from the combination of two already uncorrelated quarks, so there is a priori little physics reason to assume the parameters must be identical.

With the limited amount of junctions in the old model, none for ee and at most two for pp, these parameters previously had almost no influence on measurable observables and were therefore largely irrelevant for tuning. With the additional junctions produced by our model, these parameters can now give larger effects. Measurements of higher-spin and heavy-flavour baryon states at pp colliders are still rather limited though, and so far we are not aware of published directly usable constraints from experiments. For the time being therefore, we choose to fix the parameters to be identical to those for the production of ordinary diquarks in string breakups:

```
StringFlav:probQQ1toQQ0join = 0.027,0.027,0.027,0.027
```

The four components give the suppression when the heaviest quark is u/d, s, c or b, respectively. We stress that this is merely a starting point, hopefully to be revised soon by comparisons with new data from the LHC experiments.

II.3.2 *Hadron Colliders*

The retuning to hadron colliders consisted of tuning three main parameters:

- C_{time} (`ColourReconnection:timeDilationPar`): controls the overall strength of the colour-reconnection effect via suppression of high-boost reconnections, see section II.2.3. Can be tuned to the $\langle p_\perp \rangle$ vs n_{ch} distribution.
- C_{j} (`ColourReconnection:junctionCorrection`): multiplicative factor, $m_{0\text{j}}/m_0$, applied to the string-length measure for junction systems, thereby enhancing or suppressing the likelihood of junction reconnections. Controls the junction component of the baryon to meson fraction and is tuned to the Λ/K_s^0 ratio.
- $p_\perp^{\text{ref}}$ (`MultiPartonInteractions:pT0Ref`): lower (infrared) regularisation scale of the MPI framework. Controls the amount of low $p_\perp$ MPIs and is therefore closely related to the total multiplicity and can be tuned to the $d\langle n_{\text{ch}} \rangle / d\eta$ distribution.

By iteratively fitting each parameter to its respective most sensitive curve an overall good agreement with data was achieved (see fig. II.12) with the following parameters:

```
ColourReconnection:junctionCorrection = 1.2  # new parameter
ColourReconnection:timeDilationPar    = 0.18 # new parameter
MultiPartonInteractions:pT0Ref        = 2.15 # was 2.28
```

Note in particular this is the first time that PYTHIA has been able to describe the Λ/K_s ratio in pp collisions while remaining consistent with LEP bounds. We explore this in more detail in section II.3.4.

The $C_{\text{j}} = 1.2$ parameter shows that a slight enhancement of junction reconnections (i.e., baryon production) is needed, relative to mesonic ones. However, given the approximations used in the implementation of especially the junction structures, such a difference is not unreasonable. Small differences between the modes can be seen in the $\langle p_\perp \rangle$ vs n_{ch} and more significant differences for multiplicity distributions , cf. fig. II.13. With respect to the latter, however,

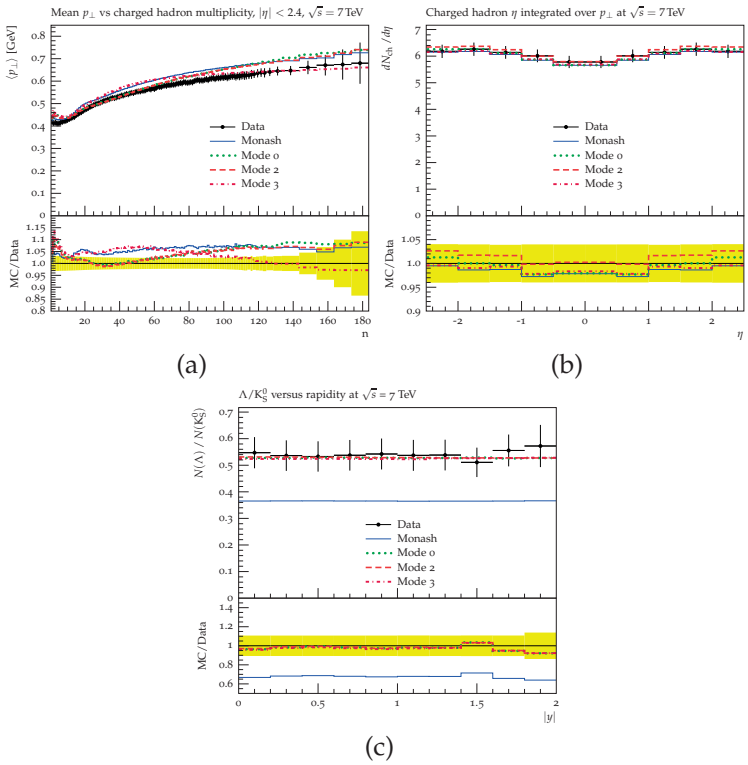

Figure II.12: The average $p_\perp$ as a function of multiplicity [52] (a), the average charged multiplicity as a function of pseudorapidity [113] (b), and the Λ/K_s ratio [114] (c). All observables from the CMS collaboration and plotted with the Rivet framework [115]. All PYTHIA simulations were non single diffractive (NSD) with a lifetime cut-off $\tau_{max} = 10$ mm/c and no $p_\perp$ cuts applied to the final state particles. The yellow error band represents the experimental 1σ deviation.

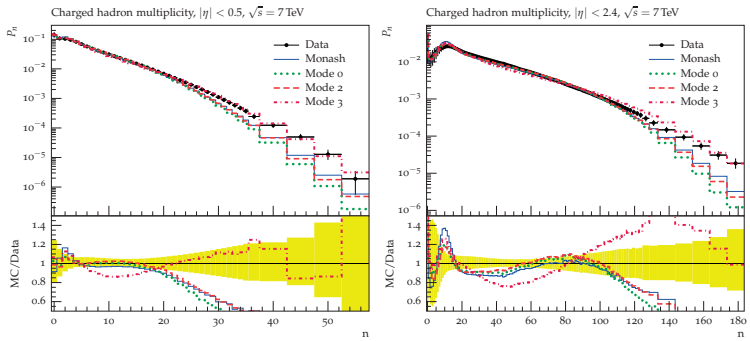

(a) $|\eta| < 0.5$ (b) $|\eta| < 2.4$

Figure II.13: The two plots show the multiplicity distributions for respectively very central tracks (a) and the full CMS tracker coverage (b), compared with CMS data [52]. All PYTHIA simulations were NSD with a lifetime cut-off ($\tau_{\text{max}} = 10$ mm/c) and no $p_\perp$ cuts were applied to the final state particles. The yellow error band represents the experimental 1σ deviation.

we note that the differences in the tails of the multiplicity distributions can be tuned away by modifying the assumed transverse matter density profile of the proton, which was kept fixed here to highlight the differences with the minimal number of retuned parameters.

The new colour treatment of the beam remnant (BR) introduces a single new parameter controlling the amount of saturation, cf. the discussion in section II.2.3. Due to the low $p_\perp$ of the BR particles, the effects are largest in the forward direction. We therefore use the forward charged multiplicity as measured by the TOTEM experiment [116] to compare different modelling choices of this aspect, see fig. II.14a. The difference between no saturation[6] ($k_{\text{saturation}} \to \infty$) and maximal saturation ($k_{\text{saturation}} = 0.1$) is about 10% and exhibits no shape difference over the TOTEM pseudo rapidity range. For illustration and completeness, we may also consider what happens over the full rapidity range, at least at the theory level. This is illustrated in fig. II.14b. In the central region, the effect of applying saturation is a slight decrease of the particle yield, and thus would already have been tuned away by $p_\perp^{\text{ref}}$. It was therefore chosen to use a relative high satura-

6 Technically: `BeamRemnants:saturation = 1E9`.

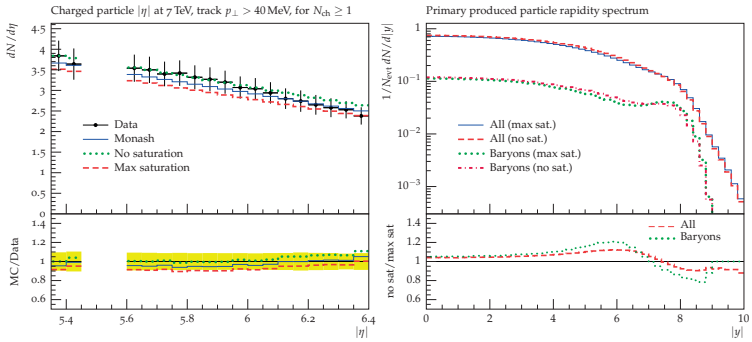

(a) TOTEM Comparison (b) Generator-Level

Figure II.14: (a): different extreme saturation choices compared with the TOTEM forward multiplicity data [116]. (The PYTHIA simulation includes all soft-QCD processes and a particle lifetime cut-off $\tau_{\text{max}} = 10$ mm/c.) The yellow error band represents the experimental 1σ deviation. (b): MC rapidity distributions for respectively all particles and baryons only. (For simplicity only non diffractive (ND) events were used, hadron decays were turned off to reflect primary hadron production, and no $p_\perp$ cuts were imposed.)

tion to mimic the effect of the earlier PYTHIA beam remnant model:

```
BeamRemnants:saturation = 5
```

We emphasise however that this is merely a starting point, and that a different balance between $p_\perp^{\text{ref}}$ and $k_{\text{saturation}}$ may be preferred in future tuning efforts, especially ones taking a more dedicated look at the forward region. In such a study the sharing of momentum between the partons in the remnant should also be considered, since it is known to alter both particle production in the forward region and the multiplicity distributions.

An interesting signal that may help to break the relative degeneracy between $p_\perp^{\text{ref}}$ and $k_{\text{saturation}}$, is to look for baryons at high rapidities, which, due to the introduction of junction structures in the BR can act as further tracers of the degree to which the BR has been disturbed. This is illustrated by the lower set of curves in fig. II.14b. The effects are indeed seen to be slightly larger for baryons, however the total cross section is also significantly lower. From this

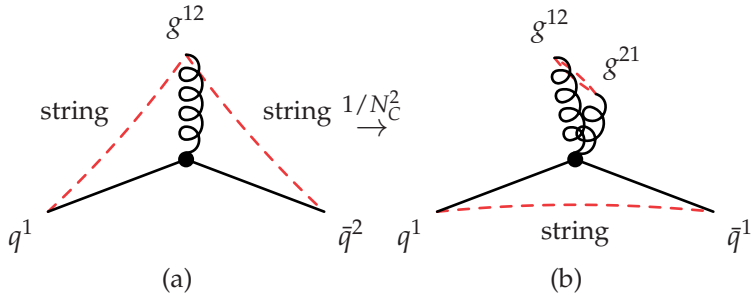

Figure II.15: (a): illustration of the correspondence between colour connections and string pieces in an ordinary (LC) 3-jet topology. b): if the gluon jet is composed of (at least) two gluons, there is probability for the $q\bar{q}$ system to be in an overall singlet. (The LC string topology remains a possibility as well, with the string-length measure λ used to decide between them.) Notation: g^{ac} denotes a gluon with colour (anticolour) index c (a). For (anti)quarks, we use $q^c \equiv q^{0c}$ and $\bar{q}^a \equiv \bar{q}^{a0}$.

simple MC study we are not able to say clearly whether such a measurement, which requires the additional non-trivial ingredient of baryon identification, would be experimentally feasible.

II.3.3 *Direct CR Constraints?*

In the preceding sections, we constrained ("retuned") the fragmentation parameters using observables like the charged-particle multiplicity and fragmentation spectrum, which are indirectly sensitive to CR effects via the modifications caused to these spectra by the minimisation of string lengths. But what about observables with more direct sensitivity to CR effects? There are two main categories of dedicated CR studies at LEP: Fully hadronically decaying WW events (looking for reconnections between the two W systems), and colour-flow sensitive observables in three-jet events. In this study we restrict our attention to the latter of these. A follow-up dedicated study of CR effects at e^+e^- colliders, both earlier as well as possible future colliders, is planned.

Without CR, the three produced jets will in general be represented by a colour string stretched from the quark via the gluon to the antiquark, illustrated in fig. II.15a. The string pieces spanned between the quark and gluon jets lead to a relatively large parti-

cle production between these jets, while there is a suppression of particle production in the phase-space region directly between the quark and antiquark jets. However, if CR is allowed, there is a $1/N_C^2$ chance that two (or more) sequentially emitted gluons end up cancelling each others' colour charges. Thus, if at least one additional gluon was produced in the FSR, the "gluon jet" may effectively become overall colour neutral, allowing it to decouple from the quark-antiquark system in colour space. This is illustrated in fig. II.15b. There is a caveat to the above, namely, if the two gluons originate from a single gluon, ie., $g \to gg$, the two gluons must form a colour octet. In the gluon-collinear limit, this colour structure dominates and the probability for the jet to end up colour neutral should therefore be strongly suppressed, below $1/N_C^2$. This aspect is not included in our model, since the history of the final state particles is not considered. The model may therefore overestimate the CR effect on three-jet events.

An additional consequence is that the jet will also have a total electric charge of zero, if all particles from the fragmentation fall within the jet. The best observable uses both of these ideas. Firstly a rapidity gap is required in order to select events with minimum radiation between the jets. This also enhances the probability that all the particles from the fragmentation falls within the jet. Secondly the jet is required to have a total charge of zero. This observable was first proposed during the LEP runs [117] and successively followed up by several of the experiments [35, 37, 40]. The studies were limited to excluding only the most extreme CR models, with no conclusions drawn between more moderate CR models and no CR; the data was located in between the two predictions.

Rather than comparing our model directly on the LEP data, we took a slightly simpler approach by only considering the difference between no CR and the new CR model in the relevant observables. The difference is found to be negligible on those observables, cf. the "No CR" and "New CR" histograms in fig. II.16. Thus we do not expect that the new CR model could be ruled out by these LEP constrains. We note that the small difference between with and without CR can be understood, by remembering the large focus on junction structures in the new CR model. Junction structures do not produce colour-singlet jets in the same manner as ordinary

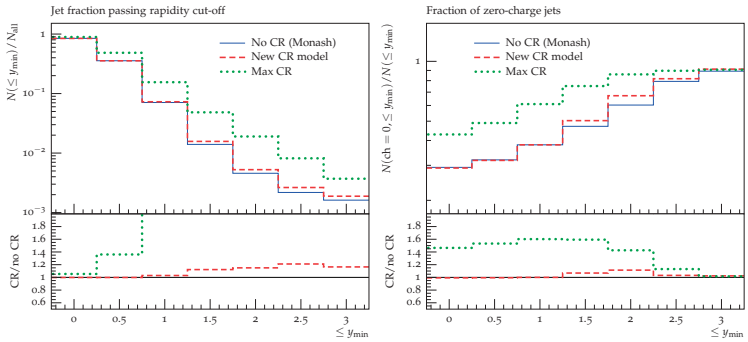

(a) Rapidity along jet axis (b) Neutral fraction

Figure II.16: Observables constraining CR in 3-jet events at LEP. (a): the minimum rapidity of the constituents of the third jet with respect to its jet axis. (b): the fraction of the third jet with total charge equal to zero as a function of minimum rapidity of particles in the third jet.

strings, and thus are not sensitive to this observable in the same way as ordinary strings reconnections. It is possible to consider a more extreme version of the new CR model where all dipoles are allowed to connect with each other, i.e. effectively replacing $1/N_C^2$ by unity! This is illustrated by the "max CR" histogram in fig. II.16. For this unphysically extreme case the difference between the two models becomes so large it most likely would have been ruled out by the experiments. However such an extreme case would also be eliminated by just considering LHC measurements (e.g. $\langle p_\perp \rangle$ vs n_{ch}).

II.3.4 *Suggestions for New Observables*

As discussed in section II.3.2, the new CR model is able to reach agreement with some key observables that have otherwise proved difficult for the string model (as implemented in PYTHIA) in the pp environment. In particular, subleading dipole connections that minimise the string-length measure can account for the rise in the $\langle p_\perp \rangle (n_{\text{ch}})$ distribution (a feature also present in earlier CR models in PYTHIA, though without the connection with subleading colour), and subleading string-junction connections can account for the observed increase in e.g. the Λ/K ratio between ee and pp collisions.

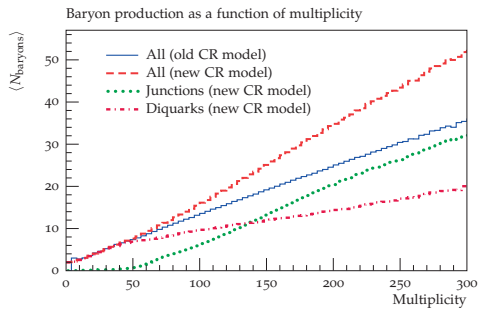

Figure II.17: average baryon multiplicity as a function of hadron multiplicity (generator-level, including all particles, hadronic decays switched off).

The price is (a few) new free parameters governing the CR modelling, so the question naturally arises to what extent this type of model can be distinguished clearly from other other phenomenological modelling attempts to describe the same data. All models we are aware of that simultaneously aim to describe both the LEP data and the LHC data (or *ee* and *pp* data more generally) rely on the higher colour/energy densities present in *pp* collisions to provide the extra baryons. The multiplicity scaling of the baryon production is therefore expected to be higher than the linear scaling of the diquark model. This is also what we observe, cf. fig. II.17. For low multiplicity, both of the CR models agree with each other, however the increase happens faster for the new model. This shape difference in the scaling with particle multiplicity could provide an additional probe to test the new model.

One also notices that there is a significant difference between the baryon production of the old model and baryon production from diquarks in the new model. This is somewhat surprising since the hadronisation model is essentially left untouched. The explanation for this is two-fold: 1) the new CR model produces a different mass spectrum of strings (with generally lower invariant masses), and 2) low-mass strings and junction structures produce fewer additional diquarks.

The first point is illustrated in fig. II.18a, which shows the invariant-mass distribution of strings in the new and old model. In the old model, the distribution is essentially flat, and includes

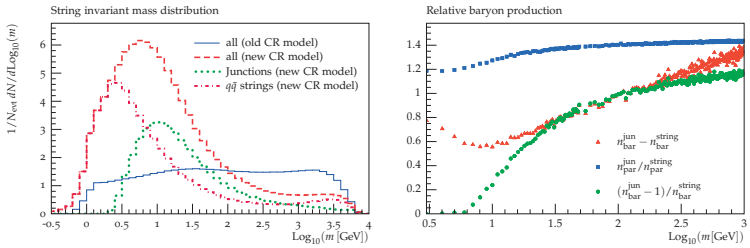

(a) (b)

Figure II.18: (a): invariant mass distribution of string systems (note logarithmic x axis). (b): the production of baryons from respectively a $q\bar{q}$ system ("string") and a qqq system ("junction") with the same total invariant mass. The red triangles show the difference of total primary-baryon multiplicities, the blue squares show the ratio of total primary-hadron multiplicities (mesons+baryons), and the green circles show the ratio for the primary-baryons multiplicities, subtracting off the extra baryon that the junction topology always produces.

a significant plateau towards very large invariant masses, whereas the distribution is strongly peaked at small invariant masses in the new model. The differences arise both from the junction cleanup procedure (by which longer strings can be split by insertion of an additional quark-antiquark pair), and from the minimisation of the λ-measure. The old model also minimised the λ-measure, however this is achieved by combining strings, giving fewer but higher-mass string systems than before the CR.

Due to energy-momentum conservation (and a greater relative importance of the quark endpoints), low-invariant-mass strings produce fewer baryons. Despite the fact that each junction system produces at least one baryon, we therefore note that this does not automatically lead to an increase in the total number of produced baryons. Since the invariant mass of a qqq junction system is distributed on three string pieces, whereas that of a $q\bar{q}$ system is carried by a single string, diquarks, which are relatively heavy, can actually be quite strongly phase-space suppressed in junction topologies, especially at low invariant masses of the string system (where the majority of the junction topologies lie cf. fig. II.18a). In addition the diquarks need to be pair produced to conserve baryon number, and the current implementation requires the pair to be on the same junc-

tion leg, leading to an even larger phase-space suppression. This effect is illustrated in fig. II.18b, where for instance a junction system with $E_{\mathrm{CM}} = 10$ GeV (in the peak of the mass distribution) has a five times lower probability to produce an (extra) diquark pair compared to a 10-GeV dipole string. At fixed multiplicity this effect is hidden in the tuned parameters, but can be observed by the different scaling.

Considering baryon production in more detail, the relative yield of different types of baryons is highly revealing. A collection of such yields for the different models are listed in tab. II.1. For most of the baryons, the new CR model predicts about $20 - 50\%$ above the old model. This is in agreement with result for Λ production shown earlier (fig. II.12). There are however also some clear order-of-magnitude differences, for charm and bottom baryons. One example is Σ_c^0 production[7], for which the new CR model predicts a rate more than a factor of 20 above that of the old model!

To understand how such large differences can occur, we need to recall how baryons are produced in ordinary string fragmentation. Since no charm is produced in string break-ups, the only way to produce a Σ_c^0 is to produce a dd-diquark and combine it with c quark from the shower. However, since dd diquarks must have spin 1 (due to symmetry), their production is heavily suppressed relative to ud ones which can also exist in the far lighter spin-0 state. Enter junctions, for which there is a priori no specific penalty associated with having two legs end on same-flavour quarks as compared to different flavours. Up to some combinatorics and symmetry factors the production of ud and dd is therefore expected to be the same for junction systems, in good agreement with the observed predictions of the new CR model. As such the production of baryons like Σ_c^0 theoretically provides an excellent probe to study the relative importance between diquark- and junction-driven baryon production.

Similar results are also observed for Σ_c^{++} as well as for the production of the analogous b-baryons. And with the large b-physics programme at the LHC, we believe this could be an interesting study, both for its physics value as well as a possible source of background for other measurements. The effect can also be seen for Ω^-, however not as clearly as for charm and bottom baryons. Moreover the

7 The Σ_c^0 is a cdd state with spin $S = 1/2$, mass $\sim$ 2.5 GeV and PDG code 4112 [26].

Particle	New CR model ($N_{\text{par}}/N_{\text{events}}$)			Old CR model
	string	junction	all	$N_{\text{par}}/N_{\text{events}}$ (all)
π^+	$2.5 \cdot 10^1$	0	$2.5 \cdot 10^1$	$2.4 \cdot 10^1$
p	2.5	1.4	3.8	3.2
n	2.4	1.3	3.7	3.2
Δ^{++}	$6.1 \cdot 10^{-1}$	$4.5 \cdot 10^{-1}$	1.1	$8.9 \cdot 10^{-1}$
Δ^+	$6.0 \cdot 10^{-1}$	$4.0 \cdot 10^{-1}$	1.0	$8.6 \cdot 10^{-1}$
Δ^0	$5.5 \cdot 10^{-1}$	$4.0 \cdot 10^{-1}$	$9.4 \cdot 10^{-1}$	$7.9 \cdot 10^{-1}$
Δ^-	$4.7 \cdot 10^{-1}$	$4.4 \cdot 10^{-1}$	$9.1 \cdot 10^{-1}$	$7.1 \cdot 10^{-1}$
K^+	5.2	0	5.2	5.1
Λ	$4.7 \cdot 10^{-1}$	$3.9 \cdot 10^{-1}$	$8.6 \cdot 10^{-1}$	$6.5 \cdot 10^{-1}$
Σ^+	$3.4 \cdot 10^{-1}$	$4.2 \cdot 10^{-1}$	$7.6 \cdot 10^{-1}$	$5.1 \cdot 10^{-1}$
Σ^0	$3.5 \cdot 10^{-1}$	$4.5 \cdot 10^{-1}$	$7.9 \cdot 10^{-1}$	$5.1 \cdot 10^{-1}$
Σ^-	$3.2 \cdot 10^{-1}$	$4.2 \cdot 10^{-1}$	$7.4 \cdot 10^{-1}$	$4.9 \cdot 10^{-1}$
Σ^{*+}	$9.6 \cdot 10^{-2}$	$8.9 \cdot 10^{-2}$	$1.9 \cdot 10^{-1}$	$1.5 \cdot 10^{-1}$
Σ^{*0}	$9.2 \cdot 10^{-2}$	$7.7 \cdot 10^{-2}$	$1.7 \cdot 10^{-1}$	$1.4 \cdot 10^{-1}$
Σ^{*-}	$8.3 \cdot 10^{-2}$	$8.7 \cdot 10^{-2}$	$1.7 \cdot 10^{-1}$	$1.3 \cdot 10^{-1}$
Ξ^-	$6.9 \cdot 10^{-2}$	$1.1 \cdot 10^{-1}$	$1.8 \cdot 10^{-1}$	$1.1 \cdot 10^{-1}$
Ω^-	$2.0 \cdot 10^{-3}$	$1.3 \cdot 10^{-2}$	$1.5 \cdot 10^{-2}$	$3.9 \cdot 10^{-3}$
D^+	$5.3 \cdot 10^{-2}$	0	$5.3 \cdot 10^{-2}$	$6.5 \cdot 10^{-2}$
Λ_c^+	$4.0 \cdot 10^{-3}$	$7.9 \cdot 10^{-3}$	$1.2 \cdot 10^{-2}$	$6.6 \cdot 10^{-3}$
Σ_c^{++}	$2.7 \cdot 10^{-4}$	$1.3 \cdot 10^{-2}$	$1.3 \cdot 10^{-2}$	$5.4 \cdot 10^{-4}$
Σ_c^+	$2.5 \cdot 10^{-4}$	$1.5 \cdot 10^{-2}$	$1.5 \cdot 10^{-2}$	$5.2 \cdot 10^{-4}$
Σ_c^0	$2.5 \cdot 10^{-4}$	$1.3 \cdot 10^{-2}$	$1.3 \cdot 10^{-2}$	$5.1 \cdot 10^{-4}$
Σ_c^{*++}	$5.1 \cdot 10^{-4}$	$1.7 \cdot 10^{-3}$	$2.2 \cdot 10^{-3}$	$9.5 \cdot 10^{-4}$
Σ_c^{*+}	$4.9 \cdot 10^{-4}$	$1.9 \cdot 10^{-3}$	$2.4 \cdot 10^{-3}$	$9.4 \cdot 10^{-4}$
Σ_c^{*0}	$4.8 \cdot 10^{-4}$	$1.7 \cdot 10^{-3}$	$2.2 \cdot 10^{-3}$	$9.1 \cdot 10^{-4}$
ccq[8]	0	$2.1 \cdot 10^{-4}$	$2.1 \cdot 10^{-4}$	$1.0 \cdot 10^{-7}$
B^+	$1.6 \cdot 10^{-3}$	0	$1.6 \cdot 10^{-3}$	$2.3 \cdot 10^{-3}$
Λ_b^0	$1.9 \cdot 10^{-4}$	$6.3 \cdot 10^{-4}$	$8.2 \cdot 10^{-4}$	$3.9 \cdot 10^{-4}$
Σ_b^+	$1.1 \cdot 10^{-5}$	$9.3 \cdot 10^{-4}$	$9.5 \cdot 10^{-4}$	$3.1 \cdot 10^{-5}$
Σ_b^0	$1.2 \cdot 10^{-5}$	$1.0 \cdot 10^{-3}$	$1.0 \cdot 10^{-3}$	$3.7 \cdot 10^{-5}$
Σ_b^-	$1.1 \cdot 10^{-5}$	$9.3 \cdot 10^{-4}$	$9.4 \cdot 10^{-4}$	$3.2 \cdot 10^{-5}$
Σ_b^{*+}	$1.1 \cdot 10^{-5}$	$9.3 \cdot 10^{-4}$	$9.5 \cdot 10^{-4}$	$3.1 \cdot 10^{-5}$
Σ_b^{*0}	$1.2 \cdot 10^{-5}$	$1.0 \cdot 10^{-3}$	$1.0 \cdot 10^{-3}$	$3.7 \cdot 10^{-5}$
Σ_b^{*-}	$1.1 \cdot 10^{-5}$	$9.3 \cdot 10^{-4}$	$9.4 \cdot 10^{-4}$	$3.2 \cdot 10^{-5}$
bcq[8]	0	$1.8 \cdot 10^{-5}$	$1.8 \cdot 10^{-5}$	0
bbq[8]	0	$1.1 \cdot 10^{-6}$	$1.1 \cdot 10^{-6}$	0

Table II.1: Primary particle and antiparticle production of identified hadrons. Ten million ND events were simulated and all particles and antiparticles were counted. Hadron decays were switched off to only look at the primary production.
[8]Double heavy baryons where the last q can be any quark.

presence of additional suppression of strange diquarks in the string fragmentation model makes Ω^- connection more complicated. We note that it can be an important validation channel however.

Due to the majority of baryons being produced by the junction mechanism in the new CR model, the baryon yields also provides a clear probe to test the spin structure of the diquarks formed from the junctions. The large difference in yield between Σ_c^{*+} and Σ_c^0 is due to the choice of spin suppression mentioned earlier in the tuning section. An actual measurement could be directly applied as a constraint for this variable. At least with the development of the present model, we now have a vehicle that allows to explore this type of phenomenology and interpret the findings.

We should note that the baryons considered above are excited states that rapidly decay through the emission of a pion, e.g. $\Sigma_c^0 \to \Lambda_c^+ \pi^-$. As such they may be quite challenging to observe experimentally. It is therefore not a given that it will be easy to utilise measurements of these yields. But it does provide a theoretical motivation for studying the production and measurement of heavy baryons.

Another special class of baryons is the double (or triple) heavy baryons containing at least two c or b quarks. These baryons can not be formed in ordinary string fragmentation and is therefore almost non-existent in the old CR scheme. The only production mechanism is via the junctions from the beams (which also means that for p^+p^+ collisions no double-heavy antibaryons are predicted). This is also observed in tab. II.1, where only a single double-heavy baryon is produced in the 10 million events. With the large amount of junctions, the new CR model provides a natural production mechanism for double-heavy baryons, and as such the expected amount is also significantly higher than for the old CR model. The effect of massive quarks in the λ-measure is not well understood, however, and possible other production mechanism might also contribute, thus the estimate is most likely rather crude. Irrespectively, a measurement of double-heavy baryons probes a region of hadronisation that the current models do not describe. And it could possible also shed some light on whether the junction mechanism might be a reasonable production mechanism.

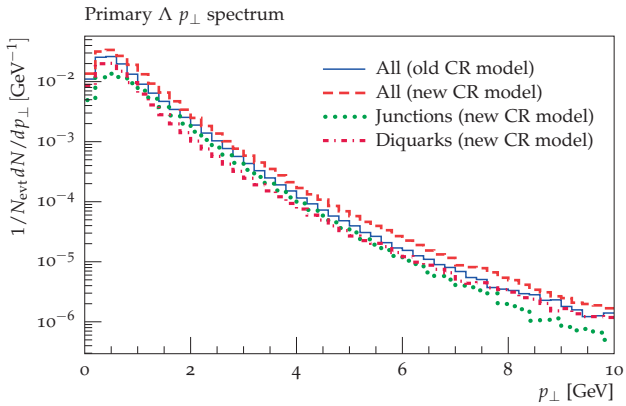

Figure II.19: The Λ $p_\perp$-distribution separated by production mechanism. Only ND events were included and hadron decays were switched off.

So far, we only considered total particle yields; more knowledge is available by studying more differential distributions. A natural next extension is the transverse momentum distributions. As the junctions are formed by minimising the λ-measure, the particles defining the junction may be expected to preferentially be moving in the same direction and thereby create a boosted baryon. This in turn leads to an expected increase in transverse momentum for such junction baryons. This is also observed in the low-$p_\perp$ region (below roughly $p_\perp \sim 4$ GeV), where the particle production peak is higher for junction baryons (fig. II.19). In the region of very high $p_\perp$ (above roughly $p_\perp \sim 4$ GeV) the particle production is dominated by jets, for which the hard high-$p_\perp$ partons are more important than the overall boost. In addition, the perturbative gluons associated with the jet already provides a low λ-measure and as such limited CR is expected inside the jet regions. This leads to the high-$p_\perp$ region being occupied predominantly by baryons produced in ordinary (diquark) string-breaks.

Transverse momentum spectra have already been measured for some of the more common baryon species and a comparison with the Λ $p_\perp$ spectrum measured by CMS is given in in fig. II.20. Sadly, the improvement is far less satisfactory here. The new CR model (as well as the old model) overshoots the production in the very low $p_\perp$ and the high $p_\perp$ region, whereas too few Λ baryons are predicted in

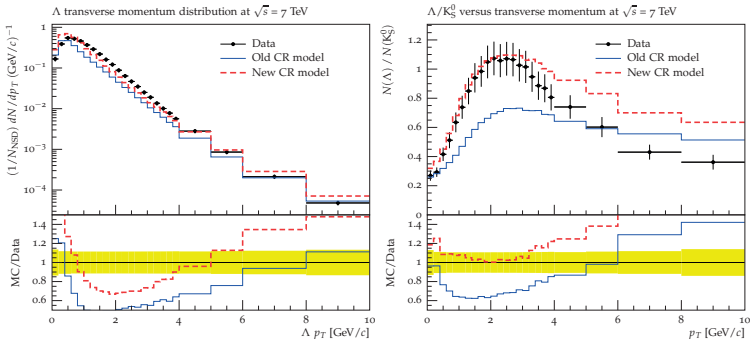

(a) (b)

Figure II.20: The (a) Λ $p_\perp$-distribution and (b) the Λ/K_s^0 $p_\perp$-distribution as measured by the CMS experiment [114]. All PYTHIA simulations were NSD with a lifetime cut-off ($\tau_{\max} = 10$ mm/c) and a rapidity cut on 2 ($|y| < 2$). The yellow error band represents the experimental 1σ deviation.

between. Thus the Λ baryons from junctions tend to fall in the right region, however the effect is not large enough. An interesting observation is that the *ratio* Λ/K_s is now well described in the low $p_\perp$ region. This shows that the problem with the $p_\perp$ distribution is not specific to baryons but is more generic. The discrepancy between data and the model for large $p_\perp$ still exists, however the baryon production in this region is primarily from diquark string breaks in jets and as such is not really unique for the new CR model. It may point to a revision needed of the spectrum of hard (leading?) baryon production in jets, which may not be unique to the pp environment, see [34].

The problem in the low $p_\perp$ domain is a common theme for all heavier hadrons (i.e. anything but pions) and would be interesting to explore further. (E.g., a measurement of ρ spectra could reveal whether it depends on the presence of strange quarks.) The PYTHIA models predict a $p_\perp$-distribution that peaks at lower values than what is actually observed. To study this in more detail, one can calculate the average $p_\perp$ for the identified hadrons and plot it a function of their mass, as done e.g. by the STAR collaboration for pp collisions at $E_{\mathrm{CM}} = 200$ GeV [118]. In purely longitudinal string fragmentation the expected result is a roughly flat curve, since no correlation between the mass of the particle and $p_\perp$ is present. The

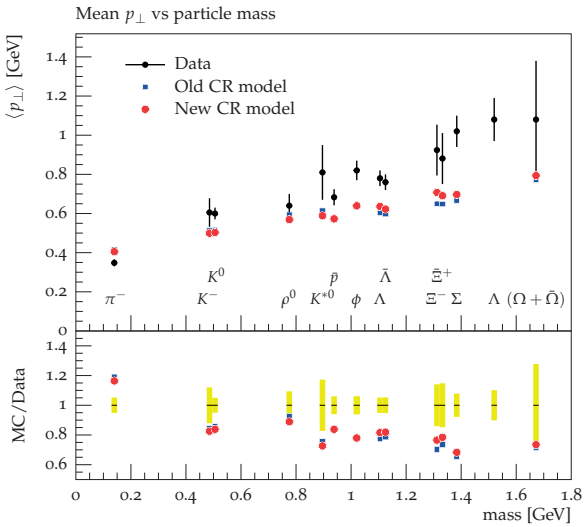

Figure II.21: Average $p_\perp$ versus hadron mass at $E_{\mathrm{CM}} = 200$ GeV, compared with STAR data [118]. The yellow error band represents the experimental 1σ deviation.

flat prediction is altered when hadron decays and jet physics are included, leading to the curve seen in fig. II.21. The prediction is also altered if the string is boosted (e.g., by partonic string endpoints), the boost is transferred to the final particles and for the same boost velocity a heavy particle will gain more $p_\perp$ than a light one. This effect can be enhanced by CR, since minimisation of the λ-measure prefers reconnections among partons moving in the same direction, thus creating boosted strings [75]. CR is therefore expected to give a sharper rise of the $\langle p_\perp \rangle$ vs mass distribution. Unfortunately, we do not observe this expected effect at any significant level (fig. II.21). To be candid, it is disappointing that the new model does not appear to address this problem at all. At the very least, it leaves room open for criticism and possibly additional new physics. Of special interest in this context are possible collective phenomena, such as (gas-like) hadron reinteractions or (hydro-like) flow, either of which could provide a (weak or strong, respectively) velocity-equalising component, and at least the latter has been applied successfully in the context of the EPOS model [72]. So-called "colour ropes" (strings carrying more than one unit of charge and hence having a

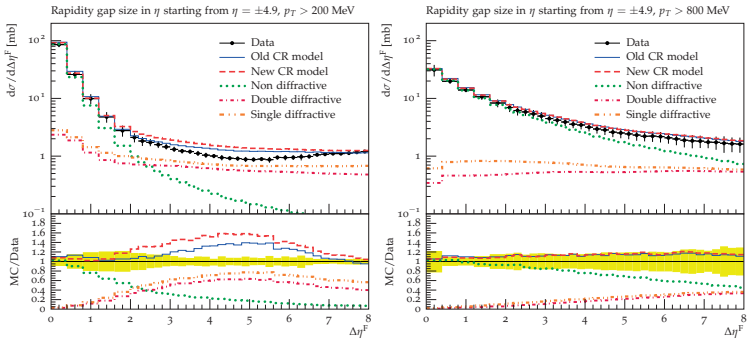

(a) (b)

Figure II.22: The rapidity gap survival for a low $p_\perp$ cut (a) and a high $p_\perp$ cut (b). The different components are also shown for the new CR model (DD/SD/ND). The gathered data is from the ATLAS experiment [119]. The yellow error band represents the experimental 1σ deviation.

higher tension) can also generate harder momentum spectra, while remaining within a string context, as was recently explored in [77]. These effects are generally not expected to be present at the relatively low energy density in pp collisions at a centre-of-mass energy of 200 GeV, however. It would therefore be of great interest to redo the measurement in detail at LHC energies, for high- and low-multiplicity samples and/or in the underlying event, to study whether the slope is steeper at the higher energy densities.

Finally, we emphasise that the rapidity gap survival is heavily affected by the choice of CR model [68, 84]. The explanation is similar to that of the three-jet LEP measurement, where the reconnected colour-singlet jet produces a rapidity gap to the other jets. The old CR model combines different strings into a single larger string, and thereby covers the same rapidity span, essentially adding kinks to an already existing string topology. Instead the new model can produce the colour-singlet union of particles in the same rapidity region. The new model is therefore expected to produce more rapidity gaps compared with the old model, which is also what we observe in fig. II.22. The new model predictions are significantly above the data in the mid-range rapidity region for low $p_\perp$ cutoffs. (For higher $p_\perp$ cuts the effect vanishes, due to the partonic description being more influential on the rapidity gap survival.)

We therefore emphasise that the new CR scenario should in principle be accompanied by a retuning of diffractive parameters. This is not straightforward however, and involves not only the shown rapidity-gap survival distributions, but several other measurements at different energies. It was therefore deemed beyond the scope of this study to perform a retuning of the diffractive components and we limit ourselves to pointing out the interplay. A future dedicated study of this aspect could also well incorporate a study of the interference between the new BR model and diffractive events.

II.4 Application to Top Mass Measurements at Hadron Colliders

Colour reconnections contribute one of the dominant uncertainties on current experimental top-mass extractions in hadronic channels (see e.g. the mini-review in [65]), and their size was recently reexamined in the context of several simplified CR schemes [71]. It is thus interesting to consider our new CR model in the same framework. We follow ref. [71], to which we refer for details on selection of the events and top mass reconstruction procedure.

Briefly stated, the idea is to select semi-leptonic top events, using the charged lepton and escaping neutrino mainly for tagging and then reconstruct the top mass from the hadronic decay. A mass window around the W mass is required and the raw top mass is extracted by fitting the invariant mass distribution of the three jets with a skewed Gaussian distribution, which fits the distributions better than a standard Gaussian [71]. For the models/tunes considered in this work (details below), the resulting shift on the calibrated top mass is below 200 MeV, which is comparable with the current level of CR uncertainty on the measurements [58, 59, 63, 64] and far below some of the "devil's-advocate" toy models considered in [71]. Characteristic for those models is that they allow some fraction of reconnections where the λ measure is increased, whereas all the models considered here involve a minimisation of λ, one way or another.

We compare six models: no CR, the existing (default) PYTHIA 8 CR model with and without early resonance decays (ERD), the new baseline CR model with and without ERD, and the new CR with

Model	$\hat{m}_{\text{top}}$ [GeV]	$\Delta\hat{m}_{\text{top}}$ [GeV]	$\Delta\hat{m}_{\text{top}}^{\text{rescaled}}$ [GeV]
no CR	169.57 ± 0.06	0	0
default ERD	169.26 ± 0.06	-0.36 ± 0.09	-0.04 ± 0.10
default	168.95 ± 0.06	-0.67 ± 0.09	$+0.17 \pm 0.10$
new model ERD	169.18 ± 0.06	-0.45 ± 0.09	$+0.03 \pm 0.10$
new model	168.97 ± 0.06	-0.66 ± 0.09	$+0.14 \pm 0.11$
max CR ERD	169.41 ± 0.06	-0.22 ± 0.09	-0.05 ± 0.10
no CR (tuned)	168.99 ± 0.06	-0.63 ± 0.09	-0.06 ± 0.10
max CR (tuned)	170.28 ± 0.07	$+0.66 \pm 0.09$	$+0.06 \pm 0.11$

Table II.2: Values of m_{top} as predicted by the different CR models. The rescaled top mass is obtained by $\hat{m}_{\text{top}}^{\text{rescaled}} = \frac{80.385}{\hat{m}_W}\hat{m}_{\text{top}}$.

maximal CR and ERD. Since the largest effect is expected for ERD, the maximal CR scenario is only considered with ERD switched on. Two versions of the "no CR" scenario were considered, one in which CR was simply switched off without any further changes (resulting in significant increase in central hadron multiplicity) and the other a semi-tuned version, where the activity ($\sum E_\perp$) in the central region ($|\eta| < 3$) for ND events was retuned. A similar approach is used for the maximal CR models, where again a non-tuned version and retuned version are considered. It should be noted that neither of the retuned models provide a good description of all MB data (for instance $\langle p_\perp \rangle (n_{\text{charged}})$ is described by neither tune). Since none of the models considered exhibit any top-specific behaviour, no additional retuning to top events was needed. The results are collected in tab. II.2.

The first observation is the large difference between the no CR model and the non ERD models for $\Delta\hat{m}_{\text{top}}$ ($\sim$ 650 MeV). Since no CR is performed for the top decay products, not much of difference was expected, and any difference observed has to reside entirely in the underlying event (UE). The CR models considered lower the total string length, and thereby the activity in the UE, which directly influences the non-scaled top mass. Since the "no CR" model uses the same tune parameters as the CR models, it has a too high activity in the UE, leading to the negative mass shifts seen. After retuning to a similar activity in the central region, the "no CR (tuned)"

model agrees with the default CR scenario within the statistical uncertainty. This emphasises the importance of using consistent UE tunes for this type of exercise, though we also note that after recalibration by the hadronic W mass, the rescaled top mass $\hat{m}_{\text{top}}^{\text{rescaled}}$ is remarkably stable.

For the ERD models the above shift in UE is still present, but the UE is now also allowed to reconnect with the top decay products. Therefore, an UE parton in close proximity to a jet from the top decay will have a large probability to be reconnected with the jet. This will result in narrower jets, leading to less of the energy falling outside the jet cone, and thereby a larger top mass. This is in agreement with the simulations, where the ERD results are above the non-ERD results. But the effect is smaller than that of the UE activity, thus the overall shift is still negative compared to the non-tuned no CR model.

Both of the above effects are magnified in the maximal CR scenario. We remind the reader that in this scenario, the $1/N_C^2$ suppression of subleading connections is switched off, hence this should be considered an unphysical extreme variation. Coincidentally, however, the two effects end up approximately canceling. A similar retuning of the central activity as above, "max CR (tuned)", shows a significant increase in the top mass shift of more than one GeV with respect to the tuned no CR model, though again, the W mass calibration removes most of it.

The fact that the rescaled top mass ($\hat{m}_{\text{top}}^{\text{rescaled}}$) is less sensitive to CR is due to a cancellation between CR in the W mass and the top mass. This is in perfect agreement with the simulations, where the deviation for all rescaled masses are below their respective non-rescaled deviations. On the other hand, this means that any interpretation of where the variations between the models arise becomes extremely difficult. We will therefore refrain from attempting this, and instead purely discuss the numerical values in term of the uncertainty on the top mass.

For the rescaled top mass, the differences between the models stay below 200 MeV. This is slightly less than what was observed earlier even for identical CR models (default) [71]. The variations in the results can be attributed to a new tune combined with a change in the PS for $t\bar{t}$ events. We regard the smaller differences

as somewhat coincidental however, and further work is needed to genuinely improve our understanding of CR effects in the top mass measurement. What we can say at least is that the results from the new model lie within those from the default CR model, and therefore do not generate a need for larger uncertainties. Even the maximal CR, which is our attempt to mimic the very large shifts seen for models that ignore MB/UE constraints, does not change this picture. Instead a pattern emerges, namely that whenever the minimisation of the λ measure is used as a guideline for the CR, the shifts stay below 300 MeV (taking the models studied in [71] into account as well). The reason for this is two-fold: firstly the coherence of the PS ensures that the jet structure is not too significantly altered; secondly, the alterations are realised in a systematic fashion leading to a similar shift in both the top and the W mass, implying that the hadronic W mass recalibration is highly robust. An increased understanding of this interplay could potentially lower the uncertainty even further.

Since these models are mainly constrained by measurements, further gains can also be achieved by improving and extending the programme of measurements sensitive to CR effects. A few new observables targeting top events specifically were already suggested in [71]. In the context of top mass uncertainties, such observables are of course especially relevant, as this is the closest to in-situ constraints as can be obtained, mimising the "extrapolation" that the model has to cover between the constraint and measurement environments.

In order to establish whether the small effects on m_t predicted by λ-minimising models are indeed conservative or not, it would be of crucial importance to test these models as directly as possible in a variety of environments, top included. The fact that our new CR models do not yet give good descriptions of identified-particle $p_\perp$ spectra should, in this context, be seen as a warning that there can be additional non-perturbative uncertainties left unaccounted for, possibly of a dynamical origin.

II.5 SUMMARY AND OUTLOOK

The question *"between which partons do confining potentials arise?"* is a fundamental one in non-perturbative QCD, which any attempt at modelling the process of hadronisation must address. In the leading-colour approximation and neglecting beam-remnant correlations, this is relatively simple: there is a one-to-one mapping between perturbative QCD dipoles and string pieces / clusters. In this paper, we have attempted to take a first step beyond leading colour, by including a randomisation over the set of possible subleading-colour topologies, with probabilities chosen according to a simplified version of the $SU(3)$ colour algebra.

We present the argument that while the LC approximation may be quite good in the environment of e^+e^- collisions (more specifically in the absence of multi-parton interactions), we expect very significant deviations from it in pp collisions, where the survival of the strict LC topology should be heavily suppressed. Although the probability for a subleading colour connection to be possible between any given pair of (uncorrelated) partons is only roughly $1/N_C^2$, it becomes increasingly unlikely *not* to have any such connections as the number of uncorrelated partons increases, as e.g. in the case when considering MPI.

This implies that a complex multi-parton system will in general have several different string/cluster configurations open to it, at the time of hadronisation; the LC one is only one among many possibilities. We invoke the string-length λ measure to choose which one is preferred, so far via a simple winner-takes-all algorithm that does not purport to always find the global minimum. Nonetheless, we believe that this model represents a significant step in the right direction, allowing us to probe for the first time the effects of subleading colour on hadronisation in a way that may be said to be systematic and consistent with (a simplified version of) QCD.

One noteworthy new aspect of our work is the use of string junctions to represent antisymmetric colour combinations, such as two colours combining to form an overall anticolour. This provides a new source of baryon production, with properties qualitatively different from the standard diquark scenario. We have shown that this aspect allows to reconcile measured baryon/meson ratios with the

string model in both pp and ee collisions simultaneously. However, we caution that the shapes of the $p_\perp$ spectra are still not well described. We had anticipated that the preference of reconnections to produce boosted string pieces should lead to an enhancement of the $\langle p_\perp \rangle$ especially for heavier hadrons, but the magnitude of this effect observed in our model is still far too low to explain the data.

We emphasised that there is a conceptual difference between colour *connections* and colour *reconnections*. The former is related to colour-space *ambiguities*, such as the unknown colour correlations between different MPI initiators or the subleading-colour connections explored in this work. Colour *reconnections* are related to *dynamical* reconfigurations of the colour/string space, via perturbative gluon exchanges or non-perturbative string interactions; i.e., they involve *momentum* exchange as well. We did not explore effects of the latter type directly in this work, though we note that the fairly realistic string-interaction scenarios constructed by Khoze and Sjöstrand in the context of $e^+e^- \to W^+W^-$ studies [43, 66, 67] also feature string-length minimisation; hence it is possible that our tuned parameters effectively attempt to cover both types. If so, the fact that the momentum spectra remain discrepant may point to the need for dynamical CR.

Finally, we presented a few suggestions for additional observables, the measurement of which would give further insight and possibly help to distinguish both physical and unphysical CR models, as well as other ideas such as models based on colour ropes [76, 77], hydrodynamics [72], or (non-hydro) hadron rescattering. We ended by considering the simplified top-mass analysis of [71] and conclude that the models presented here lead to shifts in the top mass of order 200 MeV, which is within the current level of non-perturbative uncertainties on the measurements.

Acknowledgements

Many thanks to T. Sjöstrand for his valuable comments on both our physics and our code. JRC thanks the CERN theory unit for hospitality during the main part of this study. Work supported in part by the Swedish Research Council, contract number 621-2013-4287, in part by the MCnetITN FP7 Marie Curie Initial Training Network,

contract PITN- GA-2012-315877, and in part by the Australian Research Council, contract FT130100744.

II.A MODEL PARAMETERS

A complete list of all the parameters that differ from the Monash tune for the three different models are listed in the table below.

Parameter	Monash	Mode 0	Mode 2	Mode 3
StringPT:sigma	= 0.335	= 0.335	= 0.335	= 0.335
StringZ:aLund	= 0.68	= 0.36	= 0.36	= 0.36
StringZ:bLund	= 0.98	= 0.56	= 0.56	= 0.56
StringFlav:probQQtoQ	= 0.081	= 0.078	= 0.078	= 0.078
StringFlav:ProbStoUD	= 0.217	= 0.2	= 0.2	= 0.2
StringFlav:probQQ1toQQ0join	= 0.5, 0.7, 0.9, 1.0	= 0.0275, 0.0275, 0.0275, 0.0275	= 0.0275, 0.0275, 0.0275, 0.0275	= 0.0275, 0.0275, 0.0275, 0.0275
MultiPartonInteractions:pToRef	= 2.28	= 2.12	= 2.15	= 2.05
BeamRemnants:remnantMode	= 0	= 1	= 1	= 1
BeamRemnants:saturation	-	= 5	= 5	= 5
ColourReconnection:mode	= 0	= 1	= 1	= 1
ColourReconnection:allowDoubleJunRem	= on	= off	= off	= off
ColourReconnection:m0	-	= 2.9	= 0.3	= 0.3
ColourReconnection:allowJunctions	-	= on	= on	= on
ColourReconnection:junctionCorrection	-	= 1.43	= 1.20	= 1.15
ColourReconnection:timeDilationMode	-	= 0	= 2	= 3
ColourReconnection:timeDilationPar	-	-	= 0.18	= 0.073

BIBLIOGRAPHY

[1] G. Dissertori, I. Knowles, and M. Schmelling, *Quantum Chromodynamics — High energy experiments and theory*. Oxford Science Publications, 2003.

[2] P. Skands, "Introduction to QCD," `arXiv:1207.2389 [hep-ph]`. Lectures given at TASI 2012.

[3] A. Buckley, J. Butterworth, S. Gieseke, D. Grellscheid, S. Höche, *et al.*, "General-purpose event generators for LHC physics," *Phys.Rept.* **504** (2011) 145–233, arXiv:1101.2599 [hep-ph].

[4] R. D. Ball, S. Carrazza, L. Del Debbio, S. Forte, J. Gao, *et al.*, "Parton Distribution Benchmarking with LHC Data," *JHEP* **1304** (2013) 125, arXiv:1211.5142 [hep-ph].

[5] E. Boos, M. Dobbs, W. Giele, I. Hinchliffe, J. Huston, *et al.*, "Generic user process interface for event generators," arXiv:hep-ph/0109068 [hep-ph].

[6] J. Alwall, A. Ballestrero, P. Bartalini, S. Belov, E. Boos, *et al.*, "A Standard format for Les Houches event files," *Comput.Phys.Commun.* **176** (2007) 300–304, arXiv:hep-ph/0609017 [hep-ph].

[7] A. van Hameren, C. Papadopoulos, and R. Pittau, "Automated one-loop calculations: A Proof of concept," *JHEP* **0909** (2009) 106, arXiv:0903.4665 [hep-ph].

[8] F. Cascioli, P. Maierhofer, and S. Pozzorini, "Scattering Amplitudes with Open Loops," *Phys.Rev.Lett.* **108** (2012) 111601, arXiv:1111.5206 [hep-ph].

[9] J. Alwall, M. Herquet, F. Maltoni, O. Mattelaer, and T. Stelzer, "MadGraph 5 : Going Beyond," *JHEP* **1106** (2011) 128, arXiv:1106.0522 [hep-ph].

[10] S. Alioli, S. Badger, J. Bellm, B. Biedermann, F. Boudjema, *et al.*, "Update of the Binoth Les Houches Accord for a standard interface between Monte Carlo tools and one-loop programs," *Comput.Phys.Commun.* **185** (2014) 560–571, arXiv:1308.3462 [hep-ph].

[11] G. Cullen, H. van Deurzen, N. Greiner, G. Heinrich, G. Luisoni, *et al.*, "G*OSAM*-2.0: a tool for automated one-loop calculations within the Standard Model and beyond," *Eur.Phys.J.* **C74** no. 8, (2014) 3001, arXiv:1404.7096 [hep-ph].

[12] J. Alwall, R. Frederix, S. Frixione, V. Hirschi, F. Maltoni, *et al.*, "The automated computation of tree-level and next-to-leading order differential cross sections, and their matching to parton shower simulations," *JHEP* **1407** (2014) 079, arXiv:1405.0301 [hep-ph].

[13] G. Gustafson and U. Pettersson, "Dipole Formulation of QCD Cascades," *Nucl.Phys.* **B306** (1988) 746.

[14] T. Sjöstrand and P. Z. Skands, "Transverse-momentum-ordered showers and interleaved multiple interactions," *Eur.Phys.J.* **C39** (2005) 129–154, arXiv:hep-ph/0408302 [hep-ph].

[15] Z. Nagy and D. E. Soper, "Matching parton showers to NLO computations," *JHEP* **0510** (2005) 024, arXiv:hep-ph/0503053 [hep-ph].

[16] W. T. Giele, D. A. Kosower, and P. Z. Skands, "A simple shower and matching algorithm," *Phys.Rev.* **D78** (2008) 014026, arXiv:0707.3652 [hep-ph].

[17] M. Dinsdale, M. Ternick, and S. Weinzierl, "Parton showers from the dipole formalism," *Phys.Rev.* **D76** (2007) 094003, arXiv:0709.1026 [hep-ph].

[18] S. Schumann and F. Krauss, "A Parton shower algorithm based on Catani-Seymour dipole factorisation," *JHEP* **0803** (2008) 038, arXiv:0709.1027 [hep-ph].

[19] S. Plätzer and S. Gieseke, "Coherent Parton Showers with Local Recoils," *JHEP* **1101** (2011) 024, arXiv:0909.5593 [hep-ph].

[20] K. Hamilton, P. Nason, and G. Zanderighi, "MINLO: Multi-Scale Improved NLO," *JHEP* **1210** (2012) 155, arXiv:1206.3572 [hep-ph].

[21] L. Lönnblad and S. Prestel, "Merging Multi-leg NLO Matrix Elements with Parton Showers," *JHEP* **1303** (2013) 166, arXiv:1211.7278 [hep-ph].

[22] L. Hartgring, E. Laenen, and P. Skands, "Antenna Showers with One-Loop Matrix Elements," *JHEP* **1310** (2013) 127, arXiv:1303.4974 [hep-ph].

[23] B. Andersson, *The Lund model*. Camb. Monogr. Part. Phys. Nucl. Phys. Cosmol., 1997.

[24] B. Andersson, G. Gustafson, G. Ingelman, and T. Sjostrand, "Parton Fragmentation and String Dynamics," *Phys.Rept.* **97** (1983) 31–145.

[25] G. Bali and K. Schilling, "Static quark - anti-quark potential: Scaling behavior and finite size effects in SU(3) lattice gauge theory," *Phys.Rev.* **D46** (1992) 2636–2646.

[26] **Particle Data Group** Collaboration, J. Beringer *et al.*, "Review of particle physics," *Phys. Rev.* **D86** (2012) 010001.

[27] G. Gustafson, "Dual Description of a Confined Color Field," *Phys.Lett.* **B175** (1986) 453.

[28] T. Sjöstrand, S. Mrenna, and P. Skands, "PYTHIA 6.4 physics and manual," *JHEP* **05** (2006) 026, hep-ph/0603175.

[29] T. Sjöstrand, S. Mrenna, and P. Skands, "A brief introduction to PYTHIA 8.1," *Comput. Phys. Commun.* **178** (2008) 852–867, arXiv:0710.3820 [hep-ph].

[30] T. Sjöstrand, S. Ask, J. R. Christiansen, R. Corke, N. Desai, *et al.*, "An Introduction to PYTHIA 8.2," *Comput.Phys.Commun.* **191** (2015) 159–177, arXiv:1410.3012 [hep-ph].

[31] A. Buckley, H. Hoeth, H. Lacker, H. Schulz, and J. E. von Seggern, "Systematic event generator tuning for the LHC," *Eur.Phys.J.* **C65** (2010) 331–357, arXiv:0907.2973 [hep-ph].

[32] N. Firdous and G. Rudolph, "Tuning of PYTHIA6 to Minimum Bias Data," *EPJ Web Conf.* **60** (2013) 20056.

[33] N. Fischer, S. Gieseke, S. Plätzer, and P. Skands, "Revisiting radiation patterns in e^+e^- collisions," *Eur.Phys.J.* **C74** no. 4, (2014) 2831, arXiv:1402.3186 [hep-ph].

[34] P. Skands, S. Carrazza, and J. Rojo, "Tuning PYTHIA 8.1: the Monash 2013 Tune," *Eur.Phys.J.* **C74** no. 8, (2014) 3024, arXiv:1404.5630 [hep-ph].

[35] **OPAL** Collaboration, G. Abbiendi *et al.*, "Tests of models of color reconnection and a search for glueballs using gluon jets with a rapidity gap," *Eur.Phys.J.* **C35** (2004) 293–312, arXiv:hep-ex/0306021 [hep-ex].

[36] **L3** Collaboration, P. Achard *et al.*, "Search for color reconnection effects in $e^+e^- \to W^+W^- \to$ hadrons through particle flow studies at LEP," *Phys.Lett.* **B561** (2003) 202–212, arXiv:hep-ex/0303042 [hep-ex].

[37] **L3** Collaboration, P. Achard *et al.*, "Search for color singlet and color reconnection effects in hadronic Z decays at LEP," *Phys.Lett.* **B581** (2004) 19–30, arXiv:hep-ex/0312026 [hep-ex].

[38] **DELPHI** Collaboration, M. Siebel, "A Study of the charge of leading hadrons in gluon and quark fragmentation," arXiv:hep-ex/0505080 [hep-ex].

[39] **OPAL** Collaboration, G. Abbiendi *et al.*, "Colour reconnection in $e^+e^- \to W^+W^-$ at s**(1/2) = 189-GeV - 209-GeV," *Eur.Phys.J.* **C45** (2006) 291–305, arXiv:hep-ex/0508062 [hep-ex].

[40] **ALEPH** Collaboration, S. Schael *et al.*, "Test of Colour Reconnection Models using Three-Jet Events in Hadronic Z Decays," *Eur.Phys.J.* **C48** (2006) 685–698, arXiv:hep-ex/0604042 [hep-ex].

[41] **DELPHI** Collaboration, J. Abdallah *et al.*, "Investigation of colour reconnection in WW events with the DELPHI detector at LEP-2," *Eur.Phys.J.* **C51** (2007) 249–269, arXiv:0704.0597 [hep-ex].

[42] **ALEPH** Collaboration, S. Schael *et al.*, "Measurement of the W boson mass and width in e^+e^- collisions at LEP," *Eur.Phys.J.* **C47** (2006) 309–335, arXiv:hep-ex/0605011 [hep-ex].

[43] T. Sjöstrand and V. A. Khoze, "On Color rearrangement in hadronic W+ W- events," *Z.Phys.* **C62** (1994) 281–310, arXiv:hep-ph/9310242 [hep-ph].

[44] **ALEPH, DELPHI, L3, OPAL, LEP Electroweak** Collaboration, S. Schael *et al.*, "Electroweak Measurements in Electron-Positron Collisions at W-Boson-Pair Energies at LEP," *Phys.Rept.* **532** (2013) 119–244, arXiv:1302.3415 [hep-ex].

[45] G. Marchesini and B. Webber, "Simulation of QCD Jets Including Soft Gluon Interference," *Nucl.Phys.* **B238** (1984) 1.

[46] T. Sjöstrand and M. van Zijl, "A Multiple Interaction Model for the Event Structure in Hadron Collisions," *Phys.Rev.* **D36** (1987) 2019.

[47] S. Gieseke, C. Rohr, and A. Siodmok, "Colour reconnections in Herwig++," *Eur.Phys.J.* **C72** (2012) 2225, arXiv:1206.0041 [hep-ph].

[48] **Ames-Bologna-CERN-Dortmund-Heidelberg-Warsaw** Collaboration, A. Breakstone *et al.*, "Multiplicity Dependence of Transverse Momentum Spectra at ISR Energies," *Phys.Lett.* **B132** (1983) 463.

[49] **UA1** Collaboration, C. Albajar *et al.*, "A Study of the General Characteristics of $p\bar{p}$ Collisions at $\sqrt{s}$ = 0.2-TeV to 0.9-TeV," *Nucl.Phys.* **B335** (1990) 261.

[50] **CDF** Collaboration, D. Acosta *et al.*, "Soft and hard interactions in $p\bar{p}$ collisions at $\sqrt{s} = 1800$-GeV and 630-GeV," *Phys.Rev.* **D65** (2002) 072005.

[51] **CDF** Collaboration, T. Aaltonen *et al.*, "Measurement of Particle Production and Inclusive Differential Cross Sections in p anti-p Collisions at s**(1/2) = 1.96-TeV," *Phys.Rev.* **D79** (2009) 112005, arXiv:0904.1098 [hep-ex].

[52] **CMS** Collaboration, V. Khachatryan *et al.*, "Charged particle multiplicities in pp interactions at $\sqrt{s} = 0.9$, 2.36, and 7 TeV," *JHEP* **1101** (2011) 079, arXiv:1011.5531 [hep-ex].

[53] **ATLAS** Collaboration, G. Aad *et al.*, "Charged-particle multiplicities in pp interactions measured with the ATLAS detector at the LHC," *New J.Phys.* **13** (2011) 053033, arXiv:1012.5104 [hep-ex].

[54] **ALICE** Collaboration, B. B. Abelev *et al.*, "Multiplicity dependence of the average transverse momentum in pp, p-Pb, and Pb-Pb collisions at the LHC," *Phys.Lett.* **B727** (2013) 371–380, arXiv:1307.1094 [nucl-ex].

[55] A. Karneyeu, L. Mijovic, S. Prestel, and P. Skands, "MCPLOTS: a particle physics resource based on volunteer computing," *Eur.Phys.J.* **C74** (2014) 2714, arXiv:1306.3436 [hep-ph].

[56] R. Corke and T. Sjöstrand, "Interleaved Parton Showers and Tuning Prospects," *JHEP* **1103** (2011) 032, arXiv:1011.1759 [hep-ph].

[57] P. Z. Skands and D. Wicke, "Non-perturbative QCD effects and the top mass at the Tevatron," *Eur.Phys.J.* **C52** (2007) 133–140, arXiv:hep-ph/0703081 [HEP-PH].

[58] **CDF** Collaboration, T. Aaltonen *et al.*, "Precision Top-Quark Mass Measurements at CDF," *Phys.Rev.Lett.* **109** (2012) 152003, arXiv:1207.6758 [hep-ex].

[59] **CMS** Collaboration, S. Chatrchyan *et al.*, "Measurement of the top-quark mass in $t\bar{t}$ events with lepton+jets final states in pp collisions at $\sqrt{s} = 7$ TeV," *JHEP* **1212** (2012) 105, arXiv:1209.2319 [hep-ex].

[60] **CDF, D0** Collaboration, T. A. Aaltonen *et al.*, "Combination of measurements of the top-quark pair production cross section from the Tevatron Collider," *Phys.Rev.* **D89** (2014) 072001, arXiv:1309.7570 [hep-ex].

[61] **CMS** Collaboration, S. Chatrchyan *et al.*, "Measurement of the top-quark mass in all-jets $t\bar{t}$ events in pp collisions at $\sqrt{s}$=7 TeV," *Eur.Phys.J.* **C74** (2014) 2758, arXiv:1307.4617 [hep-ex].

[62] **ATLAS, CDF, CMS, D0** Collaboration, "First combination of Tevatron and LHC measurements of the top-quark mass," arXiv:1403.4427 [hep-ex].

[63] **D0** Collaboration, V. M. Abazov *et al.*, "Precision measurement of the top-quark mass in lepton+jets final states," *Phys.Rev.Lett.* **113** (2014) 032002, arXiv:1405.1756 [hep-ex].

[64] **ATLAS** Collaboration, G. Aad *et al.*, "Measurement of the top quark mass in the $t\bar{t} \to \text{lepton} + \text{jets}$ and $t\bar{t} \to \text{dilepton}$ channels using $\sqrt{s} = 7$ TeV ATLAS data," arXiv:1503.05427 [hep-ex].

[65] A. Juste, S. Mantry, A. Mitov, A. Penin, P. Skands, *et al.*, "Determination of the top quark mass circa 2013: methods, subtleties, perspectives," *Eur.Phys.J.* **C74** no. 10, (2014) 3119, arXiv:1310.0799 [hep-ph].

[66] V. A. Khoze and T. Sjöstrand, "Color correlations and multiplicities in top events," *Phys.Lett.* **B328** (1994) 466–476, arXiv:hep-ph/9403394 [hep-ph].

[67] V. A. Khoze and T. Sjöstrand, "QCD interconnection studies at linear colliders," *Eur.Phys.J.direct* **C2** (2000) 1, arXiv:hep-ph/9912297 [hep-ph].

[68] J. Rathsman, "A Generalized area law for hadronic string re-interactions," *Phys.Lett.* **B452** (1999) 364–371, arXiv:hep-ph/9812423 [hep-ph].

[69] M. Sandhoff and P. Z. Skands, "Colour annealing - a toy model of colour reconnections," arXiv:hep-ph/0604120 [hep-ph]. FERMILAB-CONF-05-518-T.

[70] C. Buttar, S. Dittmaier, V. Drollinger, S. Frixione, A. Nikitenko, *et al.*, "Les houches physics at TeV colliders 2005, standard model and Higgs working group: Summary report," arXiv:hep-ph/0604120 [hep-ph].

[71] S. Argyropoulos and T. Sjöstrand, "Effects of color reconnection on $t\bar{t}$ final states at the LHC," *JHEP* **1411** (2014) 043, arXiv:1407.6653 [hep-ph].

[72] T. Pierog, I. Karpenko, J. Katzy, E. Yatsenko, and K. Werner, "EPOS LHC : test of collective hadronization with LHC data," arXiv:1306.0121 [hep-ph].

[73] **CMS** Collaboration, V. Khachatryan *et al.*, "Observation of Long-Range Near-Side Angular Correlations in Proton-Proton Collisions at the LHC," *JHEP* **1009** (2010) 091, arXiv:1009.4122 [hep-ex].

[74] K. Werner, I. Karpenko, and T. Pierog, "The 'Ridge' in Proton-Proton Scattering at 7 TeV," *Phys.Rev.Lett.* **106** (2011) 122004, arXiv:1011.0375 [hep-ph].

[75] A. Ortiz Velasquez, P. Christiansen, E. Cuautle Flores, I. Maldonado Cervantes, and G. Paic, "Color Reconnection and Flowlike Patterns in pp Collisions," *Phys.Rev.Lett.* **111** no. 4, (2013) 042001, arXiv:1303.6326 [hep-ph].

[76] B. Andersson and P. Henning, "On the dynamics of a color rope: The Fragmentation of interacting strings and the longitudinal distributions," *Nucl.Phys.* **B355** (1991) 82–105.

[77] C. Bierlich, G. Gustafson, L. Lönnblad, and A. Tarasov, "Effects of Overlapping Strings in pp Collisions," *JHEP* **1503** (2015) 148, arXiv:1412.6259 [hep-ph].

[78] R. Corke and T. Sjöstrand, "Multiparton Interactions and Rescattering," *JHEP* **1001** (2010) 035, arXiv:0911.1909 [hep-ph].

[79] H. Fritzsch, "Producing Heavy Quark Flavors in Hadronic Collisions: A Test of Quantum Chromodynamics," *Phys.Lett.* **B67** (1977) 217.

[80] A. Ali, J. Körner, G. Kramer, and J. Willrodt, "Nonleptonic Weak Decays of Bottom Mesons," *Z.Phys.* **C1** (1979) 269.

[81] H. Fritzsch, "How to Discover the B Mesons," *Phys.Lett.* **B86** (1979) 343.

[82] D. Eriksson, G. Ingelman, and J. Rathsman, "Colour rearrangements in B-meson decays," *Phys.Rev.* **D79** (2009) 014011, arXiv:0811.2651 [hep-ph].

[83] W. Buchmüller and A. Hebecker, "A Parton model for diffractive processes in deep inelastic scattering," *Phys.Lett.* **B355** (1995) 573–578, arXiv:hep-ph/9504374 [hep-ph].

[84] A. Edin, G. Ingelman, and J. Rathsman, "Soft color interactions as the origin of rapidity gaps in DIS," *Phys.Lett.* **B366** (1996) 371–378, arXiv:hep-ph/9508386 [hep-ph].

[85] J. Butterworth, J. R. Forshaw, and M. Seymour, "Multiparton interactions in photoproduction at HERA," *Z.Phys.* **C72** (1996) 637–646, arXiv:hep-ph/9601371 [hep-ph].

[86] S. Gieseke, S. Plätzer, A. Siodmok, and C. Röhr, "Minimum bias and underlying event developments in Herwig++,". DESY-PROC-2010-01.

[87] T. Sjöstrand and P. Z. Skands, "Multiple interactions and the structure of beam remnants," *JHEP* **0403** (2004) 053, arXiv:hep-ph/0402078 [hep-ph].

[88] **CDF** Collaboration, F. Abe *et al.*, "Transverse Momentum Distributions of Charged Particles Produced in $\bar{p}p$ Interactions at $\sqrt{s} = 630$ GeV and 1800 GeV," *Phys.Rev.Lett.* **61** (1988) 1819.

[89] **CDF** Collaboration, T. Affolder *et al.*, "Charged jet evolution and the underlying event in $p\bar{p}$ collisions at 1.8 TeV," *Phys.Rev.* **D65** (2002) 092002.

[90] **CDF** Collaboration, R. D. Field, "The Underlying event in hard scattering processes," *eConf* **C010630** (2001) P501, arXiv:hep-ph/0201192 [hep-ph].

[91] **CDF** Collaboration, R. Field and R. C. Group, "PYTHIA tune A, HERWIG, and JIMMY in Run 2 at CDF," arXiv:hep-ph/0510198 [hep-ph].

[92] T. Sjöstrand, "Colour reconnection and its effects on precise measurements at the LHC," arXiv:1310.8073 [hep-ph].

[93] D. Wicke and P. Z. Skands, "Non-perturbative QCD Effects and the Top Mass at the Tevatron," *Nuovo Cim.* **B123** (2008) S1, arXiv:0807.3248 [hep-ph].

[94] P. Z. Skands, "The Perugia Tunes," arXiv:0905.3418 [hep-ph].

[95] P. Z. Skands, "Tuning Monte Carlo Generators: The Perugia Tunes," *Phys.Rev.* **D82** (2010) 074018, arXiv:1005.3457 [hep-ph].

[96] H. Schulz and P. Skands, "Energy Scaling of Minimum-Bias Tunes," *Eur.Phys.J.* **C71** (2011) 1644, arXiv:1103.3649 [hep-ph].

[97] B. Webber, "A QCD Model for Jet Fragmentation Including Soft Gluon Interference," *Nucl.Phys.* **B238** (1984) 492.

[98] E. Avsar, G. Gustafson, and L. Lonnblad, "Small-x dipole evolution beyond the large-N(c) imit," *JHEP* **0701** (2007) 012, arXiv:hep-ph/0610157 [hep-ph].

[99] E. Avsar, "On the dipole swing and the search for frame independence in the dipole model," *JHEP* **0711** (2007) 027, arXiv:0709.1371 [hep-ph].

[100] T. Sjöstrand and P. Z. Skands, "Baryon number violation and string topologies," *Nucl.Phys.* **B659** (2003) 243, arXiv:hep-ph/0212264 [hep-ph].

[101] J. R. Gaunt and W. J. Stirling, "Double Parton Distributions Incorporating Perturbative QCD Evolution and Momentum and Quark Number Sum Rules," *JHEP* **1003** (2010) 005, arXiv:0910.4347 [hep-ph].

[102] C. Flensburg, G. Gustafson, L. Lonnblad, and A. Ster, "Correlations in double parton distributions at small x," *JHEP* **1106** (2011) 066, arXiv:1103.4320 [hep-ph].

[103] B. Blok, Y. Dokshitser, L. Frankfurt, and M. Strikman, "pQCD physics of multiparton interactions," *Eur.Phys.J.* **C72** (2012) 1963, arXiv:1106.5533 [hep-ph].

[104] M. Diehl, D. Ostermeier, and A. Schafer, "Elements of a theory for multiparton interactions in QCD," *JHEP* **1203** (2012) 089, arXiv:1111.0910 [hep-ph].

[105] A. V. Manohar and W. J. Waalewijn, "A QCD Analysis of Double Parton Scattering: Color Correlations, Interference Effects and Evolution," *Phys.Rev.* **D85** (2012) 114009, arXiv:1202.3794 [hep-ph].

[106] A. V. Manohar and W. J. Waalewijn, "What is Double Parton Scattering?," *Phys.Lett.* **B713** (2012) 196–201, arXiv:1202.5034 [hep-ph].

[107] H.-M. Chang, A. V. Manohar, and W. J. Waalewijn, "Double Parton Correlations in the Bag Model," *Phys.Rev.* **D87** no. 3, (2013) 034009, arXiv:1211.3132 [hep-ph].

[108] B. Blok, Y. Dokshitzer, L. Frankfurt, and M. Strikman, "Perturbative QCD correlations in multi-parton collisions," *Eur.Phys.J.* **C74** (2014) 2926, arXiv:1306.3763 [hep-ph].

[109] A. Snigirev, N. Snigireva, and G. Zinovjev, "Perturbative and nonperturbative correlations in double parton distributions," *Phys.Rev.* **D90** no. 1, (2014) 014015, arXiv:1403.6947 [hep-ph].

[110] S. Kirkpatrick, C. D. Gelatt, and M. P. Vecchi, "Optimization by Simulated Annealing," *Science* **220** (May, 1983) 671–680.

[111] **L3** Collaboration, P. Achard *et al.*, "Studies of hadronic event structure in e^+e^- annihilation from 30-GeV to 209-GeV with the L3 detector," *Phys.Rept.* **399** (2004) 71–174, arXiv:hep-ex/0406049 [hep-ex].

[112] W. Giele, D. Kosower, and P. Skands, "Higher-Order Corrections to Timelike Jets," *Phys.Rev.* **D84** (2011) 054003, arXiv:1102.2126 [hep-ph].

[113] **CMS** Collaboration, V. Khachatryan *et al.*, "Transverse-momentum and pseudorapidity distributions of charged hadrons in pp collisions at $\sqrt{s} = 7$ TeV," *Phys.Rev.Lett.* **105** (2010) 022002, arXiv:1005.3299 [hep-ex].

[114] **CMS** Collaboration, V. Khachatryan *et al.*, "Strange Particle Production in pp Collisions at $\sqrt{s} = 0.9$ and 7 TeV," *JHEP* **1105** (2011) 064, arXiv:1102.4282 [hep-ex].

[115] A. Buckley, J. Butterworth, L. Lonnblad, D. Grellscheid, H. Hoeth, *et al.*, "Rivet user manual," *Comput.Phys.Commun.* **184** (2013) 2803–2819, arXiv:1003.0694 [hep-ph].

[116] **TOTEM** Collaboration, G. Antchev *et al.*, "Measurement of the forward charged particle pseudorapidity density in pp collisions at $\sqrt{s} = 7$ TeV with the TOTEM experiment," *Europhys.Lett.* **98** (2012) 31002, arXiv:1205.4105 [hep-ex].

[117] C. Friberg, G. Gustafson, and J. Häkkinen, "Color connections in e+ e- annihilation," *Nucl.Phys.* **B490** (1997) 289–305, arXiv:hep-ph/9604347 [hep-ph].

[118] **STAR** Collaboration, B. Abelev *et al.*, "Strange particle production in p+p collisions at s**(1/2) = 200-GeV," *Phys.Rev.* **C75** (2007) 064901, arXiv:nucl-ex/0607033 [nucl-ex].

[119] **ATLAS** Collaboration, G. Aad *et al.*, "Rapidity gap cross sections measured with the ATLAS detector in pp collisions at $\sqrt{s} = 7$ TeV," *Eur.Phys.J.* **C72** (2012) 1926, arXiv:1201.2808 [hep-ex].

III

COLOUR RECONNECTION AT
FUTURE e^+e^- COLLIDERS

LU TP 15-25
MCnet-15-15
June 2015

Colour Reconnection at Future e^+e^- Colliders

Jesper R. Christiansen and Torbjörn Sjöstrand

Theoretical High Energy Physics,
Department of Astronomy and Theoretical Physics,
Lund University,
Sölvegatan 14A,
SE-223 62 Lund, Sweden

Eur. Phys. J. C75 (2015) 9, 441

Abstract

The effects of colour reconnection (CR) at e^+e^- colliders are revisited, with focus on recently developed CR models. The new models are compared with the LEP2 measurements for $e^+e^- \to W^+W^- \to q_1\bar{q}_2q_3\bar{q}_4$ and found to lie within their limits. Prospects for constraints from new high-luminosity e^+e^- colliders are discussed. The novel arena of CR in Higgs decays is introduced, and illustrated by shifts in angular correlations that would be used to set limits on a potential *CP*-odd admixture of the 125 GeV Higgs state.

III.1 INTRODUCTION

Multiparticle production in high-energy collisions often involves many contributing intermediate sub-sources. The cleanest such example is $e^+e^- \to W^+W^- \to q_1\bar{q}_2q_3\bar{q}_4$, or its equivalent with a $(\gamma^*/Z^0)(\gamma^*/Z^0)$ intermediate state. A more tricky one is multiparton interactions (MPIs) in hadronic collisions, wherein a variable set of (semi)perturbative partonic collisions together with the beam remnants are at the origin of the subsequent hadronization.

In neither case can a first-principles QCD calculation be carried out to describe the particle production process. Instead string or cluster models are used [1]. Both are based on an $N_C \to \infty$ limit [2], wherein each colour-anticolour pair is unique. Thus, in the string model, each quark is at the end of a string, whereas a gluon is attached to two string pieces and thus forms a kink on a longer string usually stretched between an endpoint quark and ditto antiquark [3]. In simple systems like $e^+e^- \to \gamma^*/Z^0 \to q\bar{q}g$ such principles give unique topologies, but for more complicated situations ambiguities arise. When these can be associated with the presence of unexpected colour topologies we speak of colour reconnection (CR). The historical example in this spirit is the decay $mathrmB^+ = u\bar{b} \to u\bar{c}W^+ \to (u\bar{c})(c\bar{s}) \to (u\bar{s})(c\bar{c}) \to K^+J/\psi \to K^+\mu^+\mu^-$ [4], where we have used brackets in intermediate states to delineate separate colour singlet identities.

Similarly, for $e^+e^- \to W^+W^-$, with $W^+ \to q_1\bar{q}_2$ and $W^- \to q_3\bar{q}_4$, to first approximation the $q_1\bar{q}_2$ and $q_3\bar{q}_4$ systems hadronize separately from each other. Deviations from such a production picture could be parametrized as an admixture of alternative colour-reconnected $q_1\bar{q}_4$ and $q_3\bar{q}_2$ systems. Such CR was highly relevant in the context of the W mass measurement at LEP2 [5, 6], where a potentially non-negligible uncertainty was predicted. This led to the development of dedicated studies aimed directly at measuring CR in hadronic W^+W^- events [7–10]. The most extreme CR models could be ruled out, but not enough statistics was collected to definitely distinguish between the more moderate CR models and no CR [11]. Nevertheless such moderate-model reconnection in about half of all events provided the best overall description.

Modelling and testing of CR in hadronic collisions is rather more complicated [12, 13]. And yet the case for it playing an important role is compelling, e.g. from the rise of the average transverse momentum with increasing charged multiplicity. Thus, given the predominance of hadronic colliders in recent years, first with the Tevatron and now with the LHC, recent CR studies have rather aimed to address the more complicated issues arising there, and has led to the introduction of several new models [14, 15]. These rely only on the distribution of final state partons just prior to the hadronization, making them directly applicable also to e^+e^- colliders. And even if the CR effects are expected to be significantly smaller in e^+e^- than in pp, this is compensated by a cleaner environment allowing for higher precision. On the one hand, it is therefore highly relevant to go back and check whether the newly developed models are consistent with the LEP2 data. Unfortunately the statistics is then limited, with only about 10^4 W^+W^- events per LEP experiment, giving non-negligible statistical uncertainties, of the order of 40 MeV for the W mass [11]. On the other hand, it is useful to consider what further tests may come in the future. As an example, the recently suggested 100 km e^+e^- collider [16] would produce $\mathcal{O}(10^8)$ W^+W^- pairs, resulting in a statistical uncertainty on the W mass below 1 MeV, e.g. from semileptonic decays $e^+e^- \to W^+W^- \to q_1\bar{q}_2\ell\nu_\ell$. With the calculated mass shifts in the original CR paper of the order 10-20 MeV [5] as a reference, such a precision should make it possible to rule out many CR models, and also (hopefully) definitely confirm the presence of CR effects.

With the discovery of the Higgs boson [17, 18], a new arena for CR studies opens up. The Higgs state is very narrow — the expected width is of the order of 4 MeV — meaning that it is very long-lived. Therefore hadronization of the rest of the event already happened and the produced hadrons already spread out by the time the Higgs decays. That is, the Higgs itself decays essentially in a vacuum, and has no interactions with the rest of the event, be that in e^+e^- or pp collisions. Among its key decay channels we find W^+W^- and Z^0Z^0, however, and here history repeats itself: fully hadronic decays would be sensitive to CR between the two gauge-boson systems. The variables of interest here are not only masses but even more the angles between the four hadronic jets. Such an-

gles can be modified by CR, a phenomenon which was noted e.g. in the context of top mass studies [14]. CR uncertainties thereby affect precision measurements of the Higgs properties, one of the primary purposes of future e^+e^- colliders. To be specific, the SM predicts the Higgs to be a *CP*-even state, which is also observed to be strongly favoured compared with the *CP*-odd alternative [19, 20]. Extensions of the SM Higgs sector, however, allows for the observed Higgs to be a mixture of both possibilities. One place to search for deviations from the predicted SM Higgs behaviour is precisely the angular correlations in hadronic W^+W^- (or Z^0Z^0) decays [21]. Hence CR could introduce a systematic uncertainty, and in this article we do a first study on the size of such uncertainties in various CR scenarios.

This paper is organized as follows. The different CR models we will compare are briefly summarized in section III.2. The three next sections contain studies on three different sets of observables, namely, the W mass measurement, section III.3, the search for CR effects in W^+W^- events, section III.4, and the Higgs *CP* measurements, section III.5. The article ends with a few conclusions, section III.6.

III.2 THE CR MODELS

Our current understanding of QCD does not provide a unique recipe for CR. Therefore the best we can do is contrast different plausible scenarios, and let data be the judge what works and what does not. In this article we will compare four different CR models, which provide a reasonable spread of properties and predictions. Before briefly presenting each of these models it is useful to outline some of the basic issues that are involved.

One key aspect is what role is given to colour algebra. To illustrate this, again consider $e^+e^- \to W^+W^- \to q_1\bar{q}_2q_3\bar{q}_4$. From the onset, $q_1\bar{q}_2$ form one singlet and $q_3\bar{q}_4$ another. In addition, there is a 1/9 probability that $q_1\bar{q}_4$ and $q_3\bar{q}_2$ "accidentally" form singlets. In some models such accidental matches are a prerequisite to allow a CR. In this sense, these models are not really about *re*connections but about a choice between already existing singlets. The alternative is to view CR as a dynamical process, wherein (infinitely) soft

gluons can mediate any colour exchange required to form new singlets. The original non-accidental singlets define an initial state that actively needs to be perturbed to create alternative colour topologies. As so often, these two pictures may be viewed as extremes, and the "true" behaviour may well be in between, with a bit of each.

Here another aspect enters, namely the role of geometry/causality. With a $c\tau \approx 0.1$ fm, the $W^{\pm}$ decays tend to be separated on a scale an order of magnitude below the typical hadronic size, the latter also being the size of the colour fields stretched between colour-connected partons. It would thereby seem that the W^+ and W^- colour fields fully overlap, at least in the threshold region where the W's are not too strongly boosted apart. Introducing causality, however, the colour fields take some time to grow to full size (e.g. in the SK-I model described later). Meanwhile they drift apart, thereby only partly overlapping, and with an overlap that depends on the motion of all the string pieces from each W decay. In models where geometry is allowed to play a role there is also a natural decoupling of the two W decays at energies well above the threshold region, or if the W width could be sent to zero, and this should not be spoiled by the "accidental" singlets.

Finally there is also a selection principle: if there are many potential reconnections in an event, which are the one(s) that actually occur? This could be at random or involve some bias. The most common bias is to make use of the λ measure, which characterizes the total string length [22]. That is, the smaller the λ, the better ordered are the partons along the strings. The full λ expression is rather messy, so a commonly used approximation is

$$\lambda = \sum_{ij} \ln\left(1 + \frac{m_{ij}^2}{m_0^2}\right) , \tag{III.2.1}$$

where the ij sum runs over all parton pairs connected by a string piece and m_0 is of the order of a typical hadronic mass. The average hadronic multiplicity of a string piece grows roughly logarithmically with its mass, so a reduction of λ corresponds to a reduction of the "free energy" available for particle production.

Among the four different CR models considered in this study, SK-I and SK-II were developed for W mass uncertainty studies at LEP2 [5]. The gluon move model, GM, was introduced as a simple model, among a few others, to study the effect of CR in top decays [14]. Finally, the QCD-based model, CS, was introduced to look for effects in soft QCD, especially baryon production [15]. The first two models are only applicable for the hadronic decays in diboson production, whereas the latter two could be used for any process. All of the models are available in (recent versions of) Pythia 8 [23], the first two having been (re)implemented expressly for this study. That program also contains another CR model [13], used by default, that relies on the MPI structure of hadron collisions and therefore cannot be used in e^+e^-. All of the algorithms are applied after the hard primary process and the subsequent parton-shower evolution, but before the hadronization step. Typically this means that each W contains a handful of gluons, in addition to the primary $q\bar{q}$ pair, when CR is to be considered.

Both the SK-I and SK-II model utilize the space-time picture of strings being stretched between the different decay products of the two bosons. A reconnection between two string pieces from different bosons is allowed only when these overlap in their space–time motion. Since such an overlap is assumed associated with the possibility for dynamical soft-gluon exchange between the two overlapping colour fields, there is no colour-factor suppression for reconnection. The two approaches differ in their definition of what an overlap means, taking two extreme limits by analogy with Type I and Type II superconductors, which explains their names. In SK-I the strings are imagined as elongated bags, and the probability for a reconnection is proportional to the integrated space–time overlap between two string pieces. (Up to saturation effects to ensure that probabilities stay below unity.) This model contains one parameter that directly controls the overall strength of the CR, which made it convenient for experimental LEP2 studies. For SK-II the string is considered to contain a thin core, a vortex line, where all the topological information is stored, even if the full energy still is spread over a larger volume. A reconnection can only occur when the space–time motion makes two such cores cross each other. This model introduces no special parameters, and therefore gives unique

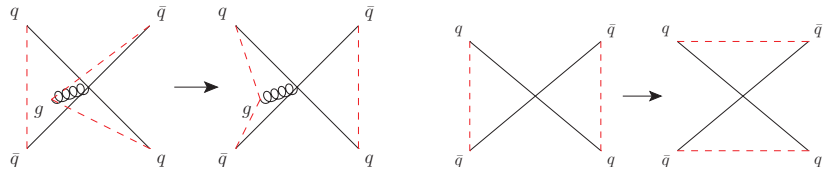

Figure III.1: Example of the gluon-move (a) and the gluon-flip (b) reconnections in the gluon-move model. The dashed lines represent the colour configuration of the partons.

predictions. (In both models one parameter is used to describe how the strings decay exponentially in proper time, and in SK-I additionally the string width is a parameter, but these parameters are almost completely fixed within the string model itself.) Normally only one reconnection is made, namely the one that happens first in proper time. By default this reconnection may either increase or decrease the total λ measure, but in the primed variants SK-I′ and SK-II′ only reconnections that reduce λ are considered. The SK models were tested at LEP2, where only the most extreme versions of SK-I were ruled out. For the SK-I model best agreement with data was obtained with parameter such that approximately 50% of all events contain a reconnection, as already mentioned.

The gluon-move (GM) model was introduced to probe uncertainties in the top mass measurement, while still providing an overall good description of data. It is a very simple framework, in which the reduction of the λ measure is at center, whereas neither colour algebra nor space–time geometry are considered at all. It contains two different types of CR, the gluon move one that gives the model its name, and a flip mechanism. In the former, the change in λ measure is calculated if any of the gluons is moved from its current location between two colour-connected partners to instead be located on the string piece of any other colour-connected pair, fig. III.1a. The move that lowers the total λ measure the most is carried out, repeatedly until the minimum λ measure is reached. The move step is quite restrictive, in that a string stretched between a q and a $\overline{\text{q}}$ endpoint will remain so; it is only the gluons in between that may change. Therefore an additional flip step is carried out after no more moves are possible. The flip mechanism flips the colour lines

between two strings when this can reduce λ, fig. III.1b, thereby mixing up also the string endpoints with each other. (This is similar in character to what in another context is called colour swing [24].) A string is only allowed to do a single flip, to avoid the formation of gluon loops. The strength of the CR can be controlled by excluding a fraction of the gluons in the above scheme, or by requiring the λ reduction in a potential move/flip to be above some minimal value. The parameters used in this study were tuned to describe the LHC minimum bias data (although not quite as well as the default model). To allow more control, three alternative versions are considered in this article: only including the move mechanism, GM-I, only the flip mechanism, GM-II, and the combination of both methods, GM-III.

The $SU(3)$-based model, CS, is similar to the GM model, in that it also minimizes the λ measure by doing flips between strings. But it differs in two major aspects. Firstly, it relies on the $SU(3)$ colour rules from QCD, together with a space–time causality requirement, to determine whether two strings are allowed to reconnect or not. Secondly, it introduces a junction type of reconnection that is unique to this model. The use of $SU(3)$ colour rules is a choice of philosophy, as already discussed. It limits which string pieces may flip with each other by requiring matching colour labels, i.e. that the colour flow is ambiguous already by the colour assignments of the partons. It is possible to change the QCD-based default value, however, in the extreme case such that all string pieces may flip with each other. For a flip between any two string pieces it is further required that they are in causal contact with each other, i.e. that each has had time to form before the other has had time to hadronize. The detailed formulation of this requirement is ambiguous, however, so a few options are available, with a tuneable parameter. The appearance of junction structures offers a clear extension relative to the other models. An (anti)junction is a point where strings stretched from three (anti)coloured quarks meet. In e^+e^- events they must be created in pairs, one junction and one antijunction. When events hadronize, one (anti)baryon is created around each (anti)junction, thereby introducing a new mechanism for baryon production. It is more important for high-energy hadronic collisions than it is for the studies in this article, how-

ever. A possibility not considered is that of colour ropes [24–26], where several parallel strings combine into one of a higher colour representation. If existing at all, ropes are more likely to play a non-negligible role in hadron or heavy-ion colliders, where the beam axis offers a natural alignment of many strings.

While the overwhelming majority of CR models have been developed for Lund string fragmentation, there have also been a few for cluster models [27, 28]. In the current Herwig++ model CR is based on a minimization of the sum of squared cluster masses (similarly to the Generalized Area Law model for strings [29]) rather than on the logarithmic λ measure used here. While the Herwig++ model can be used for W^+W^-, no studies in the spirit presented here have been performed so far.

III.3 W MASS MEASUREMENTS

One of the key tasks of LEP2 was to determine the W mass, on its own right and as a test of the Standard Model consistency. Measurements were done both in the fully hadronic and in the semileptonic channels [10, 30]. Both of them provide similar statistical errors, but the fully hadronic channel has a larger systematic uncertainty, due to the CR contribution. The uncertainty estimate depends on the analysis method as well as on the choice of CR models considered (and on their parameters), but was found to be of the same magnitude as the statistical error. The large expected decrease in the statistical error at future e^+e^- colliders would make the fully hadronic channel irrelevant for W mass measurements, unless the CR uncertainty could be constrained by other means. This was already considered at LEP2 [10], where W mass measurements for different jet cuts were used to constrain the SK-I strength parameter.

In this section we want to turn the table, and study how a precision measurement of the W mass difference between the fully hadronic and the semileptonic channels would constrain CR models and parameter values. The semileptonic channel is free of CR effects that could affect the W mass, and thus provides the "true" W mass baseline as far as CR effects are concerned. For this relative comparison a full optimization of both cuts and analysis methods

is not required. Instead we will follow the method outlined in [5] to provide a simple estimate of CR effects.

To this end, one million $e^+e^- \to W^+W^- \to q_1\bar{q}_2q_3\bar{q}_4$ events were simulated for each CR model, a number big enough to clearly discern the effects we are interested in, and also well within the reach of future e^+e^- colliders. The events are required to have exactly four jets using the Durham jet algorithm [31], with a $k_\perp$ cut of 8 GeV. In addition the jets are also required to have an energy of at least 20 GeV each and be separated by an angle of 0.5 radians. The four jets can be combined into two W bosons in three different ways. A few options for picking the "right" combination are considered:

1. With the access to Monte Carlo truth information, one can try to match each jet with a outgoing parton of the W decays. This is done by picking the match that minimizes the product of the invariant masses between each jet and its associated parton.

2. One can use that the W mass is known to be close to 80 GeV, and so minimize $|\overline{m}_W - 80|$ to find the desired match, where $\overline{m}_W$ is the average reconstructed W mass.

3. Instead of requiring the average to be close to the known W mass, both masses individually could be optimized to be close to 80 GeV, i.e. minimize $|\overline{m}_W^{(1)} - 80| + |\overline{m}_W^{(2)} - 80|$.

4. At threshold the jets from the same W are almost back-to-back. A match can therefore be found by maximizing the sum of opening angles.

To a large extent these methods pick the same combinations, and thus they give similar results. Most of the problems arise in events with hard QCD radiation, where none of the methods are expected to work well. As a separate topic it would be interesting to study the effect of perturbative QCD radiation on the hadronic W mass measurement. The Pythia shower already handles the first emission correctly [32, 33], but to go beyond that one should compare different shower algorithms with and without merging and matching to yet higher orders.

The W mass is calculated as the average of the two chosen W combinations. Since the target of this study is CR effects, the Breit-Wigner broadening of the mass spectrum is removed by subtracting the average of the produced W bosons. The results for all the methods are listed in table III.1. The results for SK-I and SK-II differ slightly from the result in the original paper [5], which is due to the $p_\perp$-ordered shower in the newer versions of PYTHIA not being identical with the older mass-ordered ones of the time.

The GM model shows an interesting behaviour; the move mechanism lowers the W mass, while the flip mechanism increases it, and the two effects accidentally cancel each other in the combined result. This may be understood as follows. If a gluon from W_1 is radiated at a large angle, such that it will move closer to the decay products from W_2, the move mechanism will connect the gluon to W_2, fig. III.1a. This will increase the mass of W_2 and decrease the mass W_1, but the decrease is larger than the increase, leading to the observed lower average mass. The flip mechanism instead will connect jets between the two Ws, and thereby increase hadronization production of particles outside the W "cones". This leads to larger opening angles, and thereby larger W masses. These two explanation will be revisited when studying the dedicated CR measurements. The complete cancellation is accidental, however, which becomes clear when the energy is varied. The SK-I and SK-II models also show opposite-sign effects, thereby further stressing the message that the mass-shift direction of CR effects cannot be taken for granted. Finally, the CS model shows no significant shifts, which will be a general trend throughout all the analyses. In this model the limitation from the colour rules and the requirement of a lower λ make the majority of the e^+e^- collider events have no CR. By removing the colour constraints (CS max), the model starts to show an effect. This extreme case is already excluded at hadron colliders, however.

A new collider should have the capacity to increase the energy beyond the W^+W^- threshold. And as was already observed for the SK-I model [5], the CR effects depend on the CM energy. There are two competing effects: firstly, the effect of a single reconnection becomes larger with increased energy, and secondly, the probability to have two overlapping strings decreases with energy. The CR mass shifts for different CM energies can be studied in tab. III.2.

Method	$\langle \Delta\overline{m}_W \rangle$ (MeV)	$\langle \delta\overline{m}_W \rangle$ (MeV)							
		SK-I	SK-II	SK-II′	GM-I	GM-II	GM-III	CS	CS max
1	-136	+18	-14	-6	-41	+49	+2	+7	+13
2	-73	+13	-13	-7	-28	+34	-1	+3	+11
3	-131	+14	-18	-9	-37	+40	-5	+6	+7
4	+131	+10	-18	-9	-27	+31	-3	+3	+10

Table III.1: Systematic mass shifts for the W mass at a center-of-mass energy of 170 GeV. The $\langle \Delta\overline{m}_W \rangle$ value is the average reconstructed minus produced W mass for the no-CR baseline. The $\langle \delta\overline{m}_W \rangle$ is the additional shift for each CR model relative to this baseline. The Monte Carlo statistical uncertainty on the latter quantity is 4 MeV.

Method	$\langle \delta\overline{m}_W \rangle$ (MeV) ($E_{cm} = 240$ GeV)						
	SK-I	SK-II	SK-II′	GM-I	GM-II	GM-III	CS
1	+95	+29	+25	-74	+400	+104	+9
2	+87	+26	+24	-68	+369	+93	+8
3	+95	+30	+26	-72	+402	+105	+10
Method	$\langle \delta\overline{m}_W \rangle$ (MeV) ($E_{cm} = 350$ GeV)						
	SK-I	SK-II	SK-II′	GM-I	GM-II	GM-III	CS
1	+72	+18	+16	-50	+369	+60	+4
2	+70	+18	+15	-50	+369	+60	+4
3	+71	+18	+16	-50	+369	+60	+3

Table III.2: Systematic W mass shifts at center-of-mass energies of 240 and 350 GeV, respectively. The $\langle \delta\overline{m}_W \rangle$ is the mass shift in the CR models relative to the no-CR result. The Monte Carlo statistical uncertainty is 5 MeV.

Method 4 is here not included, since the maximum-angle method is only reliable close to the threshold. The differences between the methods become smaller at higher energies, since the boost makes it easier to find the right combinations. The actual shifts increase at the intermediate energy, but drop when the energy is increased further. The only model that does not show this trend is the CS model, for which almost no effect is seen at any energy. The large shifts at the two higher energies for the other models provide a compelling argument to repeat the measurements at these energies. It should be recalled, however, that less statistics is expected at the higher energies.

III.4 FOUR-JET ANGULAR DISTRIBUTIONS

The direct searches for CR in W^+W^- events at LEP ruled out extreme parameter values for SK-I and potentially could also rule out some of the new CR models. Especially the GM-I and GM-II models have that potential, since they were already observed to have a larger effect on the W mass measurement than the other models.

The analysis relies on the particle multiplicities in the angular regions between two jets from the same W decay and from different W decays, respectively, to provide a ratio that is sensitive to CR. The idea is that a reconnection will form a string between jets from different W decays, thereby increasing the multiplicity between those jets. In general, we will therefore expect the same-to-different ratio to become lower when CR is switched on. Several LEP experiments [7–9] performed this measurement. The results presented in the studies are after detector simulation, however, and as such are not directly comparable with the results obtained in this study. Instead we will rely on the ratio between the CR and the no-CR results (r, see later for exact definition), since detector effects are reduced for this observable. A preliminary combination of the different experiments gave $r = 0.969 \pm 0.011(\text{stat.}) \pm 0.009(\text{syst.corr.}) \pm 0.006(\text{syst.uncorr.})$ [34] corresponding to a 2.2 standard deviation disagreement with the no-CR scenario. A later combined study [11] has increased this to disfavor the no-CR model at a 2.8 standard deviation level, by combining with the mass shift results and performing a $\Delta\chi^2$ fit. No separate r results were shown, however, and therefore we will have to rely on the preliminary combination.

The event selection and analysis procedure varied slightly between the different LEP experiments. Two of the experiments relied purely on the angles to pair the jets [8, 9], while one experiment also used the invariant masses [7]. We decided to mimic the analysis from the L3 collaboration [8]. A short recap of the event selection and analysis is presented, but for more details we refer to the experimental studies.

The event selection requires each event to have exactly four jets with the Durham jet algorithm, with $y_{\text{cut}} = 0.005$. The two smallest of the six interjet angles are required to be below 100° and be non-adjacent. These are assumed to be the two regions between the

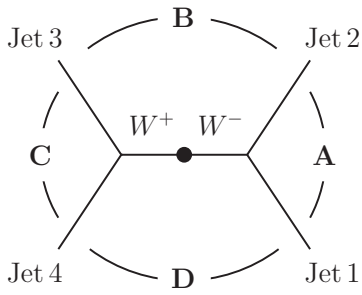

Figure III.2: Illustration of the four interjet regions used in the analysis.

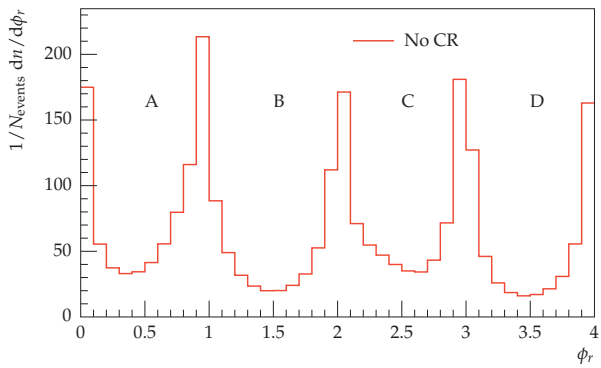

Figure III.3: The φ_r distribution at a center-of-mass energy of 183 GeV.

different W decays, and are normally referred to as regions B and D (fig. III.2). In addition two more angles are required to be between 100° and 140° and be non-adjacent. These are assumed to be the regions inside the W decays, and are normally referred to as region A and C (fig. III.2). If several combinations are allowed, the one with the largest total opening angle is chosen. For each region the particles are projected onto the plane spanned by the two jets, and all particles are assigned a rescaled angle $\varphi_r = \varphi/\varphi_{jj}$, where φ is the angle from the particle to one of the jets and φ_{jj} is the angle between the two jets. This distribution is shown in fig. III.3, where the different regions are separated by adding an integer to each. The final observable is defined as

$$R_N = \frac{\int_{0.2}^{0.8} \frac{dn}{d\varphi_r}(A+C)d\varphi_r}{\int_{0.2}^{0.8} \frac{dn}{d\varphi_r}(B+D)d\varphi_r}. \tag{III.4.1}$$

The regions closest to the jets are excluded since they are mainly sensitive to the internal jet evolution. Finally the ratio between the different CR models and the no-CR baseline is defined as $r = R_N^{CR}/R_N^{noCR}$. Thus a deviation from unity would disfavour the no-CR scenario. The results for the various CR schemes are shown in tab. III.3. As expected, all CR models, except for GM-I, predicts an r below unity. The GM-I model only allows the gluon move reconnections, and therefore it does not reconnect the quarks at the string endpoints. Instead, it can take gluons emitted at large angles and move them to the other W string, thereby actually lowering the amount of radiation in region B and D, fig. III.1a. This is the same explanation as for the lower W mass observed in section section III.3. The GM-II model only does flips, which is exactly what this observable is optimized to measure. This is in fair agreement with observations, since this model shows relative large deviations from unity. The SK-I model with default strength is quite well in agreement with the actual measurement. For comparison a SK-I max model, where a reconnection is always done, is also included. It gives too large shifts and so can be excluded. The SK-II models and the CS model do not produce any large shifts. The maximal CS model, where the $SU(3)$ rules are ignored and CR is only limited by the λ measure, shows a larger effect and it can potentially be ruled

inter-val	R_N^{noCR}	r								
		SK-I	SK-II	SK-II′	GM-I	GM-II	GM-III	CS	SK-I max	CS max
0.1–0.9	1.1031	0.9889	0.9971	0.9969	1.0132	0.9629	0.9876	0.9960	0.9614	0.9712
0.2–0.8	1.1482	0.9802	0.9916	0.9931	1.0293	0.9440	0.9918	0.9910	0.9360	0.9785
0.3–0.7	1.1402	0.9747	0.9887	0.9889	1.0404	0.9301	0.9931	0.9911	0.9196	0.9838
0.4–0.6	1.0883	0.9702	0.9823	0.9880	1.0460	0.9181	0.9882	0.9920	0.9068	0.9822

Table III.3: Results for R_N and r for different intervals in φ_r at a center-of-mass energy of 183 GeV. Two maximal CR models are included for SK-I and for the QCD based method, respectively. The Monte Carlo statistical uncertainty on r is around 0.0025.

	no CR	SK-I	SK-II	SK-II′	GM-I	GM-II	GM-III	CS	SK-I max	CS max
n_σ	2.0	0.7	1.5	1.6	3.9	1.6	1.5	1.4	2.1	0.6

Table III.4: Deviations from the measured result shown in number of standard deviations ($n_\sigma = (r_{\text{exp}} - r_{\text{th}})/(\delta r)_{\text{exp}}$), where the r_{th} are those in the 0.2–0.8 region of tab. III.3.

out by experiments. It is, however, still relatively small compared to the other maximal CR models.

In this study we consider several intervals, and not only the 0.2–0.8 considered in the original study. A clear trend shows that the smaller the interval, the more sensitive the observable becomes, i.e. varies more from unity. This is not surprising since the region closest to the jets are dominated by their perturbative behaviour. It should be noted that the statistics becomes worse for smaller intervals, but with the larger expected statistics at a new collider, a smaller interval than at LEP2 would most likely be preferable.

To check if the new models are already excluded by the LEP measurements, the number of standard deviations from the measured result is calculated, tab. III.4. The experimental uncertainties are assumed Gaussian and added in quadrature. The only model excluded at the three σ level is the GM-I model, which is the only model predicting a larger than unity r. The uncertainty is still too large to invalidate the other models, and a new collider with higher precision is needed to constrain these.

The W mass measurement was seen to be more sensitive to CR at higher energies, and hence a similar effect is expected here. The method described above cannot directly be applied at higher energies, however, since the increased boost of the W bosons changes

$\sqrt{s}$ [GeV]	R_N^{noCR}	r								
		SK-I	SK-II	SK-II′	GM-I	GM-II	GM-III	CS	SK-I max	CS max
183	1.9003	0.9900	0.9915	0.9924	1.0142	1.0247	0.9768	0.9902	0.9667	1.0153
240	1.1764	0.9820	0.9935	0.9933	0.9857	1.0130	0.9362	0.9993	0.9030	0.9762
350	1.4459	0.9829	0.9948	0.9939	0.9758	1.0022	0.9228	1.0028	0.8502	0.9586

Table III.5: Results for R_N and r for different center-of-mass energies for a fixed interval (0.2–0.8). The Monte Carlo statistical uncertainty on r is around 0.0015.

the angular distributions between the jets. Instead we apply a method similar to method 3 in the W mass section to define the two angles within the W decays. The two other angles are defined to minimize the total sum of their angles. The results for the different energies are shown in table III.5. The new method performs slightly worse at 183 GeV, i.e. the ratios lie closer to unity. This is especially evident when considering the maximal CR models. At higher energies, however, the deviation from unity becomes larger for some of the more extreme models, indicating a better sensitivity, but this observable shows no sensitivity for the CS model. The moderate models do not show any significant variation with energy, and as such it is difficult to tell whether the potential limits on CR can be stronger at higher energies. In general we expect a falling fraction of events with CR for higher energies, but more spectacular effects for the events where CR occurs, so in the future we will need to search for more selective tests.

As a slightly simpler observable, to test CR, it is possible to study the overall multiplicity. In most models CR minimizes the λ measure and therefore also lowers the total multiplicity. This is normally compensated by a retuning of the hadronization parameters or the perturbative regime. But by comparing the multiplicity in fully hadronic and semileptonic W^+W^- events, it is possible to directly probe CR. If no CR is switched on, the ratio $N_{\text{ch}}^{W^+W^-\to q_1\bar{q}_2q_3\bar{q}_4}/(N_{\text{ch}}^{W^+W^-\to q_1\bar{q}_2\ell\nu_\ell}-1)$ is expected to be exactly equal to 2 (with $\ell = e$ or μ, but excluding τ). A simple study at a center-of-mass of 170 GeV shows that indeed it is interesting to use this observable. Both the individual GM models show an effect, 1.96 and 1.97 for GM-I and GM-II, respectively. Contrary to the earlier observables, the two effects add coherently and the combined

result is 1.93. With 1.97 the CS model also shows more sensitivity in this observable as compared to the more complicated four-angle measurement. Similar results are also obtained for the SK models, so this would be an intriguing measurement for a future e^+e^- collider.

III.5 Higgs parity measurements

As discussed in the introduction, hadronic W^+W^- and Z^0Z^0 decays of the 125 GeV Higgs offers a novel system for CR effects. Like in the W^+W^- studies above we should not expect big effects, so it is unlikely to be discernible in the busy LHC environment. In a process like $e^+e^- \to \gamma^*/Z^{0*} \to H^0Z^0 \to H^0\ell^+\ell^-$, or $\mu^+\mu^- \to H^0$ for that matter, detailed studies should become possible, however, assuming sufficient luminosity. As before, reconstructed masses and angles may become affected. Rather than simply repeating discussions along the lines of the previous two sections, we choose to illustrate possible effects for another set of observables, related to setting limits for *CP* violation in Higgs decays. We are aware that such tests can be performed in purely leptonic decays, say $H \to Z^0Z^0 \to \mu^+\mu^-e^+e^-$, although with a much lower branching ratio. It can also be probed by the decay angles of the Z^0 produced in the association with the H^0 [35]. The purpose of this brief study is not to compare the relative merits of *CP*-violation tests in these different channels, but to stay with $H \to W^+W^- \to q_1\bar{q}_2q_3\bar{q}_4$ and check what CR could mean there. To this end we will use a simplistic χ^2 test on what could be the most sensitive variable.

To simulate a mixed *CP*-even and *CP*-odd Higgs boson, we will use the Higgs doublet model already implemented in Pythia, with the option to allow *CP*-violation based on the expressions in [21]. We will assume that the 125 GeV Higgs is almost completely *CP*-even, with a small admixture of *CP*-odd. Allowing for an interference term between the two, the Higgs cross section can be written as

$$\sigma \propto k_{\text{even}}^2 A + k_{\text{odd}}^2 B + k_{\text{even}}k_{\text{odd}} C\,, \tag{III.5.1}$$

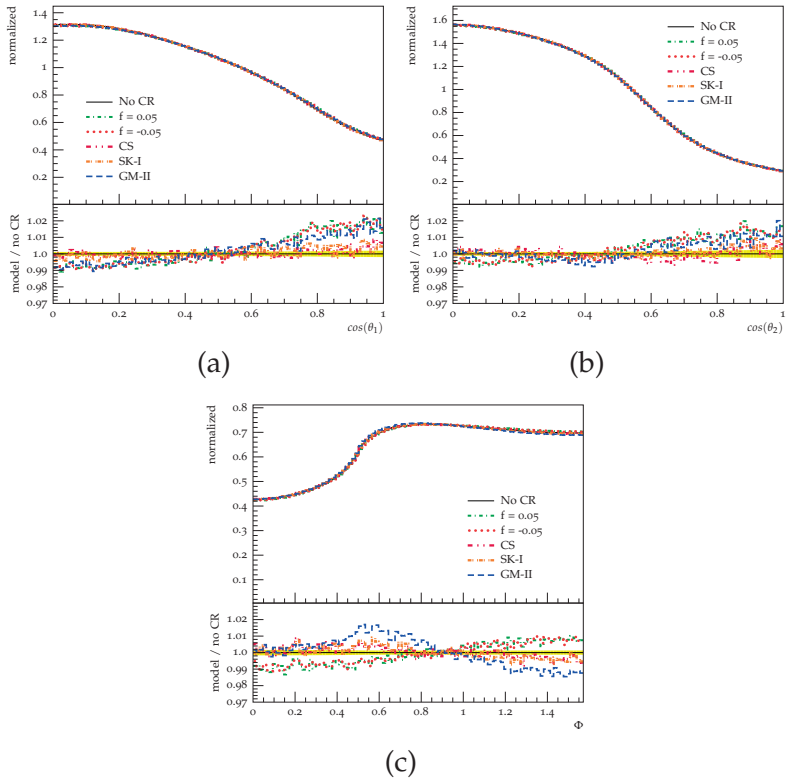

(a) (b)

(c)

Figure III.4: The three angles sensitive to the parity of the Higgs boson. Three different parity scenarios are shown together with a small selection of different CR models.

where A, B, C depends on the kinematics of the event and the k determine the contributions to the different types. Since A, B and C are not of the same order of magnitude, a characterization in terms of a mixing angle is not convenient. Instead we use a definition based on the fraction, later referred to as parity fraction, of the events coming from either of the odd and the interference parts of the cross section:

$$f = \frac{|k_{\text{odd}}^2 B| + |k_{\text{even}} k_{\text{odd}} C|}{|k_{\text{even}}^2 A| + |k_{\text{odd}}^2 B| + |k_{\text{even}} k_{\text{odd}} C|}\,. \tag{III.5.2}$$

For an almost *CP*-even Higgs, $f \approx 0$, this quantity provides a reasonable estimate of the amount of *CP*-violating interference introduced for the Higgs boson.

The parity of the Higgs can be measured by studying the angles between the fermions from the boson decays. In the standard analyses of the spin/parity of the Higgs boson (see e.g. [36, 37]), five such angles are defined, out of which three are sensitive to the parity of the Higgs. These three angles are: θ_1, the polar angle of a fermion in the rest frame of its W mother, with respect to the direction of motion of the W in the H rest frame, θ_2, similarly but for the other W, and Φ, the angle between the two planes spanned by the decay products of the respective W bosons. The rest of this section will therefore be a study on the effect of CR on these three angles.

To only have to consider the Higgs decay itself we have studied the process $\mu^+\mu^- \to H^0$, but this should only be viewed as a technical trick. All models are set up to easily handle this, whereas $e^+e^- \to H^0Z^0$ would require a bit more bookkeeping for the SK models. Otherwise the models remain unchanged relative to previous studies. The fact that at least one of the W's have to be strongly off-shell implies that its lifetime is considerably reduced, and this is taken into account in the SK models. To estimate the effect of CR on the angles, 100 million $\mu^+\mu^- \to H^0 \to W^+W^- \to q_1\bar{q}_2q_3\bar{q}_4$ events are simulated for each CR model and for each parity fraction, respectively.

The events are required to have exactly four jets using the Durham jet algorithm with a $k_\perp$ cut of 8 GeV, followed by an additional energy cut of at least 10 GeV per jet and a angular separation of 0.5. Two different methods to pair the jets were considered, either to maximize the opening angles, or to minimize $|M_W - 80|$ for a single W. The second method was found to be significantly more sensitive, and we will therefore restrict ourselves to this method. The distribution for the three angles are shown in fig. III.4. Deviations between the SM Higgs and the different parity fractions are visible by eye for all the three angles. Both of the curves with non-vanishing *CP*-oddness show almost identical behaviours, indicating that the sign of the interference term is unimportant for these observables (at least for small deviations). Comparing the pattern of variation for the *CP*-violating models and the CR models, respec-

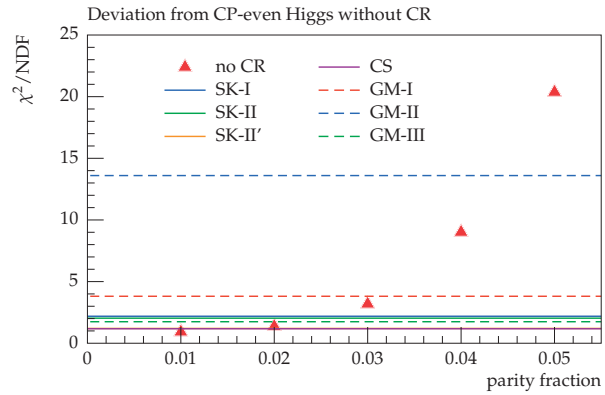

Figure III.5: Deviations between a *CP*-even Higgs without CR and models with either increased *CP*-oddness or a CR model. The deviation is quantified as the χ^2/NDF deviation for the θ_1 angle.

tively, shows an interesting picture. For θ_1 and θ_2 the deviations go in the same direction, whereas for Φ the deviations are in opposite directions. Thus a simultaneous study in principle would allow to disentangle the two potential effects.

To quantify the deviation from the no-*CP*-odd no-CR baseline, a simple χ^2 test is applied to the distributions. The most sensitive angle is θ_1, and we therefore restrict our studies to this observable. A complete experimental analysis most likely would combine all the angles in a multivariate analysis. For each parity fraction the χ^2 is calculated, fig. III.5. As expected the χ^2 increases smoothly with this fraction. Similarly, the χ^2 is also included for the different CR models. The crossover point is a simple indicator for when CR becomes an issue for Higgs parity measurements. This point occurs around 2–5%, with the higher values for somewhat more extreme CR models. Thus any limits significantly above this estimate can safely ignore CR effects. It should be stressed that also limits below 2% should be reachable, once CR is carefully taken into account. This can involve (anti)correlations between the three angles, as already noted, but also studies of particle production patterns between the jets, like the one in section III.4.

III.6 CONCLUSIONS

In this article we have studied the effects of CR at e^+e^- colliders, with emphasis on fully hadronic W^+W^- events. We find that some newer models, implemented to study CR effects at hadron colliders, show different behaviours for e^+e^-. The CS model gives rise to very limited variations, whereas for the GM models one specific scenario even shows large enough deviations to be excluded by the LEP data.

Even if the concept of CR is quite straightforward, it allows for several different mechanisms to be at play. These potentially act in opposite directions, making interpretations difficult. This is clearly illustrated by the GM models, where GM-I predicts a smaller reconstructed W mass and GM-II a larger one. This highlights the need for studying multiple models using several observables, to disentangle what is going on. It is clear that further studies will be needed, to extend the range of interesting models, to understand the pattern of potentially balancing effects within each model, to clarify which factors lead to an energy dependence of effects, and so on. There are also separate but related topics, on the one hand to improve the precision of the perturbative description, specifically that of parton showers, on the other hand to improve the modelling of the non-perturbative hadronization even in the absence of CR. Nevertheless, the outcome of the current simple study is fairly optimistic: given enough luminosity, at a few different energies, e^+e^- should offer insights into CR mechanisms that complement those obtainable at hadron colliders. This complementarity between the "clean" e^+e^- environment and the "dirty" pp one may hold the key to a deeper understanding of CR.

The $e^+e^- \to W^+W^-$ channel is not the only e^+e^- process where CR effects may be relevant. As an example we studied a Higgs parity measurement in the $H \to W^+W^- \to q_1\bar{q}_2q_3\bar{q}_4$ channel. The variations from CR were of the same size as the introduction of 2–5% *CP*-oddness into the *CP*-even Higgs, depending on the choice of CR model. The main lesson is not the precise number for this particular observable, but to highlight the need to be aware of potential CR uncertainties for any nontrivial hadronic final state.

Plans for future e^+e^- collider usually include the possibility to reach the $t\bar{t}$ threshold. Then hadronic final states will start out

with three colour singlets: one W from each top decay, plus one encompassing the b and $\bar{b}$ from the two decays. Like for the $W^+W^-(\gamma^*/Z^0)$ background this increases the possibilities for CR effects. Some early studies are found in [38], but updated and extended studies should be performed, including the new models. At the very least, it will be needed in order to estimate the expected CR uncertainty in the measurements of the top properties for possible future colliders. Many of the necessary tools are already in place in PYTHIA 8, although e.g. the administrative machinery in the SK models needs to be extended appropriately.

ACKNOWLEDGMENTS

Work supported in part by the Swedish Research Council, contract number 621-2013-4287, and in part by the MCnetITN FP7 Marie Curie Initial Training Network, contract PITN-GA-2012-315877. Peter Skands is acknowledged for useful comments.

BIBLIOGRAPHY

[1] A. Buckley, J. Butterworth, S. Gieseke, D. Grellscheid, S. Hoche, *et al.*, "General-purpose event generators for LHC physics," *Phys.Rept.* **504** (2011) 145–233, arXiv:1101.2599 [hep-ph].

[2] G. 't Hooft, "A Planar Diagram Theory for Strong Interactions," *Nucl.Phys.* **B72** (1974) 461.

[3] B. Andersson, G. Gustafson, G. Ingelman, and T. Sjöstrand, "Parton Fragmentation and String Dynamics," *Phys.Rept.* **97** (1983) 31–145.

[4] H. Fritzsch, "How to Discover the *B* Mesons," *Phys.Lett.* **B86** (1979) 343.

[5] T. Sjöstrand and V. A. Khoze, "On Color rearrangement in hadronic W+ W- events," *Z.Phys.* **C62** (1994) 281–310, arXiv:hep-ph/9310242 [hep-ph].

[6] T. Sjöstrand and V. A. Khoze, "Does the W mass reconstruction survive QCD effects?," *Phys.Rev.Lett.* **72** (1994) 28–31, arXiv:hep-ph/9310276 [hep-ph].

[7] **OPAL** Collaboration, G. Abbiendi *et al.*, "Colour reconnection in e+ e- $\to$ W+ W- at s**(1/2) = 189-GeV - 209-GeV," *Eur.Phys.J.* **C45** (2006) 291–305, arXiv:hep-ex/0508062 [hep-ex].

[8] **L3** Collaboration, P. Achard *et al.*, "Search for color reconnection effects in $e^+e^- \to W^+W^- \to$ hadrons through particle flow studies at LEP," *Phys.Lett.* **B561** (2003) 202–212, arXiv:hep-ex/0303042 [hep-ex].

[9] **DELPHI** Collaboration, J. Abdallah *et al.*, "Investigation of colour reconnection in WW events with the DELPHI detector at LEP-2," *Eur.Phys.J.* **C51** (2007) 249–269, arXiv:0704.0597 [hep-ex].

[10] **ALEPH** Collaboration, S. Schael *et al.*, "Measurement of the *W* boson mass and width in e^+e^- collisions at LEP," *Eur.Phys.J.* **C47** (2006) 309–335, arXiv:hep-ex/0605011 [hep-ex].

[11] **ALEPH, DELPHI, L3, OPAL, LEP Electroweak** Collaboration, S. Schael *et al.*, "Electroweak Measurements in Electron-Positron Collisions at W-Boson-Pair Energies at LEP," *Phys.Rept.* **532** (2013) 119–244, arXiv:1302.3415 [hep-ex].

[12] T. Sjöstrand and M. van Zijl, "A Multiple Interaction Model for the Event Structure in Hadron Collisions," *Phys.Rev.* **D36** (1987) 2019.

[13] T. Sjöstrand and P. Z. Skands, "Multiple interactions and the structure of beam remnants," *JHEP* **0403** (2004) 053, arXiv:hep-ph/0402078 [hep-ph].

[14] S. Argyropoulos and T. Sjöstrand, "Effects of color reconnection on $t\bar{t}$ final states at the LHC," *JHEP* **1411** (2014) 043, arXiv:1407.6653 [hep-ph].

[15] J. R. Christiansen and P. Z. Skands, "String Formation Beyond Leading Colour," arXiv:1505.01681 [hep-ph].

[16] **TLEP Design Study Working Group** Collaboration, M. Bicer *et al.*, "First Look at the Physics Case of TLEP," *JHEP* **1401** (2014) 164, arXiv:1308.6176 [hep-ex].

[17] **CMS** Collaboration, S. Chatrchyan *et al.*, "Observation of a new boson at a mass of 125 GeV with the CMS experiment at the LHC," *Phys.Lett.* **B716** (2012) 30–61, arXiv:1207.7235 [hep-ex].

[18] **ATLAS** Collaboration, G. Aad *et al.*, "Observation of a new particle in the search for the Standard Model Higgs boson with the ATLAS detector at the LHC," *Phys.Lett.* **B716** (2012) 1–29, arXiv:1207.7214 [hep-ex].

[19] **ATLAS** Collaboration, G. Aad *et al.*, "Study of the spin and parity of the Higgs boson in diboson decays with the ATLAS detector," arXiv:1506.05669 [hep-ex].

[20] **CMS** Collaboration, S. Chatrchyan *et al.*, "Measurement of the properties of a Higgs boson in the four-lepton final state," *Phys.Rev.* **D89** no. 9, (2014) 092007, arXiv:1312.5353 [hep-ex].

[21] A. Skjold and P. Osland, "Angular and energy correlations in Higgs decay," *Phys.Lett.* **B311** (1993) 261–265, arXiv:hep-ph/9303294 [hep-ph].

[22] B. Andersson, G. Gustafson, and B. Söderberg, "A Probability Measure on Parton and String States," *Nucl.Phys.* **B264** (1986) 29.

[23] T. Sjöstrand, S. Ask, J. R. Christiansen, R. Corke, N. Desai, *et al.*, "An Introduction to PYTHIA 8.2," arXiv:1410.3012 [hep-ph].

[24] C. Bierlich, G. Gustafson, L. Lönnblad, and A. Tarasov, "Effects of Overlapping Strings in pp Collisions," *JHEP* **1503** (2015) 148, arXiv:1412.6259 [hep-ph].

[25] T. Biro, H. B. Nielsen, and J. Knoll, "Color Rope Model for Extreme Relativistic Heavy Ion Collisions," *Nucl.Phys.* **B245** (1984) 449–468.

[26] A. Bialas and W. Czyz, "Chromoelectric Flux Tubes and the Transverse Momentum Distribution in High-energy Nucleus-nucleus Collisions," *Phys.Rev.* **D31** (1985) 198.

[27] B. R. Webber, "Color reconnection and Bose-Einstein effects," *J. Phys.* **G24** (1998) 287–296, arXiv:hep-ph/9708463 [hep-ph].

[28] S. Gieseke, C. Rohr, and A. Siodmok, "Colour reconnections in Herwig++," *Eur. Phys. J.* **C72** (2012) 2225, arXiv:1206.0041 [hep-ph].

[29] J. Rathsman, "A Generalized area law for hadronic string re-interactions," *Phys.Lett.* **B452** (1999) 364–371, arXiv:hep-ph/9812423 [hep-ph].

[30] **DELPHI** Collaboration, J. Abdallah *et al.*, "Measurement of the Mass and Width of the W Boson in e^+e^- Collisions at $\sqrt{s}$ = 161-GeV - 209-GeV," *Eur.Phys.J.* **C55** (2008) 1–38, arXiv:0803.2534 [hep-ex].

[31] S. Catani, Y. L. Dokshitzer, M. Olsson, G. Turnock, and B. Webber, "New clustering algorithm for multi - jet

cross-sections in e+ e- annihilation," *Phys.Lett.* **B269** (1991) 432–438.

[32] M. Bengtsson and T. Sjöstrand, "Coherent Parton Showers Versus Matrix Elements: Implications of PETRA - PEP Data," *Phys. Lett.* **B185** (1987) 435.

[33] E. Norrbin and T. Sjöstrand, "QCD radiation off heavy particles," *Nucl. Phys.* **B603** (2001) 297–342, arXiv:hep-ph/0010012 [hep-ph].

[34] **ALEPH, DELPHI, L3, OPAL, LEP Electroweak Working Group** Collaboration, J. Alcaraz *et al.*, "A Combination of preliminary electroweak measurements and constraints on the standard model," arXiv:hep-ex/0612034 [hep-ex].

[35] A. Skjold and P. Osland, "Testing CP in the Bjorken process," *Nucl.Phys.* **B453** (1995) 3–16, arXiv:hep-ph/9502283 [hep-ph].

[36] Y. Gao, A. V. Gritsan, Z. Guo, K. Melnikov, M. Schulze, *et al.*, "Spin determination of single-produced resonances at hadron colliders," *Phys.Rev.* **D81** (2010) 075022, arXiv:1001.3396 [hep-ph].

[37] S. Bolognesi, Y. Gao, A. V. Gritsan, K. Melnikov, M. Schulze, *et al.*, "On the spin and parity of a single-produced resonance at the LHC," *Phys.Rev.* **D86** (2012) 095031, arXiv:1208.4018 [hep-ph].

[38] V. A. Khoze and T. Sjöstrand, "Color correlations and multiplicities in top events," *Phys.Lett.* **B328** (1994) 466–476, arXiv:hep-ph/9403394 [hep-ph].

IV

EFFECTS OF COLOUR RECONNECTION
ON HADRON FLAVOUR OBSERVABLES

LU TP 15-26
MCnet-15-16

Effects of Colour Reconnection on Hadron Flavour Observables

Christian Bierlich and Jesper R. Christiansen

Department of Astronomy and Theoretical Physics,
Lund University, Sölvegatan 14A,
SE-223 62 Lund, Sweden

Submitted to Phys. Rev. D

Abstract

We present a comparison between two recently developed colour reconnection models, the new colour reconnection model in PYTHIA and the DIPSY rope hadronization model. Specifically we investigate ratios of identified hadron yields as a function of the final-state activity, as measured by the charged multiplicity. Since both models have a nontrivial dependence on the final-state activity, the above observables serve as excellent probes to test the effect of these models. Both models show a clear baryon enhancement with increasing multiplicity, while only the DIPSY rope model leads to a strangeness enhancement. Flow-like patterns, previously found to be connected to colour reconnection models, are investigated for the new models. Only PYTHIA shows a $p_\perp$-dependent enhancement of the Λ/K ratio as the final-state activity increases, with the enhancement being largest in the mid-$p_\perp$ region.

IV.1 INTRODUCTION

The first run of LHC has provided a large number of measurements probing both soft and hard QCD, and thereby a large number of tests for the Monte Carlo event generators. Even though the overall performance of the event generators have been quite good, there are still some phenomena that are insufficiently understood [1]. One of the more intriguing soft QCD deviations is the observed enhancement of Λ production [2, 3]. No model has been simultaneously able to describe the identified hadron spectra at both LEP and LHC. This has led to the development of several phenomenological models [4–6], partly aimed to address this problem. With the planned low pile-up runs at the beginning of the second LHC run, it is now an ideal time to test these models further, and thereby probe the physical origin of the Λ enhancement. In this study we consider two of the models: the new colour reconnection (CR) model in the PYTHIA event generator [5, 7] and the colour rope model in the DIPSY event generator [4, 8, 9]. The models have previously been compared to pp data at $\sqrt{s}$ of 200, 900 and 7000 GeV. In this paper new possible observables to test the models are suggested, and predictions are made for collisions at $\sqrt{s} = 13$ TeV. Both colour reconnection models are built upon the Lund model for string hadronization [10]. Nonperturbative differences can therefore be ascribed to differences in the new phenomenological ideas.

One of the key ideas for the two models in question is *jet universality*. Stated in terms of the string model, it essentially means that fragmentation of a string does not depend on how the string is formed. Free strings at both lepton and hadron colliders should thus hadronize in a similar fashion. Fragmentation parameters are therefore tuned in the clean $e^+e^- \to Z \to q\bar{q}$ environment, and then directly applied to hadron colliders. Any discrepancy has to be due to physical phenomena not active at lepton colliders. For all the models attempting to describe the Λ enhancement, the enhancement is linked to the increased density of quarks and gluons in the final state at hadron colliders[1]. It would therefore be of natural interest to measure the Λ enhancement as a function of this density. The quark-gluon density is experimentally ill-defined, however, and

1 Sometimes also referred to as string density, colour density, or energy density.

we suggest to use the number of charged tracks in the forward region as a measure of final-state activity. A similar idea for using the hyperon-to-meson ratio to search for indications of a miniQGP was suggested in ref. [11]. We suggest ratios that allows for separation of strangeness enhancement from baryon enhancement, which both could be present in the hyperon-to-meson ratio.

Another puzzling observation is the indication of collective effects in high-multiplicity pp collisions [12, 13], often interpreted as the presence of flow. These effects were only expected in the dense medium of heavy ion collisions, where the pressure gradients give rise to flow effects. A study of the models for pp collisions showed that CR generated similar effects even without the introduction of a thermalized medium [14]. We therefore consider one of the standard observables in heavy ion physics, that of identified particle ratios as a function of $p_\perp$, separated into bins of centrality, and compare the model predictions for pp collisions. Since centrality is not experimentally well defined in pp collisions, the number of charged tracks in the forward region is used as a measure of activity.

The outline of the paper is as follows. In section IV.2 we will briefly recap the most important features of the two models considered. Comparison to existing pp data at $\sqrt{s}$ of 200 GeV and 7 TeV is shown in section IV.3. The event selection and tuning for 13 TeV is described in section IV.4. In section IV.5, the predictions at $\sqrt{s} =$ 13 TeV, for the second run of LHC, are presented. Finally, in section IV.6, we summarize and present an outlook.

IV.2 THE MODELS

Both models for colour reconnection are built upon the Lund string model for hadronization. In this model, outgoing partons are connected with stringlike colour fields, which fragment into hadrons when moving apart. The model contains two main parameters relevant to this study, which determine the suppression of strange quarks and of diquarks (giving baryons) in the break ups. Assuming jet universality, these parameters are tuned to LEP data.

Baryons can in addition be created around string junctions, which can arise as a consequence of colour reconnection. Consider the simple configuration of two $q\bar{q}$ dipoles in fig. IV.1, which for exam-

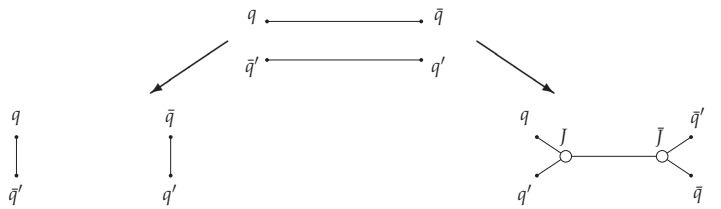

Figure IV.1: Sketch of how two $q\bar{q}$ dipoles (top) can be reconnected to different colour topologies (left and right). The right connection gives rise to a double junction, which in turn will produce baryons. Notice that the placement of the pairs differs in the junction figure.

ple could have originated from a decay of two W-bosons in a LEP environment, as described in ref. [15]. What essentially could be described as a quadrupole configuration is instead described as either the original (on top) or the left configuration in fig. IV.1. Without CR only the original configuration is considered. Extending this type of colour reconnection to hadron colliders has been shown [16] to be a necessary condition to describe the rising of $\langle p_\perp \rangle (N_{ch})$ distributions. The QCD ε-tensor gives rise to the rightmost configuration, containing two junction connections, depicted as empty circles. Since such junctions constitute proto-baryons, in the same way string segments constitute proto-mesons, they become an additional source of baryons.

IV.2.1 *Colour reconnection in* Pythia

The new CR model in Pythia is situated just prior to the hadronization. It takes the leading-colour ($N_c \to \infty$) strings and transform them to a different colour configuration based on three principles: firstly the SU(3) colour rules from QCD determine if two strings are colour compatible (e. g.there is only a $1/9$ probability that the top configuration of fig. IV.1 can transform to the left configuration purely from colour considerations). Secondly a simplistic space-time picture to check causal contact between the strings. Finally the λ measure (which is a string-length measure) to decide whether a possible reconnection is actually favoured. Since the model relies purely on the outgoing partons, it is in principle applicable to any

type of collision. So far it has only been tested for pp [5] and ee collisions [17]. The main extension compared to the other CR models in PYTHIA is the introduction of reconnections that form junction structures. From a pure colour consideration the probability to form a junction topology is three times larger than an ordinary reconnection. The junction will introduce additional strings, however, and it is therefore often disfavoured due to a larger λ measure. Given the close connection between junctions and baryons, the new model predicts a baryon enhancement. It was shown to be able to simultaneously describe the Λ production for both LEP and LHC experiments, which neither of the earlier PYTHIA tunes have been able to.

The new CR model essentially contains two new parameters: a parameter that constrains the overall strength of the CR, and a parameter that controls the baryon enhancement. Both of these parameters were tuned to data [3, 18] from the LHC experiments at 7 TeV.

IV.2.2 *Rope hadronization in* DIPSY

The DIPSY model for rope hadronization and final-state swing [4] is a (partly) dynamic model, implemented as corrections during the evolution of the final-state parton shower and also during the hadronization, depending on the local configuration of the density of quarks and gluons.

The model is based upon the idea that when several parton pairs are next to each other in geometric space, they can act together coherently to form a colour rope. Each string is treated as a flux tube with a fixed radius, and the amount of overlap between strings, in impact parameter space and rapidity, can be directly calculated.

If such an overlap is found to exist, it can have different effects, determined by SU(3) colour rules. The overlapping strings can end up in a colour singlet configuration. This is handled by a final-state "swing", that reconnects colour dipoles, in the final-state parton shower as the transformation from the top to the bottom left configuration in fig. IV.1. In all other cases, the strings end up forming a "rope". This is hadronized with a higher effective string tension, reflecting the fact that more energy is available for the fragmenta-

tion, in accordance with results from lattice QCD. In some cases, the strings forming the rope end up in a junction structure. In such cases the junction pair is handled using a simple approach, where the two junctions collapse to either two diquarks or two quarks, with a probability controlled by a tuneable parameter. The resulting strings are then hadronized with the appropriate effective string tension.

An increased string tension results in more strange quarks and diquarks produced in string breakups. Since the effect increases with the density of quarks and gluons in the final state, the expected outcome is more baryons and strangeness among the resulting hadrons. The model includes two free parameters; the string radius and the probability for a junction to resolve to diquarks. Both are tuned to LHC data [3] at 7 TeV.

IV.3 COMPARISON TO DATA

The models performs as intended when comparing to existing data. Ratios of baryons to mesons are enhanced for both models, whereas ratios of particles with strange quark content is enhanced only in the DIPSY rope model. Comparisons are done to ratios of integrated yields of identified particles, using the analyses published through the Rivet [19] framework. The raw results from comparing the Monte Carlo to data using Rivet, are integrated to give figure IV.2, using Matplotlib [20]. Error estimates are conservative, as they assume the error of all bins are fully correlated.

In figure IV.2 comparison to STAR data [21–23] at 200 GeV indicated that the description of the baryon to meson ratios[2] improves with both models, while the description of the Ξ/Λ ratio only improves with the DIPSY rope model. The change in the $K^{\pm}/\pi$ ratio is not visible on this scale for this energy.

Comparison to 7 TeV data from ALICE [24, 25] and CMS [3] confirms that the description improves, even for the Ω/Ξ ratio. The description of the p/π ratio is seen to be somewhat worse with the new models. This could either have a mundane explanation

2 We denote a particle and its antiparticle with just a single letter such that e. g. p means both proton and anti-proton. Special cases are π with denotes $\pi^+\pi^-$, K which denotes $K^+K^-K_s^0K_L^0$ and Ξ which denotes $\Xi^+\Xi^-$.

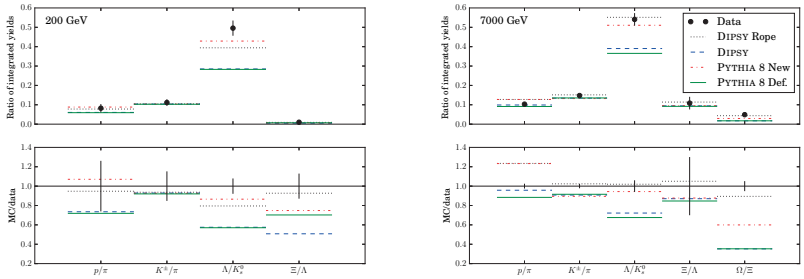

Figure IV.2: Comparison to pp data at 200 GeV from STAR (left) and at 7 TeV from ALICE and CMS (right).

originating in the fact that the very low-$p_\perp$ area of the individual distributions (which contains most of the multiplicity) are not fully understood, or have further reaching consequences. We point to the measurements suggested in the next section of this paper to shed light on this issue.

IV.4 TUNING AND EVENT SELECTION

Before studying exclusive observables at 13 TeV, it is necessary to verify that the baselines for the two models agree reasonable well. Normally this is achieved by tuning the models to the available data. Since this study was begun before any 13 TeV data was available, the DIPSY model was instead tuned to the PYTHIA predictions for $\mathrm{d}N_{ch}/\mathrm{d}\eta$, $\langle p_\perp \rangle (N_{ch})$ and the multiplicity distribution. Both models will eventually have to be retuned, when more data, in a suitable format for tuning, become available. Only small effects are expected from the retuning, firstly due to fragmentation mainly being determined from LEP data, and secondly since the already presented results at 13 TeV show a good agreement between the Monash tune and the data [26, 27].

An event and particle selection was implemented to mimic a possible experimental setup. Each particle is required to have $p_\perp > 0.15$ GeV. Two different η regions are used; a forward region ($2 < |\eta| < 5$) to measure the activity, and a central region ($|\eta| < 1$) to measure the identified hadron yields. The reason for the split is to avoid any potential bias, which otherwise happens

at low N_{ch}, in particular for ratios involving both charged and non-charged hadrons. Since DIPSY does not have a model for diffraction, only non-diffractive events are considered for both models. To reflect this in the event selection, only events with at least six forward charged particles are considered.

All particles with $c\tau > 10$ mm are treated as stable. In practice this means that π, K, Λ, Ξ and Ω are all stable whereas φ (which decays strongly) is not. This introduces some double counting in the φ/K-ratio, where a φ can potentially be counted in the numerator and its decay products in the denominator.

IV.5 PREDICTIONS FOR 13 TEV

Differences between the colour reconnection models are best determined using observables controlled by hadronization effects. Ratios of identified particles is exactly such an observable, since particle species production is determined by the quark and diquark content in string breaks. In the first part of this section, ratios of identified particles are shown as a function of N_{ch} in the forward region, as a measure of event activity. Then flow-like effects are considered, by showing $(\Lambda/K)\,(p_\perp)$ in four different bins of N_{ch} in the forward region.

IV.5.1 *Particle ratios*

Ratios of hadrons with different strange and baryon numbers as function of event activity, measured as functions of N_{ch}^{fwd}, are shown in fig. IV.3. The strangeness enhancement in meson production is probed by the K/π and φ/K ratios, for which the numerator always contains one more strange quark than the denominator. As expected, only the DIPSY rope model shows an enhancement relative to the baseline, since it contains a strangeness enhancement. The new PYTHIA CR model lies slightly below the baseline, but a slight difference in tuning can potentially explain this. It should be recalled that both the new as well as the old models are capable of describing the total K_s^0 yield at 7 TeV. Thus, the limited effects in this ratio is somewhat expected. The φ/K ratio shows more

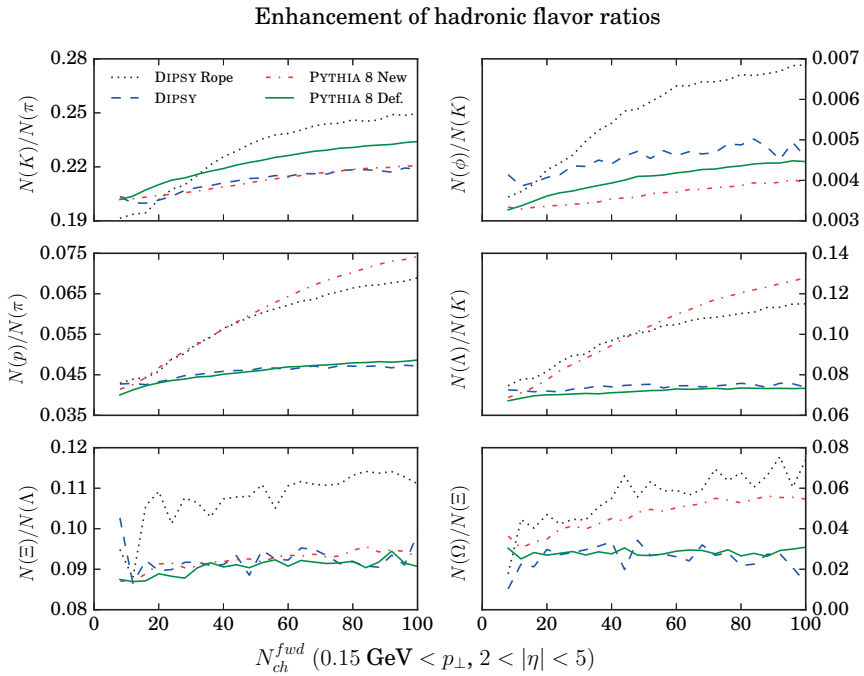

Figure IV.3: Ratios of identified hadrons as functions of N_{ch}^{fwd} at $\sqrt{s} = 13$ TeV. The top row shows meson ratios with the numerator having one more strange quark than the denominator. The middle row shows baryon to meson ratios, with same amount of strange quarks. The bottom row shows baryon ratios with the numerator having one more strange quark than the denominator. Note that the vertical axis differs between the figures and that zero is suppressed.

promise as a means to distinguish between the two models, since the DIPSY model shows a larger enhancement. It is, however, more experimentally challenging.

The baryon enhancement is tested for both hadrons containing zero or one strange quark, p/π and Λ/K. For both ratios, and both models, clear enhancements are expected and seen. For the Λ/K ratio both models agree quite well, which is not surprising, given that both models are tuned to describe the inclusive Λ/K distributions at 7 TeV. A similar picture is seen for the p/π ratio, indicating similar predictions for the baryon enhancement from both the models.

The multistrange baryon enhancement is tested in the same way as the strange-meson enhancement by considering the ratios Ξ/Λ and Ω/Ξ. The large variations at low multiplicity for both distributions are due to statistical fluctuations. For Ξ/Λ the DIPSY rope model shows a clear enhancement as opposed to the new PYTHIA CR model. The Λ/p ratio is not shown, but the enhancement is similar to the enhancement of Ξ/Λ. An enhancement is seen for both models in the Ω/Ξ, with the enhancement factor being around 2.5 for the DIPSY rope model in the highest multiplicity bins. This is larger than any of the other enhancements seen. The enhancement for the new PYTHIA CR model is somewhat surprising, as the increased junction production should be equal for both Ξ and Ω. The production of Ω in the standard PYTHIA fragmentation is, however, significantly suppressed, as the production of *ss*-diquarks is disfavoured. This suppression is not present in the junction handling, since it takes two already formed quarks and combine into a diquark. The enhancement in the new PYTHIA model should therefore not be interpreted as a "real" strangeness enhancement, but more as an absence of suppression of *ss* diquarks. For the DIPSY model the above effect is also present, but there is an additional enhancement of strangeness and diquarks. It should be noted that the Ω baseline from LEP is not that well constrained, due to a large experimental uncertainty, and the model predictions are below the actual measurements [28]. A measurement of $(\Omega/\Xi)\,(N_{ch})$ would cast light on whether an actual activity-based enhancement takes place.

Increased hyperon production in high activity pp events have previously been associated with production of a miniQGP [11]. The hyperon-to-pion ratio is only indirectly shown in fig. IV.3, but the rise is similar to the one predicted by miniQGP. The new models therefore provide an alternative explanation, if such an enhancement is observed.

IV.5.2 *Flow-like effects*

The Λ/K ratio as a function of $p_\perp$ for different N_{ch}^{fwd} ranges is shown in fig. IV.4. The two models show different behaviours for the different multiplicity ranges: the DIPSY rope model only gives a small enhancement ($\sim$ 10% at maximum) between the lowest and highest multiplicity regions. Even though the differential enhancement is generally below 10 %, the enhancement of the ratio of integrated yields is about 20 %, which is in good agreement with fig. IV.3. It should be noted that the DIPSY model is inadequate in describing the high $p_\perp$ tails ($p_\perp >\sim 4$ GeV). This was observed for 900 GeV and 7 TeV in ref. [4].

The new PYTHIA CR model shows a clear change in $p_\perp$ with increasing multiplicity. The enhancement is largest in the mid-$p_\perp$ region ($p_\perp \sim 2-6$ GeV), leading to a "peak" structure. This structure looks qualitatively similar to what is observed in $PbPb$ and pPb collisions [29, 30]. The peak also moves towards larger $p_\perp$ with increased multiplicity, an effect normally attributed to radial flow in heavy ion collisions [31]. That the new CR model predicts a qualitatively similar effect in pp collisions is quite intriguing and strengthens the hint at a potential connection between flow and CR effects already observed [14].

IV.6 CONCLUSIONS

The new CR models can be separated by measuring the identified hadron yields as a function of the multiplicity. The new CR model in PYTHIA only contains a baryon enhancement with increasing multiplicity, while the DIPSY rope models contains both a baryon and a strangeness enhancement. The multistrange hyperon ratios, as well

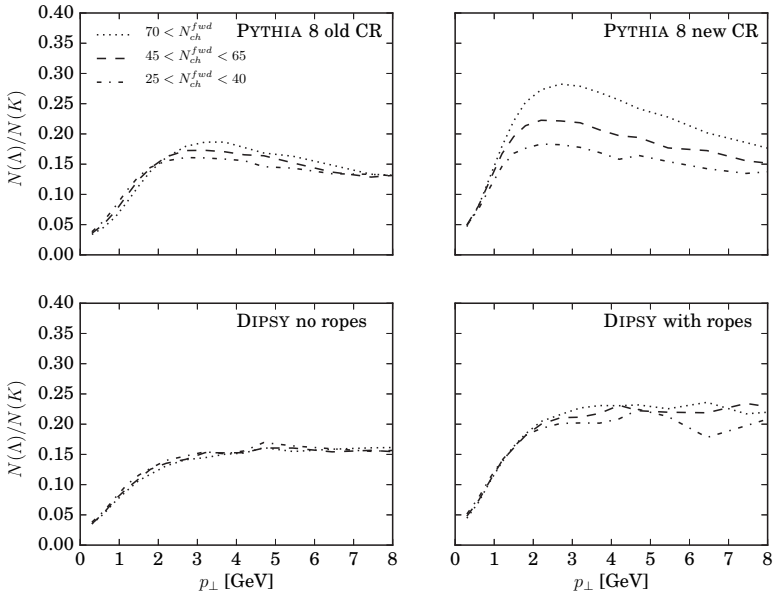

Figure IV.4: Ratio of Λ/K as a function of $p_\perp$ in three bins of N_{ch}^{fwd}. In the right column the new colour reconnection models are shown, and in the left column the old ones.

as the φ/K ratio, provide clear observables for distinguishing between the two models. It should be mentioned that this is already possible to observe in inclusive measurements, but the separation into different multiplicity regions highlights the enhancement.

One of the most important points is the power to distinguish, not only between the two new models, but also between the new models and the old models. Both new models are based on interactions between strings in the hadronization phase, and confirmation of the common predictions made by the two models is a direct hint that colour reconnections among strings are of physical importance. Both baseline models show almost no dependency on multiplicity for the identified hadron yield ratios. Therefore, any observed dependency would provide a clearer indication that the old models miss a feature, better than an inclusive measurement alone could provide. We therefore strongly suggest that these observables should be measured at the LHC experiments. In this paper we only studied the effects at a center-of-mass energy of 13 TeV,

but the effects should also be visible in the already collected data at 7 TeV.

We have also shown that one of the CR models predicts effects similar to those normally attributed to radial flow in heavy ion collisions. This is in agreement with earlier indications that also hint at a connection between the two phenomena. It should however be recalled that neither of the models provide a satisfactory description of the individual $p_\perp$ spectra for the identified hadrons. And before these are fully understood, claims of connections between flow and CR may be premature.

IV.7 ACKNOWLEDGMENTS

We thank Leif Lönnblad and Torbjörn Sjöstrand for useful discussions and comments. Work supported in part by the MCnetITN FP7 Marie Curie Initial Training Network, contract PITN-GA-2012-315877 and the Swedish Research Council, contract 621-2013-4287.

BIBLIOGRAPHY

[1] A. De Roeck, "Experimental results on quantum chromo dynamics: what is next?," *Phys.Scripta* **T158** (2013) 014001.

[2] **ALICE** Collaboration, K. Aamodt *et al.*, "Strange particle production in proton-proton collisions at $\sqrt{s} = 0.9$ TeV with ALICE at the LHC," *Eur.Phys.J.* **C71** (2011) 1594, arXiv:1012.3257 [hep-ex].

[3] **CMS** Collaboration, V. Khachatryan *et al.*, "Strange Particle Production in pp Collisions at $\sqrt{s} = 0.9$ and 7 TeV," *JHEP* **1105** (2011) 064, arXiv:1102.4282 [hep-ex].

[4] C. Bierlich, G. Gustafson, L. Lönnblad, and A. Tarasov, "Effects of Overlapping Strings in pp Collisions," *JHEP* **1503** (2015) 148, arXiv:1412.6259 [hep-ph].

[5] J. R. Christiansen and P. Z. Skands, "String Formation Beyond Leading Colour," arXiv:1505.01681 [hep-ph].

[6] T. Pierog, I. Karpenko, J. Katzy, E. Yatsenko, and K. Werner, "EPOS LHC : test of collective hadronization with LHC data," arXiv:1306.0121 [hep-ph].

[7] T. Sjöstrand, S. Ask, J. R. Christiansen, R. Corke, N. Desai, *et al.*, "An Introduction to PYTHIA 8.2," *Comput.Phys.Commun.* **191** (2015) 159–177, arXiv:1410.3012 [hep-ph].

[8] E. Avsar, G. Gustafson, and L. Lönnblad, "Energy conservation and saturation in small-x evolution," *JHEP* **07** (2005) 062, hep-ph/0503181.

[9] C. Flensburg, G. Gustafson, and L. Lönnblad, "Inclusive and Exclusive observables from dipoles in high energy collisions," *JHEP* **1108** (2011) 103, arXiv:1103.4321 [hep-ph].

[10] B. Andersson, G. Gustafson, G. Ingelman, and T. Sjöstrand, "Parton Fragmentation and String Dynamics," *Phys.Rept.* **97** (1983) 31–145.

[11] V. Topor Pop, M. Gyulassy, J. Barrette, C. Gale, and A. Warburton, "Can hyperon/meson ratios in rare high multiplicity pp collisions at Large Hadron Collider energies provide signatures of mini-quark-gluon plasma formation?," *Phys.Rev.* **C86** (2012) 044902, arXiv:1203.6679 [hep-ph].

[12] A. Kisiel, "Signatures of collective flow in high multiplicity pp collisions," *Phys.Rev.* **C84** (2011) 044913, arXiv:1012.1517 [nucl-th].

[13] **CMS** Collaboration, V. Khachatryan *et al.*, "Observation of Long-Range Near-Side Angular Correlations in Proton-Proton Collisions at the LHC," *JHEP* **1009** (2010) 091, arXiv:1009.4122 [hep-ex].

[14] A. Ortiz Velasquez, P. Christiansen, E. Cuautle Flores, I. Maldonado Cervantes, and G. Paić, "Color Reconnection and Flowlike Patterns in *pp* Collisions," *Phys.Rev.Lett.* **111** (2013) 042001, arXiv:1303.6326 [hep-ph].

[15] T. Sjöstrand and V. A. Khoze, "On Color rearrangement in hadronic W+ W- events," *Z.Phys.* **C62** (1994) 281–310, arXiv:hep-ph/9310242 [hep-ph].

[16] T. Sjöstrand and M. van Zijl, "A Multiple Interaction Model for the Event Structure in Hadron Collisions," *Phys.Rev.* **D36** (1987) 2019.

[17] J. R. Christiansen and T. Sjöstrand, "Colour Reconnection at Future e^+e^- Colliders," arXiv:1506.09085 [hep-ph].

[18] **ATLAS** Collaboration, G. Aad *et al.*, "Charged-particle multiplicities in pp interactions measured with the ATLAS detector at the LHC," *New J.Phys.* **13** (2011) 053033, arXiv:1012.5104 [hep-ex].

[19] A. Buckley *et al.*, "Rivet user manual," arXiv:1003.0694 [hep-ph].

[20] J. D. Hunter, "Matplotlib: A 2d graphics environment," *Computing In Science & Engineering* **9** no. 3, (2007) 90–95.

[21] **STAR** Collaboration, B. I. Abelev *et al.*, "Systematic Measurements of Identified Particle Spectra in pp, d^+ Au and Au+Au Collisions from STAR," *Phys. Rev.* **C79** (2009) 034909, arXiv:0808.2041 [nucl-ex].

[22] **STAR** Collaboration, B. I. Abelev *et al.*, "Strange particle production in p+p collisions at s**(1/2) = 200-GeV," *Phys. Rev.* **C75** (2007) 064901, arXiv:nucl-ex/0607033 [nucl-ex].

[23] **STAR** Collaboration, J. Adams *et al.*, "Identified hadron spectra at large transverse momentum in p+p and d+Au collisions at s(NN)**(1/2) = 200-GeV," *Phys. Lett.* **B637** (2006) 161–169, arXiv:nucl-ex/0601033 [nucl-ex].

[24] **ALICE** Collaboration, J. Adam *et al.*, "Measurement of pion, kaon and proton production in proton–proton collisions at $\sqrt{s} = 7$ TeV," *Eur. Phys. J.* **C75** no. 5, (2015) 226, arXiv:1504.00024 [nucl-ex].

[25] **ALICE** Collaboration, B. Abelev *et al.*, "Multi-strange baryon production in pp collisions at $\sqrt{s} = 7$ TeV with ALICE," *Phys. Lett.* **B712** (2012) 309–318, arXiv:1204.0282 [nucl-ex].

[26] **ATLAS** Collaboration, "Charged-particle distributions in $\sqrt{s} = 13$ TeV pp interactions measured with the ATLAS detector at the LHC," *ATLAS-CONF-2015-028, ATLAS-COM-CONF-2015-046* (2015) .

[27] **ATLAS** Collaboration, "Detector level leading track underlying event distributions at 13 TeV measured in ATLAS," *ATL-PHYS-PUB-2015-019* (2015) .

[28] P. Skands, S. Carrazza, and J. Rojo, "Tuning PYTHIA 8.1: the Monash 2013 Tune," *Eur.Phys.J.* **C74** no. 8, (2014) 3024, arXiv:1404.5630 [hep-ph].

[29] **ALICE** Collaboration, B. B. Abelev *et al.*, "K^0_S and Λ production in Pb-Pb collisions at $\sqrt{s_{NN}}$ = 2.76 TeV," *Phys.Rev.Lett.* **111** (2013) 222301, arXiv:1307.5530 [nucl-ex].

[30] **ALICE** Collaboration, B. B. Abelev *et al.*, "Multiplicity Dependence of Pion, Kaon, Proton and Lambda Production in p-Pb Collisions at $\sqrt{s_{NN}}$ = 5.02 TeV," *Phys.Lett.* **B728** (2014) 25–38, arXiv:1307.6796 [nucl-ex].

[31] R. Fries and B. Müller, "Heavy ions at LHC: Theoretical issues," *Eur.Phys.J.* **C34** (2004) S279–S285, arXiv:nucl-th/0307043 [nucl-th].

V

MERGING WEAK AND QCD SHOWERS
WITH MATRIX ELEMENTS

LU TP 15-41
MCnet-15-28

Merging weak and QCD showers with matrix elements

Jesper Roy Christiansen[1], Stefan Prestel[2]

[1]: Department of Astronomy and Theoretical Physics, Lund University, Sölvegatan 14, Lund, Sweden

[2]: SLAC National Accelerator Laboratory, Menlo Park, CA 94025, USA

Abstract

We present a consistent way of combining associated weak boson radiation in hard dijet events with hard QCD radiation in Drell-Yan-like scatterings. This integrates multiple tree-level calculations with vastly different cross sections, QCD- and electroweak parton shower resummation into a single framework. The new merging strategy is implemented in the PYTHIA event generator and predictions are confronted with LHC data. Improvements over the previous strategy are observed. Results of the new electroweak-improved merging at a future 100 TeV proton collider are also investigated.

V.1 INTRODUCTION

With the Large Hadron Collider entering its 13 TeV run phase, new phenomena will be investigated in previously inaccessible regions of phase space. Accurate calculations for background processes in the Standard Model (SM) thus have to be reliable when singling out phase space regions by applying intricate analysis techniques to the collider data. General Purpose Event Generators [1] that are combined with multi-parton fixed-order cross section calculations provide the most flexible assessments of SM backgrounds. The problems to address in these methods are to ensure that no momentum configurations are over- or under-counted, and that the perturbative accuracy of the fixed-order matrix element calculation (ME) and parton shower (PS) resummation merge without either being undermined. These obstacles were tackled in matching [2–13] and merging [14–24] methods, with next-to-next-to-leading order matching [25–30] and next-to-leading order merging [31–36] currently providing the most precise predictions.

It is crucial to note that these state-of-the art methods inherit both strengths and weaknesses from less precise methods, in particular from choices made in leading-order merging. These choices stem from uncontrolled or missing ingredients in the parton shower. More comprehensive parton showers will lead to less freedom and more precise predictions. This is also true for electroweak shower resummation [37, 38], which are shown to be important for the accurate modelling of jets at large transverse momenta. In this article, we discuss how to combine multi-jet calculations with QCD and weak parton showers in the context of W-boson production, which highlights that

a) processes that are disjoint at lowest-order need to be combined, yielding a “merging of mergings", (e.g. Drell-Yan W-boson production and QCD $2 \to 2$ production both contribute to $pp \to jjW$),

b) weak parton showers are necessary to describe weak bosons close to or inside jets, and to disentangle how a “merging of mergings" should proceed,

c) merging is necessary for an inclusive prediction, and to set starting conditions for the weak showers.

Note that if these points are not satisfactorily answered within a leading-order merging method, then the uncertainty due to the resulting choices can only partially be remedied by a more precise (e.g. NLO) merging method. Thus, to start with the simplest merging approach, we improve the CKKW-L leading-order merging prescription [23] in the PYTHIA 8 event generator [39] to address these issues. The improvements should then carry over when merging NLO calculations. We present results for both LHC and at a potential future 100 TeV proton collider.

In section V.2 we review the weak parton showers in PYTHIA, followed by a brief introduction to CKKW-L merging in section V.3. In these sections, we also highlight choices that have been made in both approaches. A merging of QCD and weak showers with multi-parton cross sections, which resolves these choices, is presented in section V.4. Validations of the implementation are presented in section V.5. We then move on to discuss results for LHC and a future 100 TeV collider in section V.6 and conclude in section V.7.

V.2 WEAK PARTON-SHOWER FORMALISM

Scattering processes containing massless partons with very different transverse momenta exhibit logarithmic divergences that limit the applicability of perturbative calculations. Fortunately, it is possible to derive factorisation theorems and sum logarithmic terms to all orders in perturbation theory. This leads to a reliable, finite calculation with an extended range of validity. Leading-logarithmic contributions can be summed in a process- and observable-independent fashion by using PS programs[1].

Large scale hierarchies involving massless particles still lead to logarithmic enhancements that should, for a stable prediction, be summed to all orders in perturbation theory. The resummation of logarithmic electro-weak enhancements becomes important when

1 Note that many other universal subleading effects are also included in parton showers, and that for specific observables, better accuracy, than the formal leading log, can be achieved [40, 41].

processes contain low transverse-momentum weak bosons and jets with transverse momentum much larger than the boson mass. It has been shown in fixed-order calculations that weak Sudakov corrections can indeed become relevant at LHC energies [42–47] and especially when considering potential future proton colliders [48]. Including all-order electroweak effects in flexible, commonly used programs facilitates realistic studies of these effects.

General Purpose Event generators include an approximation of all-order effects with the help of parton showers. Parton showers produce all-order (QCD or QED) results by resumming real-emission corrections into exponentiated no-emission probabilities. These no-emission probabilities are related to Sudakov form factors by application of DGLAP evolution [49–51]. Electro-weak resummation is a natural extension to the QCD and QED showering. EW showers have, due to the dominance of QCD effects, only recently been investigated in event generators [37, 38]. The EW shower allows for an equal treatment of QCD, QED and weak radiation and naturally includes competition between emissions of gluons, photons or weak gauge bosons. In this section a short summary of the major issues are given, with a specific focus on aspects relevant for merging parton showers with matrix element calculations.

There are two major differences between γ emission and $W^{\pm}$ emissions. Firstly, the emission of a $W^{\pm}$ boson changes the flavour of the radiator, and secondly, the $W^{\pm}$ is massive. Flavour changes are handled according to the CKM matrix, with additional care needed for the evaluation of PDFs. A phase space mapping for emissions of massive particles was previously given in the context of a Hidden-Valley PS model [52], and the weak showers can directly reuse the corresponding structures in PYTHIA.

The massive phase space does not include the collinear and soft divergences, since the weak boson has to carry at least enough energy to be on its mass shell. The introduction of mass should also affect the PS splitting kernels. The normal massless collinear approximation in the PS is therefore not sensible for radiation of weak gauge bosons. Thus, a complicated assessment of mass effects seems necessary. However, this can be avoided if the full, massive matrix elements are used as splitting kernels. The weak parton shower in PYTHIA thus heavily relies on ME corrections [53–56].

All emissions are corrected with a fully massive $2 \to 3$ matrix element. The corrections vary depending on the type of process – an s-channel process will for example carry a different correction factor than a t-channel process. Different corrections are mandatory in order to obtain a reasonable agreement between the PS prediction and gauge-invariant subsets of the full ME calculations (including all interferences). Note however that the weak parton shower only recovers the $pp \to jjV$ matrix elements (where $V = W, Z$). The weak shower further omits interference terms between different fermion lines. It is further only possible to choose the correct ME correction if the underlying type of process is known. Therefore the weak shower resorts to (artificial) choices if the evolution is not started from a $2 \to 1$ or a $2 \to 2$ process. As will be described in detail later, this problem is resolved through the introduction of PS histories.

The introduction of weak parton showers leads to potential double counting in an inclusive event generation. If the desired process is dijet + $W^{\pm}$ it can be interpreted in two ways: either as a Drell-Yan-like $W^{\pm}$-boson process followed by two QCD emissions, or as a $2 \to 2$ QCD process radiating a $W^{\pm}$-boson. Allowing these two possibilities to separately cover the full phase space results in double counting. Disallowing QCD emissions above the weak boson mass for Drell-Yan-like processes would ameliorate this double counting, yet result in an unconvincing data description of the pure PS result. Instead, a strategy using the $k_{\perp}$ jet algorithm was adopted. If the jet separation between a $W^{\pm}$-boson and a parton proves the minimal scale, then the events are removed from the Drell-Yan-like sample. Conversely, dijet states whose minimal jet separation is between partons are removed from the $2 \to 2$ QCD event sample. This artificial separation will be corrected upon merging weak and QCD showers with multi-parton matrix elements.

The weak coupling to a fermion depends on its spin. In the weak shower this is handled in a simplistic way, by assigning each fermion line a randomly chosen spin. The spin is then kept fixed through the whole PS. For a single weak emission it corresponds to using averaged spin results, but it introduces a slight enhancement for multiple weak gauge bosons to be emitted from the same fermion line.

The overall performance of the weak PS is surprisingly good. It is capable of describing a large number of measurements that earlier has only been possible to describe with merged samples. Notable the rate of $W + n$ jets could be described up to the highest measured ($n = 7$) bin without using more than $W + 2$ jet matrix elements. But the PS still does not provide a perfect description, and especially the description of angular distributions (e.g. $\Delta\varphi$ between leading and second leading jet) is poor. Merging is expected to significantly improve the results.

V.3 MERGING

Many interesting multi-jet observables at a hadron collider are difficult to predict with calculations containing a fixed (or limited) number of outgoing partons in fixed-order perturbation theory. Parton showers are then necessary to spread the fixed-order calculation over a broader multi-jet phase space. Standard examples are jet rates, where fixed-order calculations become prohibitively expensive, or azimuthal separations between (reconstructed) heavy bosons and a hardest jet, which are naturally sensitive to momentum configurations with a variable number of hard jets [57]. To describe such genuine multi-jet observables, many multi-parton calculations need to be combined into an inclusive sample describing configurations with $n \leq N$ jets with fixed-order accuracy, where N should be as large as possible.

Matrix element merging is a process-independent method that invokes the PS to facilitate this combination. The main steps in a merging procedure are[2]:

- choose a "history" of intermediate states through which a pre-calculated input multi-parton state has evolved from a lowest-multiplicity state (see e.g. fig. V.1),
- use this history to make the state exclusive (i.e. additive) by calculating and applying the necessary no-emission probabilities (which are intimately linked to Sudakov form factors),

2 We will call a physical flavour, colour and momentum configuration a "state".

- reweight the input state with additional factors (e.g. $\alpha_s(p_\perp^2)$, PDF weights) that would have been applied by the PS, had it produced the input state by following the history of intermediate states (this is necessary to not impair the accuracy of the PS, or the event generator prediction more generally),
- combine the result of all such post-processed input states for all parton multiplicities.

This immediately highlights that omissions in the shower lead to uncertainties in the merging prescription, which are commonly disposed of by judicious selection. Since we are interested in combining with weak parton showers, let us look at producing an inclusive sample of W-boson + N jets through CKKW-L merging, and assume $N \leq 3$ for simplicity.

Figure V.1: Two examples of possible histories for a pp $\to$ ggW process. The two histories have different hard processes, either as a Drell-Yan process (left) or as a $2 \to 2$ QCD process (right).

In this example, the lowest-multiplicity state (W-boson production) should be used to describe very inclusive observables like e.g. the W-boson rapidity. The interface to the PS is straightforward since no partons are present initially – we only have to ensure that the PS does not produce hard jets, as such configurations should be covered by higher-multiplicity matrix elements. This leads to the introduction of a "merging scale" with arbitrary functional definition and value t_{MS}. States that are classified as "below" t_{MS} will be produced by showering, while states "above" t_{MS} are governed by higher-order matrix elements. Any functional form of the merging scale should be allowed, as long as the function acts as a regularising cut on the fixed-order input calculations. Commonly used merging scale definitions are the minimum of all jet separations in the k_T algorithm [58], or the minimum of parton shower evolution variables measured on the state. Merging methods have to ensure that the dependence of exclusive and inclusive observables on the

merging scale are small. For inclusive jet observables, the merging scale dependence can be removed to reasonable accuracy[3].

Coming back to our example, the next calculation to be added is W-boson in association with one parton. As outlined above, a PS history has to be chosen for such states. These histories are well-defined if the QCD parton shower can (at least in principle) cover the full single-emission phase space. In order to pick all histories in the proportion in which the PS would have produced the output state, the probability for a specific history is given by the product of splitting functions characterising each intermediate evolution step. This reduces the merging scale dependence of exclusive observables. Upon choosing a history, it is simple to reweight with no-QCD-emission probabilities (i.e. QCD Sudakov factors) and to account for the dynamic renormalisation and factorisation scales used in the PS evolution. Using the shower directly to produce the no-QCD-emission probabilities reduces the t_{MS} dependence. The starting conditions for PS emissions off the W + parton state are uniquely determined by the chosen history.

Including a W-boson in association with two partons uncovers further uncertainties, because no ordered PS will cover the full double-emission phase space. Thus, some states accessible to the fixed-order calculation will not yield any ordered PS history[4]. The reweighting of such a state is ambiguous due to ambiguous renormalisation and factorisation scale choices. Although this ambiguity has very small numerical impact for inclusive observables, it can have an uncomfortably large impact on more exclusive observables [23]. Furthermore, some flavour configurations are inaccessible to a QCD parton shower, meaning that no PS history can be reconstructed. Ambiguities in the treatment of such genuine non-shower (commonly called incomplete) states have vanishingly small impact on inclusive observables and yield only very minor variations of exclusive observables [23]. A precise method should however avoid having to make choices. The PS starting conditions are fixed once a history is chosen.

3 The method of section V.4 will, when applied in unitarised merging [24], allow to cancel the t_{MS} dependence of inclusive cross sections exactly.

4 In the following, we will use the phrase “unordered states" when talking about input states that do not yield any ordered PS history.

No new problems occur for higher-multiplicity processes. The issues related to unordered states outlined in the last paragraph can be aggravated in more exclusive observables, however, as the PS phase space coverage will be worse for higher multiplicities. It is still important to remember that merging offers a consistent way to set the PS starting conditions for multi-parton states – which is not the case in plain (QCD or EW) parton showers.

V.4 WEAK SHOWERS AND THE MERGING OF MERGED CALCULATIONS

In the previous sections, we have seen that the construction of weak parton showers as well as multi-jet merging involves compromises. Summarising the most severe choices, we have addressed that:

- Weak showers are currently limited to dijet processes, while inclusive predictions require an ambiguous mixing with Drell-Yan-like configurations.
- Matrix element merging is ambiguous starting at W-boson + two partons, leading to uncomfortable compromises related to unordered states and incomplete histories.

The combination of weak parton showers and multi-jet merging remedies these deficiencies and should provide a more physical picture of multi-parton states. This will further mean that matrix element merging, which is usually regarded to realise corrections to one underlying process, is generalised to incorporate many underlying processes that mix at higher perturbative orders.

To explain the reasoning behind our new merging scheme, let us look at states including one weak boson and two final state partons for illustration. If the outgoing partons have very different transverse momenta, and if the $p_\perp$ of the W-boson is thus comparable to the $p_\perp$ of the harder parton, then it is natural to associate the partons with DGLAP evolution of the incoming beams. For a reliable perturbative prediction, a fixed-order calculation with large scale separation should then be supplemented with no-emission probabilities resumming unresolved QCD emissions. This W-boson + two parton state is an example for corrections to W-boson production.

If the state instead contains two partons with comparable and large $p_\perp$ and a W-boson with small transverse momentum, it is prudent to resum large logarithms associated with the difference between the parton and W-boson transverse momenta. Then Sudakov form factors resumming the dominant weak virtual corrections need to be supplemented. Hence, the two-parton + W-boson state is an example for corrections to dijet production. This correction can be approximated by weak parton showers.

Thus we find that, when going to $\mathcal{O}\left(\alpha_s^2\alpha_w\right)$, it is not possible to disentangle QCD corrections to W-boson production and weak corrections to dijet production[5]. Beyond $\mathcal{O}\left(\alpha_s^2\alpha_w\right)$, W-boson production and dijet production share a single evolution, so that only a combined treatment of these two processes (which are disjoint at lowest multiplicity) will yield a satisfactory prediction. This means that it is necessary to combine multi-jet merged corrections to W-boson production with multi-jet merged corrections for dijet production. These corrections then mix by virtue of weak showers[6]. This in a sense constitutes a "merging of mergings".

Summarising, we have argued that a clean description of W + jets states necessitates a combination of QCD no-emission probability-reweighted corrections to to W-boson production and weak no-emission probability-reweighted dijet production. Within this framework, it is possible to address and amend the choices in weak showering and merging that we have previously highlighted.

The first feature of the combined merging is the possibility to recombine W-boson radiation with other partons. As a natural consequence of this the lowest-multiplicity process is, as desired, no longer forced to be a colour-singlet Drell-Yan-like state if the input state contained W-bosons. The new clustering is illustrated in fig. V.1, where two very different possible histories are shown[7].

5 α_w is used as proxy of the weak coupling constant, which will differ depending on the type of the radiated boson.

6 To be fully consistent, it would be necessary to be inclusive both in QCD and EW outgoing particles. A complete description of a $A, B \to 4$ particle state should contain any admixture of W-bosons and partons with four or less outgoing particles. This article only addresses the combination of dijet and W-boson production, since processes with multiple W-bosons are rare, and assuming that many radiated W-bosons escape detection further seems unrealistic.

7 Note that in the SHERPA [59] event generator, this method is also used, albeit without taking the corresponding weak no-emission probabilities into account [60].

The decision which of these histories to choose should again ensure that the merging scale variation of exclusive observables is small. This means we should attempt to answer the question *how would the (QCD+EW) parton shower have produced this state?* The answer will minimise merging artefacts at the boundary between PS and fixed-order ME regions. With the parton shower probabilistically sampling all ways to evolve into a particular state, we again decide to pick histories with different underlying process probabilistically. For instance the two histories shown in fig. V.1 would have the following probabilities:

$$\mathcal{P}_{\text{left path}} = \frac{\mathcal{P}^{(1)}_{\text{QCD FSR}}\,\mathcal{P}^{(2)}_{\text{QCD ISR}}\,\mathcal{P}^{(3)}_{\text{weak W production}}}{\sum_{\text{all paths}}\prod_{\substack{\text{nodes j}\\ \text{in path i}}}\mathcal{P}^{(j)}_{\text{type}}} \tag{V.4.1}$$

$$\mathcal{P}_{\text{right path}} = \frac{\mathcal{P}^{(1)}_{\text{weak ISR}}\,\mathcal{P}^{(2)}_{\text{QCD jet production}}}{\sum_{\text{all paths } i}\prod_{\substack{\text{nodes j}\\ \text{in path i}}}\mathcal{P}^{(j)}_{\text{type}}} \tag{V.4.2}$$

where $\mathcal{P}^{(j)}_{\text{type}}$ indicates probability associated to the j'th clustering in the path, with "type" indicating what type of transition occurred.

The coupling between fermion and weak gauge bosons depends on the spin of the fermion. To capture this effect in the merging, histories for all possible spin assignments for fermions are considered. One improvement of spin treatment could be to use fully spin dependent input matrix elements. However, in order for this to be consistent, improvements in the spin handling within the PS would be required.

An additional constraint on the probabilities comes from insisting on $p_\perp$-ordered histories: clusterings of states with lower multiplicity have to have a larger $p_\perp$ than clusterings of higher-multiplicity states. For instance, if the event consists of two hard jets and a soft W-boson, it is very unlikely to cluster it to a Drell-Yan hard process and obtain a $p_\perp$-ordered clustering sequence. Within a combined merging of dijet and W-boson production, the dominant scale hi-

Also, histories are picked by choosing probabilistically at each history node, while PYTHIA generates all histories before choosing a whole path probabilistically.

erarchies are correctly identified. Hence, the amount of unordered states is drastically reduced.

The necessity for weak clusterings and the weak showering effects introduces two new weights to the merging procedure: an α_W weight and the weak no-emission probability. The α_W weight is required because a dynamical scale setting is also assumed when evaluating α_W.

The weak no-emission probability can be generated by trial showering. To treat QCD-like and electroweak emissions on equal footing, we include W-bosons in the merging scale definition, meaning that "soft" W-bosons will be generated by the PS, while "hard" W-bosons are generated with the help of a fixed-order matrix element generator. This also means that in non-highest multiplicity states, any first PS response producing states with a hard W-boson (or, of course, hard QCD emissions) will lead to an event rejection. The impact of the weak no-emission probabilities can, due to the large W-boson mass and the small value of α_W, be minor for many observables. However, for observables with large hierarchies between the scales associated to QCD emissions and scales of EW effects, larger effects are anticipated. An idealised observable highlighting weak resummation effects would be very inclusive over multi-parton states and fully exclusive for weak emissions (i.e. all weak bosons can be resolved). We will return to this in the result section, where the effect of the weak no-emission probabilities at a future 100 TeV collider is considered.

While this new method leads to a more physical description of multi-parton states in association with W-bosons, it should be noted that the formal accuracy of neither QCD resummation nor fixed-order calculation is improved. However, this merging for the first time supplements arbitrary multi-jet states with weak resummation effects within a matrix-element-merged prediction. Thus, the electro-weak all-order structure improves over previous results.

To round off this section, remember that merging methods allow the combination of different jet multiplicities. A combination is only possible because the inclusive fixed-order input states (describing N or more particles) are converted into exclusive calculations (describing exactly N resolved particles) by supplementing no-emission probabilities which resum logarithmic enhancements due

to large scale hierarchies. It would thus at first glance seem that a state containing two soft QCD emissions at vastly different scales and a W-boson with transverse momentum commensurate with the larger jet scale is in some sense "more exclusive" than a dijet state with jets of similar $p_\perp$ and a soft W-boson. In the former case two scale differences require resummation, while in the latter, only one hierarchy has to be considered. However, note that the dijet cross section is not well-defined unless jet cuts are applied. These cuts make the cross section exclusive in the sense that at least two jets above a resolution scale are required. That the cross section contains exactly the desired number of jets (and no further resolved jets) is then again achieved by reweighting with no-emission probabilities. As an aside, note that multi-parton interaction (MPI) models [61–63] are derived from the condition that the dijet cross section needs to be regularised, and that this regularisation can be achieved in the same way that no-emission probabilities regularise parton-shower real-emission cross sections. The no-MPI-probabilities motivated by this argument should be correctly included in any merging scheme to ensure that the input states do not overlap with MPI, adding yet another layer of exclusivity. Our implementation in PYTHIA includes a consistent handling of interleaved MPI [64] as outlined in [23].

V.5 VALIDATION

When developing an improved merging scheme, detailed tests validating the method and implementation are necessary. We have tested that the new implementation recovers the correct scales, probabilities and underlying states by directly comparing a reconstructed PS evolution history against the evolution as picked by the parton shower. Such technical comparisons are of course not particularly enlightening for the reader, so that below, we will focus on two hopefully convincing tests.

The weak PS relies on ME corrections for the process $pp \to \mathrm{jjW}$. As such, an excellent agreement between merged and default weak PS results for such $2 \to 3$ processes is expected. We illustrate the agreement for the process $\mathrm{u\bar{u}} \to \mathrm{s\bar{c}W^+/\bar{s}cW^-}$, only including the $\mathcal{O}\left(\alpha_s^2\alpha_w\right)$ contributions as fixed-order inputs. This is an s-channel process, where only final state radiation is possible (assuming a di-

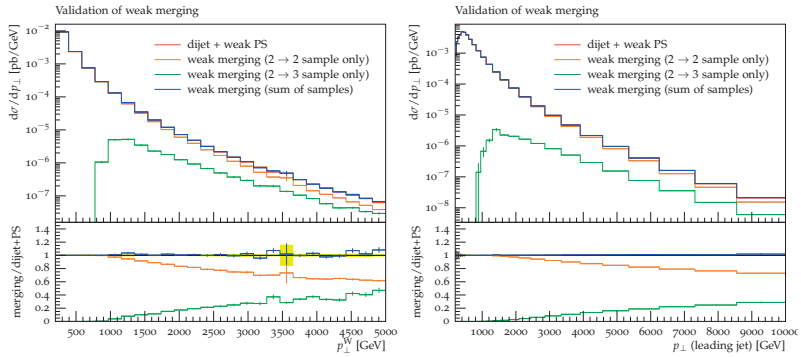

Figure V.2: The figure shows the cross section for $u\bar{u} \to s\bar{c}W^+/\bar{s}cW^-$ as a function of respectively $p_\perp$ of the $W^\pm$ (left) and $p_\perp$ of leading jet (right). The cross section is calculated in two ways: Either through merging of $2 \to 2$ and $2 \to 3$ MEs, or as a $2 \to 2$ ME with weak shower.

agonal CKM matrix). α_{em} was set to 0.1 to increase the statistics and the merging scale was 1000 GeV. The merged curve and the weak PS agree nicely over the whole kinematic range, as illustrated by both the W-boson $p_\perp$ and the leading jet $p_\perp$ distributions (fig. V.2). The merged result thus correctly applies all factors present in the weak PS resummation.

To further validate the implementation, fig. V.3 shows the probability with which states are identified as corrections to a Drell-Yan-like or a $2 \to 2$ QCD hard scattering. Each path is expected to dominate in a specific region of phase-space. If the scales associated to jet production are low and exhibit a hierarchy, then a Drell-Yan-like underlying process should be expected. States with two hard jets at comparable scales should yield a $2 \to 2$ QCD underlying process. We investigate this expectation on the process $pp \to jjW$, using different $p_\perp$ cuts on the leading jet (fig. V.3). As expected, the lower the $p_\perp^{\text{leading jet}}$ cut is, the more likely states will lead to a Drell-Yan-like underlying process. Conversely, for a fixed leading jet $p_\perp$, softer W $p_\perp$'s and more back-to-back jet systems yield predominantly QCD $2 \to 2$ scatterings as underlying process.

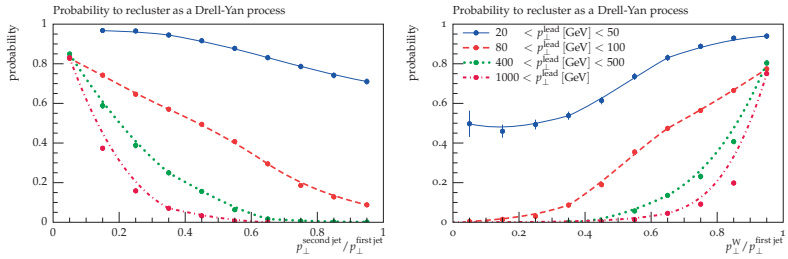

Figure V.3: The figure shows the competition for either clustering a pp $\to$ jjW process as a Drell-Yan process or a $2 \to 2$ QCD process. The probability is shown as a function of the fraction between either the second leading jet $p_\perp$ divided by the leading jet $p_\perp$ (left) or the fraction between the W $p_\perp$ and the leading jet $p_\perp$ (right). The minimum $p_\perp$ for any jet is 5 GeV and the centre-of-mass energy is 7 TeV. The vertical lines indicate the statistical MC uncertainty and smooth curves have been added as a visual help.

V.6 RESULTS

This section presents predictions of merging QCD+EW showers with multi-parton matrix elements. We begin by comparing with studies from both ATLAS and CMS and follow up by a study of the weak no-emission probability at 100 TeV.

V.6.1 *Comparison with LHC data*

In this section, we contrast results of the default CKKW-L merged prescription in PYTHIA and the new QCD+EW merging with LHC data.

To compare against LHC data, we merge five tree-level event samples for W-boson + $\leq$ 4 jets, generated with MadGraph5_aMC@NLO [13] using the CTEQ6m PDF set [67]. The merging scale was defined as the minimum of all PYTHIA transverse momentum separations between partons, while no cut was applied to the the W-boson. This means that the phase space for real weak parton showers is vanishing, thus making the inclusion

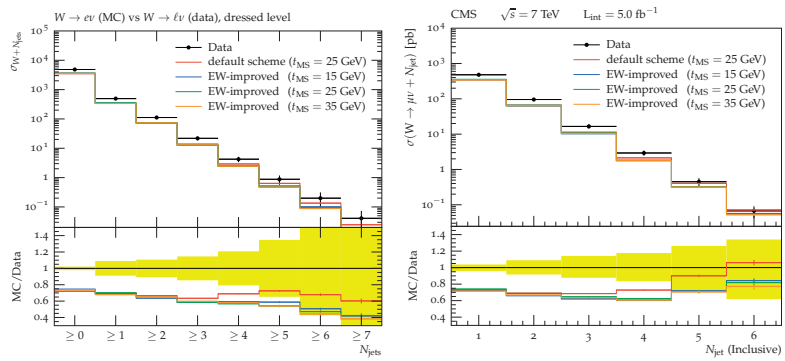

Figure V.4: PYTHIA predictions in comparison to ATLAS data [65] (left) and CMS data [66] (right) for W + jets as a function inclusive jet multiplicity. The yellow error band indicates the one sigma experimental uncertainty and the vertical line on the MC prediction is the statistical MC uncertainty.

of pure-QCD samples unnecessary[8]. Thus, this setup can be used in particular to check the impact of the "weak clustering" outlined in section V.4. The Monash tune [68] was used, but with $\alpha_s(M_Z)$ lowered to $\alpha_s(M_Z) = 0.118$.

Our results only contain tree-level normalisation, and an overall rescaling due to virtual corrections is missing. The results are therefore not expected to match the normalisation of the data. We choose to not rescale our results since we believe that presenting unnormalised experimental data adds additional information and should be encouraged. We do not want to undermine such efforts by rescaling tree-level results. The differential shape of the data should however be described by a tree-level merged prediction (i.e. the ratio between the data and the prediction should be flat for all distributions). All the data comparisons are done using the Rivet framework [69].

In the following, we will refer to the default CKKW-L implementation in PYTHIA as "default scheme", while the new QCD+EW merging will be called "EW-improved" scheme. The EW-improved results are shown for three different merging scales, $t_{MS} = 15$ GeV, $t_{MS} = 25$ GeV and $t_{MS} = 35$ GeV. The uncertainty due to this merging

8 Real W-boson emissions can only enter through 5-parton events or, for lower-multiplicity events, if a QCD emission below t_{MS} is followed by a weak emission. Both contributions have a negligible effect.

scale variation is very small for all observables we have investigated, and is nearly indistinguishable from statistical fluctuations for the observables below. The very small variation is a result of the PS both correctly recovering the W + 1 j matrix element as well as hard (dijet-like) parts of the W + 2 j matrix elements, thus pushing the merging scale dependence to yet higher orders.

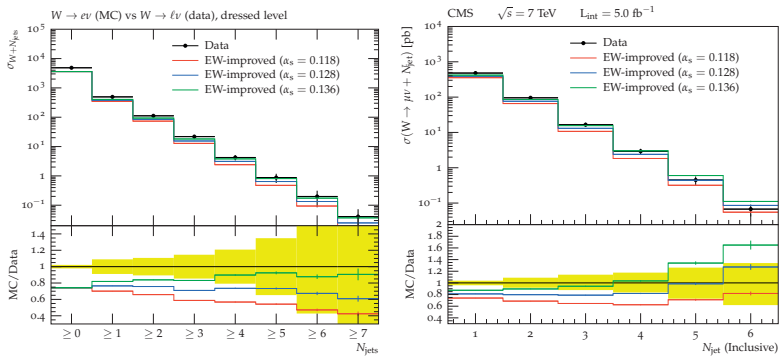

Figure V.5: PYTHIA predictions in comparison to ATLAS data [65] (left) and CMS data [66] (right) for W + jets as a function inclusive jet multiplicity. The yellow error band indicates the one sigma experimental uncertainty and the vertical line on the MC prediction is the statistical MC uncertainty. "$\alpha_s = 0.136$" stands for the values of the Monash tune [68].

The inclusive jet multiplicity in W-boson events is well described by both the default and the EW-improved merging (fig. V.4). The EW-improved model predicts a slightly lower cross section for large jet multiplicities, but given the large experimental uncertainty it is difficult to distinguish between the models. Also, the value chosen for $\alpha_s(M_Z)$ greatly influences the shape of the distribution (fig. V.5). The default value used in the Monash tune overshoots the tail, whereas the PDG best fit value undershoots it. Choosing an in-between value leads to a good agreement for all multiplicities. However, it should be noted that $\alpha_s(M_Z)$ in the parton shower is tuned to jet-shapes (in e^+e^- and hadron-hadron collisions) and just changing the value on a process-by-process means a significant loss of predictivity. An optimal solution would be a full retuning of the merged event generator to observables that have been measured for the purpose of tuning. This would result in a sensible best-fit value of $\alpha_s(M_Z)$ that should be used for merged predictions of, say, the jet

multiplicities. We refrain from providing a merged tune here, since distinguishing between the “uncertainties" and the “tunable parameters" of merged predictions is beyond the scope of this study. All observables presented below are not very sensitive to $\alpha_s(M_Z)$, up to overall normalisations. We thus use $\alpha_s(M_Z) = 0.118$ for all further studies.

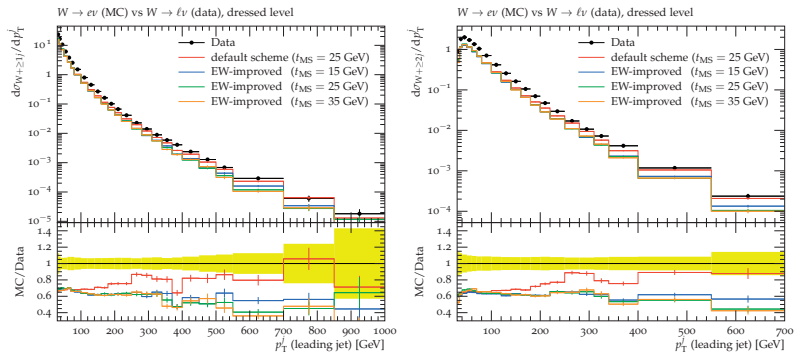

Figure V.6: PYTHIA predictions in comparison to ATLAS data [65] for W + jets as a function of the leading jet transverse momentum in inclusive $n-$jet events. The yellow error band indicates the one sigma experimental uncertainty and the vertical line on the MC prediction is the statistical MC uncertainty.

The $p_\perp$ distributions of individual jets (fig. V.6) provide a better test of the default and EW-improved merging schemes. The fall-off observed in data is not captured by the default model, whereas the EW-improved model describes the shape of the data much better. This is the result of a more sensible scale setting, when the event is clustered to a $2 \to 2$ QCD process, and of the correct inclusion of the weak no-emission probability. The default merging scheme had to compromise to determine the no-emission probability for the unordered states. No such compromise is necessary now, since the EW-improved scheme will instead naturally yield an underlying $2 \to 2$ QCD process and reweight accordingly. This clearly showcases that the “merging of mergings" scheme is favoured by data.

More inclusive hardness-measures like the scalar $p_\perp$ sum of jets S_T (fig. V.7) encourage the same conclusion. The effect is even more pronounced for these observables. One of the observables that proved difficult to describe in the original experimental study

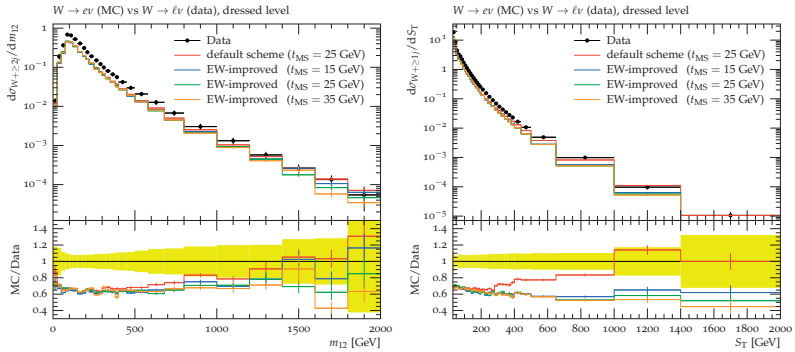

Figure V.7: PYTHIA predictions in comparison to ATLAS data [65] for W + jets as a function of m_{12} and S_T. The yellow error band indicates the one sigma experimental uncertainty and the vertical line on the MC prediction is the statistical MC uncertainty.

was the invariant mass between the two leading jets, m_{12}. Again, the EW-improved merging scheme describes this observable well.

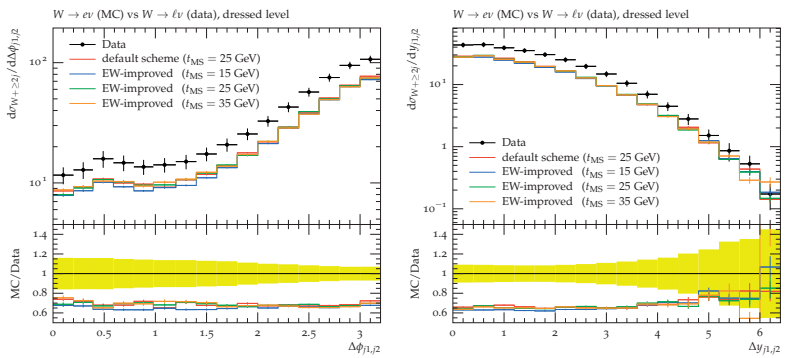

Figure V.8: PYTHIA predictions in comparison to ATLAS data [65] for W + jets as a function of $\Delta\varphi_{12}$ and Δy_{12}. The yellow error band indicates the one sigma experimental uncertainty and the vertical line on the MC prediction is the statistical MC uncertainty.

Angular distributions are problematic for the weak parton showers. The inclusion of merging is expected to improve this. This is exactly what is seen for $\Delta\varphi_{12}$ and Δy_{12} distributions (fig. V.8). Both the default and the EW-improved merging schemes provide almost identical, and good, descriptions of the data.

v.6.2 *Predictions at 100 TeV*

When comparing with LHC data, we choose to highlight the importance of assigning the correct underlying process, and disregarded other weak resummation effects to not obscure the picture. In this section, we instead combine pure QCD multi-parton states with W-boson + jets states. We therefore include W-bosons in the merging scale cut: soft W-bosons will be produced by the shower, while states containing hard W-bosons will be given by the fixed-order result.

In order to assess the full effect of the merging QCD+EW showers with multi-parton matrix elements, it is preferable to consider 100 TeV pp collisions due to larger logarithmic enhancement with increasing energy. Observable that are commonly used to highlight weak resummation effects mostly relate to exclusive dijet production. However, in a combined resummation of QCD and EW logarithms, effects of weak resummation will be completely dwarfed by all-order QCD. We will therefore consider fully inclusive QCD and fully exclusive weak dijet production. Basically, whenever a weak boson is produced the event will not enter the histograms. This should of course not be regarded as experimentally feasible, since a perfect W/Z tagging is doubtful. However, the setup can provide valuable insight into the maximal size of effects related to the weak no-emission probability. As event selection, we require at least two jets with $p_\perp > 500$ GeV and the leading jet above $p_\perp > 1500$ GeV and no weak bosons.

The effects of the weak no-emission probability can seen in fig. V.9, where we compare the result of including/not including the weak PS when merging multi-jet with up to three outgoing partons. The merging scales value is $t_{\text{MS}} = 500$ GeV. As expected the weak no-emission probability becomes more important for higher $p_\perp$ scales and reaches roughly 25% for a leading jet $p_\perp$ of 20 TeV. Even at lower energies it might become important for high precision measurements. This result is in agreement with the prediction from the stand-alone weak PS [37].

A similar observable is the exclusive weak production of a $W^\pm$ boson in association with at least two jets (fig. V.9). In addition to the multi-jet samples, this simulation also requires W + $\leq$ 2

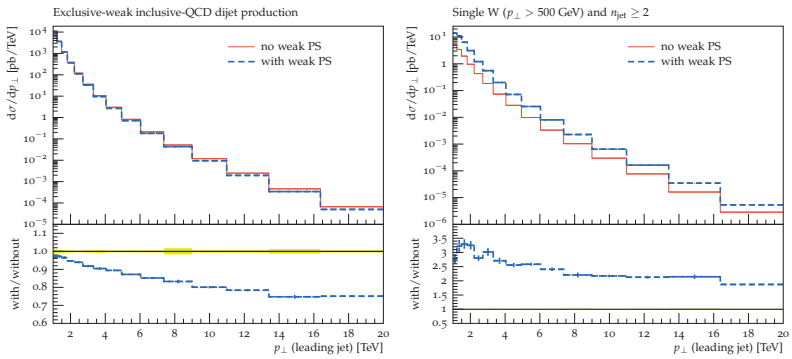

Figure V.9: Predictions for 100 TeV respectively with and without including the weak PS for weak-exclusive dijet production (left) and weak-exclusive W + $\geq$ 2 jets (right). The yellow error band and the vertical lines indicate statistical MC uncertainty.

jets samples. As such, this simulation presents a fully inclusive merging of processes with vastly different cross sections. The event selection applies the jet selection outlined above, but additionally requires exactly one W with $p_\perp > 500$ GeV, and no further weak bosons. The interpretation in terms of resummation effects is not as straightforward for this observable. The inclusion of the weak PS both adds real radiation while simultaneously lowering the cross section due to the inclusion of no-emission probabilities. However, the real emission enhancement is overwhelming and leads to a factor of 2–3 enhancement of the cross section. This clearly shows the need for including weak corrections, since the prediction from the ME alone is too low. If higher jet multiplicities (e.g. W + 4 jet) are included, this effect is expected to become milder.

An earlier study [48] of the electroweak corrections showed significantly larger effects, reaching up to $\sim 80\,\%$ for lower jet energies. This earlier study calculates the full EW NLO and compares the differences between LO and NLO. The studies are not directly compatible, due to different treatment of multiple effects, including: handling of photons, competition between QCD and weak bosons, Bloch-Nordsieck violations [70] and different analysis conditions. Further studies to get a better handle on weak Sudakov effects would be of great interest.

V.7 CONCLUSIONS

We have presented a new consistent way of combining associated weak boson radiation in hard dijet production with hard QCD radiation in Drell-Yan-type events. It captures the strengths of both the merging technique and the weak PS, while removing issues intrinsic to either. More specifically, we provide a first matrix element merged prediction that consistently includes weak all-order effects. The combination of weak and QCD corrections leads to the concept of a "merging of mergings": processes with vastly different lowest-order cross sections are combined into a single consistent sample. We have addressed the problem of unordered states in this context, and a dynamical solution based on the dominance of certain scale hierarchies (i.e. evolution histories) in certain phase space regions has been presented. The novel prescription will be made available with the next release of PYTHIA 8.

The new merging scheme is compared to experimental data from ATLAS and CMS. For all considered distributions the new EW-improved merging scheme does as least as well as the old default merging. For a large fraction of the distributions, the EW-improved scheme shows a significant improvement over the previous results. Especially for high S_T, where the EW-improved merging predicts a lower production rate by a more physical scale setting, by including weak no-emission probabilities, and by identifying a $2 \to 2$ QCD scattering as underlying process.

The importance of the weak Sudakov for dijet production have been assessed in the EW-improved merging scheme. The effects are shown to be about 25 % at large jet $p_\perp$ at a 100 TeV proton collider. Further studies comparing the predicted corrections in the EW-improved merging scheme with NLO EW calculation would be an interesting next step.

This study only includes the merging of W bosons and jets, but the Sudakov coming from both $W^\pm$ and Z^0 bosons is accounted for. The implementation of Z^0 in the same merging framework is purely a technical, and is expected to simpler than that of the $W^\pm$.

In this study the weak merging scheme was only implemented for the CKKW-L merging of leading-order matrix elements, as this relatively simple merging method allows us to isolate and address

generic problems without obscuring the discussion by irrelevant details. A natural, and intriguing, next step is to extend the novel prescription to the UMEPS and UNLOPS schemes implemented in PYTHIA. Especially the latter would be of great interest, since it would yield an event simulation that contains multiple NLO calculations for multiple processes consistently combined with both QCD and EW resummation. The challenge of such a generalisation is expected to be technical rather than conceptual.

ACKNOWLEDGMENTS

We thank Leif Lönnblad and Torbjörn Sjöstrand for many enlightening discussions and for their comments on the manuscript. SP gratefully acknowledges discussions about merging with Stefan Höche. JRC is in part supported by Swedish Research Council, contract number 621-2013-4287, and in part by the MCnetITN FP7 Marie Curie Initial Training Network, contract PITN-GA-2012-315877. SP is supported by the US Department of Energy under contract DE–AC02–76SF00515.

BIBLIOGRAPHY

[1] A. Buckley *et al.*, "General-purpose event generators for LHC physics," *Phys. Rept.* **504** (2011) 145–233, arXiv:1101.2599 [hep-ph].

[2] S. Frixione and B. R. Webber, "Matching NLO QCD computations and parton shower simulations," *JHEP* **06** (2002) 029, hep-ph/0204244.

[3] P. Nason, "A new method for combining NLO QCD with shower Monte Carlo algorithms," *JHEP* **11** (2004) 040, hep-ph/0409146.

[4] S. Frixione, P. Nason, and C. Oleari, "Matching NLO QCD computations with parton shower simulations: the POWHEG method," *JHEP* **11** (2007) 070, arXiv:0709.2092 [hep-ph].

[5] S. Frixione, F. Stoeckli, P. Torrielli, and B. R. Webber, "NLO QCD corrections in Herwig++ with MC@NLO," *JHEP* **01** (2011) 053, arXiv:1010.0568 [hep-ph].

[6] P. Torrielli and S. Frixione, "Matching NLO QCD computations with PYTHIA using MC@NLO," *JHEP* **04** (2010) 110, arXiv:1002.4293 [hep-ph].

[7] S. Alioli, P. Nason, C. Oleari, and E. Re, "A general framework for implementing NLO calculations in shower Monte Carlo programs: the POWHEG BOX," *JHEP* **06** (2010) 043, arXiv:1002.2581 [hep-ph].

[8] S. Höche, F. Krauss, M. Schönherr, and F. Siegert, "Automating the POWHEG method in SHERPA," *JHEP* **04** (2011) 024, arXiv:1008.5399 [hep-ph].

[9] S. Höche, F. Krauss, M. Schönherr, and F. Siegert, "W+n-jet predictions with MC@NLO in Sherpa," *Phys.Rev.Lett.* **110** (2013) 052001, arXiv:1201.5882 [hep-ph].

[10] S. Plätzer and S. Gieseke, "Dipole Showers and Automated NLO Matching in Herwig++," *Eur.Phys.J.* **C72** (2012) 2187, arXiv:1109.6256 [hep-ph].

[11] S. Jadach, W. Placzek, S. Sapeta, A. Siodmok, and M. Skrzypek, "Matching NLO QCD with parton shower in Monte Carlo scheme - the KrkNLO method," arXiv:1503.06849 [hep-ph].

[12] S. Höche, F. Krauss, M. Schönherr, and F. Siegert, "A critical appraisal of NLO+PS matching methods," *JHEP* **09** (2012) 049, arXiv:1111.1220 [hep-ph].

[13] J. Alwall, R. Frederix, S. Frixione, V. Hirschi, F. Maltoni, O. Mattelaer, H. S. Shao, T. Stelzer, P. Torrielli, and M. Zaro, "The automated computation of tree-level and next-to-leading order differential cross sections, and their matching to parton shower simulations," *JHEP* **07** (2014) 079, arXiv:1405.0301 [hep-ph].

[14] S. Catani, F. Krauss, R. Kuhn, and B. R. Webber, "QCD matrix elements + parton showers," *JHEP* **11** (2001) 063, hep-ph/0109231.

[15] L. Lönnblad, "Correcting the colour-dipole cascade model with fixed order matrix elements," *JHEP* **05** (2002) 046, hep-ph/0112284.

[16] M. L. Mangano, M. Moretti, and R. Pittau, "Multijet matrix elements and shower evolution in hadronic collisions: $Wb\bar{b} + n$-jets as a case study," *Nucl. Phys.* **B632** (2002) 343–362, hep-ph/0108069.

[17] J. Alwall *et al.*, "Comparative study of various algorithms for the merging of parton showers and matrix elements in hadronic collisions," *Eur. Phys. J.* **C53** (2008) 473–500, arXiv:0706.2569 [hep-ph].

[18] N. Lavesson and L. Lönnblad, "Merging parton showers and matrix elements – back to basics," *JHEP* **04** (2008) 085, arXiv:0712.2966 [hep-ph].

[19] K. Hamilton, P. Richardson, and J. Tully, "A modified CKKW matrix element merging approach to angular-ordered parton showers," *JHEP* **11** (2009) 038, arXiv:0905.3072 [hep-ph].

[20] K. Hamilton and P. Nason, "Improving NLO-parton shower matched simulations with higher order matrix elements," *JHEP* **06** (2010) 039, arXiv:1004.1764 [hep-ph].

[21] S. Höche, F. Krauss, M. Schönherr, and F. Siegert, "NLO matrix elements and truncated showers," *JHEP* **08** (2011) 123, arXiv:1009.1127 [hep-ph].

[22] S. Plätzer, "Controlling inclusive cross sections in parton shower + matrix element merging," *JHEP* **08** (2013) 114, arXiv:1211.5467 [hep-ph].

[23] L. Lönnblad and S. Prestel, "Matching Tree-Level Matrix Elements with Interleaved Showers," *JHEP* **03** (2012) 019, arXiv:1109.4829 [hep-ph].

[24] L. Lönnblad and S. Prestel, "Unitarising Matrix Element + Parton Shower merging," *JHEP* **02** (2013) 094, arXiv:1211.4827 [hep-ph].

[25] K. Hamilton, P. Nason, E. Re, and G. Zanderighi, "NNLOPS simulation of Higgs boson production," *JHEP* **10** (2013) 222, arXiv:1309.0017 [hep-ph].

[26] A. Karlberg, E. Re, and G. Zanderighi, "NNLOPS accurate Drell-Yan production," arXiv:1407.2940 [hep-ph].

[27] K. Hamilton, P. Nason, and G. Zanderighi, "Finite quark-mass effects in the NNLOPS POWHEG+MiNLO Higgs generator," *JHEP* **05** (2015) 140, arXiv:1501.04637 [hep-ph].

[28] S. Höche, Y. Li, and S. Prestel, "Higgs-boson production through gluon fusion at NNLO QCD with parton showers," *Phys.Rev.* **D90** (2014) 054011, arXiv:1407.3773 [hep-ph].

[29] S. Höche, Y. Li, and S. Prestel, "Drell-Yan lepton pair production at NNLO QCD with parton showers," arXiv:1405.3607 [hep-ph].

[30] S. Alioli, C. W. Bauer, C. Berggren, F. J. Tackmann, and J. R. Walsh, "Drell-Yan Production at NNLL'+NNLO Matched to Parton Showers," arXiv:1508.01475 [hep-ph].

[31] N. Lavesson and L. Lönnblad, "Extending CKKW-merging to one-loop matrix elements," *JHEP* **12** (2008) 070, arXiv:0811.2912 [hep-ph].

[32] T. Gehrmann, S. Höche, F. Krauss, M. Schönherr, and F. Siegert, "NLO QCD matrix elements + parton showers in e^+e^- $\to$hadrons," *JHEP* **01** (2013) 144, arXiv:1207.5031 [hep-ph].

[33] S. Höche, F. Krauss, M. Schönherr, and F. Siegert, "QCD matrix elements + parton showers: The NLO case," *JHEP* **04** (2013) 027, arXiv:1207.5030 [hep-ph].

[34] R. Frederix and S. Frixione, "Merging meets matching in MC@NLO," *JHEP* **12** (2012) 061, arXiv:1209.6215 [hep-ph].

[35] S. Alioli, C. W. Bauer, C. J. Berggren, A. Hornig, F. J. Tackmann, *et al.*, "Combining Higher-Order Resummation with Multiple NLO Calculations and Parton Showers in GENEVA," *JHEP* **09** (2013) 120, arXiv:1211.7049 [hep-ph].

[36] L. Lönnblad and S. Prestel, "Merging Multi-leg NLO Matrix Elements with Parton Showers," *JHEP* **03** (2013) 166, arXiv:1211.7278 [hep-ph].

[37] J. R. Christiansen and T. Sjöstrand, "Weak Gauge Boson Radiation in Parton Showers," *JHEP* **04** (2014) 115, arXiv:1401.5238 [hep-ph].

[38] F. Krauss, P. Petrov, M. Schoenherr, and M. Spannowsky, "Measuring collinear W emissions inside jets," *Phys. Rev.* **D89** no. 11, (2014) 114006, arXiv:1403.4788 [hep-ph].

[39] T. Sjöstrand, S. Ask, J. R. Christiansen, R. Corke, N. Desai, P. Ilten, S. Mrenna, S. Prestel, C. O. Rasmussen, and P. Z. Skands, "An Introduction to PYTHIA 8.2," *Comput.Phys.Commun.* **191** (2015) 159–177, arXiv:1410.3012 [hep-ph].

[40] S. Catani, B. R. Webber, and G. Marchesini, "QCD coherent branching and semiinclusive processes at large x," *Nucl. Phys.* **B349** (1991) 635–654.

[41] Z. Nagy and D. E. Soper, "On the transverse momentum in Z-boson production in a virtuality ordered parton shower," *JHEP* **03** (2010) 097, arXiv:0912.4534 [hep-ph].

[42] S. Dittmaier, A. Huss, and C. Speckner, "Weak radiative corrections to dijet production at hadron colliders," *JHEP* **11** (2012) 095, arXiv:1210.0438 [hep-ph].

[43] P. Ciafaloni and D. Comelli, "The Importance of weak bosons emission at LHC," *JHEP* **09** (2006) 055, arXiv:hep-ph/0604070 [hep-ph].

[44] S. Moretti, M. R. Nolten, and D. A. Ross, "Weak corrections and high E(T) jets at Tevatron," *Phys. Rev.* **D74** (2006) 097301, arXiv:hep-ph/0503152 [hep-ph].

[45] A. Denner, "Electroweak radiative corrections at high-energies," *PoS* **HEP2001** (2001) 129, arXiv:hep-ph/0110155 [hep-ph].

[46] U. Baur, "Weak Boson Emission in Hadron Collider Processes," *Phys. Rev.* **D75** (2007) 013005, arXiv:hep-ph/0611241 [hep-ph].

[47] J. M. Campbell, D. Wackeroth, and J. Zhou, "Electroweak Corrections at the LHC with MCFM," in *23rd International Workshop on Deep-Inelastic Scattering and Related Subjects (DIS 2015) Dallas, Texas, United States, April 27-May 1, 2015*. 2015. arXiv:1508.06247 [hep-ph].

[48] K. Mishra *et al.*, "Electroweak Corrections at High Energies," arXiv:1308.1430 [hep-ph].

[49] V. N. Gribov and L. N. Lipatov, "Deep inelastic *e-p* scattering in perturbation theory," *Sov. J. Nucl. Phys.* **15** (1972) 438–450.

[50] Y. L. Dokshitzer, "Calculation of the structure functions for deep inelastic scattering and e^+e^- annihilation by perturbation theory in quantum chromodynamics," *Sov. Phys. JETP* **46** (1977) 641–653.

[51] G. Altarelli and G. Parisi, "Asymptotic freedom in parton language," *Nucl. Phys.* **B126** (1977) 298–318.

[52] L. Carloni, J. Rathsman, and T. Sjöstrand, "Discerning Secluded Sector gauge structures," *JHEP* **04** (2011) 091, arXiv:1102.3795 [hep-ph].

[53] M. Bengtsson and T. Sjöstrand, "Coherent Parton Showers Versus Matrix Elements: Implications of PETRA - PEP Data," *Phys. Lett.* **B185** (1987) 435.

[54] M. H. Seymour, "Matrix-element corrections to parton shower algorithms," *Comp. Phys. Commun.* **90** (1995) 95–101, hep-ph/9410414.

[55] G. Miu and T. Sjöstrand, "W production in an improved parton-shower approach," *Phys. Lett.* **B449** (1999) 313–320, arXiv:hep-ph/9812455.

[56] E. Norrbin and T. Sjöstrand, "QCD radiation off heavy particles," *Nucl. Phys.* **B603** (2001) 297–342, arXiv:hep-ph/0010012 [hep-ph].

[57] M. Wobisch and K. Rabbertz, "Dijet azimuthal decorrelations for $\Delta\varphi_{\text{dijet}} < 2\pi/3$ in perturbative QCD," arXiv:1505.05030 [hep-ph].

[58] S. Catani, Y. L. Dokshitzer, M. H. Seymour, and B. R. Webber, "Longitudinally-invariant $k_\perp$-clustering algorithms for hadron–hadron collisions," *Nucl. Phys.* **B406** (1993) 187–224.

[59] T. Gleisberg, S. Höche, F. Krauss, M. Schönherr, S. Schumann, F. Siegert, and J. Winter, "Event generation with SHERPA 1.1," *JHEP* **02** (2009) 007, arXiv:0811.4622 [hep-ph].

[60] A. Schälicke and F. Krauss, "Implementing the ME+PS merging algorithm," *JHEP* **07** (2005) 018, hep-ph/0503281.

[61] T. Sjöstrand and M. van Zijl, "A multiple-interaction model for the event structure in hadron collisions," *Phys. Rev.* **D36** (1987) 2019.

[62] S. Alekhin *et al.*, "HERA and the LHC - A workshop on the implications of HERA for LHC physics: Proceedings Part A," hep-ph/0601012.

[63] M. Bähr, S. Gieseke, and M. H. Seymour, "Simulation of multiple partonic interactions in Herwig++," *JHEP* **07** (2008) 076, arXiv:0803.3633 [hep-ph].

[64] T. Sjöstrand and P. Z. Skands, "Multiple interactions and the structure of beam remnants," *JHEP* **03** (2004) 053, hep-ph/0402078.

[65] **ATLAS** Collaboration, G. Aad *et al.*, "Measurements of the W production cross sections in association with jets with the ATLAS detector," *Eur. Phys. J.* **C75** no. 2, (2015) 82, arXiv:1409.8639 [hep-ex].

[66] **CMS** Collaboration, V. Khachatryan *et al.*, "Differential cross section measurements for the production of a W boson in

association with jets in proton–proton collisions at $\sqrt{s} = 7$ TeV," *Phys. Lett.* **B741** (2015) 12–37, arXiv:1406.7533 [hep-ex].

[67] J. Pumplin, D. R. Stump, J. Huston, H. L. Lai, P. Nadolsky, and W. K. Tung, "New generation of parton distributions with uncertainties from global QCD analysis," *JHEP* **07** (2002) 012, hep-ph/0201195.

[68] P. Skands, S. Carrazza, and J. Rojo, "Tuning PYTHIA 8.1: the Monash 2013 Tune," *Eur. Phys. J.* **C74** no. 8, (2014) 3024, arXiv:1404.5630 [hep-ph].

[69] A. Buckley, J. Butterworth, L. Lönnblad, D. Grellscheid, H. Hoeth, *et al.*, "Rivet user manual," *Comput.Phys.Commun.* **184** (2013) 2803–2819, arXiv:1003.0694 [hep-ph].

[70] F. Bloch and A. Nordsieck, "Note on the radiation field of the electron," *Phys. Rev.* **52** (Jul, 1937) 54–59.